2014

SYNTHESIS, CHARACTERIZATION, AND BIOLOGICAL STUDIES OF PYRAZOLONE SCHIFF BASES AND THEIR TRANSITION METAL COMPLEXES

by **Omoruyi Gold Idemudia**

A dissertation, submitted in fulfillment of the requirements for the award of Doctor of Philosophy in Chemistry (PhD) in the Faculty of Science and Agriculture, University of Fort Hare

Supervisors

Professor A. P. Sadimenko

Professor A. J. Afolayan

Synthesis, Characterization, and Biological Studies of Pyrazolone Schiff Bases and their Transition Metal Complexes

By

Idemudia Omoruyi Gold (200805777)
B.Sc (Hons) Industrial Chemistry (Univ. of Benin, Nigeria), B.Sc (Hons), M.Sc Chemistry (Univ. of Fort Hare, South Africa)

Being a dissertation submitted to the Faculty of Science and Agriculture in fulfillment of the requirements for the award of the degree of Doctor of Philosophy in Chemistry (PhD)

University of Fort Hare
Together in Excellence

Supervisors: Professor A. P. Sadimenko
Professor A. J. Afolayan

March 2014

Table of Contents

Declaration 9

Acknowledgements 10

Dedication 11

List of Tables 12

List of Figures 13

List of Abbreviations 17

List of Journal Abbreviations 20

Research Output 26

Abstract 28

1. Introduction 30

2. Review of Literature 33

    2.1. Schiff Bases 33

    2.2. Transition Metal Complexes of Schiff Bases 37

    2.3. Pyrazolone Schiff Bases and Metal Complexes 39

    2.4. Transition Metal Ions under Investigation 54

    2.5. Antibacterial Activity 57

    2.6. Antioxidant Activity 61

    2.7. Diseases andResistance to Drugs 62

3. Experimental and Characterization Techniques 65

    3.1. Materials 65

    3.2. Synthesis of Schiff Bases 65

3.2.1. Synthesis of 4-Acetyl-3-methyl-1-phenyl-2-pyrazolin-5-one Phenylhydrazine 65
3.2.2. Synthesis of 4-Acetyl-3-methyl-1-phenyl-2-pyrazolin-5-one Dinitrophenylhydrazine 66
3.2.3. Synthesis of 4-Acetyl-3-methyl-1-phenyl-2-pyrazolin-5-one Sulfanilamide 67
3.2.4. Synthesis of 4-Benzoyl-3-methyl-1-phenyl-2-pyrazolin-5-one Phenylhydrazine 67
3.2.5. Synthesis of 4-Benzoyl-3-methyl-1-phenyl-2-pyrazolin-5-one Dinitrophenylhydrazine 68
3.2.6. Synthesis of 4-Benzoyl-3-methyl-1-phenyl-2-pyrazolin-5-one Sulfanilamide 69
3.3. Synthesis of Transition Metal Complexes of Pyrazolone Schiff Bases 70
3.3.1. Synthesis of $Mn(Ampp\text{-}Ph)_2(H_2O)_2 \cdot 2H_2O$ 70
3.3.2. Synthesis of $Co(Ampp\text{-}Ph)_2(H_2O)_2 \cdot 2H_2O$ 70
3.3.3. Synthesis of $Ni(Ampp\text{-}Ph)_2(H_2O)_2 \cdot H_2O$ 71
3.3.4. Synthesis of $Cu(Ampp\text{-}Ph)_2(H_2O)_2$ 72
3.3.5. Synthesis of $Mn(Bmpp\text{-}Ph)_2(H_2O)_2 \cdot 2H_2O$ 72
3.3.6. Synthesis of $Co(Bmpp\text{-}Ph)_2(H_2O)_2 \cdot H_2O$ 73
3.3.7. Synthesis of $Ni(Bmpp\text{-}Ph)_2(H_2O)_2 \cdot 2H_2O$ 73
3.3.8. Synthesis of $Cu(Bmpp\text{-}Ph)_2(H_2O)_2 \cdot H_2O$ 74

3.3.9. Synthesis of $Mn(Ampp\text{-}Dh)_2(H_2O)_2 \cdot H_2O$ 74

3.3.10. Synthesis of $Co(Ampp\text{-}Dh)_2(H_2O)_2$ 75

3.3.11. Synthesis of $Ni(Ampp\text{-}Dh)_2(H_2O)_2$ 76

3.3.12. Synthesis of $Cu(Ampp\text{-}Dh)_2(H_2O)_2$ 76

3.3.13. Synthesis of $Mn(Bmpp\text{-}Dh)_2(H_2O)_2$ 77

3.3.14. Synthesis of $Co(Bmpp\text{-}Dh)_2(H_2O)_2 \cdot H_2O$ 77

3.3.15. Synthesis of $Ni(Bmpp\text{-}Dh)_2(H_2O)_2 \cdot H_2O$ 78

3.3.16. Synthesis of $Cu(Bmpp\text{-}Dh)_2(H_2O)_2 \cdot 2H_2O$ 78

3.3.17. Synthesis of $Mn(Ampp\text{-}Sn)_2(H_2O)_2 \cdot H_2O$ 79

3.3.18. Synthesis of $Co(Ampp\text{-}Sn)_2(H_2O)_2$ 79

3.3.19. Synthesis of $Ni(Ampp\text{-}Sn)_2(H_2O)_2 \cdot H_2O$ 80

3.3.20. Synthesis of $Cu(Ampp\text{-}Sn)_2(H_2O)_2 \cdot H_2O$ 81

3.3.21. Synthesis of $Mn(Bmpp\text{-}Sn)_2(H_2O)_2$ 81

3.3.22. Synthesis of $Co(Bmpp\text{-}Sn)_2(H_2O)_2 \cdot H_2O$ 82

3.3.23. Synthesis of $Ni(Bmpp\text{-}Sn)_2(H_2O)_2 \cdot H_2O$ 82

3.3.24. Synthesis of $Cu(Bmpp\text{-}Sn)_2(H_2O)_2$ 83

3.4. Melting Point 83

3.5. Elemental Analysis 83

3.6. Conductivity Measurements 84

3.7. Infrared-Spectroscopy 84

3.8. Electronic (UV-Vis) Spectroscopy 85

3.9. NMR Spectroscopy 86

3.10. Mass Spectroscopy 87

3.11. Magnetic Susceptibility Measurements 87

3.12. X-Ray Crystallography Analysis 89

3.13. Thermogravimetric analysis 90

3.14. Antibacterial Assay 91

3.14.1. Preparation of Nutrient Broth 91

3.14.2. Preparation of Mueller–Hinton Agar 91

3.14.3 Preparation of Test Samples 92

3.15. Antioxidant Assay 93

4. Results and Discussion 95

4.1. Acylpyrazolone Derived Phenylhydrazine Schiff Bases and Their Metal Complexes 95

4.1.1. Synthesis 96

4.1.2. Elemental Analysis 97

4.1.3. ^{1}H and ^{13}C NMR Spectroscopy 97

4.1.4. Mass Spectroscopy 100

4.1.5. Infrared Spectroscopy 101

4.1.6. UV-Vis Spectroscopy and Magnetic Moments 103

4.1.7. X-Ray Crystallography 109

4.1.8. Thermogravimetric Studies 115

4.1.9. Antibacterial Activity Study 123

4.1.10 Antioxidant (Free Radical Scavenging) Activity 125

4.2. Acylpyrazolone Derived Dinitrophenylhydrazine Schiff Bases and Their Metal Complexes 127

4.2.1. Synthesis 128

4.2.2. Elemental Analysis 129

4.2.3. ^{1}H and ^{13}C NMR Spectroscopy 130

4.2.4. Mass Spectroscopy 133

4.2.5. Infrared Spectroscopy 134

4.2.6. UV-Vis Spectroscopy and Magnetic Moments 135

4.2.7. X-Ray Crystallography 140

4.2.8. Thermogravimetric Studies 143

4.2.9. Antibacterial Activity Study 150

4.2.10. Antioxidant (Free Radical Scavenging) Activity 151

4.3. Acylpyrazolone Derived Dinitrophenylhydrazine Schiff Bases and Their Metal Complexes 153

4.3.1. Synthesis 154

4.3.2. Elemental Analysis 155

4.3.3. ^{1}H and ^{13}C NMR Spectroscopy 156

4.3.4. Mass Spectroscopy 158

4.3.5. Infrared Spectroscopy 159

4.3.6. UV-Vis Spectroscopy and Magnetic Moments 160

4.3.7. X-Ray Crystallography 164

4.3.8. Thermogravimetric Studies 169

4.3.9. Antibacterial Activity Study 177

4.3.10. Antioxidant (Free Radical Scavenging) Activity 178

5. Conclusion 181

References 185

Appendix 205

A1. IR Spectra of Metal Complexes 205

A2. Crystal Structure Data 209

Declaration

I hereby declare that this dissertation, submitted to the University of Fort Hare (UFH) for the award of Doctor of Philosophy (PhD) in Chemistry, in the Faculty of Science & Agriculture and the work contained therein, is my original work with exemption to the available citations. I further declare that neither the whole work nor any part of it has been, is being, or shall be submitted at any other university for the award of a degree.

Name: _____

Signature: _____

Date: _____

Acknowledgements

My sincere gratitude goes to everyone who has contributed knowingly or unknowingly towards the success of this study. To my supervisors, Professor A. P. Sadimenko and Professor A. J. Afolayan, for their tremendous understanding, guidance, and support, just to mention but a few. Special thanks to Prof. A. P. Sadimenko for his remarkable technical contributions.

I am thankful to Govan Mbeki Research Development Centre (GMRDC) University of Fort Hare for financial support.

I would like to thank Dr. D. M. Katwire, head of the Department of Chemistry, University of Fort Hare, for his continuous encouragement and for space to carry out my research work. Also, I recognize my research group members, Emmanuel Ajayi and Siyambusa Zimela, thank you for having me.

My appreciation also goes to my aunty Mrs. B. A. Ogunmwonyi, my mum Mrs. E. O. Imasuen and my siblings for their understanding, continuous support and prayers. I cannot forget the moral support of Engr. Eghosa O. Uzunuigbe, Mr. and Mrs. Osaze G. Inneh, and Mr. Anthony Curtis Idemudia in my life, it has kept me going.

I acknowledge my friends, Eric Akinnawo, Osadolor Omo–osagie, Justin Omogiate, Godwin Ogiemwonyi, Okiemute Onome, Etinosa Igbinosa, Mykel Obiapi, Idowu Seriki and others, too numerous to mention, thank you, guys, for believing in me. To Ngoakoana Lettie Chokoe, thank you for your love and been there for me. OSA URUESE!

Dedication

To my grandmother, Late Madam Edowaye Amadasu and her children

List of Tables

Table 1. Magnetic Properties of d^n Configurationsof Interest 89

Table 2. Composition of Nutrient Broth 92

Table 3. Composition of Mueller-Hinton Agar 92

Table 4. Crystal and Refinement Data for Bmpp-Ph 109

Table 5. Crystal and Refinement Data for $C_{38}H_{38}CoN_4O_6$ 112

Table 6. Zone of Growth Inhibition Exhibited by Ligands and Metal Complexes at 40 mg/mL 124

Table 7. Antioxidant Scavenging Activity Data of Phenylhydrazine Schiff Bases and Their Metal Complexes (%) 126

Table 8. Crystal and Refinement Data for Bmpp-Dh 140

Table 9. Zone of Growth Inhibition Exhibited by Dinitrophenylhydrazine Schiff Bases and Metal Complexes at 40 mg/mL (mm) 150

Table 10. Antioxidant Scavenging Activity Data of Dinitrophenylhydrazine Schiff Bases and Their Metal Complexes (%) 151

Table 11. Crystal and Refinement Data for Bmpp-Sn 165

Table 12. Crystal and Refinement data for $Co(Bmpp)_2(DMF)_2$ 168

Table 13. Zone of Growth Inhibition Exhibited by Sulfanilamide Schiff Bases and Metal Complexes at 40 mg/mL (mm) 178

Table 14. Antioxidant Scavenging Activity Data of Sulfanilamide Schiff Bases and Their Metal Complexes (%) 179

List of Figures

Figure 1. ^{1}H NMR Spectrum of Bmpp-Ph 98

Figure 2. ^{1}H NMR Spectrum of Ampp-Ph 99

Figure 3. ^{13}C NMR Spectrum of Bmpp-Ph 99

Figure 4. ^{13}C NMR Spectrum of Ampp-Ph 100

Figure 5. Mass Spectrum of Bmpp-Ph 101

Figure 6. Mass Spectrum of Ampp-Ph 101

Figure 7. Electronic Spectrum of $Mn(Bmpp\text{-}Ph)_2(H_2O)_2\cdot 2H_2O$ 104

Figure 8. Electronic Spectrum of $Mn(Ampp\text{-}Ph)_2(H_2O)_2\cdot 2H_2O$ 105

Figure 9. Electronic Spectrum of $Co(Bmpp\text{-}Ph)_2(H_2O)_2\cdot H_2O$ 106

Figure 10. Electronic Spectrum of $Co(Ampp\text{-}Ph)_2(H_2O)_2\cdot 2H_2O$ 106

Figure 11. Electronic Spectrum of $Ni(Bmpp\text{-}Ph)_2(H_2O)_2\cdot 2H_2O$ 107

Figure 12. Electronic Spectrum of $Ni(Ampp\text{-}Ph)_2(H_2O)_2\cdot H_2O$ 107

Figure 13. Electronic Spectrum of $Cu(Bmpp\text{-}Ph)_2(H_2O)_2\cdot H_2O$ 108

Figure 14. Electronic Spectrum of $Cu(Ampp\text{-}Ph)_2(H_2O)_2$ 108

Figure 15. Molecular structure of $Bmpp\text{-}Ph(C_{23}H_{20}N_4O)$ 110

Figure 16. Inter and Intramolecular Hydrogen Bonding in Bmpp-Ph 111

Figure 17. Molecular Packing Diagram of Bmpp-Ph 111

Figure 18. The Molecular Structure of $[Co(C_{17}H_{13}N_2O_2)_2(C_2H_6O)_2]$ 114

Figure 19. Hydrogen Bonding in $[Co(C_{17}H_{13}N_2O_2)_2(C_2H_6O)_2]$ 114

Figure 20. Crystal Packing Diagram of $[Co(C_{17}H_{13}N_2O_2)_2(C_2H_6O)_2]$ 115

Figure 21. TGA and DTG Curves of $Mn(Bmpp\text{-}Ph)_2(H_2O)_2\cdot 2H_2O$ 116

Figure 22. TGA and DTG Curve of $Mn(Ampp\text{-}Ph)_2(H_2O)_2\cdot 2H_2O$ 117

Figure 23. TGA and DTG curve of $Co(Bmpp\text{-}Ph)_2(H_2O)_2\cdot H_2O$ 118

Figure 24. TGA and DTG Curve of $Co(Ampp\text{-}Ph)_2(H_2O)_2\cdot 2H_2O$ 118

Figure 25. TGA and DTG curve of $Ni(Bmpp\text{-}Ph)_2(H_2O)_2\cdot 2H_2O$ 119

Figure 26. TGA and DTG curve of $Ni(Ampp\text{-}Ph)_2(H_2O)_2\cdot H_2O$ 120

Figure 27. TGA and DTG Curve of $Cu(Bmpp\text{-}Ph)_2(H_2O)_2\cdot H_2O$ 121

Figure 28. TGA and DTG Curve of $Cu(Ampp\text{-}Ph)_2(H_2O)_2$ 121

Figure 29. Chart Showing the Scavenging Activity of Bmpp-Ph and its Metal Complexes 126

Figure 30. Chart Showing the Scavenging Activity of Ampp-Ph and its Metal Complexes 127

Figure 31. ^1H NMR Spectrum of Bmpp-Dh 130

Figure 32. ^1H NMR Spectrum of Ampp-Dh 131

Figure 33. ^{13}C NMR Spectrum of Bmpp-Dh 132

Figure 34. ^{13}C NMR Spectrum of Ampp-Dh 133

Figure 35. Mass-Spectrum of Bmpp-Dh 133

Figure 36. Mass-Spectrum of Ampp-Dh 134

Figure 37. Electronic Spectrum of $Mn(Bmpp\text{-}Dh)_2(H_2O)_2$ 136

Figure 38. Electronic Spectrum of $Mn(Ampp\text{-}Dh)_2(H_2O)_2\cdot H_2O$ 136

Figure 39. Electronic Spectrum of $Co(Bmpp\text{-}Dh)_2(H_2O)_2\cdot H_2O$ 137

Figure 40. Electronic Spectrum of $Co(Ampp\text{-}Dh)_2(H_2O)_2$ 137

Figure 41. Electronic Spectrum of $Ni(Bmpp\text{-}Dh)_2(H_2O)_2\cdot H_2O$ 138

Figure 42. Electronic Spectrum of $Ni(Ampp\text{-}Dh)_2(H_2O)_2$ 138

Figure 43. Electronic Spectrum of $Cu(Bmpp\text{-}Dh)_2(H_2O)_2\cdot 2H_2O$ 139

Figure 44. Electronic Spectrum of $Cu(Ampp\text{-}Dh)_2(H_2O)_2$ 139

Figure 45. Molecular crystal structure of $C_{23}H_{18}N_6O_5 \cdot C_2H_6O$ 141

Figure 46. Hydrogen Bonding in $C_{23}H_{18}N_6O_5 \cdot C_2H_6O$ 142

Figure 47. Packing Diagram of $C_{23}H_{18}N_6O_5 \cdot C_2H_6O$ 142

Figure 48. TGA and DTG curves of $Mn(Bmpp\text{-}Dh)_2(H_2O)_2$ 143

Figure 49. TGA and DTG Curves of $Mn(Ampp\text{-}Dh)_2(H_2O)_2 \cdot H_2O$ 144

Figure 50. TGA and DTG Curves of $Co(Bmpp\text{-}Dh)_2(H_2O)_2 \cdot H_2O$ 145

Figure 51. TGA and DTG Curves of $Co(Ampp\text{-}Dh)_2(H_2O)_2$ 145

Figure 52. TGA and DTG Curves of $Ni(Bmpp\text{-}Dh)_2(H_2O)_2 \cdot H_2O$ 146

Figure 53. TGA and DTG Curves of $Ni(Ampp\text{-}Dh)_2(H_2O)_2$ 147

Figure 54. TGA and DTG Curves of $Cu(Bmpp\text{-}Dh)_2(H_2O)_2 \cdot 2H_2O$ 148

Figure 55. TGA and DTG Curves of $Cu(Ampp\text{-}Dh)_2(H_2O)_2$ 148

Figure 56. Chart Showing the Scavenging Activity of Bmpp-Dh and its Metal Complexes 152

Figure 57. Chart Showing the Scavenging Activity of Ampp-Dh and its Metal Complexes 152

Figure 58. ^1H NMR Spectrum of Bmpp-Sn 156

Figure 59. ^1H NMR Spectrum of Ampp-Sn 157

Figure 60. ^{13}C NMR Spectrum of Bmpp-Sn 157

Figure 61. ^{13}C NMR Spectrum of Ampp-Sn 158

Figure 62. Mass Spectrum of Bmpp-Sn 159

Figure 63. Mass Spectrum of Ampp-Sn 159

Figure 64. Electronic Spectrum of $Mn(Bmpp\text{-}Sn)_2(H_2O)_2$ 161

Figure 65. Electronic Spectrum of $Mn(Ampp\text{-}Sn)_2(H_2O)_2 \cdot H_2O$ 161

Figure 66. Electronic Spectrum of $Co(Bmpp\text{-}Sn)_2(H_2O)_2 \cdot H_2O$ 162

Figure 67. Electronic Spectrum of $Co(Ampp\text{-}Sn)_2(H_2O)_2$ 162

Figure 68. Electronic Spectrum of $Ni(Bmpp\text{-}Sn)_2(H_2O)_2 \cdot H_2O$ 163

Figure 69. Electronic Spectrum of $Ni(Ampp\text{-}Sn)_2(H_2O)_2 \cdot H_2O$ 163

Figure 70. Electronic Spectrum of $Cu(Bmpp\text{-}Sn)_2(H_2O)_2$ 164

Figure 71. Electronic Spectrum of $Cu(Ampp\text{-}Sn)_2(H_2O)_2 \cdot H_2O$ 164

Figure 72. Molecular Crystal Structure of $Bmpp\text{-}Sn \cdot H_2O$ 166

Figure 73. Hydrogen Bonding in $Bmpp\text{-}Sn \cdot H_2O$ 167

Figure 74. Molecular Packing Diagram of $Bmpp\text{-}Sn \cdot H_2O$ 167

Figure 75. Molecular Crystal Structure of $Co(Bmpp)_2(DMF)_2$ 169

Figure 76. Molecular Packing Diagram of $Co(Bmpp)_2(DMF)_2$ 169

Figure 77. TGA and DTG Curve of $Mn(Bmpp\text{-}Sn)_2(H_2O)_2 \cdot H_2O$ 171

Figure 78. TGA and DTG Curve of $Mn(Ampp\text{-}Sn)_2(H_2O)_2 \cdot H_2O$ 171

Figure 79. TGA and DTG Curve of $Co(Bmpp\text{-}Sn)_2(H_2O)_2 \cdot H_2O$ 172

Figure 80. TGA and DTG Curve of $Co(Ampp\text{-}Sn)_2(H_2O)_2$ 172

Figure 81. TGA and DTG Curve of $Ni(Bmpp\text{-}Sn)_2(H_2O)_2 \cdot H_2O$ 173

Figure 82. TGA and DTG Curve of $Ni(Ampp\text{-}Sn)_2(H_2O)_2 \cdot H_2O$ 174

Figure 83. TGA and DTG Curve of $Cu(Bmpp\text{-}Sn)_2(H_2O)_2$ 175

Figure 84. TGA and DTG Curve of $Cu(Ampp\text{-}Sn)_2(H_2O)_2 \cdot H_2O$ 175

Figure 85. Chart Showing the Scavenging Activity of Bmpp-Sn and its Metal Complexes 180

Figure 86. Chart Showing the Scavenging Activity of Ampp-Sn and its Metal Complexes 180

List of Abbreviations

Ac	Acyl
Ampp-Dh	4-Acetyl-3-methyl-1-phenyl-2-pyrazolin-5-one dinitrophenyl-hydrazone
Ampp-Ph	4-Acetyl-3-methyl-1-phenyl-2-pyrazolin-5-one phenylhydra-zone
Ampp-Sn	4-Acetyl-3-methyl-1-phenyl-2-pyrazolin-5-one sulfanilamide
APCI	Atmospheric-pressure chemical ionization
AST	Antibacterial susceptibility testing
BM	Bohr magneton
Bmpp-Dh	4-Benzoyl-3-methyl-1-phenyl-2-pyrazolin-5-one dinitro-phenylhydrazone
Bmpp-Ph	4-Benzoyl-3-methyl-1-phenyl-2-pyrazolin-5-one phenylhydra-zone
Bmpp-Sn	4-Benzoyl-3-methyl-1-phenyl-2-pyrazolin-5-one sulfanilamide
Bu	Butyl
Cy	Cyclohexyl
DIP	Direct insertion probe
DMF	Dimethylformamide
DMSO	Dimethylsulfoxide
DPPH	1,1-diphenyl-2-picrylhydrazyl
DTG	Differential thermal analysis

ESBL	Extended–spectrum *beta–lactamases*
ESI	Electrospray ionization
Et	Ethyl
EUCAST	European Committee for Antimicrobial Susceptibility Testing
IR	Infrared
MALDI	Matrix-assisted laser desorption/ionization
MBC	Minimum bactericidal concentration
MDR	Multidrug resistance
Me	Methyl
MIC	Minimum inhibitory concentration
MRSA	Methicillin/oxacillin–resistant *Staphylococcus aureus*
Naphth	Naphthyl
NMR	Nuclear magnetic resornance
OLED	Organic light-emitting diode
Ph	Phenyl
ppm	Parts Per Million
Pr	Propyl
PRSP	Penicillin–resistant *Streptococcus pneumonia*
TGA	Thermogravimetric analysis
TLC	Thin layer chromatography
TMS	Trimethylsilane
Tol	Tolyl

UV-Vis	Ultraviolent Visible
VRE	Vancomycin–resistant *enterococci*

List of Journal Abbreviations

A	Analyst
AAC	Antimicrobial Agents and Chemotherapy
ACM	Anti-CorrosionMethods and Materials
ACS	Acta Chemical Scandinavica
ADD	Advanced Drug Delivery Reviews
AIC	Advances of Inorganic Chemistry
AJ	American Journal of Chemistry
AJB	African Journal of Biotechnology
AJP	American Journal of Clinica Pathology
AL	Analytical Letters
AOC	Applied Organometallic Chemistry
APP	Acta Polonica Pharmaceutica Drug Research
APR	Archives of Pharmaceutical Research
AS	Analytical Sciences
AX(A)	Acta Crystallographica Section A Foundations of Crystallography
AX(C)	Acta Crystallographica Section C Crystal Structure Communications
AX(E)	Acta Crystallographica Section E Crystal Structure Reports
BBR	Biochemicaland Biophysical Research Communications
BCA	Bioinorganic Chemistry and Applications

BCE	Bulletin of the Chemical Society of Ethiopia
BCH	Biochemistry
BCJ	Bulletin of the Chemical Society of Japan
BJM	Brazilian Journal of Microbiology
BKC	Bulletin of the Korean Chemical Society
BMB	Biochemistryand Molecular Biology Education
BPH	Biochemical Pharmacology
BSF	Bulletin de la Société Chimique de France
CAM	BMC Complementary andAlternative Medicine
CB	Chemische Berichte
CCL	Chinese Chemistry Letters
CCR	Coordination Chemistry Reviews
CHJ	Chinese Journal of Chemistry
CJS	Chinese Journal of Structural Chemistry
CMI	Clinical Microbiology and Infection
COC	Current Organic Chemistry
CPB	Chemical and Pharmaceutical Bulletin
CRS	Cancer Research
CRV	Chemical Reviews
CSR	Chemical Society Reviews
CUS	Current Science (India)
D	Dalton Transactions

DP	Dyes and Pigments
ECA	Electrochimica Acta
EJC	E-Journal of Chemistry
EJM	European Journal of Medicinal Chemistry
EJO	European Journal of Organic Chemistry
EQ	Eclética Química
EXP	Experimental Physiology
IC	Inorganic Chemistry
ICA	Inorganica Chimica Acta
ICC	Inorganic Chemistry Communications
IJC	Indian Journal of Chemistry
IJE	International Journal of Electrochemical Science
IJM	International Journal of Molecular Science
IJP	International Journal of Pharmacy and Pharmaceutical Science
IPH	International Journal of Pharmacology
IPS	International Journal of Physical Sciences
JA	Journal of the American Chemical Society
JAC	Journal of Antimicrobial Chemotherapy
JAF	Journal of Agricultural and Food Chemistry
JAX	Journal of Applied Crystallography
JBC	Journal of Brazilian Chemical Society
JCC	Journal of Coordination Chemistry

JCH	Journal of Chilean Chemical Society
JCHE	Journal of Chemistry
JCM	Journal of Clinical Microbiology
JCPR	Journal of Chemical Pharmaceutical Research
JCT	Journal of Chemotherapy
JCX	Journal of Chemical Crystallography
JEI	Journal of Enzyme Inhibition and Medicinal Chemistry
JEP	Journal of Ethnopharmacology
JIB	Journal of Inorganic Biochemistry
JIC	Journal of the Indian Chemical Society
JID	Journal of Infectious Diseases
JIM	Journal of Inorganic Medicinal Chemistry
JIN	Journal of the Indian Council of Chemists
JINC	Journal of Inorganic and Nuclear Chemistry
JIR	Journal of the Iranian Chemical Society
JME	Journal of Medicinal Chemistry
JMI	Journal of Microbiology and Infectious Diseases
JMS	Journal of Molecular Structure
JMS(T)	Journal of Molecular Structure Theochem
JOM	Journal of Organometallic Chemistry
JPA	Journal of Pure and Applied Sciences
JPC	Journal of Physical Chemistry

JPH	Journal of Pharmacy Research
JPR	Journal für praktische Chemie
JPP(A)	Journal of Photochemistry and Photobiology A: Chemistry
JRN	Journal of Radioanalytical and Nuclear Chemistry
JSC	Journal of Structural Chemistry
JSI	Journal of Scientific and Industrial Research
LAM	Letters in Applied Microbiology
MBD	Metal-Based Drugs
MI	Miscellaneous (books)
MIO	Memorias do Instituto Oswaldo Cruz
MOL	Molecules
MRR	Medicinal Research Reviews
NAT	Nature
NBT	Nature Biotechnology
NJC	New Journal of Chemistry
NJM	The New England Journal of Medicine
NRM	Nature Reviews MolecularCell Biology
OC	Organic Communications
PHC	Phytochemistry
PHE	Physical Education
PHR	Pharmacology Reviews

PIA	Proceedings of the Indian Academy of Sciences, Chemical Sciences
PIC	Progress in Inorganic Chemistry
PJP	Pranama – Journal of Physics
POL	Polyhedron
RJP	Research Journal of Pharmacutical, Biological, and Chemical Science
SA(A)	Spectrochimica Acta Part A: Molecular and Biomolecular Spectroscopy
SAB	South African Journal of Botany
SC	Sctructural Chemistry
SCI	Science
SRI	Synthesis and Reactivity in Inorganic, Metal-Organic and Nano-Metal Chemistry
T	Tetrahedron
TJB	Turkish Journal of Biology
TJC	Turkish Journal of Chemistry
TJP	Turkish Journal of Pharmaceutical Science
TMC	Transition Metal Chemistry

Research Output

Published Papers

O. G. Idemudia, A. P. Sadimenko, and E. C. Hosten, 4-{[2-(2,4-Dinitrophenyl)hydrazinylidene](phenyl)methyl}-5-methyl-2-phenyl-1H-pyrazol-3(2H)-one Ethanol Monosolvate, *Acta Crystallogr.*, **E68**, o3380 (2012).

O. G. **Idemudia** and E. C. Hosten, Bis(4-benzoyl-3-methyl-1-phenyl-1H-pyrazol-5-olato-κ^2O,O')bis(ethanol-κO)cobalt(II), *Acta Crystallogr*., **E68**, m1107 (2012).

O. G. **Idemudia,** A. P. Sadimenko, A. J. Afolayan, and E. C. Hosten, 3-Methyl-1-phenyl-4-[(phenyl)(2-phenylhydrazin-1-yl)methylidene]-1H-pyrazol-5(4H)-one, *Acta Crystallogr.*, **E68**, o1280 (2012).

Academic conference presentations

O. G. **Idemudia**, A. P. Sadimenko, and A. J. Afolayan, Potential Therapeutic Acylpyrazolone Heterocycles and Their Metal Complexes, *41st SACI Convention*, 1st–6th December 2013, River Park Conference Center, East London, South Africa. (Oral presentation)

O. G. **Idemudia**, A. P. Sadimenko, and A. J. Afolayan, New bioactive 4-benzoyl-3-methyl-1-phenyl pyrazolone-5-one phenylhydrazones and their metal complexes, *IUPAC 9th International Conference on Novel Materials and their Synthesis (NMS-VIII) & 23rd International Symposium on Fine Chemis-*

try and Functional Polymers (FCFP-XXIII), October 17th–22th, 2013, Fudan University, Shanghai, China (Oral presentation)

O. G. **Idemudia**, A. P. Sadimenko, and A. J. Afolayan, Potential Therapeutic Mn^{2+} and Ni^{2+} Complexes of New Acylpyrazolone Based Phenylhydrazone, *15th IUPAC International Conference and Symposium on Macromolecular Complexes MMC-15*, August 13th-16th, 2013 Greenville, South Carolina, USA (oral presentation).

O. G. **Idemudia**, A. P. Sadimenko, and A. J. Afolayan, Newly Synthesized Biologically Active Pyrazolone Based Dinitophenylhydrazone and its Cobalt(II) Complex as Potential Therapeutic Agents, *Gordons Research Conference and Seminars on Medicinal Chemistry 2013*, 03rd-09thAugust 2013, New England, New Hampshire, USA (poster presentation)

O. G. **Idemudia**, A. P. Sadimenko, and A. J. Afolayan, Bioactive Pyrazolone Based Dinitrophenylhydrazone and its Nickel Complex, *12th Annual UNESCO/IUPAC Workshop & Conference on Macromolecules and Materials*, 24th-28th March 2013, Stellenbosch, South Africa (poster presentation).

O. G. **Idemudia**, A. P. Sadimenko, and A. J. Afolayan, Synthesis of Biologically Active Heterocyclic Acypyrazolone Based Phenylhydrazone and its Co(II) Complex, *Third Annual South African Young Scientists' Conference ASSAf*, Brummeria, Pretoria, South Africa, 16th-18th October 2012 (oral and postal presentation).

Abstract

Some new acylpyrazolone Schiff bases have been synthesized from the condensation reaction of two acylpyrazolone diketone precursors with phenylhydrazine, 2,4-dinitrophenylhydrazine and sulfanilamide. They have been fully characterized by elemental analysis and spectroscopic techniques (IR, ^{1}H and ^{13}C NMR, and mass-spectra). The single crystal structure of the benzoyl derivative acylpyrazolone Schiff bases have been obtained and analyzed by X-ray crystallography technique. Solid state X-ray diffraction revealed a keto tautomer Schiff base in solid state.

Mn(II), Co(II), Ni(II) and Cu(II) complexes with the Schiff bases have been synthesized and characterized by elemental analysis, IR and UV-VIS spectroscopy, magnetic susceptibility measurements, and thermal studies (TGA and DTG). An octahedral geometry around the transition metal ion, consisting of two bidentate Schiff base ligands bonding through the azomethine nitrogen and ketonic oxygen have been proposed based on careful interpretation of available analytical and spectroscopic characterization results. Two water molecules as ligands complete the octahedral geometry in all cases. Using the *invitro* disc diffusion method for screening synthesized compounds against selected gram positive and gram negative bacterial at 40 mg/mL, and the DPPH free radical scavenging methods at 0.50, 0.25 and 0.13 mg/mL, the synthesized Schiff base and metal complexes showed varying biological activities. 4-benzoyl-3-methyl-1-phenyl-2-pyrazolin-5-one sul-

fanilamide showed more activity generally, exhibiting a broad spectrum activity against all selected bacterial in some cases. Mn(II), Co(II) and Ni(II) complexes of sulfanilamide Schiff base with the acetylpyrazolone derivative 4-acetyl-3-methyl-1-phenyl-2-pyrazolin-5-one sulfanilamide, exhibited a stronger and very good DPPH radical scavenging activity as good as ascorbic acid on comparing, but not with Cu(II). As such they could be important antitumour candidates.

1. Introduction

Heterocyclic compounds have been useful therapeutic agents and active pharmacological compounds, many of which have been in use clinically, for example **1**-**3**. Some are of natural origin (an example of this is the discovery of antibiotic penicillin), and they have been employed either alone or in co-ordination with metal ions as medicinal metal complexes (03MRR697).

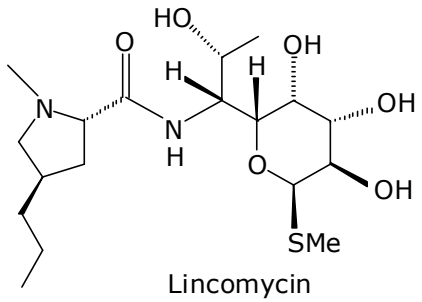

Lincomycin
1

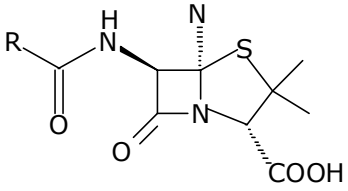

Peniclillin
2

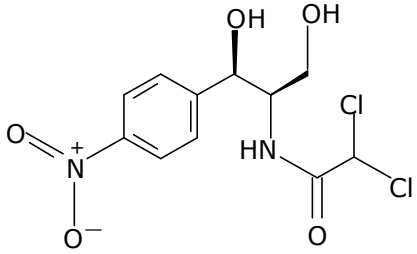

Chloramephenicol
3

Heterocycles play a vital role in the organic processes of all living systems required for life. The essential amino acids, proline, histidine, and tryptophan**4** are examples. Also the pyrimidine and purine bases, adenine**5** and guanine, just to mention but a few, are the major constituents of the generic material DNA and RNA. In addition, the hormones epinephrine, kinetine**6** and heteroauxin are heterocycles needed for the proper functioning of the living cells. Their applications in chemistry, both in fundamental and theoretical studies, can be attributed to their complexity of being able to form a variety of structurally novel compounds with a wide range of physical, chemical and biological properties, bringing about a broad spectrum of reactivity and stability.

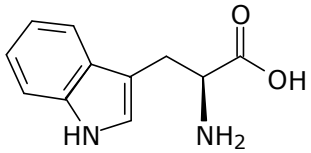

L-Tryptophan

4

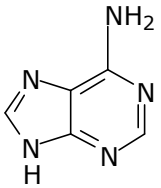

Adenine

5

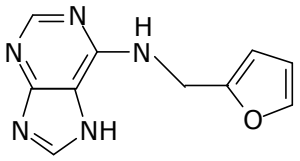

Kinetine

6

Studies on Schiff bases, products of the condensation of a carbonyl group with an amine, have been an active and steadily growing area of research. This has been ascribed to its versatile coordination properties, as well as its potential chemotherapeutic capabilities (01PIA257, 07CPB1070, 11IJP26). They are mostly nitrogen, oxygen, or sulfur donor ligands, particularly towards transition metal ions, and have amongst their flexible coordination characteristics, stability, potential application in the field of oxidation catalysis, metal ion extraction in electrochemistry as well as known biological attributes and as such have received a lot of research attention (03D748, 03MOL439, 04D2404, 07MOL1910). Their transition metal complexes have been receiving appreciable interest as they have been observed to possess improved biological activities (79JINC1229). Taking into consideration high affinity of Schiff bases towards transition metal ions and therapeutic activity of the relevant coordination compounds (91TMC276 and 03TMC229), we undertook synthesis, structural characterization, as well as the study of biological activity of heterocyclic pyrazolone-based Schiff bases and their transition metal complexes. The study seeks to address the ongoing problems of in-

creasing resistance of diseases pathogens to commonly administered drugs and their toxicity effects.

Previous work on pyrazolone Schiff bases highlighted herein, have revealed their interesting significant biological and pharmacological applications, their high reactivity and chelating properties with metal ions. In line with this motivation and bearing in mind the huge need for the design/synthesis of new molecules with novel characteristics as a possible replacement for disease-resistant drugs and taking advantage of the modification of molecules, resulting in an overall change in properties, this work is aimed at synthesizing new acylpyrazolone Schiff bases and their Mn(II), Co(II), Ni(II) and Cu(II) complexes that may be of therapeutic importance.

The specific objectives towards attaining this aim are;

- To synthesize acetyl and benzoyl derivative of acylpyrazolone.
- To synthesize the acylpyrazolone Schiff bases.
- To synthesize the Mn^{2+}, Co^{2+}, Ni^{2+} and Cu^{2+} complexes of the synthesized Schiff bases.
- To characterize the synthesized Schiff bases and their transition metal complexes.
- To evaluate the *in-vitro* antibacterial activities of the synthesized Schiff bases and their transition metal complexes.
- To evaluate the free radical antioxidant scavenging activities of the synthesized Schiff base and their transition metal complexes.

2. Review of Literature

2.1. Schiff Bases

Azomethine functional group is the common characteristic part of a group of organic compounds known as Schiff bases which have a general formula RR'C=NR" where R and R' represent hydrogen, an alkyl, an aryl, a cycloalkyl or heteroaryl, whereas R" could be an alkyl or an aryl group. They are referred to as anils when R" is an aryl. Schiff bases with aryl group bonded to the nitrogen or carbon of the C=N with effective conjugation, are generally more stable, and more readily synthesized. Those with alkyl substituent are relatively unstable, and they decompose or polymerize rapidly (87MI1). The electrophilic carbon atoms of aldehyde and ketone carbonyl groups serve as good target sites for the nucleophilic attack of amines. During Schiff base-formation, the carbonyl group C=O is replaced by a C=NR azomethine or imine group and can be structurally said to be a nitrogen analog of aldehydes and ketones (03CRV893). They are weak bases and in general stable in alkaline solutions. Hydrolysis of a Schiff base to yield the corresponding amine and an aldehyde occurs when in aqueous solutions. They occur through a reversible condensation reaction and generally proceed under acidic or basic condition as in eq. 1. The reaction mechanism for the formation of a Schiff base is a nueclophillic addition scheme, where the amine is the neuclophile. First, the amine reacts with the aldehyde or ketone to

form an unstable addition intermediate called carbinolamine, which successively loses water by way of an acid-catalyzed hydration (eq. 2).

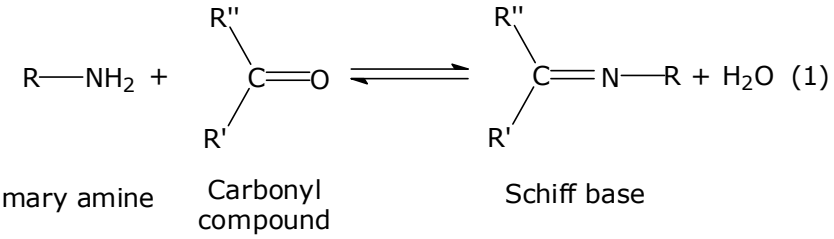

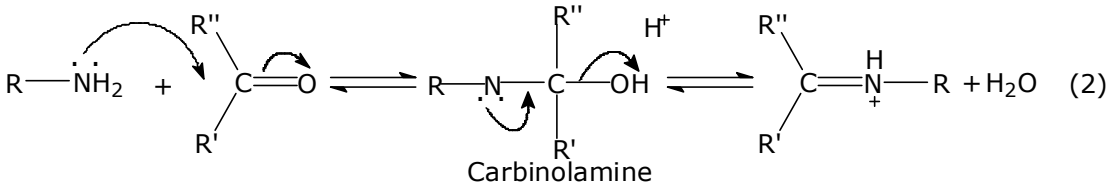

Aldehydes form Schiff bases more readily than ketones because the latter contain an extra electron donating carbon, making it more sterically hindered and less electrophilic (98MI1). Schiff bases are easily synthesized and form very stable complexes with transition metals, and hence they are widely used compounds. In chemistry, they are been employed as the components of dyes and pigments, carbon-nitrogen bonds intermediates in organic and inorganic synthesis, as catalysts and as polymer stabilizers (02T5357, 06DP71, 06POL1915, 07DP653). Furylglyoxal and *para*-toluidene based Schiff base that showed antibacterial activities towards *Staphylococcus aureus, Escherichia coli*, *Bacillus subtilis* and *Proteus vulgaris* was synthesized (87JIC685) from N-ethylethane-1,2-diamine and N-(2-hydroxyethyl)ethane-1,2-diamine as starting materials with 4-methoxysalicylaldehyde**7** and 3-

ethoxysalicylaldehyde**8**, respectively, for the synthesis of salicylaldehyde Schiff bases, which showed urease inhibitory activity (11ICC1636).

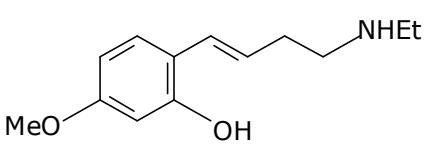

7

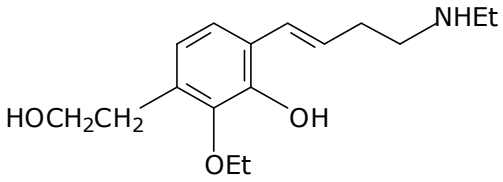

8

In the presence of anhydrous sodium acetate in ethanol, heterocyclic 4-thiazolidinone derivatives**9** have been synthesized *via* cyclisation by the reaction of enaminolactones with ethyl 2-bromo propionate, a regiospecific cyclisation mechanism involving one of the nitrogen atoms and sulfur site was proposed (10OC14).

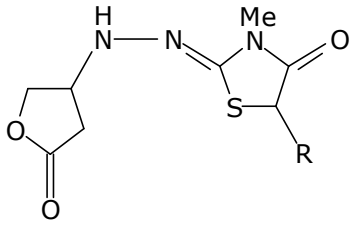

R = H, Me

9

The presence of a carbonyl region and hydroxyl group in some synthesized hydrazine Schiff bases with flavanoids have been reported to be the reason they possess activity against methicillin-resistant *Staphylococcus aureus* strain (10JCPR558). It was observed that the hydrazones having electron donor group at the *para*-position of the aryl group showed a higher antimicrobial activity than those at the *ortho*- or *meta*-positions amongst some synthesized quinoxaline derivatives (09APP169).

Ethyl 2-arylhydrazone-3-oxobutyrate**10** showed activity against *staphyloccocus aureus* amongst other derivatives which did not exhibit any activity (99EJM153).

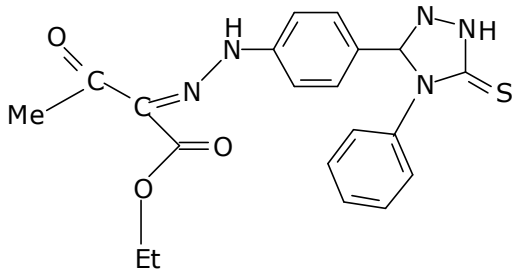

10

Schiff bases have shown metal corrosion inhibitory activity, some thiosemicarbazides exhibited corrosion inhibition properties for mild steel in H_2SO_4 studied at different temperature and varying concentrations (10IJM2473), and inhibitory properties have been attributed to their spatial arrangement and electronic structure (02ECA1365, 05JMST61, 06JPC8928, 08ECA8287). Other interesting Schiff bases that can inhibit corrosion processes have been reported in literature (81BCJ3157, 89BSF297, 08ACM60, 12IJE3222).

For a series of 2-acetylpyridine thiosemicarbazones**11**, the N, N-disubstituted Schiff bases have a higher activity than those which were N-monosubstituted (R^1 = H) (80AAC27). Furthermore their investigation gave an insight on how the nitrogen atom in the pyrimidine ring contributed to the biological activity of the synthesized test compound by way of replacing the

nitrogen atom in the ring with a carbon atom to form a derivative of the Schiff base which gave a reduced activity.

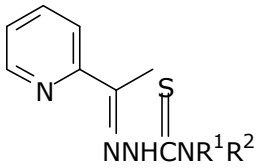

11

R^1 = H, R^2 = H, Me, Et, *n*-Pr, $CH_2CH{=}CH_2$, $CH_2C{\equiv}CH$, *n*-Bu, Ph, $PhCH_2$, o-Tol, p-Tol, Cy, Naphth, and others

$R^1 = R^2$ = Me, Et, *i*-Bu; R^1 = Me, R^2 = Cy

Much work has been done on thiosemicarbazones, their biological significance follows from numerous applications such as antimalarial (79JME855), antiviral (92JMC3288, 97TMC1), antineoplastic and antileukemic (56CRS167), as well as antibacterial activities, part of which have been mentioned earlier in this review chapter.

2.2 Transition Metal Complexes of Schiff Bases

Transition metals are capable of forming stable compounds with Schiff bases basically because they are good Lewis acids that can form a wide range of complexes with nitrogen, oxygen, and sulfur donor ligands. Most first row transition metal complexes are characterized by octahedral geometry and to a lesser extent tetrahedral. Distorted geometries may also be found, for example a d^9 Cu(II) complex. Schiff bases can form stable complexes with most transition metal ions in their various oxidation states. Perhaps, their huge interest in coordination chemistry is based on their easy synthesis and remarkable applications. They have been usually prepared by direct interaction of components. Some of the features of preparative methods have been outlined in a review on complexes of metal–Salen Schiff base

(04CSR410). Properties of the Schiff base metal complexes depend on the nature of a ligand and that of a metal ion. A particular Schiff base exhibits a certain electronic environment around a metal ion which determines the general behavior of a metal complex. Hence, their huge interest in bioinorganic chemistry. More Schiff base metal complexes of salicylaldehyde have been synthesized and thouroughly studied (66PIC83). The structures of N-substituted Schiff bases of salicylaldimine and their Co^{3+} and Cu^{2+} complexes were proposed by way of spectroscopic analysis, magnetic behavior, and single crystal X-ray analysis (98IJC(A)1010). Zinc and beryllium complexes of Schiff bases derived from calixarene cyclic oligomer exhibited blue luminescence, making them good light emission and charge transporter in organic light emitting diodes (OLEDs) (03CCL263). Some first row transition metal complexes of newly synthesized chelating (1-formylferrocene)-3, 5-dibenzyloxybenzoyl hydrazone exhibited antibacterial activity against *Esclerichia coli* (07SRI263). Tetradentate mononuclear $Cu^{2+}$and Zn^{2+}complexes of 2-((2-(2-hydroxyethylamino)ethylimino)methyl)-4-nitrophenol, **12**-**14**, and those of some Schiff bases that showed positive activity to urease inhibition is reported (08TMC1013, 10EJM3196, 10ICC996).

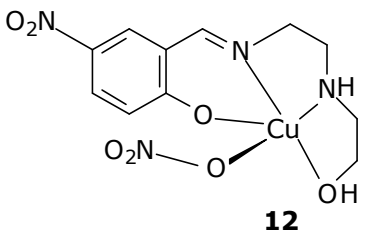

12

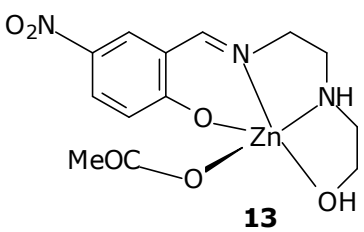

13

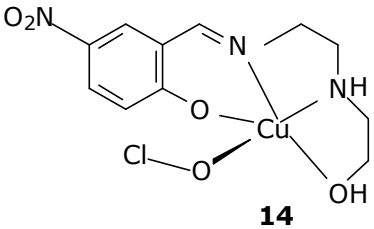

14

Vanadium crystal structures of oxovanadium(V) complexes, **15**, that also inhibited nickel-containing metalloenzyme (urease) causing the formation of unwanted excess of ammonia and carbamate, which affect the pH level of living systems negatively, have been investigated and it was concluded based on structure–activity relationship that Schiff base ligands with shorter terminal groups form stronger urease inhibiting oxovanadium (V) complexes (11ICC636).

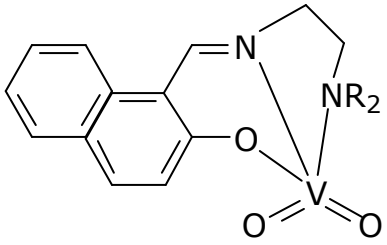

R = Me, Et

15

There are known insulin-enhancing activities of some Schiff base metal complexes of vanadium (10JEI599, 10JIB851).

2.3. Pyrazolone Schiff Bases and Metal Complexes

Pyrazolone is a ketone derivative of a five-membered ring heterocyclic pyrazole. Studies on pyrazolone compounds have been on since 1883 when Knorr synthesized its first derivative (83CB546, 12AJ52). By reacting phenyl hydrazine with ethylacetoacetate he synthesized a novel 1-phenyl-3-methyl-5-pyrazolone. Their tautomerism and ability to exist either in enol or keto form gives them the potential to form different types of interesting coordination compounds (07SC909, 10JPH2856). Acylpyrazolones are diketone de-

rivatives of pyrazolone substituted at the position 4, hence mostly called 4-acylpyrazolones. A suitable method for acylpyrazolone synthesis was reported (59ACS1668) after it was first discovered in the nineteenth century (97JPR145). They have been employed alone, as Schiff bases or in the form of their metal complexes in the field of analytical chemistry (04BKC1121, 07ICA1599), as useful metal extractants and chelating reagents in the spectroscopic determination of metals in trace amounts (09JIR345, 04JOM2192), because of their versatile coordination properties (03MI1).

Pyrazolones have become a more important class of heterocycles due to their significant applications in pharmacological and biological activities (08IJC(B)1555, 96JME3920, 09EJM3480, 09IPH220), although their prototypes antipyrines have been synthesized and used as clinical drugs over two decades ago. O-((3-Methyl-5-oxo-pyrazolin-1-yl)acetyl)salicylamide as a direct precursor to the Schiff bases reveals anti-inflammatory and analgesic activities (01APR171).

4-Acetyl-5-methyl-2-phenyl-2, 4-dihydropyrazol-3-one and alkyl amines form Schiff bases existing practically exclusively in the enol-imine form **16** in a solution and in a solid state (09JSC1159). Forms imine-one, **17** and **18**, as well as amine-one **19**, are not revealed in any ways. Stabilizing factor for **16** is hydrogen bonding between amine hydrogen and the pyrazolone carbonyl oxygen. In contrast, for 1-phenyl-3-methyl-4-aminomethylene pyrazolones the tautomer similar to **19** and displayed as **20** (X = S, Se; R = Me, Ph; R^1

= H, Me, Et, *i*-Pr, *t*-Bu, Ph) is stabilized due to the intramolecular hydrogen bond (01JMS15).

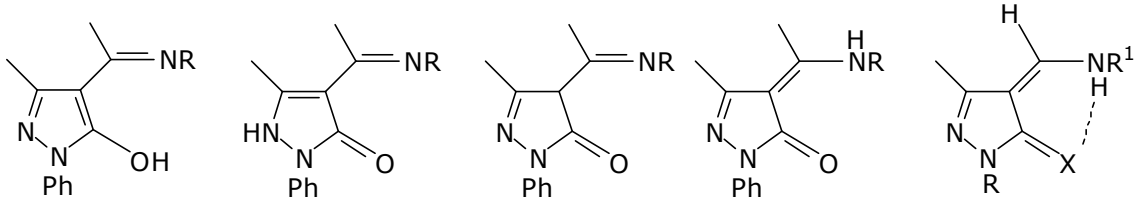

16 **17** **18** **19** **20**

Schiff bases derived from 3-methyl-1-(4'-methylphenyl)-2-pyrazoline-5-one and aromatic amines can exist in three tautomeric forms: keto-imine **21**, imine-enol **22**, and keto-amine **23**, the ketoamine form **23** being predominant in the solid state (04POL2465), which follows from the rigorous structural proof. In **21**-**23**, $R^1 = R^2 = R^3 = H$; R^1 =Me, Cl, $R^2 = R^3 = H$; $R^1 = H$, R^2 = Me, Cl, $R^3 = H$; $R^1 = R^2 = H$, R^3 = Me, Cl. All the ligands form the distorted octahedral geometry **24**, on reaction with $VOSO_4 \cdot 5H_2O$ (07POL1677) as obtained from spectral data. Their mononuclear copper(II) complexes **25** prepared using copper(II) nitrate have a distorted octahedral geometry around the copper(II) ion, and are NO coordinated. Conclusions on the complexes proposed geometry follow basically from the spectral but not structural data only.

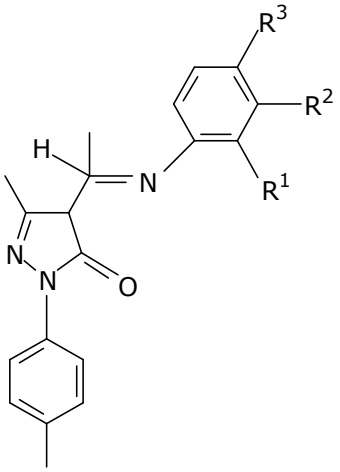

21

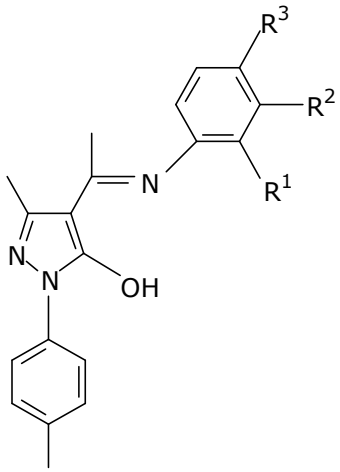

22

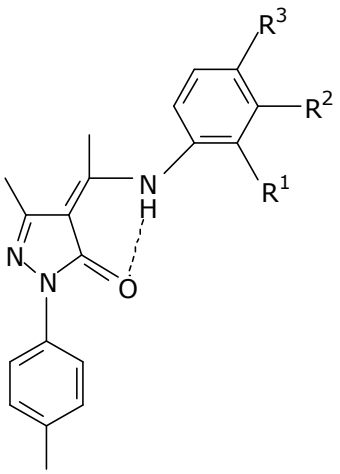

23

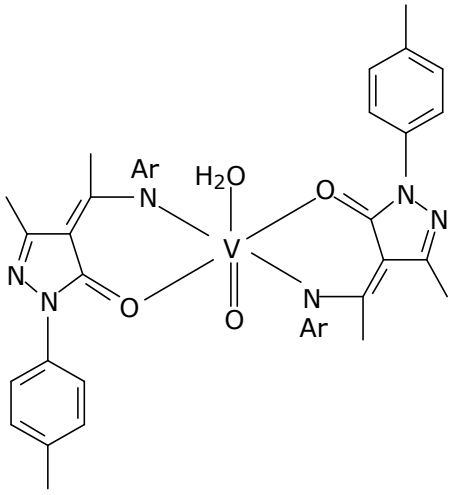

24

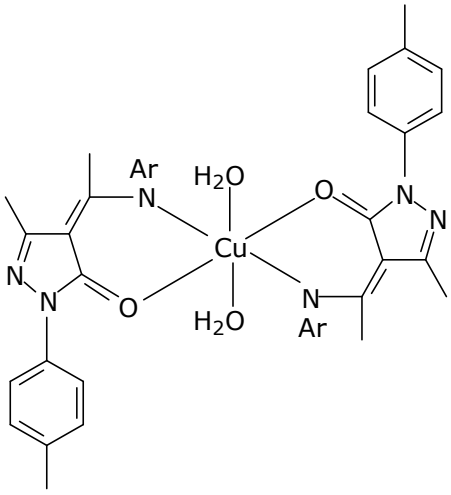

25

The ligand prepared by condensation of 1-phenyl-3-methyl-4-benzoyl-5-pyrazolone with *p*-aminoacetophenone gives neutral copper(II) complex **26** with a distorted trigonal bipyramidal coordination unit (03AX(E)m128).

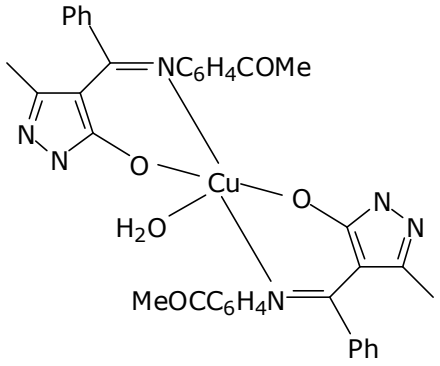

26

N-(3’-Methyl-1’-phenyl-4’-valerylidene-2’-pyrazolin-5’-one)sulfadiazine, N-(3’-methyl-1’-phenyl-4’-valerylidene-2’-pyrazolin-5’-one)sulfaguanidine, N-(3’-methyl-1’-phenyl-4’-valerylidene-2’-pyrazolin-5’-one)-sulfanilamide, and N’(-3’-methyl-1’-phenyl-4’-valerylidene-2’-pyrazolin-5’-one) sulfameth-oxazole with $VOSO_4 \cdot 5H_2O$ form square-pyramidal bis-chelates **27** as judged from spectral measurements, (06JMS24).

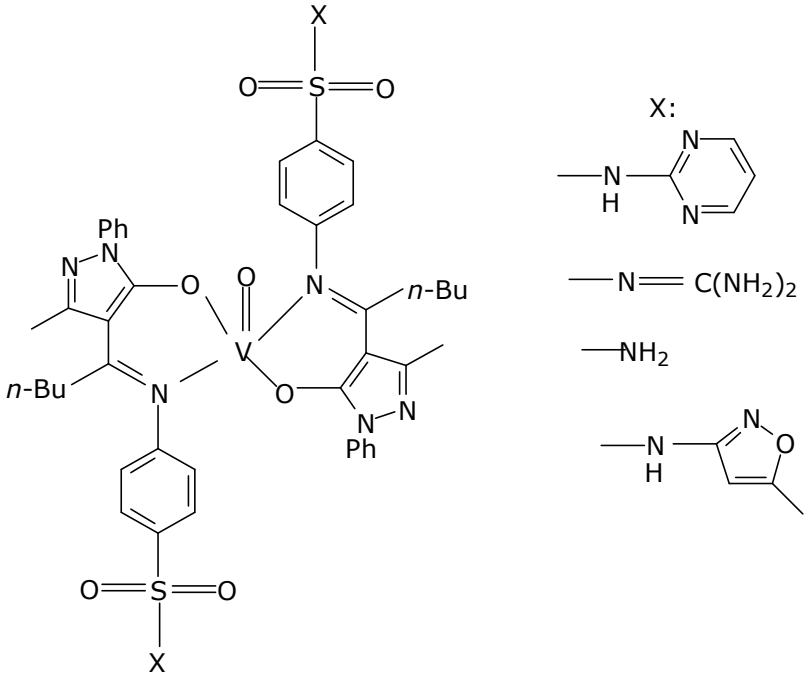

27

Condensation of acyl pyrazolones with 2-amino phenol gives rise to a series of Schiff bases **28** (R^1 = Me, Ph, R^2 = R^3 = H, R^2 = Me, R^3 = H; R^1 = Me, R^2 = H, R^3 = Cl) (10JPA68). With copper acetate, ligands form dimeric square-planar dinuclear complex **29**, according to spectral data only.

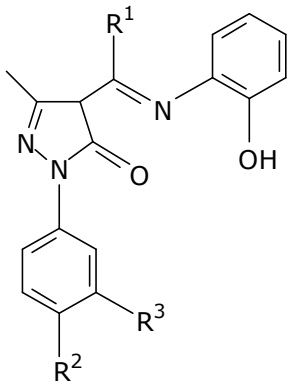

28

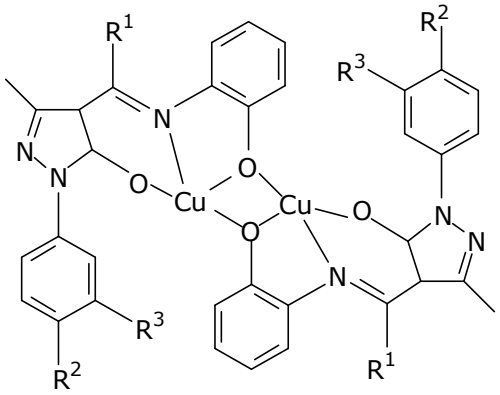

29

1-(*n*-Hexyl)-3-methyl-4-[1-phenylaminopropylidene]-2-pyrazolin-5-one with $Cu(CH_3COO)_2 \cdot H_2O$ gives bis-chelate **30** (08JCH1689).

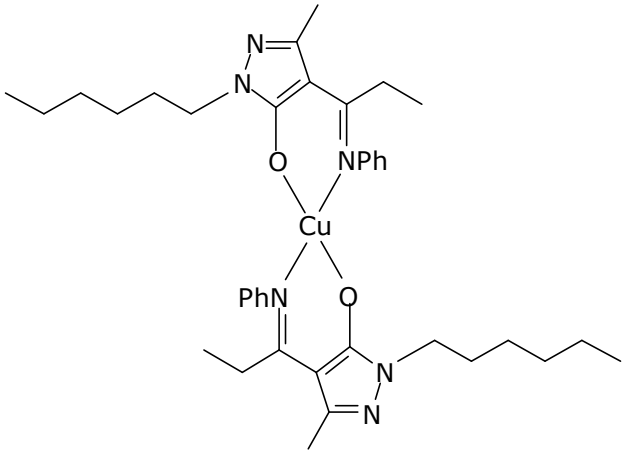

30

Phenylglyoxal-4-iminoantipyrine **31** and 4-N-(*m*-phenoxybenzylidene)-4-iminoantipyrine **32** form a number of metal complexes, for which ONO-coordination sites is postulated for the chelates of **31** and NO-coordination

sites for the chelates of **32** with manganese(II), cobalt(II), nickel(II), chromium(III), and iron(III) (03JIN61) on the basis of microanalysis and spectral data only. The products possess notable antifungal activity.

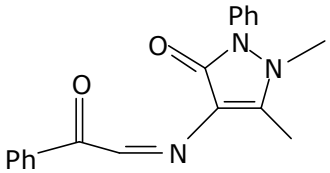

31

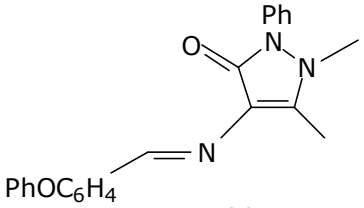

32

N,N'-Bis(1-(*n*-hexyl)-3-methyl-5-oxo-2-pyrazolin-4-ylethyliden-1-yl) ethylenediamine, N,N'-Bis(1-(*n*-hexyl)-3-methyl-5-oxo-2-pyrazolin-4-ylethyliden-1-yl)-1,2-diaminopropane, and N,N'-bis(1-(*n*-hexyl)-3-methyl-5-oxo-2-pyrazolin-4-ylpropyliden-1-yl]ethylenediamine (04AX(C)o705, 05JBC179) with $Mn(CH_3COO)_3 \cdot CH_3OH$ and then lithium chloride give manganese(III) chloro **33** (R = Me, Et, Y = $(CH_2)_2$; R = Me, Y = CH_2CHMe) (05NJC283). X-ray structural proof is available. Oxidation of the products using $NH_4OH \cdot MeOH$ and then NaOCl gives manganese(V) nitride **34** with the same set of R and Y. These products are promising agents in the nitrogen transfer reactions.

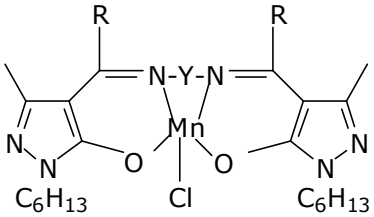

33

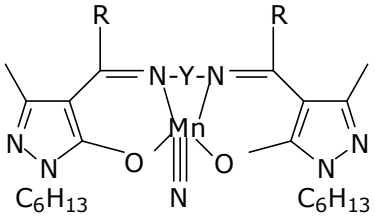

34

Bis-ketimino derivatives of 4-acetyl-3-methyl-1-phenyl-2-pyrazolin-5-one and 4-acetyl-3-methyl-1-(3'-chlorophenyl)-2-pyrazolin-5-one **35** (R = Ph, 3-ClC_6H_4; X = *o*-C_6H_4, *m*-C_6H_4, *p*-C_6H_4, CH_2-CH_2) may exist not only in the tautomeric form **35**, but also **36** or **37** (04SRI697). Spectral and magnetic studies (no X-ray structures) suggest that octahedral mononuclear chelates **38** based on **37** are formed, although for *o*- and *m*-phenylene derivatives dimeric **39** is not excluded. Schiff bases prepared by the condensation of 4-butyryl-3-methyl-1-phenyl-2-pyrazolin-5-one with *o*-, *m*-, *p*-phenylenediamine, benzidine, and ethylenediamine form nickel(II) and cobalt(II) chelates similar to **38** and **39** when reacted with nitrate salt of these metals (09JCC2388).

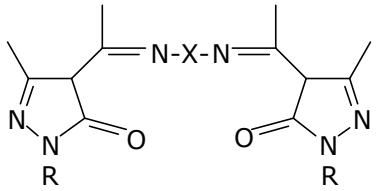

35

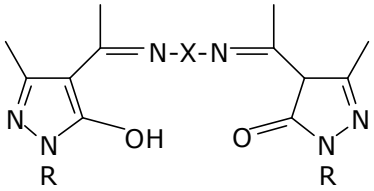

36

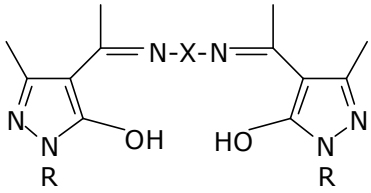

37

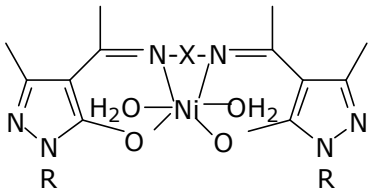

38

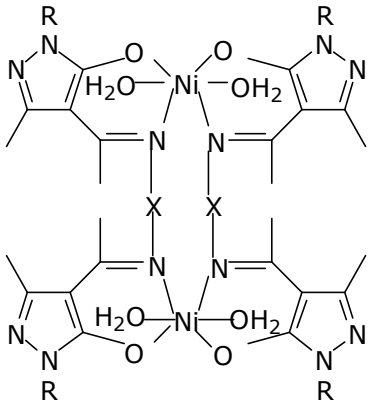

39

The Schiff base derived from 4-aminoantipyrine, 3-hydroxy-4-nitrobenzaldehyde and acetylacetone with copper(II), nickel(II), zinc(II) chlorides, and vanadyl(IV) sulfate forms square-planar (metal ions) and square-pyramidal (vanadyl) chelates **40** and **41** with promising antimicrobial properties (09JIC738).

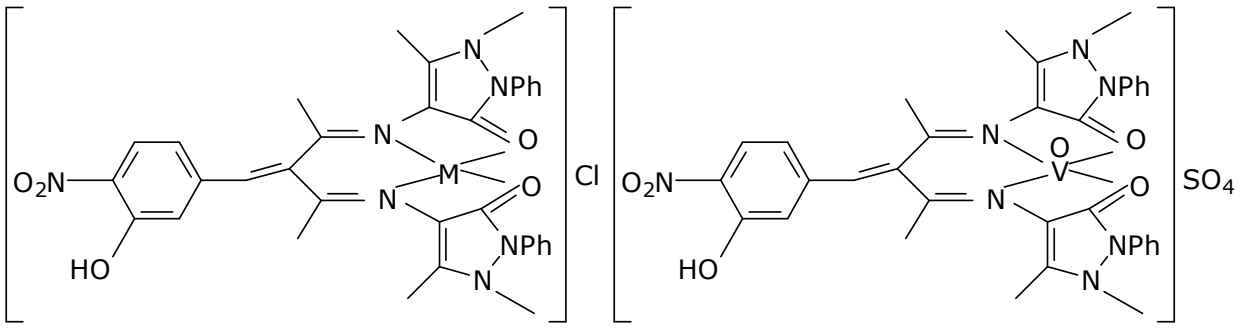

40 **41**

N,N'-Bis((1-phenyl-3-methyl-5-oxo-4-pyrazolinyl)-α-furylmethylidyne)-1,2-propylenediimine and N,N'-bis[(1-phenyl-3-methyl-5-oxo-4-pyrazolinyl)-α-furylmethylidyne)-1,3-propylenediimine with $UO_2(NO_3)_2 \cdot 6H_2O$ give neutral

42 and **43** and with $Th(NO_3)_4 \cdot 4H_2O$ give cationic **44** and **45** (03JRN693). Structural elucidation is based on spectral results.

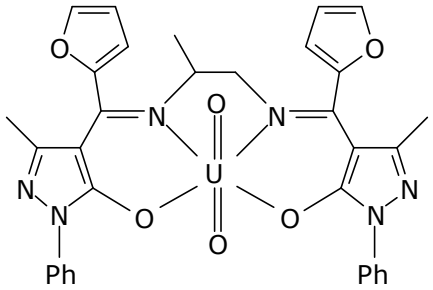

42

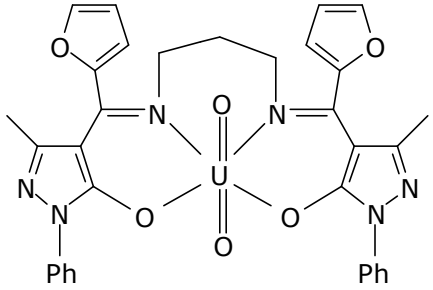

43

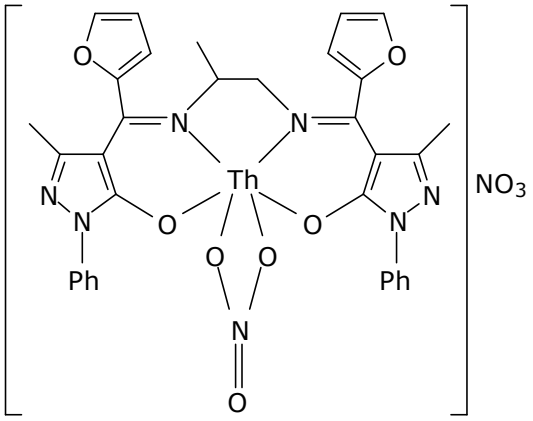

44

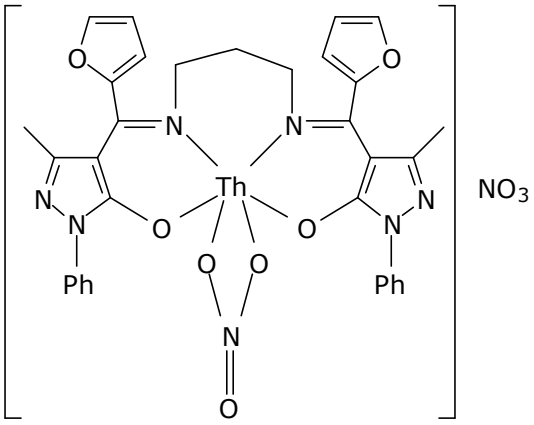

45

Oximes derived from 4-acylpyrazolones **46**-**53** are characterized by a variety of both tautomers and E/Z-diastereoisomers at the C=N double bond and were stabilized by intramolecular hydrogen bonds (03EJO1209). For 4-benzoyl-5-methyl-2-phenyl-3H-pyrazol-3-one and its methyl derivatives they are present in enamino pyrazolone form **52**, according to rigorous structural proof, theoretical computations, and chemical evidence, in the solid state and in a solution (03EJO1209).

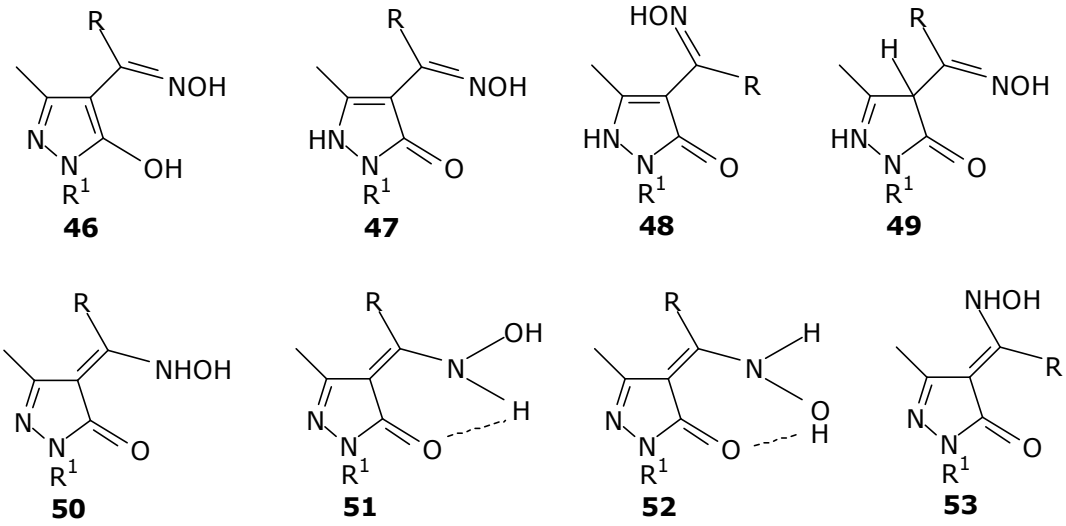

1,3-Diphenyl-4-(salicylidenehydrazone)-phenylethylenepyrazolone-5 (H_2L) with sodium hydroxide in methanol and $Cu(MeCOO)_2{\cdot}H_2O$ gives $[Cu_2L_2]$ **54** (04ICC1306). The distorted square-planar structure was characterized by the NNOO-coordination unit, and enol tautomeric form of the pyrazolones Schiff base derivative. Under similar synthetic conditions, zinc acetate provides $[Zn_4L_4]$ **55**. Here, tetradenticity of the ligand is preserved. However, each phenolic oxygen atom in addition serves as a bridge connecting two zinc sites, and coordination number of each zinc site is five. In contrast, N-(1,3-Diphenyl-4-benzal-5-pyrazolone)-salicylidene hydrazone (H_2L) forms the mononuclear complex $Zn(HL)_2{\cdot}2CH_3OH$ **56** where phenolic oxygen atoms are not involved in the octahedral coordination unit (08JCX837).

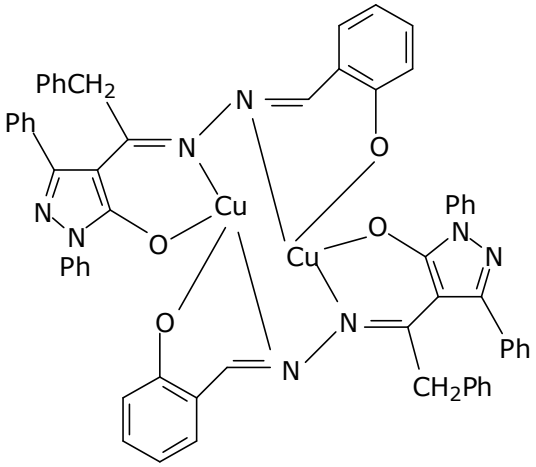
PhCH2
Ph
N
N
O
Cu
N
N
Ph
O
Cu
O
Ph
N
N
O
N
Ph
N
CH2Ph

54

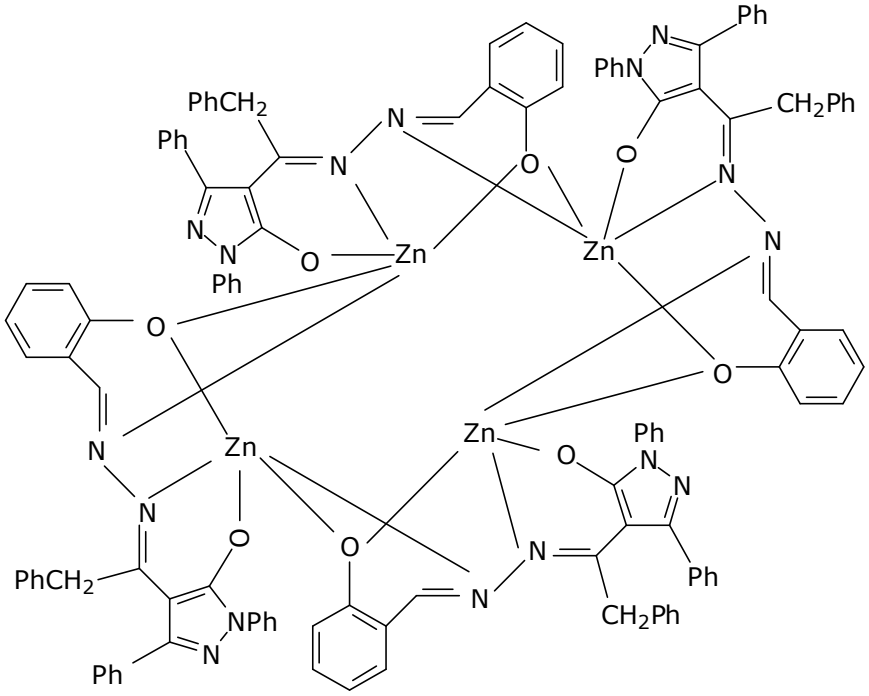
Ph
N
PhN
CH2Ph
PhCH2
Ph
N
N
O
O
N
N
N
Ph
O
Zn
Zn
N
O
O
N
Zn
Zn
Ph
N
O
N
N
PhCH2
O
O
N
Ph
NPh
N
CH2Ph
Ph

55

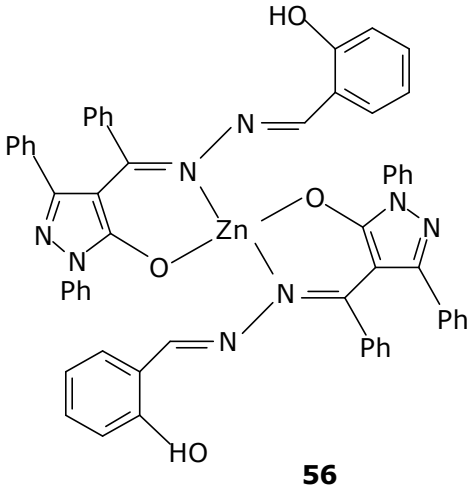

56

N-(α-(1-Phenyl-3-methyl-5-pyrazolone-4-ylidene)benzyl)-*N'*-3,4,5-trimethoxybenzoylhydrazine is characterized by keto-enol tautomerism **57⇆58** (05ASx289). The inter or intramolecular N–H···O hydrogen bonds, together with π–π stacking interactions make structure **58** more favorable. Similarly, N-(1-phenyl-3-methyl-4-benzalpyrazolone-5)-salicylidene hydrazine contains two kinds of tautomers: the enol form predominating in the solid state (02JCX255). Isomerization of the enol and keto forms is governed by the intramolecular proton transfer.

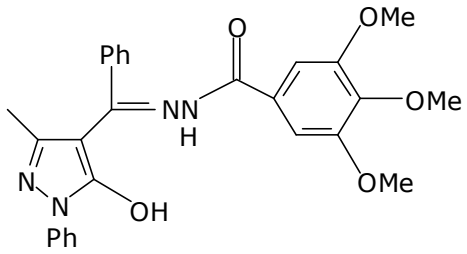

57

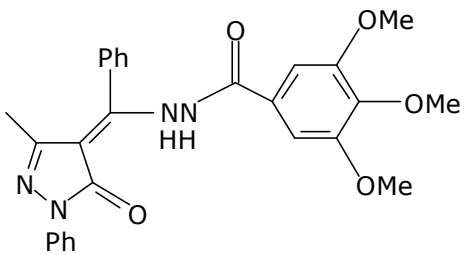

58

Photochromism of 1-phenyl-3-methyl-4-benzyl-5-one pyrazole S-methyl thiosemicarbazone is due to the photoisomerization from the enol **59** to the keto-tautomer **60** by the route of an intermolecular proton transfer

(03JMS221). 1-Phenyl-3-methyl-4-benzal-5-pyrazolone 4-ethylthio-semicarbazone in the process of photocolouration also transforms from the enol form **61** by the route of two proton transfers: from N–H to the S atom to form intermediate **62** and from hydroxyl group to the nitrogen atom in thiosemicarbazone moiety under UV-irradiation to yield keto form **63** (04JMS217). 1-Phenyl-3-methyl-4-benzoylpyrazol-5-one thiosemicarbazone and 1-phenyl-3-methyl-4-benzoylpyrazol-5-one *S*-methylthio-semicarbazone exhibited photochromic properties (00JPP(A)23). The photocolouration involves an intermolecular proton transfer from O-hydroxyl group to the nitrogen atom of adjoining molecular pyrazolone ring. With $Co(OAc)_2{\cdot}4H_2O$, 1-phenyl-3-methyl-4-benzyl-5-one pyrazole S-methyl thiosemicarbazone (HL) gives $CoL_2{\cdot}2H_2O$ of octahedral geometry and ONS-coordination mode **64** (02JCX505). The Schiff base loses a proton from the tautomeric thiol form of the type **62** and acts as a singly charged tridentate ligand.

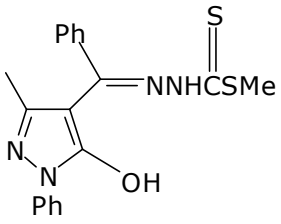

59

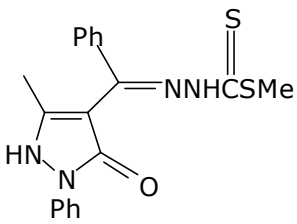

60

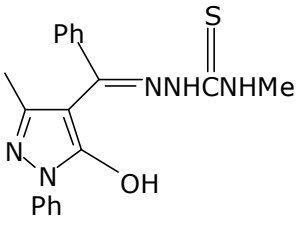

61

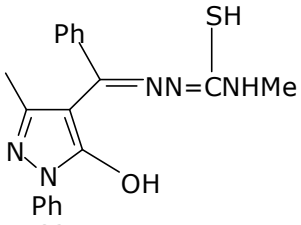

62

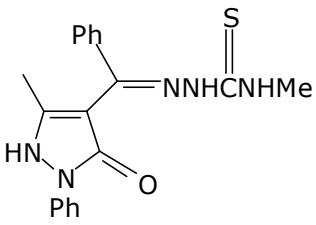

63

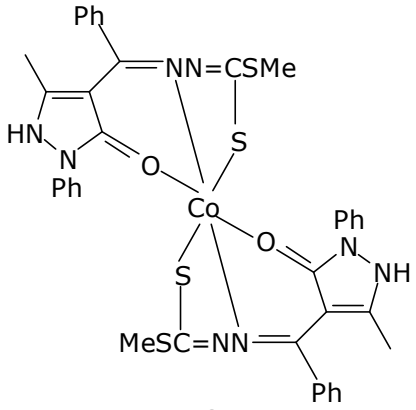

64

4-(*p*-Bromo-α-methylaminothiocarbonyl hydrazonobenzal)-2,5-dihydro -3-methyl-5-oxo-1-phenyl pyrazole, remarkable for its photochromism, may exist as tautomers **65**-**68** (03JPP(A)117, 06CHJ569). Transformation of tautomers from **65** through the stage of **66** to **67** occurs in the process of photocolouration reaction and involves intra- and intermolecular proton transfers. 1-Phenyl-3-methyl-4-(salicylaldehyde hydrazone)-propenylidene-5-pyrazolone, according to the structural data, exists mainly exists mainly in enamino pyrazolone form **69** but not in a more common NH form **68** (05JCX497).

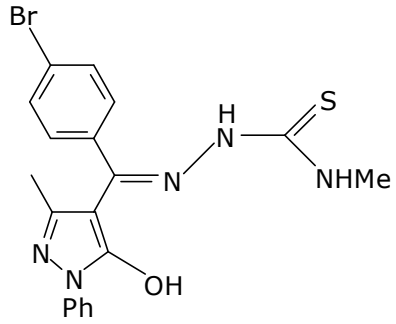

65

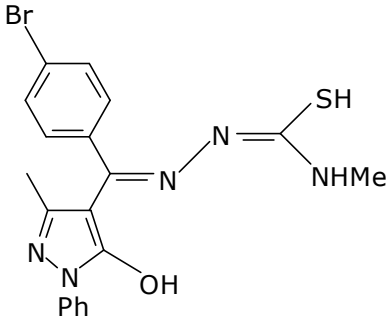

66

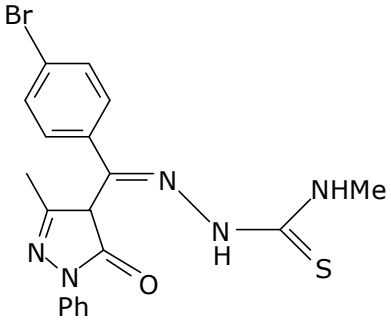

67

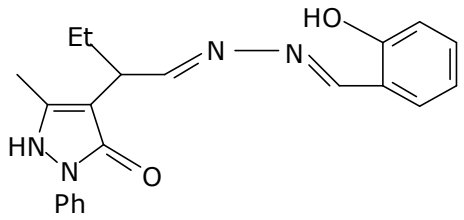

68

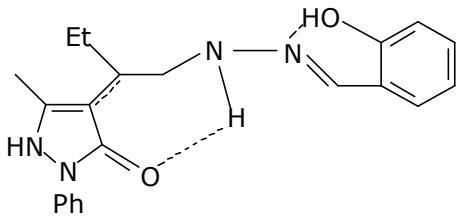

69

1-Phenyl-3-methyl-4-(4'-methylbenzal)-pyrazolone-5 thiosemicarbazone prepared as **70** under UV-irradiation transforms into the keto-form **71** (solid-state photochromism). In solution this form is largely presented as the zwitterionic form **72**, which in acidic medium is converted to species **73**, the process of mutual transformation **72⇆73** being reversible in acidic/basic medium (05JPP(A)243).

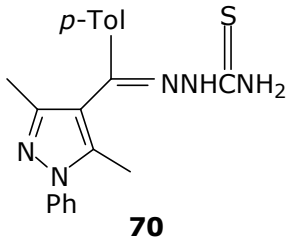

70

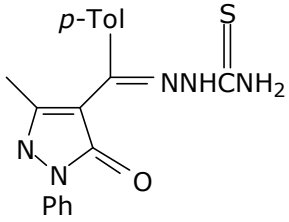

71

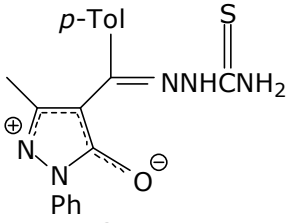

72

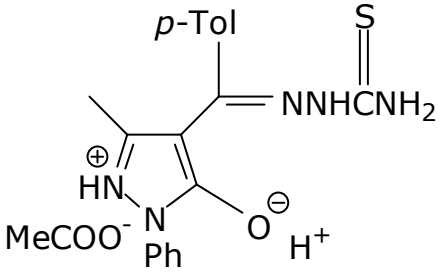

73

2.4. Transition Metal Ions under Investigation

Mn^{2+} is the most important oxidation state of manganese complexes due to its stability and resistance to oxidation. A four-coordinated Mn^{2+} complex of either a tetrahedral or square-planar geometry and a six-coordinated oc-

tahedral configuration are common. Based on Laporte selection rule, four spin-forbidden bands usually of very low intensity with an ε_{max} value being approximately 0.01, typical of manganese(II) complexes, are observed at around 18800 cm^{-1}, 23000 cm^{-1}, 24900 cm^{-1}, and 25100 cm^{-1} in the visible region of their electronic spectra, corresponding to $^6A_{1g}\rightarrow{}^4T_{1g}$, $^6A_{1g}\rightarrow{}^4T_{2g}$, $^6A_{1g}\rightarrow{}^4E_g$ and $^6A_{1g}\rightarrow{}^4A_{1g}$ transitions, respectively. They also may exhibit $^6A_{1g}\rightarrow{}^4E_g(D)$, $^6A_{1g}\rightarrow{}^4T_{1g}(P)$, $^6A_{1g}\rightarrow{}^4A_{2g}(F)$, $^6A_{1g}\rightarrow{}^4T_{1g}(F)$, and $^6A_{1g}\rightarrow{}^4T2g(F)$ transitions (94MI1). Studies on the reactivity of manganese complexes have increased because of the importance of manganese ion sites in biological systems (89AIC197, 90PIC97, 09JSIR181). Manganese ions are useful components in the metabolism of manganese peroxidase (95BCH7773), superoxide dismutase (91JA4069), and manganese dioxygenase (96BCH160). Complexes of manganese with Schiff bases have shown good activity in biocatalysis (10JPH2856).

Cobalt(II) complexes are the most important group of transition metal complexes with a d^7 configuration. They mostly exist in an octahedral or tetrahedral geometry. Octahedral cobalt(II) species exhibit three transitions $v_1(^4T_{2g}\rightarrow{}^4T_{1g})$, $v_2(^4A_{2g}\rightarrow{}^4T_{1g})$, and $v_3(^4T_{1g}(p)\rightarrow{}^4T_{1g})$. The $v_1(^4T_2\rightarrow{}^4A_2)$, $v_2(^4T_1\rightarrow{}^4A_2)$, and $v_3(^4T_1(p)\rightarrow{}^4A_2)$ transitions are peculiar for tetrahedral Co(II), all three transitions however are equal to 10 Dq and those for the six-coordinated situation are not exactly 10 Dq. This in turn makes it possible for the transitions to be observed easily in the four-coordinate species

spectra rather than in the six-coordinate spectra. The $v_2(^4A_{2g}\rightarrow{}^4T_{1g})$ transition is usually observed as a weak band because the energy difference v_2 - v_1 is exactly equal to 10 Dq (68MI1). Cobalt complexes in different coordination numbers and geometry have generally been useful in biological systems, as potential antimicrobial agents amongst others (04BCA193, 13JCH1).

Ni(II) commonly forms four-coordinate square planar complexes, as well as spin-free d^8 octahedral complexes. Their electronic spectra usually have three bands in the visible region due to d-d transitions. These transitions are assigned as $^3A_{2g}\rightarrow{}^3T_{1g}(p)$ (υ3), $^3A_{2g}\rightarrow{}^3T_{1g}(F)$ (υ2) and $^3A_{2g}\rightarrow{}^3T_{1g}(F)$ (υ1) (68MI1).

Copper complexes mostly exist in its +2 oxidation state. The d^9 Cu^{2+} is characterized by a high degree of distortions bringing about unequal bond lengths and inter-bond angles, hence their electronic spectra transitions cannot be assigned for certain to justify the structure. The +1 and +2 oxidation states are common and more stable than +3, which is uncommon. Electronic spectrum of an octahedral copper(II) complex has an absorption band which is due to $^2Eg\rightarrow{}^2T_{2g}$ or $^2T_2\rightarrow{}^2E$ transitions. The roles of copper *in-vivo* have received a lot of attention. Cu(III) compounds although uncommon have played a role in some biological processes. They generally form low-spin diamagnetic complexes.

2.5 Antibacterial activity

Antibacterial susceptibility testing (AST) has been employed for the determination of the efficacy of potential antimicrobials (ligands and metal complexes) against preselected bacterial isolates. Furthermore the MIC (minimum inhibitory concentration) and MBC (minimum bactericidal concentration) may be used to differentiate the kind of activity and the specific amount of an antibacterial agent that is responsible for the specific activity. The methods of diffusion assay (disc and agar well diffusion methods), dilution assay (agar dilution and broth–dilution methods), and bioautography assay have been used to study the antimicrobial activities of potential therapeutic compounds. The differences in these methods are in varying inoculum concentrations, pH of the medium, and components of the medium (75AAC15). Many factors have been found to influence results from these methods, making standardization technique difficult. Also, standardized methods are often more likely to be reproducible experimentally than unstandardized methods as this may affect the outcome of activity screening and these methods may significantly influence inter- and intralaboratory reproducibility (03CMI1). These factors include culture medium composition, microorganisms, extraction method in the case of extracts from natural products, pH and solubility of the test sample in the culture medium (88JEP127).

The agar diffusion assay uses either a disc, a well, or a cylinder as reservoirs for a test substance, which is grounded on the lead where the reservoir containing an antimicrobial sample is brought into contact with an inoculated medium (88JEP127).The diffusion of the test sample solution into the agar is attained on reaching equilibrium. Filter paper cut into the circular disc is prepared by way of sterilizing in a dry oven at 120^{o}C for one hour and is used as the test sample carrier in the disc diffusion method, while agar well is bored on the solidified agar medium in the case of agar diffusion technique. The test sample solution diffuses into the solidified agar medium and if the inoculated organisms show no growth in the area around the disc or agar, it means that the test sample inhibits the growth and hence referred to as positively active against the selected microbial isolate. This area of no visible growth is known as the zone of inhibition. Also, certain conditions are employed during screening process like the nutrient agar, the amount of organism, concentration of the antimicrobial agent in solution, and incubation conditions, such as time, temperature, and atmosphere are constantly maintained to give room for a variability of zone of inhibition in the disc diffusion susceptibility method, for an optimum result. Turbidity standard is used to standardize the selected microorganisms, and this may be a visual approximation with the McFarlan standard of 0.5 or by using a spectrophotometer at 600 nm with optical density of 1.0.

Diffusion methods are more suitable for the preliminary testing of pure compounds or an established chemical component. In the agar well diffusion method it is important that the test samples are highly water-soluble to allow for proper diffusion into the solidified water-agar solution. Also, it affects alongside the antimicrobial agent molecular size, the extent of the area of solution infiltration around the disc, which is an important determining factor for the exact zone of inhibition. This method is not suitable for water-insoluble synthetic compounds as with most synthesized ligands and metal complexes regardless of if it is applied in a non polar solvent or not. Therefore, the disc diffusion method is preferred for the antibacterial activity investigation in this study.

The dilution bioassay technique is carried out using different experimental concentrations by way of serial dilution from a starting stock solution of known concentration. Reports have shown that methanol and acetone as solvents for antimicrobial test samples are advisable, because in addition to the test samples being completely soluble in them they show no inhibition of the microbes even at 2% final concentration (95JEP109, 97JEP177, 00PHC93). DMSO, with a dipole moment of 3.96 D has also been successfully used for dissolving antimicrobial agents (96JET27, 00LAM379, 06TJB65). Increased sensitivity for small amount of an antimicrobial agent is one of dilution technique strong points, thereby having the ability to distinguish between bacteriostatic and bactericidal effect of test samples. Micro dilution

method is a cheap and affordable technique, it gives room for reproducible results, and it can be used for a wide variety of microorganisms. The use of serial dilution assay for the quantitative determination of MIC values of some bioactive compounds have been reported (98JMI113, 04JEP(94)279). For non-fastidious organisms a recommended temperature of 35–37^{o}C in air for 16–20 hours has been reported (03CMI1), and in the incubator at 37^{o}C (04JEP(95)253). Changes in turbidity of test plates is usually an indication of organism growth (98JMI113), in some other cases, spectroscopy is used to observe them (02BJM97). Indicators like tetrazolium salts or resazurin dye have also been used (08AJB1797).

In bioautography technique, a determined amount of an antimicrobial agent is applied to a silica 60 gel TLC plate and developed with an appropriate solvent; a suspension of the selected test bacterial is sprayed onto the TLC plate. Growth detection is observed using tetrazolium salts as microbial indicators (05MIO779). After spraying the plates with the detector, they are reincubated at 25^{o}C for 20 hours or at 37^{o}C for 3–4 hours (96SAJB158, 06CAM11). TLC plates disruptions of synergism between active constituents in an antimicrobial agent, thereby reducing activity, is a disadvantage of the bioautography technique, and it is also not an ideal method for the quantification of biological activities of plant extract (94IPH87).

The chelation of Schiff bases to metal ion have been shown to increase in their overall biological activity compared to that of the Schiff base. This is

based on the theory of the overtone concept of cell permeability (86SRI257) and that of chelation (93IJC(A)446). The overtone cell permeability theory says that the lipid membrane surrounding a microorganism cell, allows for the passage of only lipid soluble materials, as a result liposolubility is a useful factor affecting antimicrobial activity (86SRI257). Chelation theory explains that the polarity of the metal ion is greatly reduced due to the overlap of the Schiff base orbital as a result of the partial sharing of the metal ion positive charge with donor groups. In addition, it increases the delocalization of π electrons over the chelate ring enhancing the lipophilicity of metal complex. The penetration of the complex into the lipid membrane is therefore enhanced by the increased lipophilicity thereby blocking the metal binding sites on the enzymes of the microorganism and bringing about cell death.

2.6. Antioxidant Activity

Free radicals of any form within the cell tissue damage it. They could be generated naturally witin the system and sometimes could be synthesized and introduced into it by some biological processes (97EXP291). The damage-free radicals may lead to the growth of cancerous cells. These extensive cellular damage ranges from the polypeptides modification, lipid peroxidation, and nucleic acid strand scission just to mention but a few (01CUS1179). Antioxidants are capable of protecting the cell tissues by reacting with these free radicals thereby stabilizing them. By so doing, they

slow down the oxidative chemical reaction that produces free radicals that start chain reactions damaging cells.

2.7. Diseases and Resistance to Drugs

Medicinal clinical drugs usually inhibit the function of a biomolecule in a living system responsible for a disease, thereby bringing therapeutic benefits to a patient. But when a drug no longer serves the function of curing an ailment for which it is responsible, the unavoidable disease resistance sets in, which have been reported to be caused by the rapid replication and evolution of microbes (93JCT361). It has been reported that disease resistance to drugs has become a worldwide public health problem (05ADD1446, 06BPH1036). This phenomenon predates to the discovery of antimicrobials itself. The excessive use of antimicrobial drugs is ascribed to drug resistance wide spread level (92SCI1050, 92SCI1064).

Also, it has been reported that resistance rates of gram-negative pathogens in developing countries is higher than those in the developed countries. Trimethoprim resistance for instance has been reported at high levels of 25 to 68% in South America, Asia, and Africa (85JID1107, 89JAC(23)143, 89JAC(23)151, 89JAC(24)973, 90NJM285). It is observed that these resistant isolates are easily transferred by travelers who are not open to antimicrobial agents (82NJM130, 90AAC515). Microbes can commonly acquire encoding genes *via* transfer from members of their own species or completely unrelated family, making them unnoticeable by the administered drug.

The abuse and misuse of drugs have been attributed to the mutation of microbes, hence helping them to survive in the presence of an antimicrobial agent. It has been reported that when rapid mutation takes place within the microbial population, it is impossible to eradicate disease resistance (99MI1). Multidrug resistance (MDR) is the resistance of tumor cells to the cytostatic or cytotoxic actions of multiple, structurally dissimilar, and functionally divergent drugs commonly used in cancer chemotherapy (93CRS747). It could be intrinsic when the disease is refractory to chemotherapy from the outset, or acquired; or when the disease becomes insensitive to treatment upon relapse. MDR has been responsible for the overall poor efficacy of cancer chemotherapy. With the identification of proteins that could mediate multidrug resistance, development of related drugs has been attempted (90PHR155). Amongst these multidrug resistant organisms are methicillin/oxacillin–resistant *Staphylococcus aureus* MRSA, vancomycin–resistant *enterococci* VRE, extended–spectrum *beta–lactamases* (which are resistant to cephalosporins and monobactams) ESBL, and penicillin–resistant *Streptococcus pneumonia* PRSP (90PHR155). Studies on drugs have revealed that there is no obvious chemical similarity that brings about multidrug resistance by microbes (93CR747). Enzymatic inactivation is the common mode of mechanism used by the disease microbes to become resistant, which can chemically modify the antibiotic, render it inactive through physical removal from the cell, or modify target site so that it is not recognized by

the antibiotic. In this process, an existing cellular enzyme is modified to react with the antibiotic in such a way that it no longer affects the microorganism. Disease microbe antibiotic target sites alteration has been seen in most drug resistance cases. Chloramphenicol, for instance, is affected by reduced uptake into the cell system, tetracycline by active efflux from the cell, β–lactams, erythromycin, lincomycin by its elimination or reduction of binding to cell target and sulfonamides/trimethoprim is affected by metabolic bypass of inhibition reaction and the over-production of antibiotic target (12MI1). There have been reports on antimicrobial resistance in *Salmonella*, research on this has been possible in the countries, with excellent systems to monitor resistance to antibiotics (02JCM3574). A high level of bacterial resistance which is the cause of acquired infections within the community has also been documented (08IPS177).

3. Experimental and Characterization Techniques

3.1. Materials

Analytical grade reagents, manganese(II) chloride tetrahydrate $MnCl_2 \cdot 4H_20$, cobalt(II) chloride hexahydrate $CoCl_2 \cdot 6H_20$, nickel(II) chloride hexahydrate $NiCl_2 \cdot 6H_20$, copper(II) acetate monohydrate $(MeCOO)_2Cu \cdot H_2O$, phenylhydrazine, 2,4-dinitrophenylhydrazine, 4-aminobenzenedulfonamide, 3-methyl-1-phenyl-2-pyrazolin-5-one, calcium hydroxide and solvents were used as supplied by Sigma Aldrich. 4-Benzoyl-3-methyl-1-phenyl-2-pyrazolin-5-one**74** and 4-acetyl-3-methyl-1-phenyl-2-pyrazolin-5-one**75** were synthesized and purified as reported (04POL2465, 12IC1152).

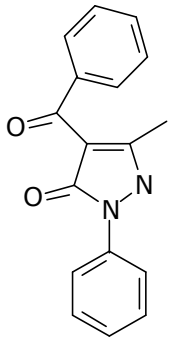

74

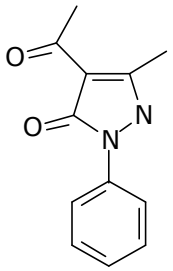

75

3.2. Synthesis of Schiff bases

3.2.1. Synthesis of 4-Acetyl-3-methyl-1-phenyl-2-pyrazolin-5-one Phenylhydrazine

To a solution of 4-acetyl-3-methyl-1-phenyl-2-pyrazolin-5-one (2.0 mmol, 0.43 g) in methanol (40 mL) was added in drops phenylhydrazine (2.0 mmol, 0.22 g) in methanol (10 mL) and Ampp-Ph was precipitated. Af-

ter 4 h of reflux the pale yellow solid was filtered, washed with methanol, dried at room temperature and stored over fused $CaCl_2$. Yield: 74%. M.p.: 183−185°C.^{1}H NMR (600 MHz, DMSO): δ (ppm) = 12.40 (br, 1H, phenylhydrazine –NH), 8.60 (s, 1H, C=N-H), 6.80 - 8.00 (m, 10H, Ar-H), 2.40(s, 3H, CH_3).^{13}C NMR (600 MHz, DMSO): δ (ppm) = 168.7 (s, C=O), 165.5 (s, C=N), 147.3 – 97.3 (s, aromatic carbons), 17.3 (s, pyrazolone CH_3), 14.6 (s, acetyl CH_3). IR (KBr, cm^{-1}): 3497 ν(N-H), 2928 ν(C-H), 1630 ν(C=N), 1501 ν(C=O). Elemental analysis for $C_{18}H_{18}N_4O$ (%): found C 70.14, H 5.84, N 18.13; calculated C 70.55, H 5.93, N 18.30. Mol. mass (g/mol): 306.15. AP-CI-MS: *m/z* 307.15 ($[M + H]^+$, 100%).

3.2.2. Synthesis of 4-Acetyl-3-methyl-1-phenyl-2-pyrazolin-5-one Dinitrophenylhydrazine

To 4-acetyl-3-methyl-1-phenyl-2-pyrazolin-5-one (2.0 mmol, 0.43 g) in methanol (40 mL) was added in drops dinitrophenylhydrazine (2.0 mmol, 0.40 g) dissolved in hot methanol (40 mL) while stirring and Ampp-Dh was precipitated in good yield. After 4 h of reflux, the red solid was filtered, washed with methanol, dried at room temperature and stored over fused $CaCl_2$. Yield: 74%. M.p.: 217−218°C. ^{1}H NMR (600 MHz, DMSO): δ (ppm) = 10.8 (br, 1H, phenylhydrazine –NH), 8.8 (s, 1H, C=N-H), 8.4–7.2 (m, 8H, aromatic-H), 2.30(s, 3H, CH_3).^{13}C NMR (600 MHz, DMSO): δ (ppm) = 146.2 (s, C=O), 137.7 (s, C=N), 137.9 – 116.0 (s, aromatic carbons), 16.2 (s, pyrazolone CH_3), 14.9 (s, acetyl CH_3). IR (KBr, cm^{-1}): 3486 ν(N-H), 2913 ν(C-

H), 1627 ν(C=N), 1501 ν(C=O). Elemental Analysis for $C_{18}H_{16}N_6O_5$ (%): found C 54.20, H 4.11, N 20.98; calculated C 54.53, H 4.07, N 21.21. Mol. mass (g/mol): 396.12. APCI-MS: *m/z* 397.12 ($[M + H]^+$, 100%).

3.2.3. Synthesis of 4-Acetyl-3-methyl-1-phenyl-2-pyrazolin-5-one Sulfanilamide

To a solution of 4-acetyl-3-methyl-1-phenyl-2-pyrazolin-5-one (2.0 mmol, 0.43 g) in methanol (40 mL) was added in drops sulfanilamide (2.0 mmol, 0.34 g) in hot methanol (40 mL) while stirring and Ampp-Sn was precipitated. After 4 h of reflux the yellow solid was filtered, washed with methanol, dried at room temperature and stored over fused $CaCl_2$. Yield: 74%. M.p.: 232−234°C. ^{1}H NMR (600 MHz, DMSO): δ (ppm) = 13.1 (s, 1H, –NH), 8.0 (s, 1H, C=N-H), 7.9 – 7.2 (m, 9H, aromatic-H), 2.4 (s, 3H, CH_3).^{13}C NMR (600 MHz, DMSO): δ (ppm) = 165.4 (s, C=O), 164.5 (s, C=N), 148.2 (s, C–S)142.8 – 116.6 (s, aromatic carbons), 17.6 (s, pyrazolone CH_3), 17.5 (s, acetyl CH_3). IR (KBr, cm^{-1}): 3496 ν(N-H), 2954 ν(C-H), 1633 ν(C=N), 1503 ν(C=O). Elemental analysis for $C_{18}H_{18}N_4O_3S$ (%): found C 58.42, H 4.88, N 15.18; calculated C 58.36, H 4.90, N 15.13. Mol. mass (g/mol): 370.11. APCI-MS: *m/z* 371.11 ($[M + H]^+$, 100%).

3.2.4. Synthesis of 4-Benzoyl-3-methyl-1-phenyl-2-pyrazolin-5-one Phenylhydrazine

To a solution of 4-benzoyl-3-methyl-1-phenyl-2-pyrazolin-5-one (2.0 mmol, 0.56 g) in methanol (40 mL) was added in drops phenylhydrazine

(2.0 mmol, 0.22 g) in methanol (10 mL) while stirring and Bmpp-Dh was precipitated. After 4 h of reflux the yellow solid was filtered, washed with methanol, dried at room temperature and stored over fused $CaCl_2$. Suitable block-like golden yellow single crystals of Bmpp-Ph for x-ray diffraction were grown at room temperature from slow evaporation of methanol solution after four days. Yield: 71%. M.p.: 197−199^{o}C. ^{1}H NMR (600 MHz, DMSO): δ (ppm) = 12.2 (br, 1H, phenylhydrazine –NH), 9.5 (br, 1H, C=N-H), 8.4−6.8 (m, 15H, aromatic-H), 1.9(s, 3H, CH_3).^{13}C NMR (600 MHz, DMSO): δ (ppm) = 168.0 (s, C=O), 165.5 (s, C=N), 148−115.3 (m, aromatic carbons), 15.8 (s, pyrazolone CH_3). IR (KBr, cm^{-1}): 3491 ν(N-H), 2919 ν(C-H), 1634 ν(C=N), 1501 ν(C=O). Elemental analysis for $C_{23}H_{20}N_4O$ (%): found C 74.61, H 5.65, N 15.14; calculated C 74.97, H 5.47, N 15.21. Mol. mass (g/mol): 368.16. APCI-MS: *m/z* 369.17 ($[M + H]^+$, 100%).

3.2.5. Synthesis of 4-Benzoyl-3-methyl-1-phenyl-2-pyrazolin-5-one Dinitrophenylhydrazine

To a solution of 4-benzoyl-3-methyl-1-phenyl-2-pyrazolin-5-one (2.0 mmol, 0.56 g) in methanol (40 mL) was added in drops dinitrophenylhydrazine (2.0 mmol, 0.40 g) in hot methanol (40 mL) while stirring and Bmpp-Dh was precipitated. After 4 h of reflux, the red solid was filtered, washed with methanol, dried at room temperature, and stored over fused $CaCl_2$. Block-like red single crystals of Bmpp-Dh suitable for X-ray diffraction were grown at room temperature from slow evaporation of methanol solution after three

days. Yield: 73%. M.p.: 240−242°C. ^{1}H NMR (600 MHz, DMSO): δ (ppm) = 11.6 (s, 1H, phenylhydrazine –NH), 8.9 (s, 1H, C=N-H), 8.5−7.3 (m, 13H, aromatic-H), 1.9(s, 3H, CH_3). ^{13}C NMR (600 MHz, DMSO): δ (ppm) = 148.9 (s, C=O), 147.4 (s, C=N), 144.6–117.2 (m, aromatic carbons), 13.6 (s, pyrazolone CH_3). IR (KBr, cm^{-1}): 3489 ν(N-H), 2954 ν(C-H), 1642 ν(C=N), 1501 ν(C=O). Elemental Analysis for $C_{23}H_{18}N_6O_5$ (%): found C 60.18, H 3.58, N 18.40; calculated C 60.24, H 3.96, N 18.34. Mol. mass (g/mol): 458.13. APCI-MS: *m/z* 459.14 ($[M + H]^+$, 100%).

3.2.6. Synthesis of 4-Benzoyl-3-methyl-1-phenyl-2-pyrazolin-5-one Sulfanilamide

To a solution of 4-benzoyl-3-methyl-1-phenyl-2-pyrazolin-5-one (2.0 mmol, 0.56 g) in methanol (40 mL) was added in drops sulfanilamide (2.0 mmol, 0.34 g) in hot methanol while stirring and Bmpp-Sn was precipitated. After 4 h of reflux, the yellow solid was filtered, washed with methanol, dried at room temperature, and stored over fused $CaCl_2$. Suitable thread-like yellow single crystals of Bmpp-Dh for X-ray diffraction were grown at room temperature from slow evaporation of methanol solution after seven days. Yield: 69%. M.p.: 102−104°C. ^{1}H NMR (600 MHz, DMSO): δ (ppm) = 12.8 (br, 1H, –NH), 8.0 (s, 1H, C=N-H), 7.8 – 7.1 (m, 14H, aromatic-H), 2.2 (s, 3H, CH_3). ^{13}C NMR (600 MHz, DMSO): δ (ppm) = 190.5 (s, C=O), 139.3 (s, C=N), 148.2 (s, C–S) 132.2–110.7 (s, aromatic carbons), 16.5 (s, pyrazolone CH_3). IR (KBr, cm^{-1}): 3497 ν(N-H), 2927 ν(C-H), 1639 ν(C=N), 1504

ν(C=O). Elemental analysis for $C_{23}H_{20}N_4O_3S$ (%): found C 63.84, H 4.67, N 12.79; calculated C 63.87, H 4.66, N 12.96. Mol. mass (g/mol): 432.13. AP-CI-MS: *m/z* 433.13 ($[M + H]^+$, 100%).

3.3. Synthesis of Transition Metal Complexes of Pyrazolone Schiff Bases

3.3.1. Synthesis of $Mn(Ampp\text{-}Ph)_2(H_2O)_2{\cdot}2H_2O$

To a solution of Ampp-Ph (2 mmol, 0.61g) in hot ethanol (40 mL) was added in drops aqueous solution of $MnCl_2{\cdot}6H_2O$ (1 mmol, 0.23 g) while stirring under reflux and followed by the addition of NaOH (2 mmol, 0.08 g) to precipitate the metal complex. After 4 h of reflux, the pale yellow solid was filtered, washed with ethanol/water (1:1), dried at room temperature, and stored over fused $CaCl_2$. Yield: 76%. M.p.: 140−142°C. Mol. Cond. (10^{-3} M in DMF): 4.04 ohm^{-1} cm^2 mol^{-1}. μ_{eff}(B.M.): 5.98. UV-Vis (DMF) λ_{max} nm: 230 (π→π*), 311, 321 (n→π*), 396 (d→d). IR (KBr, cm^{-1}): 3475 ν(N-H), 3387 ν(O–H), 2930 ν(C-H), 1620 ν(C=N), 839 ν(H_2O), 632 ν(M-N), 485 ν(M-O). Elemental analysis for $C_{36}H_{42}N_8O_6Mn$ (%): found C 58.57, H 5.62, N 15.01; calculated C 58.60, H 5.74, N 15.19. Mol. mass (g/mol): 737.26.

3.3.2. Synthesis of $Co(Ampp\text{-}Ph)_2(H_2O)_2{\cdot}2H_2O$

To a solution of Ampp-Ph (2 mmol, 0.61 g) in hot ethanol (40 mL) was added in drops, aqueous solution of $CoCl_2{\cdot}4H_2O$ (1 mmol, 0.20 g) while stirring under reflux and followed by the addition of NaOH (2 mmol, 0.08 g) to precipitate the metal complex. After 4 h of reflux, the pink solid was filtered,

washed with ethanol/water (1:1), dried at room temperature, and stored over fused $CaCl_2$. Yield: 75%. M.p.: 160−162°C. Molar cond. (10^{-3} M in DMF): 6.78 ohm^{-1} cm^2 mol^{-1}. μ_{eff}(B.M.): 4.49.UV-Vis (DMF) λmax nm: 223 (π→π*), 313, 324 (n→π*), 390, 536, 600 (d→d). IR (KBr, cm^{-1}): 3485 ν(N-H), 3391 ν(O–H), 2923 ν(C-H), 1619 ν(C=N), 844 ν(H_2O), 621 ν(M-N), 489 ν(M-O). Elemental analysis for $C_{36}H_{42}N_8O_6Co$ (%): found C 57.95, H 5.63, N 15.40; calculated C 58.28, H 5.71, N 15.11, Mol. mass (g/mol): 741.25.

3.3.3. Synthesis of $Ni(Ampp\text{-}Ph)_2(H_2O)_2 \cdot H_2O$

To a solution of Ampp-Ph (2 mmol, 0.61 g) in hot ethanol (40 mL) was added in drops, aqueous solution of $NiCl_2 \cdot 4H_2O$ (1 mmol, 0.20 g) while stirring under reflux and followed by the addition of NaOH (2 mmol, 0.08 g) to precipitate the metal complex. After 4 h of reflux, the pale green solid was filtered, washed with ethanol/water (1:1), dried at room temperature, and stored over fused $CaCl_2$. Yield: 73%. M.p.: 176−178°C. Molar Cond. (10^{-3} M in DMF): 14.55 ohm^{-1} cm^2 mol^{-1}. μ_{eff}(B.M.): 2.87. UV-Vis (DMF) λ_{max} nm: 226(π→π*), 322, 354 (n→π*), 407, 597, 793 (d→d). IR (KBr, cm^{-1}): 3483 ν(N-H), 3390 ν(O–H), 2925 ν(C-H), 1621 ν(C=N), 842 ν(H_2O), 623 ν(M-N), 490 ν(M-O). Elemental analysis for $C_{36}H_{40}N_8O_5Ni$ (%): found C 59.92, H 5.55, N 15.23; calculated C 59.75, H 5.58, N 15.49, Mol. mass (g/mol): 723.00.

3.3.4. Synthesis of $Cu(Ampp\text{-}Ph)_2(H_2O)_2$

To a solution of Ampp-Ph (2 mmol, 0.61 g) in hot ethanol (40 mL) was added in drops aqueous solution of $Cu(CH_3COO)_2 \cdot H_2O$ (1 mmol, 0.20 g) while stirring under reflux and followed by the addition of NaOH (2 mmol, 0.08 g) to precipitate the metal complex. After 4 h of reflux, the light brown solid was filtered, washed with ethanol/water (1:1), dried at room temperature and stored over fused $CaCl_2$. Yield: 79%. M.p.: 212−213°C. Molar cond. (10^{-3} M in DMF): 12.05 ohm^{-1} cm^2 mol^{-1}. μ_{eff}(B.M.): 1.93. UV-Vis (DMF) λ_{max} nm: 217 (п→п*), 310, 323 (n→п*), 401, 594 (d→d). IR (KBr, cm^{-1}): 3493 ν(N-H), 3399 ν(O–H), 2926 ν(C-H), 1618 ν(C=N), 821 ν(H_2O), 628 ν(M-N), 478 ν(M-O). Elemental Analysis for $C_{36}H_{38}N_8O_4Cu$ (%): found C 60.49, H 5.11, N 15.40; calculated C 60.86, H 5.40, N 15.78, Mol. mass (g/mol): 709.85.

3.3.5. Synthesis of $Mn(Bmpp\text{-}Ph)_2(H_2O)_2 \cdot 2H_2O$

To a solution of Bmpp-Ph (2 mmol, 0.74 g) in hot ethanol (40 mL) was added in drops aqueous solution of $MnCl_2 \cdot 6H_2O$ (1 mmol, 0.23 g) while stirring under reflux and followed by the addition of NaOH (2 mmol, 0.08 g) to precipitate the metal complex. After 4 h of reflux, the pale-yellow solid was filtered, washed with ethanol/water (1:1), dried at room temperature, and stored over fused $CaCl_2$. Yield: 73%. M.p.: 120−121°C. Molar cond. (10^{-3} M in DMF): 8.28 ohm^{-1} cm^2 mol^{-1}. μ_{eff}(B.M.): 5.63. UV-Vis (DMF) λ_{max} nm: 228 (п→п*), 303 (n→п*), 393 (d→d). IR (KBr, cm^{-1}): 3492 ν(N-H), 3397 ν(O–

H), 2943 ν(C-H), 1621 ν(C=N), 841 ν(H_2O), 631 ν(M-N), 486 ν(M-O). Elemental analysis for $C_{46}H_{46}N_8O_6Mn$ (%): found C 64.00, H 5.53, N 13.07; calculated C 64.09, H 5.38, N 13.01, Mol. mass (g/mol): 861.29.

3.3.6. Synthesis of $Co(Bmpp\text{-}Ph)_2(H_2O)_2\cdot H_2O$

To a solution of Bmpp-Ph (2 mmol, 0.74 g) in hot ethanol (40 mL) was added in drops aqueous solution of $CoCl_2\cdot 4H_2O$ (1 mmol, 0.20 g) while stirring under reflux and followed by the addition of NaOH (2 mmol, 0.08 g) to precipitate the metal complex. After 4 h of reflux, the pink solid was filtered, washed with ethanol/water (1:1), dried at room temperature and stored over fused $CaCl_2$. Slow evapouration of a solution of $Co(Bmpp\text{-}Ph)_2(H_2O)_2\cdot H_2O$ in ethanol afforded crystals of $Co(Bmpp)_2(EtOH)_2$ suitable for X-ray crystallography. Yield: 72%. M.p.: 125−127°C. Molar cond. (10^{-3} M in DMF): 10.02 ohm^{-1} cm^2 mol^{-1}. μ_{eff}(B.M.): 4.45. UV-Vis (DMF) λ_{max} nm: 230 (π→π*), 317 (n→π*), 554, 627, 708 (d→d). IR (KBr, cm^{-1}): 3480 ν(N-H), 3373 ν(O–H), 2949 ν(C-H), 1618 ν(C=N), 826 ν(H_2O), 641 ν(M-N), 485 ν(M-O). Elemental analysis for $C_{46}H_{44}N_8O_5Co$ (%): found C 65.06, H 4.96, N 13.14; calculated C 65.15, H 5.23, N 13.22, Mol. mass (g/mol): 847.28.

3.3.7. Synthesis of $Ni(Bmpp\text{-}Ph)_2(H_2O)_2\cdot 2H_2O$

To a solution of Bmpp-Ph (2 mmol, 0.74 g) in hot ethanol (40 mL) was added in drops aqueous solution of $NiCl_2\cdot 4H_2O$ (1 mmol, 0.20 g) while stirring under reflux and followed by the addition of NaOH (2 mmol, 0.08 g) to precipitate the metal complex. After 4 h of reflux, the pale-green solid was

filtered, washed with ethanol/water (1:1), dried at room temperature, and stored over fused $CaCl_2$. Yield: 72%. M.p.: 213−215°C. Molar cond. (10^{-3} M in DMF): 11.43 ohm^{-1} cm^2 mol^{-1}. μ_{eff}(B.M.): 2.94. UV-Vis (DMF) λ_{max} nm: 232 (π→π*), 309 (n→π*), 678, 808 (d→d). IR (KBr, cm^{-1}): 3487 ν(N-H), 3393 ν(O–H), 2935 ν(C-H), 1619 ν(C=N), 845 ν(H_2O), 639 ν(M-N), 498 ν(M-O). Elemental Analysis for $C_{46}H_{46}N_8O_6Ni$ (%): found C 63.80, H 5.79, N 12.18; calculated C 63.81, H 5.36, N 12.95, Mol. mass (g/mol): 865.05.

3.3.8. Synthesis of $Cu(Bmpp\text{-}Ph)_2(H_2O)_2{\cdot}H_2O$

To a solution of Bmpp-Ph (2 mmol, 0.74 g) in hot ethanol (40 mL) was added in drops aqueous solution of $Cu(CH_3COO)_2{\cdot}H_2O$ (1 mmol, 0.20 g) while stirring under reflux and followed by the addition of NaOH (2 mmol, 0.08 g) to precipitate the metal complex. After 4 h of reflux, the brown solid was filtered, washed with ethanol/water (1:1), dried at room temperature, and stored over fused $CaCl_2$. Yield: 80%. M.p.: 195−197°C. Molar cond. (10^{-3} M in DMF): 5.98 ohm^{-1} cm^2 mol^{-1}. μ_{eff}(B.M.): 1.94.UV-Vis (DMF) λ_{max} nm: 215 (π→π*), 304, 317 (n→π*),516, (d→d). IR (KBr, cm^{-1}): 3483 ν(N-H), 3378 ν(O–H), 2923 ν(C-H), 1618 ν(C=N), 848 ν(H_2O), 627 ν(M-N), 482 ν(M-O). Elemental analysis for $C_{46}H_{46}N_8O_6Cu$ (%): found C 64.76, H 5.02, N 13.13; calculated C 64.80, H 5.21, N 13.15, Mol. mass: (g/mol): 851.89.

3.3.9. Synthesis of $Mn(Ampp\text{-}Dh)_2(H_2O)_2{\cdot}H_2O$

To a solution of Ampp-Dh (2 mmol, 0.79 g) in hot ethanol (40 mL) was added in drops aqueous solution of $MnCl_2{\cdot}6H_2O$ (1 mmol, 0.23 g) while stir-

ring under reflux and followed by the addition of NaOH (2 mmol, 0.08 g) to precipitate the metal complex. After 4 h of reflux, the dark red solid was filtered, washed with ethanol/water (1:1), dried at room temperature, and stored over fused $CaCl_2$. Yield: 70%. M.p.: 209−211°C. Molar cond. (10^{-3} M in DMF): 8.09 ohm^{-1} cm^2 mol^{-1}. μ_{eff}(B.M.): 5.67.UV-Vis (DMF) λ_{max} nm: 270 (π→π*), 324, (n→π*), 451 (d→d). IR (KBr, cm^{-1}): 3489 ν(N-H), 3395 ν(O–H), 2925 ν(C-H), 1620 ν(C=N), 840 ν(H_2O), 621 ν(M-N), 485 ν(M-O). Elemental analysis for $C_{36}H_{36}N_{12}O_{13}Mn$ (%): found C 48.57, H 5.42, N 18.10; calculated C 48.04, H 4.03, N 18.69, mol. mass (g/mol): 899.19.

3.3.10. Synthesis of $Co(Ampp\text{-}Dh)_2(H_2O)_2$

To a solution of Ampp-Dh (2 mmol, 0.79 g) in hot ethanol (40 mL) was added in drops aqueous solution of $CoCl_2{\cdot}4H_2O$ (1 mmol, 0.20 g) while stirring under reflux and followed by the addition of NaOH (2 mmol, 0.08 g) to precipitate the metal complex. After 4 h of reflux, the red solid was filtered, washed with ethanol/water (1:1), dried at room temperature, and stored over fused $CaCl_2$. Yield: 71%. M.p.: 199−201°C. Molar cond. (10^{-3} M in DMF): 11.80 ohm^{-1} cm^2 mol^{-1}. μ_{eff}(B.M.): 4.47.UV-Vis (DMF) λ_{max} nm: 268 (π→π*), 324, (n→π*),414, 493 (d→d). IR (KBr, cm^{-1}): 3493 ν(N-H), 3384 ν(O–H), 2929 ν(C-H), 1618 ν(C=N), 843 ν(H_2O), 630 ν(M-N), 484 ν(M-O). Elemental analysis for $C_{36}H_{34}N_{12}O_{12}Co$ (%): found C 48.61, H 3.63, N 18.79; calculated C 48.80, H 3.87, N 18.98, Mol. mass (g/mol): 885.17.

3.3.11. Synthesis of $Ni(Ampp\text{-}Dh)_2(H_2O)_2$

To a solution of Ampp-Dh (2 mmol, 0.79 g) in hot ethanol (40 mL) was added in drops aqueous solution of $NiCl_2 \cdot 4H_2O$ (1 mmol, 0.20 g) while stirring under reflux and followed by the addition of NaOH (2 mmol, 0.08 g) to precipitate the metal complex. After 4 h of reflux, the red solid was filtered, washed with ethanol/water (1:1), dried at room temperature and stored over fused $CaCl_2$. Yield: 69%. M.p.: 154−156°C. Molar cond. (10^{-3} M in DMF): 4.40 ohm^{-1} cm^2 mol^{-1}. μ_{eff}(B.M.): 2.92. UV-Vis (DMF) λ_{max} nm: 278 (π→π*), 324 (n→π*), 436, (d→d). IR (KBr, cm^{-1}): 3495 ν(N-H), 3388 ν(O–H), 2921 ν(C-H), 1617 ν(C=N), 849 ν(H_2O), 633 ν(M-N), 486 ν(M-O). Elemental analysis for $C_{36}H_{34}N_{12}O_{12}Ni$ (%): found C 48.70, H 3.85, N 18.74; calculated C 48.82, H 3.87, N 18.99, Mol. mass (g/mol): 884.93.

3.3.12. Synthesis of $Cu(Ampp\text{-}Dh)_2(H_2O)_2$

To a solution of Ampp-Dh (2 mmol, 0.79 g) in hot ethanol (40 mL) was added in drops aqueous solution of $Cu(CH_3COO)_2 \cdot H_2O$ (1 mmol, 0.20 g) while stirring under reflux and followed by the addition of NaOH (2 mmol, 0.08 g) to precipitate the metal complex. After 4 h of reflux, the red solid was filtered, washed with ethanol/water (1:1), dried at room temperature, and stored over fused $CaCl_2$. Yield: 78%. M.p.: 222−223°C. Molar cond. (10^{-3} M in DMF): 11.80 ohm^{-1} cm^2 mol^{-1}. μ_{eff}(B.M.): 1.97. UV-Vis (DMF) λ_{max} nm: 251 (π→π*), 342 (n→π*), 467, 598, (d→d). IR (KBr, cm^{-1}): 3498 ν(N-H), 3390 ν(O–H), 2935 ν(C-H), 1619 ν(C=N), 833 ν(H_2O), 620 ν(M-N),

492 ν(M-O). Elemental analysis for $C_{36}H_{34}N_{12}O_{12}Cu$ (%): found C 48.49, H 3.96, N 18.54; calculated C 48.55, H 3.85, N 18.89. Mol. mass (g/mol): 889.79.

3.3.13. Synthesis of $Mn(Bmpp\text{-}Dh)_2(H_2O)_2$

To a solution of Bmpp-Dh (2 mmol, 0.92 g) in hot ethanol (40 mL) was added in drops aqueous solution of $MnCl_2 \cdot 6H_2O$ (1 mmol, 0.23 g) while stirring under reflux and followed by the addition of NaOH (2 mmol, 0.08 g) to precipitate the metal complex. After 4 h of reflux, the orange solid was filtered, washed with ethanol/water (1:1), dried at room temperature, and stored over fused $CaCl_2$. Yield: 76%. M.p.: 240−241°C. Molar cond. (10^{-3} M in DMF): 11.40 ohm^{-1} cm^2 mol^{-1}. μ_{eff}(B.M.): 5.65. UV-Vis (DMF) λ_{max} nm: 280 (π→π*), 324 (n→π*), 436, 462, (d→d). IR (KBr, cm^{-1}): 3496 ν(N-H), 3392 ν(O–H), 2923 ν(C-H), 1619 ν(C=N), 833 ν(H_2O), 629 ν(M-N), 486 ν(M-O). Elemental Analysis for $C_{46}H_{36}N_{12}O_{12}Mn$ (%): found C 54.78, H 3.51, N 16.41; calculated C 55.02, H 3.62, N 16.75. Mol. mass (g/mol): 1003.19.

3.3.14. Synthesis of $Co(Bmpp\text{-}Dh)_2(H_2O)_2 \cdot H_2O$

To a solution of Bmpp-Dh (2 mmol, 0.92 g) in hot ethanol (40 mL) was added in drops aqueous solutions of $CoCl_2 \cdot 4H_2O$ (1 mmol, 0.20 g) while stirring under reflux and followed by the addition of NaOH (2 mmol, 0.08 g) to precipitate the metal complex. After 4 h of reflux, the orange solid was filtered, washed with ethanol/water (1:1), dried at room temperature, and stored over fused $CaCl_2$. Yield: 72%. M.p.: 248−250°C. Molar cond. (10^{-3} M

in DMF): 10.91 ohm^{-1} cm^2 mol^{-1}. μ_{eff}(B.M.): 4.48. UV-Vis (DMF) λ_{max} nm: 271 (π→π*), 323 (n→π*),425, 460 (d→d). IR (KBr, cm^{-1}): 3484 ν(N-H), 3396 ν(O–H), 2926 ν(C-H), 1620 ν(C=N), 832 ν(H_2O), 622 ν(M-N), 487 ν(M-O). Elemental analysis for $C_{46}H_{38}N_{12}O_{13}Co$ (%): found C 53.40, H 3.92, N 16.22; calculated C 53.84, H 3.74, N 16.39, Mol. mass (g/mol): 1025.20.

3.3.15. Synthesis of $Ni(Bmpp\text{-}Dh)_2(H_2O)_2 \cdot H_2O$

To a solution of Bmpp-Dh (2 mmol, 0.92 g) in hot ethanol (40 mL) was added in drops aqueous solutions of $NiCl_2 \cdot 4H_2O$ (1 mmol, 0.20 g) while stirring under reflux and followed by the addition of NaOH (2 mmol, 0.08 g) to precipitate the metal complex. After 4 h of reflux, the red solid was filtered, washed with ethanol/water (1:1), dried at room temperature, and stored over fused $CaCl_2$. Yield: 72%. M.p.: 247−249°C. Molar cond. (10^{-3} M in DMF): 6.34 ohm^{-1} cm^2 mol^{-1}. μ_{eff}(B.M.): 2.90.UV-Vis (DMF) λ_{max} nm: 274 (π→π*), 324 (n→π*), 431, 463 (d→d). IR (KBr, cm^{-1}): 3494 ν(N-H), 3394 ν(O–H), 2925 ν(C-H), 1619 ν(C=N), 832 ν(H_2O), 624 ν(M-N), 478 ν(M-O). Elemental analysis for $C_{46}H_{38}N_{12}O_{13}Ni$ (%): found C 53.68, H 3.80, N 16.32; calculated C 53.86, H 3.74, N 16.39. Mol. mass (g/mol): 1024.96.

3.3.16. Synthesis of $Cu(Bmpp\text{-}Dh)_2(H_2O)_2 \cdot 2H_2O$

To a solution of Bmpp-Dh (2 mmol, 0.92 g) in hot ethanol (40 mL) was added in drops aqueous solution of $Cu(CH_3COO)_2 \cdot H_2O$ (1 mmol, 0.20 g) while stirring under reflux and followed by the addition of NaOH (2 mmol, 0.08 g)to precipitate the metal complex. After 4 h of reflux, the brown solid

was filtered, washed with ethanol/water (1:1), dried at room temperature and stored over fused $CaCl_2$. Yield: 79%. M.p.: 250−251°C. Molar cond. (10^{-3} M in DMF): 9.96 ohm^{-1} cm^2 mol^{-1}. μ_{eff}(B.M.): 1.95. UV-Vis (DMF) λ_{max} nm: 268 (π→π*), 324 (n→π*), 426, 449 (d→d). IR (KBr, cm^{-1}): 3493 ν(N-H), 3396 ν(O–H), 2930 ν(C-H), 1619 ν(C=N), 830 ν(H_2O), 623 ν(M-N), 487 ν(M-O). Elemental Analysis for $C_{46}H_{40}N_{12}O_{14}Cu$(%): found C 52.65, H 3.75, N 15.83; calculated C 52.68, H 3.89, N 16.04, Molar. mass (g/mol): 1047.82.

3.3.17. Synthesis of $Mn(Ampp\text{-}Sn)_2(H_2O)_2{\cdot}H_2O$

To a solution of Ampp-Sn (2 mmol, 0.74 g) in hot ethanol (40 mL) was added in drops aqueous solution of $MnCl_2{\cdot}6H_2O$ (1 mmol, 0.23 g) while stirring under reflux and followed by the addition of NaOH (2 mmol, 0.08 g) to precipitate the metal complex. After 4 h of reflux, the golden yellow solid was filtered, washed with ethanol/water (1:1), dried at room temperature, and stored over fused $CaCl_2$. Yield: 81%. M.p.: 210−212°C. Molar cond. (10^{-3} M in DMF): 14.40 ohm^{-1} cm^2 mol^{-1}. μ_{eff}(B.M.): 5.61. UV-Vis (DMF) λ_{max} nm: 259 (π→π*), 377 (n→π*), 431 (d→d). IR (KBr, cm^{-1}): 3484 ν(N-H), 3392 ν(O–H), 2920 ν(C-H), 1624 ν(C=N), 824 ν(H_2O), 634 ν(M-N), 488 ν(M-O). Elemental Analysis for $C_{36}H_{40}N_8O_9S_2Mn$ (%): found C 51.01, H 4.58, N 13.21; calculated C 50.99, H 4.76, N 13.22, Molar. mass (g/mol): 847.17.

3.3.18. Synthesis of $Co(Ampp\text{-}Sn)_2(H_2O)_2$

To a solution of Ampp-Sn (2 mmol, 0.74 g) in hot ethanol (40 mL) was added in drops aqueous solution of $CoCl_2{\cdot}4H_2O$ (1 mmol, 0.20 g) while stir-

ring under reflux and followed by the addition of NaOH (2 mmol, 0.08 g) to precipitate the metal complex. After 4 h of reflux, the pink solid was filtered, washed with ethanol/water (1:1), dried at room temperature, and stored over fused $CaCl_2$. Yield: 82%. M.p.: 150−151°C. Molar cond. (10^{-3} M in DMF): 11.22 ohm^{-1} cm^2 mol^{-1}. μ_{eff}(B.M.): 4.43. UV-Vis (DMF) λ_{max} nm: 274 (π→π*), 377 (n→π*), 408, 632, 699 (d→d). IR (KBr, cm^{-1}): 3491 ν(N-H), 3391 ν(O–H), 2923 ν(C-H), 1619 ν(C=N), 831 ν(H_2O), 631 ν(M-N), 486 ν(M-O). Elemental analysis for $C_{36}H_{38}N_8O_8S_2Co$ (%): found C 51.61, H 4.51, N 13.11; calculated C 51.85, H 4.60, N 13.45, Mol. mass (g/mol): 833.16.

3.3.19. Synthesis of $Ni(Ampp\text{-}Sn)_2(H_2O)_2{\cdot}H_2O$

To a solution of Ampp-Sn (2 mmol, 0.74 g) each in hot ethanol (40 mL) was added in drops aqueous solution of $NiCl_2{\cdot}4H_2O$ (1 mmol, 0.20 g) while stirring under reflux and followed by the addition of NaOH (2 mmol, 0.08 g) to precipitate the metal complex. After 4 h of reflux the greenish-yellow solid was filtered, washed with ethanol/water (1:1), dried at room temperature, and stored over fused $CaCl_2$. Yield: 79%. M.p.: 157−158°C. Molar cond. (10^{-3} M in DMF): 16.02 ohm^{-1} cm^2 mol^{-1}. μ_{eff}(B.M.): 2.93. UV-Vis (DMF) λ_{max} nm: 257 (π→π*), 324 (n→π*), 596, 674 (d→d). IR (KBr, cm^{-1}): 3488 ν(N-H), 3398 ν(O–H), 2934 ν(C-H), 1620 ν(C=N), 823 ν(H_2O), 622 ν(M-N), 488 ν(M-O). Elemental analysis for $C_{36}H_{40}N_8O_9S_2Ni$ (%): found C 50.65, H 4.71, N 13.30; calculated C 50.77, H 4.74, N 13.16, Mol. mass (g/mol): 850.93.

3.3.20. Synthesis of $Cu(Ampp\text{-}Sn)_2(H_2O)_2{\cdot}H_2O$

To a solution of Ampp-Sn (2 mmol, 0.74 g) in hot ethanol (40 mL) was added in drops aqueous solution of $Cu(CH_3COO)_2{\cdot}H_2O$ (1 mmol, 0.20 g) while stirring under reflux and followed by the addition of NaOH (2 mmol, 0.08 g) to precipitate the metal complex. After 4 h of reflux, the green solid was filtered, washed with ethanol/water (1:1), dried at room temperature, and stored over fused $CaCl_2$. Yield: 83%. M.p.: 298−299°C. Molar cond. (10^{-3} M in DMF): 7.04 ohm^{-1} cm^2 mol^{-1}. μ_{eff}(B.M.): 1.90. UV-Vis (DMF) λ_{max} nm: 261 (π→π*), 365 (n→π*), 618, (d→d). IR (KBr, cm^{-1}): 3482 ν(N-H), 3392 ν(O–H), 2922 ν(C-H), 1617 ν(C=N), 850 ν(H_2O), 628 ν(M-N), 498 ν(M-O). Elemental analysis for $C_{36}H_{40}N_8O_9S_2Cu$ (%): found C 50.44, H 4.59, N 13.21; calculated C 50.48, H 4.71, N 13.09, Mol. mass (g/mol): 855.78.

3.3.21. Synthesis of $Mn(Bmpp\text{-}Sn)_2(H_2O)_2$

To a solution of Bmpp-Sn (2 mmol, 0.87 g)in hot ethanol (40 mL) was added in drops aqueous solution of $MnCl_2{\cdot}6H_2O$ (1 mmol, 0.23 g) while stirring under reflux and followed by the addition of NaOH (2 mmol, 0.08 g) to precipitate the metal complex. After 4 h of reflux, the golden-yellow solid was filtered, washed with ethanol/water (1:1), dried at room temperature, and stored over fused $CaCl_2$. Yield: 82%. M.p.: 180−182°C. Molar cond. (10^{-3} M in DMF): 8.19 ohm^{-1} cm^2 mol^{-1}. μ_{eff}(B.M.): 5.82. UV-Vis (DMF) λ_{max} nm: 277 (π→π*), 378 (n→π*), 424, 589 (d→d). IR (KBr, cm^{-1}): 3483 ν(N-H), 3398 ν(O–H), 2938 ν(C-H), 1623 ν(C=N), 844 ν(H_2O), 619 ν(M-N), 470

ν(M-O). Elemental Analysis for $C_{46}H_{42}N_8O_8S_2Mn$ (%): found C 57.72, H 4.14, N 11.22; calculated C 57.91, H 4.44, N 11.75, Mol. mass (g/mol): 953.19.

3.3.22. Synthesis of $Co(Bmpp\text{-}Sn)_2(H_2O)_2{\cdot}H_2O$

To a solution of Bmpp-Sn (2 mmol, 0.87 g) in hot ethanol (40 mL) was added in drops aqueous solution of $CoCl_2{\cdot}4H_2O$ (1 mmol, 0.20 g) while stirring under reflux and followed by the addition of NaOH (2 mmol, 0.08 g) to precipitate the metal complex. After 4 h of reflux, the pale-pink solid was filtered, washed with ethanol/water (1:1), dried at room temperature, and stored over fused $CaCl_2$. Yield: 89%. M.p.: 144−146°C. Molar cond. (10^{-3} M in DMF): 10.30 ohm^{-1} cm^2 mol^{-1}. μ_{eff}(B.M.): 4.46. UV-Vis (DMF) λ_{max} nm: 262 (π→π*), 376 (n→π*), 408, 540 (d→d). IR (KBr, cm^{-1}): 3492 ν(N-H), 3398 ν(O–H), 2925 ν(C-H), 1618 ν(C=N), 849 ν(H_2O), 624 ν(M-N), 489 ν(M-O). Elemental analysis for $C_{46}H_{44}N_8O_9S_2Co$ (%): found C 56.33, H 4.92, N 11.16; calculated C 56.60, H 4.55, N 11.49, Mol. mass (g/mol): 975.20.

3.3.23. Synthesis of $Ni(Bmpp\text{-}Sn)_2(H_2O)_2{\cdot}H_2O$

To a solution of Bmpp-Sn (2 mmol, 0.87 g)in hot ethanol (40 mL) was added in drops aqueous solution of $NiCl_2{\cdot}4H_2O$ (1 mmol, 0.20 g) while stirring under reflux and followed by the addition of NaOH (2 mmol, 0.08 g) to precipitate the metal complex. After 4 h of reflux, the pale-green solid was filtered, washed with ethanol/water (1:1), dried at room temperature, and stored over fused $CaCl_2$. Yield: 85%. M.p.: 190−192°C. Molar cond. (10^{-3} M in DMF): 11.62 ohm^{-1} cm^2 mol^{-1}. μ_{eff}(B.M.): 2.89. UV-Vis (DMF) λ_{max} nm:

278 (π→π*), 377 (n→π*), 410, 683 (d→d). IR (KBr, cm^{-1}): 3489 ν(N-H), 3390 ν(O–H), 2935 ν(C-H), 1619 ν(C=N), 849 ν(H_2O), 625 ν(M-N), 486 ν(M-O). Elemental Analysis for $C_{46}H_{44}N_8O_9S_2Ni$ (%): found C 57.01, H 4.29, N 11.30; calculated C 56.62, H 4.55, N 11.49, Mol. mass (g/mol): 974.96.

3.3.24. Synthesis of $Cu(Bmpp\text{-}Sn)_2(H_2O)_2$

To a solution of Bmpp-Sn (2 mmol, 0.87 g) in hot ethanol (40 mL) was added in drops aqueous solution of $Cu(CH_3COO)_2{\cdot}H_2O$ (1 mmol, 0.20 g) while stirring under reflux and followed by the addition of NaOH (2 mmol, 0.08 g)to precipitate the metal complex. After 4 h of reflux, the pale-green solid was filtered, washed with ethanol/water (1:1), dried at room temperature, and stored over fused $CaCl_2$. Yield: 92%. M.p.: 238−240°C. Molar cond. (10^{-3} M in DMF): 6.41 ohm^{-1} cm^2 mol^{-1}. μ_{eff}(B.M.): 1.93.UV-Vis (DMF) λ_{max} nm: 273 (π→π*), 378 (n→π*), 442, 751 (d→d). IR (KBr, cm^{-1}): 3498 ν(N-H), 3399 ν(O–H), 2935 ν(C-H), 1617 ν(C=N), 840 ν(H_2O), 623 ν(M-N), 484 ν(M-O). Elemental Analysis for $C_{46}H_{42}N_8O_8S_2Cu$ (%): found C 57.19, H 4.31, N 11.32; calculated C 57.39, H 4.40, N 11.65, Mol. mass (g/mol): 961.80.

3.4. Melting Point

The Gallenkamp melting point apparatus was used for all synthesized compounds in this study.

3.5. Elemental Analysis

The composition of a compound often expressed in terms of mass percentage can be determined by the quantitative and qualitative elemental analysis. The information obtained helps for the proposition of the structure of an unknown compound. It also gives some information on the purity of the compound. This method utilizes the combustion analysis. When the test compound is burned in excess of oxygen, the carbon dioxide, water, and nitric oxide fractions are trapped and used to calculate the individual elemental component. The CHN elemental analysis of the synthesized ligands and metal complexes in this investigation were determined on a LECO.TRUSpec Micro CHNS elemental analyzer. The correctness of proposed structure and purity is when there is not more than 0.5% difference between the calculated theoretical mass percentage of the synthesized compounds components and the found elemental analysis values.

3.6. Conductivity Measurements

Conductivity measurement can give some information on the behavior of metal complexes in solutions. Their structures in solution can thus be related to that in solid state. The theory relates the conductivity values of the metal complexes to the electrolyte type (71CCR81). The conductivity measurement was determined using CON 6/TDS 6 hand–held conductivity/TDS meter.

3.7. Infrared Spectroscopy

The theory of infrared spectroscopy is based on exchange of the vibrational energy between a molecule and the electromagnetic field. This occurs when $h\nu = \Delta E$, where ΔE is the difference between initial and final quantized states. This method of characterization is usually employed to determine the formation, breaking or/and modification of functional groups bonds. The IR spectra of established standard compounds are compared with the spectra of the newly obtained molecule to determine and ascertain changes. Infrared absorption spectra usually cover the range 200-4000 cm^{-1}. Most times infrared spectrometers provide the spectrum in the form of % transmittance vs. wavenumber cm^{-1}. Transmittance spectra give an idea of how weak or strong absorptions in the spectrum are and it is dependent on the concentration of sample compound. Hence spectra of the same sample recorded at different concentrations display different relative peak heights. Solid samples are usually prepared in KBr disc while liquid samples in Nujol mull and mounted using a NaCl window. In this study IR spectra were measured as KBr pellets (4000–370 cm^{-1}) on a Perkin-Elmer Model System 2000 FTIR spectrophotometer ensuring that the pellets are moisture-free.

3.8. Electronic (UV-Vis) Spectroscopy

Transition metal complexes often have absorption bands displayed at the visible region of the electronic spectra which is usually a result of the d-d electron transfer (an excitation only due to the transition metal d-orbitals)

or/and charge-transfer transitions. When there is more than one electron in the d orbital of a transition metal complex or ion, there is more than one d-d transitions. This is because the electrons feel each others' presence and interacts with one another, hence repel each other. In the presence of charge transfer in a ligand field, more distinct terms are possible leading to many possible transitions (10MI1). In this study, electronic spectra of metal complexes and ligands were recorded on a Perkin-Elmer Lambda 25 spectrophotometer.

3.9. NMR Spectroscopy

The technique of characterization has been used to deduce the molecular component and structure of organic and inorganic samples, hence giving information on the purity of the sample compound. For an unknown compound, it can help matching its molecular composition with spectral libraries and proposing possible structures. The theory is based on the fact that the molecules have many nuclei, ^{1}H and ^{13}C inclusive, and behave as a magnet moving randomly about an axis because they have spin and are electrically charged. In the presence of an external magnetic field, an energy transfer is established between the base energy to another higher energy level, causing the nuclei to spin flip. The nuclei are said to be in resonance with the applied radiation when this spin flip takes place. This energy transfer process occurs at a wavelength corresponding to radio frequencies and when the spin returns to its base level, energy is emitted at the same frequency. The signal

that matches this transfer is measured and processed into an NMR spectrum representing the nucleus concerned. ^{1}H and ^{13}C NMR spectra in deuterated DMSO were recorded on a Bruker 600 MHz Avance II NMR spectrophotometer with residual protons of deuterated DMSO as internal standards (DMSO-D_6 2.5 ppm; $CDCl_3$ 7.26 ppm) using trimethylsilane TMS as reference point. Chemical shifts are given in ppm (δ scale).

3.10. Mass Spectroscopy

The property of mass to charge ratio of ions is used to identify and then quantify molecules in both simple and complex mixtures in a characterization technique known as mass spectroscopy. This technique was developed for measuring elemental molar atomic masses and the natural abundance of specific isotopes almost a century back (88MI1). It was first used in biological sciences to trace heavy isotopes (04BMB93) and in proteomics, the study of proteins in biological systems (05NRM577, 10NBT695), which have been enabled by the development of macromolecule ionization methods, including electrospray ionization (ESI) and matrix-assisted laser desorption/ionization (MALDI) (81NAT270, 89SCI64, 90BBR686). A more robust ionization method is the atmospheric-pressure chemical ionization (APCI). Mass spectra for ligands were determined by Bruker micrOTOF-Q II 10390 mass spectrometer. All the ligands were analyzed with ACPI using a direct insertion probe (DIP). An external calibration with sodium formate was performed to attain the correct accurate mass.

3.11. Magnetic Susceptibility Measurements

Unpaired electrons of paramagnetic species can be attracted by a magnetic field. Magnetic susceptibility is a property that measures the force with which magnetic field attracts or repels. The degree of this attraction can be measured by calculating magnetic moment. In other words, magnetic moment of a compound is related to the number of unpaired electrons it has. The electronic spectra of transition metal complexes can be studied by the magnetic moment measurement using the method of Guoy which is still the simplest. It was invented by Louis Georges Gouy, it determines the magnetic susceptibility of molecules by measuring the obvious changes in the mass of the molecule as it is repelled or attracted by the poles of an external magnetic field (68PHE272). The unpaired electron spinning of the paramagnetic d-block ions creates a magnetic field. The magnetic susceptibility, μ, as a result of the spinning of the unpaired electrons is given by the spin-only formula:

$$\mu(spin - only) = \sqrt{n(n+2)}$$

Here, n is the number of unpaired electrons. This spin-only method of calculating magnetic moment in BM (Bohr Magneton) usually works well with the first row transition metals. Magnetic property of d^n configuration numbers of transition metals under investigation is displayed in Table 1.

Table 1. Magnetic Properties of d^n Configurations of Interest

Metal ion	d^n configuration	μ_{eff} (spin-only)	μ_{eff} (observed)
Mn^{2+}	d^5	5.92	5.7-6.0
Co^{2+}	d^7	3.87	4.3-5.2
Ni^{2+}	d^8	2.83	2.9-3.9
Cu^{2+}	d^9	1.73	1.9-2.1

There could also be a d-orbital contribution to the overall magnetic moment which is usually controlled by the spin-orbit coupling constant applied in another expression. Magnetic susceptibility measurement was carried out on a Sherwood Scientific magnetic susceptibility balance with powder samples of complexes at room temperature and diamagnetism corrections were estimated from Pascal's constants.

3.12. X-Ray Crystallography Analysis

Atoms are arranged in a periodic manner in what is known as the crystal structure of that molecule. X-ray crystallography can give information in detail of a three-dimensional structure of compounds. For a successful x-ray diffraction, the single crystal of the molecule must be grown, which is mounted on the x-ray diffractometer with the help of an x-ray source and a detector, and the three-dimensional structure is obtained. Single crystal x-ray diffraction studies were performed at 200 K using a Bruker Kappa Apex II diffractometer with graphite monochromator, Mo Kα radiation (λ = 0.71073 Å). APEXII (07MI1) was used for data collection and SAINT (07MI1) for cell refinement and data reduction. The structure was solved by direct

methods using SHELXS-97 (08AX(A)112) and refined by least-squares procedures using SHELXL-97 (08AX(A)112) with SHELXLE (11JAX1281) as a graphical interface. Platon (03JAX7) and Ortep-3 (97AJC565, 08JAX466) were used to prepare material and diagrams respectively.

The carbon-bound H atoms were placed in calculated positions (C-H 0.95 Å for the aromatic carbon atoms and C-H 0.98 Å for the methyl group) and were included in the refinement in the riding model approximation, with *U*(H) set as1.2*U*~eq~(C). The H atoms of the methyl group were allowed to rotate with a fixed angle around the C—C bond to best fit the experimental electron density (HFIX 137 in the SHELXprogram suite (08AX(A)112), with U(H) set to 1.5*U*~eq~(C)). The nitrogen-bound H atoms were located on a difference Fourier map and refined freely with isotropic parameters.

3.13. Thermogravimetric analysis

The change in the physical and chemical properties of compounds as a function of increasing temperature at a selected constant heating rate can be monitored and measured in a thermal analysis process known as thermogravimetric analysis(TGA). Molecular structures of materials can be predicted with TGA, which is usually used to corroborate proposed structure from spectroscopic and other characterization techniques. This is achievable by way of measuring the organic and inorganic (ash content) of the molecule through decomposition patterns. The instrument is continuously weighing and recording the mass of the pre-weighed test sample as the temperature

increases at a specific heating rate. A plot of temperature of the decompositions *versus* percentage mass loss gives a TGA thermogam. The TGA curve is usually compared with the DTG which gives information about the major decomposition points and also to what is attributed to the decomposition. Thermal analyses were done on a NETZSCH STA 449 C instrument at a temperature range of 20–900 ^{o}C with a heating rate of 15^{o}Cmin^{-1} in nitrogen gas.

3.14. Antibacterial Assay

The concept of antimicrobial assay has been highlighted in the previous chapter. Presented herein is the detailed procedure employed for this investigation. *In-vitro* antibacterial activity of the synthesized Schiff bases and their transition metal complexes were screened against Gram positive *Staphylococcus aureus*, *Bacillus pumilus* and Gram negative *Proteus vulgaris*, *Aeromonas hydrophila* bacterial isolates at 40 mg/mL concentrations in DMSO using the Kirby-Bauer disc diffusion technique based on the size of inhibition zone formed around the paper discs with some modifications (96AJP493).

3.14.1. Preparation of Nutrient Broth

Following the preparatory standard, 16 g of nutrient broth was completely dissolved in 1 L of distilled water. The prepared solution was dispensed in test tubes with a cork and autoclaved at 160^{o}C for 1h.

Table 2. Composition of Nutrient Broth

Meat extract	1.0
Yeast extract	2.0
Peptone	5.0
Sodium chloride	8.0
pH	7.1 ± 0.2

3.14.2. Preparation of Mueller–Hinton Agar

Also with standard method, 38 g of the solid Mueller–Hinton agar was dissolved in 1 L of distilled water while stirring and heated to boil. The Mueller–Hinton agar solution was dispensed into McCartney bottles and autoclaved for 1 h at 160^{o}C.

Table 3. Composition of Mueller–Hinton Agar

Meat infusion	5.0
Casein hydrolysate	17.5
Soluble starch	1.5
Agar	14.0
pH	7.4 ± 0.2

3.14.3 Preparation of Test Samples

Test samples (Schiff bases, metal complexes, and the standard drug, chloramphenicol), 400 mg, was each dissolved in 10 ml of DMSO to form a stock solution of 40 mg/mL.

Bacterial isolates were grown in freshly prepared nutrient broth media to obtain a minimum of 0.1 optical density OD suitable for screening. 0.1mL of test bacteria was spread over the surface of solidified 20 mL Mueller-Hinton agar in Petri plates using a sterilized spreader. Pre-sterilized filter paper

discs having a diameter of 6 mm which were impregnated into prepared solutions of synthesized test samples solutions, were placed in the inoculated Petri plates ensuring a reasonable equidistance from each other. Filter paper disc treated with DMSO was used as control while antibacterial chloramphenicol served as a standard drug and was used as a reference to compare the potency of the tested compounds under the same conditions. The Petri dishes were left for a few hours in the refrigerator for pre-diffusion and finally transferred to an incubator at 37^{o}C for 24 h. This procedure was performed in triplicates. The bactericidal activities were determined by measuring the diameter of the zones showing complete inhibition of bacterial growth in millimeters minus the diameter of the filter paper disc and values calculated as mean of triplicates.

3.15. Antioxidant assay

Free radical scavenging activity of Schiff bases and its metal complexes was tested against the free stable radical of 1,1-diphenyl-2-picrylhydrazyl (DPPH), employing the method of Blois (58NAT1199) with few modifications. A solution of 0.1 mmol DPPH in methanol was prepared, and 1 mL of this solution was added to 3 mL of the prepared solutions of the test compounds in a mixture of DMSO and methanol in a mole ratio of 9:1, respectively at different concentrations (0.13, 0.25 and 0.50 mg/mL). The same procedure was carried out for standard drug, ascorbic acid and an equal volume of a dissolving solvent as control. The mixture was shaken vigorously and al-

lowed to stand at room temperature in the dark for 30 min. With the use of a spectrophotometer at a wavelength of 517 nm, the absorbance was measured. The capability of synthesized compounds to scavenge DPPH radical was calculated using the expression:

$$Scavenging\ activity\ (\%) = \frac{A_0 - A_i}{A_0} \times 100$$

Here A_0 is the absorbance with control reaction sample and A_i is the absorbance with test samples including that of a standard drug.

4. Results and Discussion

4.1. Acetylpyrazolone-Based Phenylhydrazone Schiff Bases and their Metal Complexes

The water soluble phenylhydrazine $PhNHNH_2$ with a molecular formula $C_6H_8N_2$ and of molar mass 108 g/mol exists as a golden yellow oily liquid at room temperature. Analytically, it can be determined in aqueous solution using its reducing ability. It reduces Cu(II) to Cu(I), and this has been used as a basis for spectroscopic analytical method for measuring colored complexes (88AL633, 88AL1917), although the method is not specific as it can be due to other reducing compounds (88AL633). Phenylhydrazine turns reddish-brown in the presence of oxygen due to auto oxidation, which is enhanced by heating.

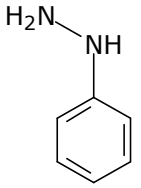

76

Phenylhydrazine **76** has been used mainly as a chemical intermediate in the pharmaceutical, agrochemical and chemical industries. They form important compounds in the form of Schiff bases, generally referred to as hydrazones. Two new Schiff base ligands, 4-benzoyl-3-methyl-1-phenyl-2-pyrazolin-5-one phenylhydrazone Bmpp-Ph and 4-acetyl-3-methyl-1-phenyl-2-pyrazolin-5-one phenylhydrazone Ampp-Ph alongside their Mn(II), Co(II),

Ni(II) and Cu(II) complexes have been characterized, applied, and discussed accordingly in this chapter.

4.1.1. Synthesis

Synthesized acetyl and benzoyl pyrazolone Schiff base precursors were reacted with phenylhydrazine in a condensation reaction to afford the Schiff bases 4-acetyl-3-methyl-1-phenyl-2-pyrazolin-5-one Phenylhydrazine and 4-benzoyl-3-methyl-1-phenyl-2-pyrazolin-5-one Phenylhydrazine (eq. 3).

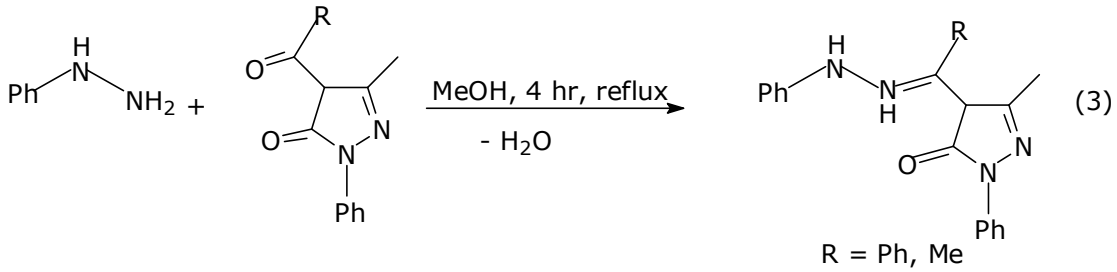

(3)

They exist in hygroscopic solid form, stable at room temperature and are soluble in methanol, ethanol and most common organic solvents. Schiff bases were precipitated in good yield and purity was monitored by TLC after washing continuously with solvents used for synthesis, which was corroborated by a sharp melting point range. Due to their favorable solubility the single crystal structure of Bmpp-Ph has been obtained but not for Ampp-Ph, even with appropriate mixed solvent systems. They have been fully characterized by elemental analysis, IR, UV-VIS, ^{1}H and ^{13}C NMR, mass spectroscopy. In addition, X-ray crystallographic analysis is available for Bmpp-Ph.

All the metal complexes were synthesized by the treatment of Bmpp-Ph or Ampp-Ph with the appropriate metal salt in a general synthetic scheme

formulated as eq. 4. They are in solid form and in unlike colours. The complexes are generally insoluble in water, ethanol and in most non-coordinating solvents but completely soluble in polar solvents with strong donor strength like DMF and DMSO, and as such attempts to grow their single crystals were unsuccessful. Their molar conductance values inferred non–electrolyte behavior in DMF (71CCR81, 75MI1).

$$MX_2 \cdot nH_2O + 2L \xrightarrow{EtOH/H_2O} ML_2(H_2O)_2 \cdot nH_2O \quad (4)$$

L = Bmpp-Ph or Ampp-Ph; M = Mn, Co, Ni, X = Cl; M = Cu, X = MeCOO

4.1.2. Elemental Analysis

The percentage CHN composition data of Bmpp-Ph, Ampp-Ph and their metal complexes found, were in agreement with calculated values according to proposed structures. Octahedral metal complexes formed with the corresponding Schiff base are proposed. The metal ion is coordinated with two molecules each of the Schiff base and two molecules of water to complete its octahedral geometry. Some of their physical properties, melting point range, electrical molar conductivities, elemental composition and percentage yields are presented in the experimental section of chapter 3.

4.1.3. ^{1}H and ^{13}C NMR Spectroscopy

^{1}H and ^{13}C NMR spectra of the Schiff bases, Bmpp-Ph and Ampp-Ph (Fig.1-4) were recorded in DMSO-d_6 solutions, and chemical shift assigned with trimethylsilane TMS as an internal reference. The ^{1}H-NMR spectra displayed two broad peaks downfield which were almost unnoticeable at around

12.2 and 9.5 ppm integrating for approximately one proton each assigned to the hydrogen atoms of the –NH and the C=NH azomethine group respectively in Bmpp-Ph.

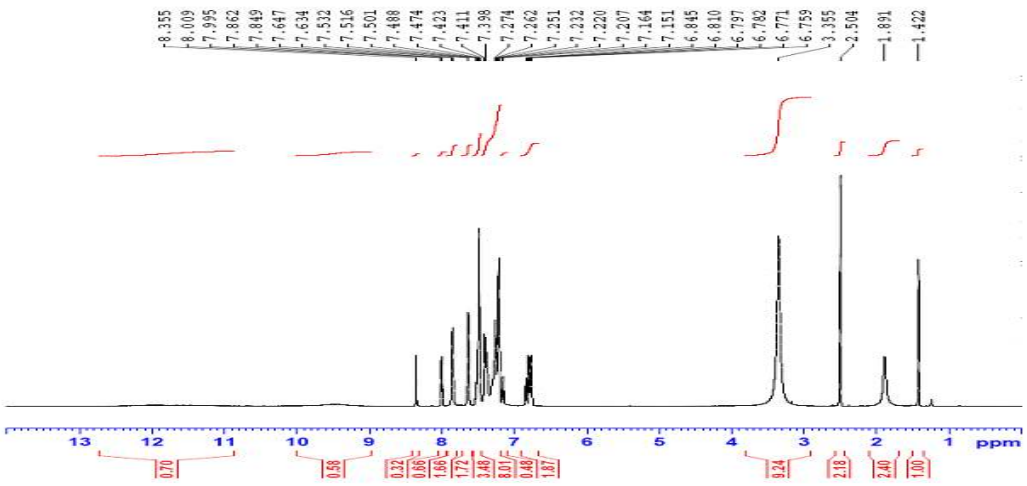

Figure 1. ^{1}H NMR Spectrum of Bmpp-Ph

In Ampp-Ph, the proton of the–NH showed chemical shift at 12.4 ppm and the azomethine C=NH proton at a lower chemical shift at 8.6 ppm, both integrating for one proton each. The aromatic protons H–Ar were observed as a multiplet at 6.8–8.4 and at 6.8-8.0 in Bmpp-Ph and Ampp-Ph respectively. The resonating peak in the aliphatic region with a chemical shift of 1.9 ppm in Bmpp-Ph and at 2.4 ppm in Ampp-Ph spectra is due to the methyl protons attached to the pyrazolone ring each integrating for approximately three protons. The peak at around 3.4 ppm in both spectra integrating at an unusually large value is due to the presence of acetone probably within the NMR tube. This peak was peculiar to all the spectra.

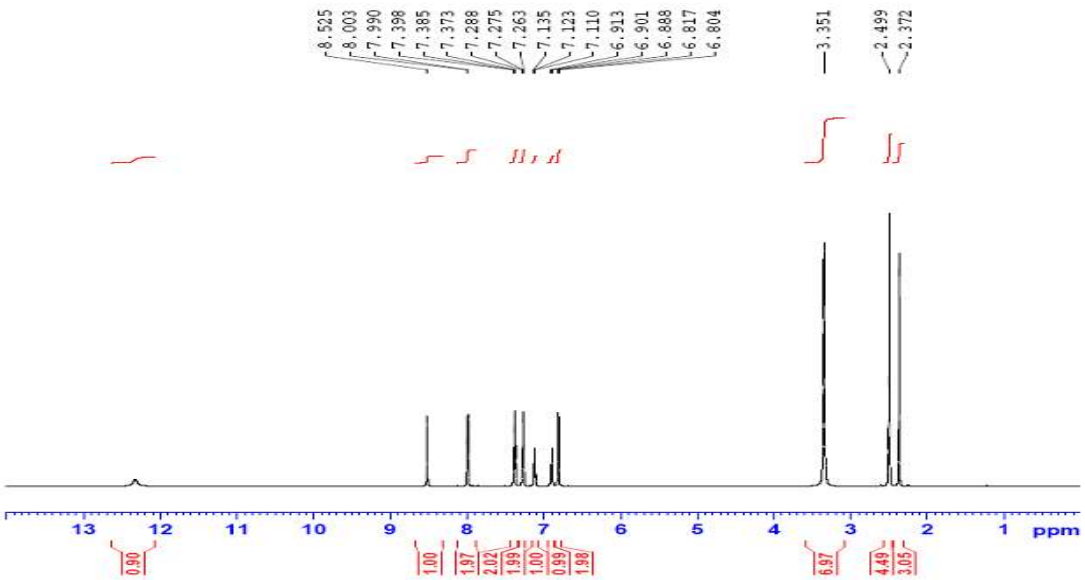

Figure 2. ^{1}H NMR Spectrum of Ampp-Ph

^{13}C NMR of Bmpp-Ph and Ampp-Ph in DMSO-d_6 solution displayed clear signals that add value to information obtained from ^{1}H NMR. The signals at 168.0 ppm in Bmpp-Ph may be assigned to carbon of the pyrazolone bonded to oxygen C=O, and the signal at 165.5 ppm is due to the azomethine carbon atom C=N (10COC281).

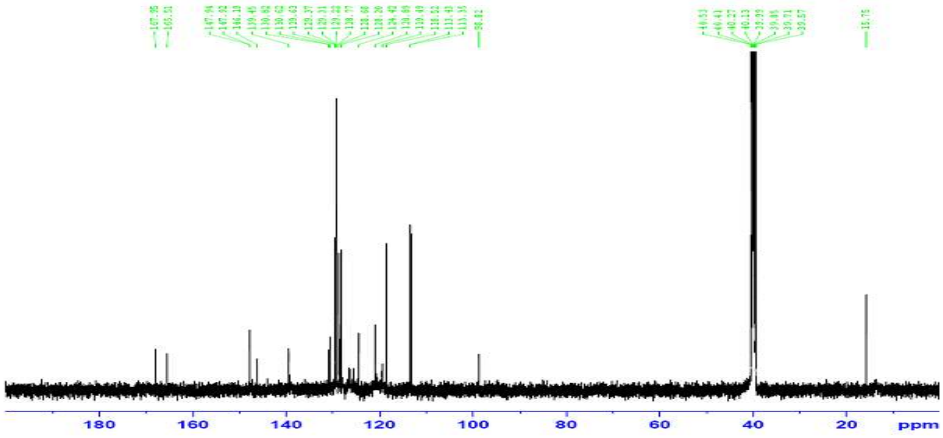

Figure 3. ^{13}C NMR Spectrum of Bmpp-Ph

These signals were observed at 168.7 and 165.5 ppm respectively in Ampp-Ph. Aromatic ring carbon atoms of Bmpp-Ph resonated at 115.3–148.0 ppm in Bmpp-Ph and at 116.5–148.0 ppm in Ampp-Ph. Signals due to pyrazolone methyl carbon resonates at 15.8 ppm in Bmpp-Ph and at 17.3 ppm in Ampp-Ph. The second methyl group carbon in Ampp-Ph was observed at 14.6 ppm.

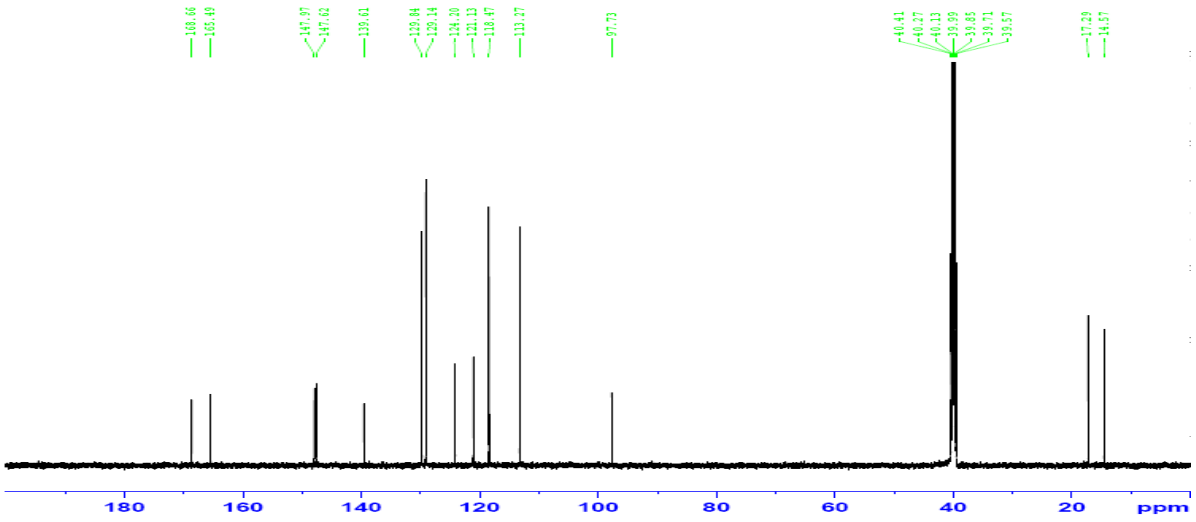

Figure 4. ^{13}C NMR Spectrum of Ampp-Ph

4.1.4. Mass Spectroscopy

The mass spectra of Schiff bases were investigated to further justify results obtained from NMR spectroscopy. Molecular ion peak M^+ was observed at *m/z* 369 in Bmpp-Ph (Fig.5) and at *m/z* 307 in Ampp-Ph(Fig.6) corresponding to $[M + H]^+$.

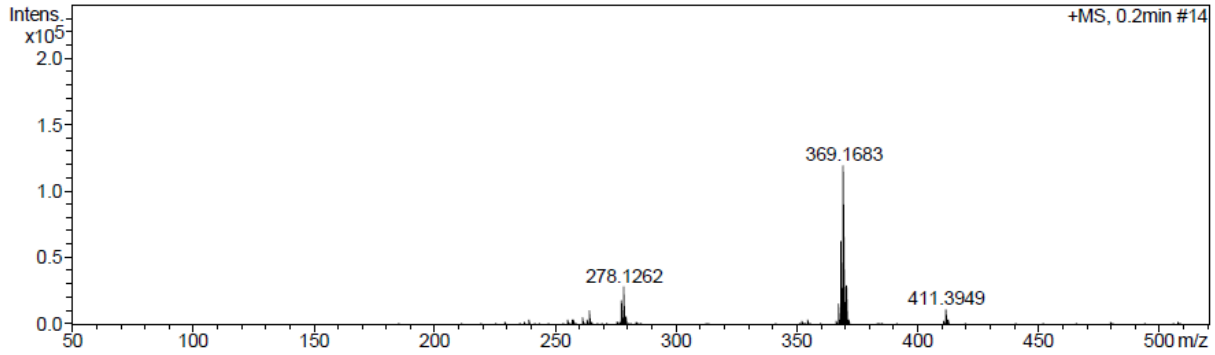

Figure 5. Mass Spectrum of Bmpp-Ph

Fragmentation of the corresponding Schiff base precursors (Bmpp and Ampp) is peculiar with the mass spectrum of both Schiff bases. These peaks were seen at *m/z* 278 in Bmpp-Ph and *m/z* 216 in Ampp-Ph (Fig.6) which agreed with theoretical mass and due to $C_{17}H_{13}N_2O_2$ and $C_{12}H_{11}N_2O_2$, respectively.

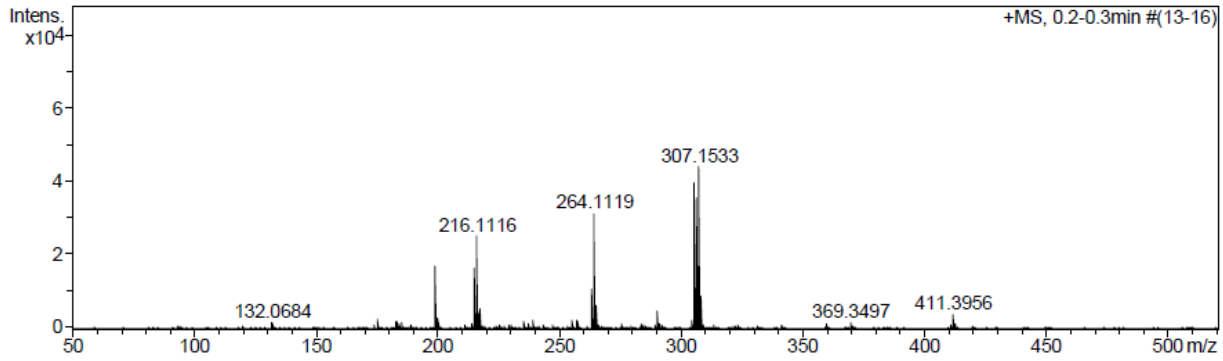

Figure 6. Mass Spectrum of Ampp-Ph

4.1.5. Infrared Spectroscopy

Relevant bands from infrared spectra of ligands and metal complexes were carefully assigned and presented in the experimental section. The possible coordination donor sites of these Schiff base ligands are the azome-

thine nitrogen, the heterocyclic pyrazolone nitrogen and the ketonic oxygen. It is proposed that the ligand bond to the metal ion in a bidentate form through the azomethine nitrogen –C=N and the ketonic oxygen –C=O. The existence of a band observed at 1634 and 1630 cm^{-1} in Bmpp-Ph and Ampp-Ph respectively due to azomethine group –C=N (78JINC793, 81D1241, 94TMC611), formed from the combination of the carbonyl carbon of the ketone and nitrogen N of the amine, peculiar to Schiff base ligands, is an evidence of the formation of the acylpyrazolone phenylhydrazone, corroborating the X-ray crystal structure of Bmpp-Ph reported (12AX(E)1280). These strong bands are modified and appeared at a significantly lower wavenumber of 1618 -1621 cm^{-1} in the spectra of the complexes indicative of the interaction of the transition metal ion, hence the coordination through the nitrogen of the azomethine. A broad band peaking at around 3491 cm^{-1} in Bmpp-Ph and at 3497cm^{-1} in Ampp-Ph corresponding to the ν(N-H) stretching vibration (01TMC131), which is due to the inter- and intramolecular hydrogen bonding were observed in the metal complexes in the range of 3493 to 3373 cm^{-1}, but also due to ν(O-H) stretching vibration associated with either the coordinated or the non-coordinated water molecule alongside ν(N-H). The coordination of the water molecule to the central ion is evident and complemented by the existence of a band in the far-infrared region at 848 - 821 cm^{-1} in the spectra of all eight metal complexes reported in this chapter (97MI1). Also, in the IR-spectra of ligands, the band vibrating at 1501 cm^{-1}

due to the ketone carbonyl C=O, and evidence of the existence of the Schiff base ligands in keto tautomer form was seen as a small band or have disappeared in the spectra of the metal complexes, an evidence that the second coordination site of the bidentate ligands is through the pyrazolone keto oxygen (00POL2599). New bands observed at the regions 641-621 cm^{-1} and 498-478 cm^{-1} may be assigned to M-N and M-O, respectively (06MOL904, 07TJC623). IR spectra of all the compounds in this study are presented in the appendix.

4.1.6. UV-Vis Spectroscopy and Magnetic Moments

The electronic spectra of all the reported metal complexes show absorption bands in the UV region due to the organic Schiff base conjugate bonds in DMF. These absorption bands, usually intense, are assigned to charge transfer from the π orbital of the donor ligand to the d orbital of the metals, d$\leftarrow\pi^*$ and inter-ligand n$\rightarrow\pi^*$ transitions (97POL1771, 09JCC156). However, the assignment of a particular band to the type of transition is not clear-cut, as quantum-mechanical calculation is needed. Also charge transfer transitions may interfere with each other hence preventing the observation of the expected transitions in the electronic spectra of compounds (93TMC221). Weak to medium intensities are peculiar for the electronic spectra of metal complexes as compared to the UV-region strong intensity bands of free Schiff base ligands. The UV-VIS absorption bands of Bmpp-Ph, Ampp-Ph and

their metal complexes have been assigned and presented in the experimental chapter.

In the electronic spectra of $Mn(Bmpp\text{-}Ph)_2(H_2O)_2{\cdot}2H_2O$ and $Mn(Ampp\text{-}Ph)_2(H_2O)_2{\cdot}2H_2O$ (Fig. 7 and 8)there is a single absorption band appearing weak at 393 and 395 nm, respectively close to the UV region. The other visible region transition bands expected of a high spin d^5 octahedral Mn(II) may have superimposed on each other and hence are not visible. It may also be worth of noting that Mn(II) complexes with a ^6S ground term cannot be made to split by the crystal field of any symmetry. Also, their pale yellow colour may be another contributing factor for this observation, which makes them show d-d transitions rarely. These bands may be assigned to $^6A_{1g}\rightarrow{}^4A_{1g}$ transition (86JA2309,94IC1875). In corroboration of the spin $3d^5$ configuration of the manganese complexes, the magnetic susceptibility measurement gavemagnetic moments of 5.63 and 5.98 BM for $Mn(Bmpp\text{-}Ph)_2(H_2O)_2{\cdot}2H_2O$ and $Mn(Ampp\text{-}Ph)_2(H_2O)_2{\cdot}2H_2O$ respectively, expected for an octahedral Mn(II) (07PJP301).

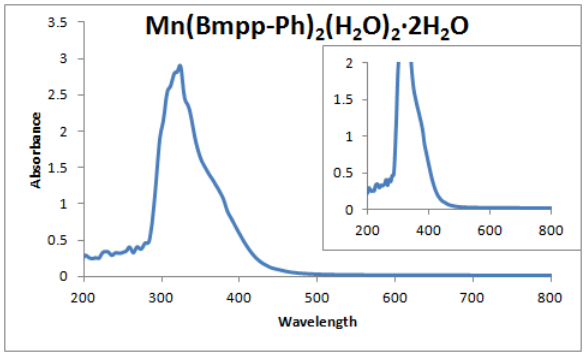

Figure 7. Electronic Spectrum of $Mn(Bmpp\text{-}Ph)_2(H_2O)_2{\cdot}2H_2O$

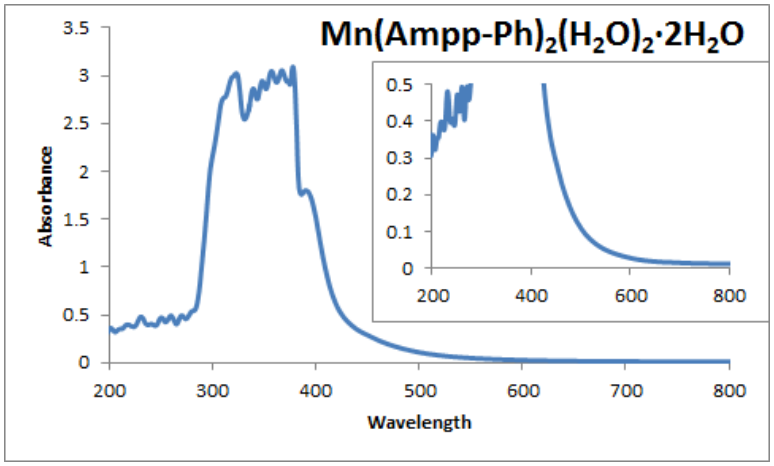

Figure 8. Electronic Spectrum of $Mn(Ampp\text{-}Ph)_2(H_2O)_2\cdot 2H_2O$

Both cobalt complexes show three d-d bands each, in the visible region (Fig.9 and 10). $Co(Bmpp\text{-}Ph)_2(H_2O)_2\cdot H_2O$ exhibits a very weak, broad and almost unnoticeable band at 554 nm, followed by a second band at 627 nm shoulder to a third band at 708 nm. The respective band positions for $Co(Ampp\text{-}Ph)_2(H_2O)_2\cdot 2H_2O$ are 390 nm, 536 nm, and 600 nm. These bands may be assigned to ($^4T_{2g}\rightarrow{}^4T_{1g}$), ($^4A_{2g}\rightarrow{}^4T_{1g}$) and ($^4T_{1g}(p)\rightarrow{}^4T_{1g}$) transitions, respectively, attributed to the octahedral Co(II) (66JIM521). Magnetic moment values of 4.45 and 4.49 BM were obtained for $Co(Bmpp\text{-}Ph)_2(H_2O)_2\cdot H_2O$ and $Co(Ampp\text{-}Ph)_2(H_2O)_2\cdot 2H_2O$ respectively, which falls within the range of 4.40 to 4.53 B.M. expected for a high-spin octahedral Co(II) with a d^7 configuration (07EQ7).

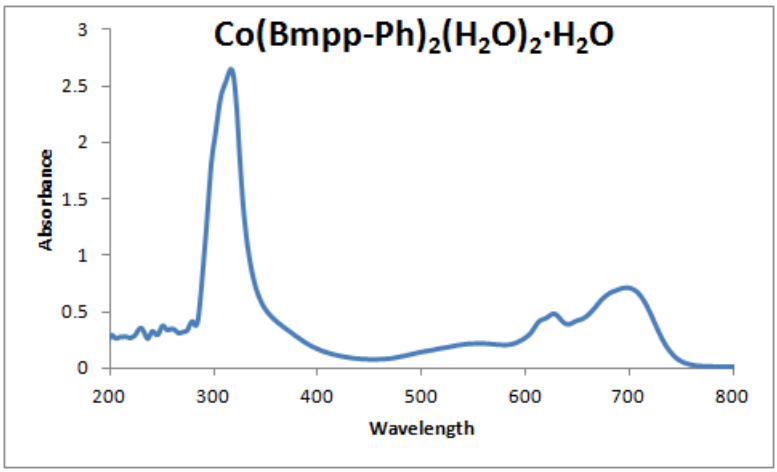

Figure 9. Electronic Spectrum of $Co(Bmpp\text{-}Ph)_2(H_2O)_2 \cdot H_2O$

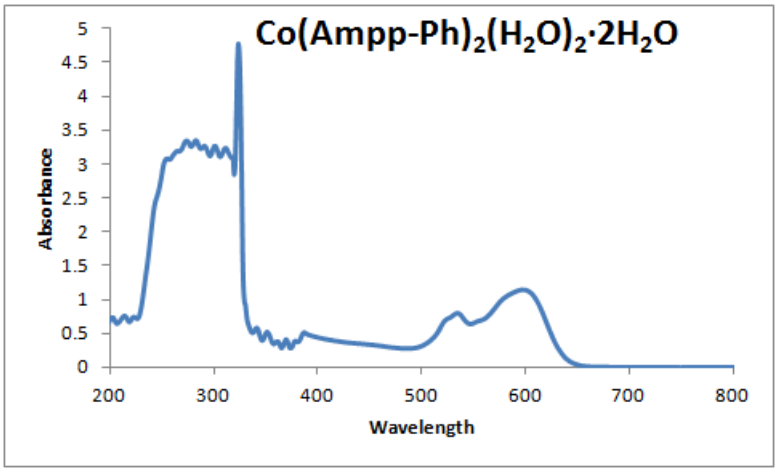

Figure 10. Electronic Spectrum of $Co(Ampp\text{-}Ph)_2(H_2O)_2 \cdot 2H_2O$

Two bands in the visible region were observed in $Ni(Bmpp\text{-}Ph)_2(H_2O)_2 \cdot 2H_2O$ at 678 nm and 808nm assigned to $^3A_{2g} \rightarrow {}^3T_{1g}(F)$ and $^3A_{2g} \rightarrow {}^3T_{2g}(F)$, respectively (Fig.11). $Ni(Ampp\text{-}Ph)_2(H_2O)_2 \cdot H_2O$ exhibited a sharp band close to the UV region at 407 nm, followed by two weak bands at 597nm and 793 nm assigned to $^3A_{2g} \rightarrow {}^3T_{1g}(p)$, $^3A_{2g} \rightarrow {}^3T_{1g}(F)$, and $^3A_{2g} \rightarrow {}^3T_{2g}(F)$ respectively. The electronic transitions of both complexes correspond to an octahedral Ni(II). The magnetic moment of 2.94 BM for Ni(Bmpp-

$Ph)_2(H_2O)_2 \cdot 2H_2O$ and 2.87 BM for $Ni(Bmpp\text{-}Ph)_2(H_2O)_2 \cdot 2H_2O$ were obtained which further supports the proposed octahedral geometry around the nickel ion in agreement with reported data (02SRI819).

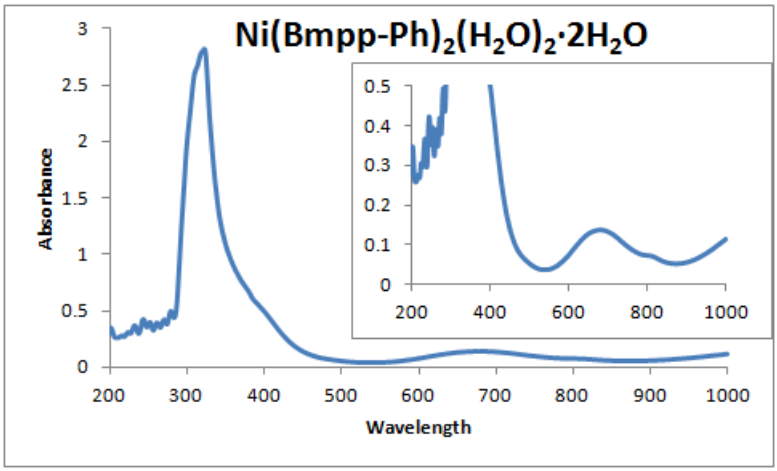

Figure 11. Electronic Spectrum of $Ni(Bmpp\text{-}Ph)_2(H_2O)_2 \cdot 2H_2O$

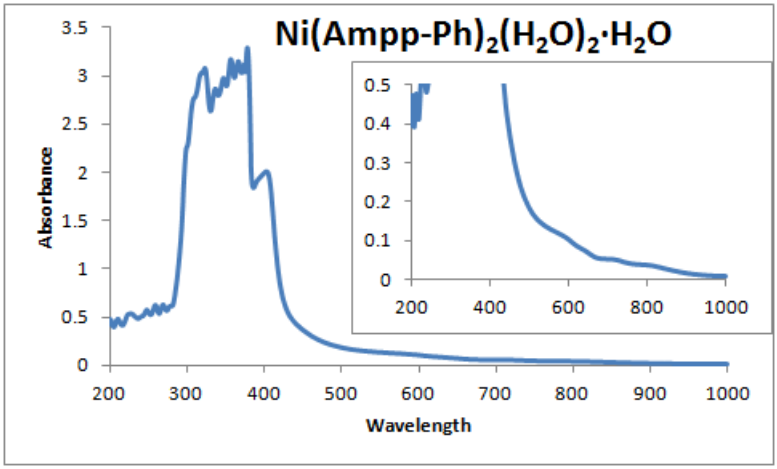

Figure 12. Electronic Spectrum of $Ni(Ampp\text{-}Ph)_2(H_2O)_2 \cdot H_2O$

A broad band corresponding to a distorted octahedral Cu(II) with a d^9 configuration at 516 nm assigned to $^2B_{1g} \rightarrow {}^2B_{2g}$ transition was observed in $Cu(Bmpp\text{-}Ph)_2(H_2O)_2 \cdot H_2O$ spectrum (Fig.13). In Fig.14, the same transition is seen as a weak but broad band at 594 nm for $Cu(Ampp\text{-}Ph)_2(H_2O)_2$

(07JIB95, 08EJC529). $Cu(Bmpp\text{-}Ph)_2(H_2O)_2 \cdot H_2O$ showed a magnetic moment of 1.94 BM and 1.93 BM for $Cu(Ampp\text{-}Ph)_2(H_2O)_2$ which corroborates the d^9 octahedral Cu(II) complex proposed (07PJP301, 12BCE95).

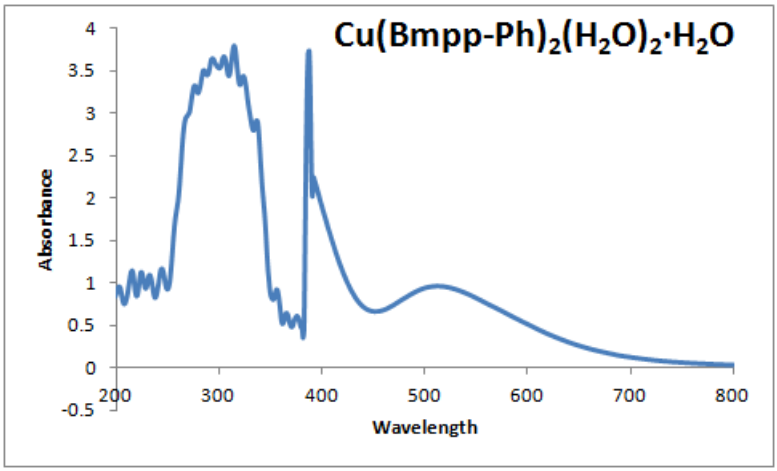

Figure 13. Electronic Spectrum of $Cu(Bmpp\text{-}Ph)_2(H_2O)_2 \cdot H_2O$

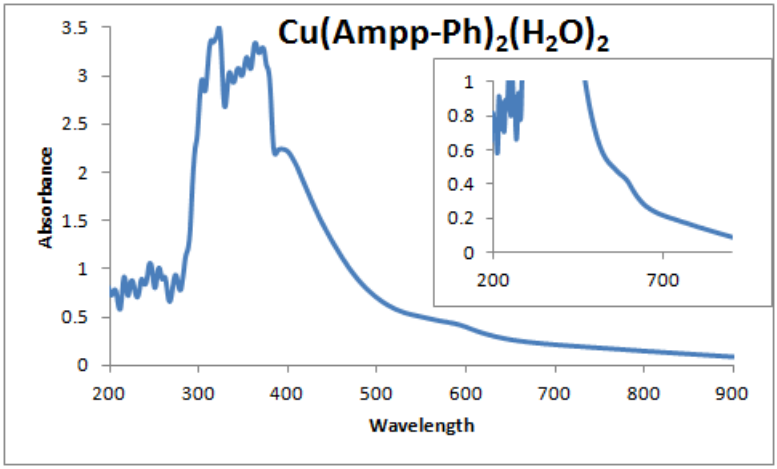

Figure 14. Electronic Spectrum of $Cu(Ampp\text{-}Ph)_2(H_2O)_2$

4.1.7. X-Ray Crystallography

Single crystal of Bmpp-Ph reported as 3-Methyl-1-phenyl-4-[(phenyl)(2-phenylhydrazin-1-yl)methylidene]-1H-pyrazol-5(4H)-one (12AX(C)o1280) was grown by slow evaporation of a methanol solution of Bmpp-Ph at room

temperature. A summary of crystal data (crystallographic and refinement parameters) is presented in Table 4. Molecular structure with the atom numbering scheme is shown in Figure 4.15. Bmpp-Ph crystallizes in a monoclinic space group $P2_1/c$.

Table 4. Crystal and Refinement Data for Bmpp-Ph

Compound	Bmpp-Sn
Formula	$C_{23}H_{20}N_4O$
Crystal colour and form	Golden Yellow/Block like
Formula mass	368.43
Crystal system	monoclinic
Space group	$P2_1/c$
a	8.6806 (2) (Å)
b	20.4319 (4) (Å)
c	10.6100 (2) (Å)
β	99.713(1)°
V	1854.83 (7) (Å^3)
Z	4
$D_{(calc)}$	1.319 (Mg cm^{-1})
F(000)	776
θ range	2.6-26.6 (°)
Crystal size	0.59 x 0.40 x 0.22 (mm)
Reflections measured	17965
Independent/observed	4607/3891
Mu(MoKa)	0.084(/mm)
Temperature	200 (K)
Parameters	262

In the crystal structure π-stacking occurs between the phenyl groups of adjacent phenylhydazone moieties with a centroid to centroid distance of 3.6512 (7) Å and slippage of 0.922 Å (Fig. 15).

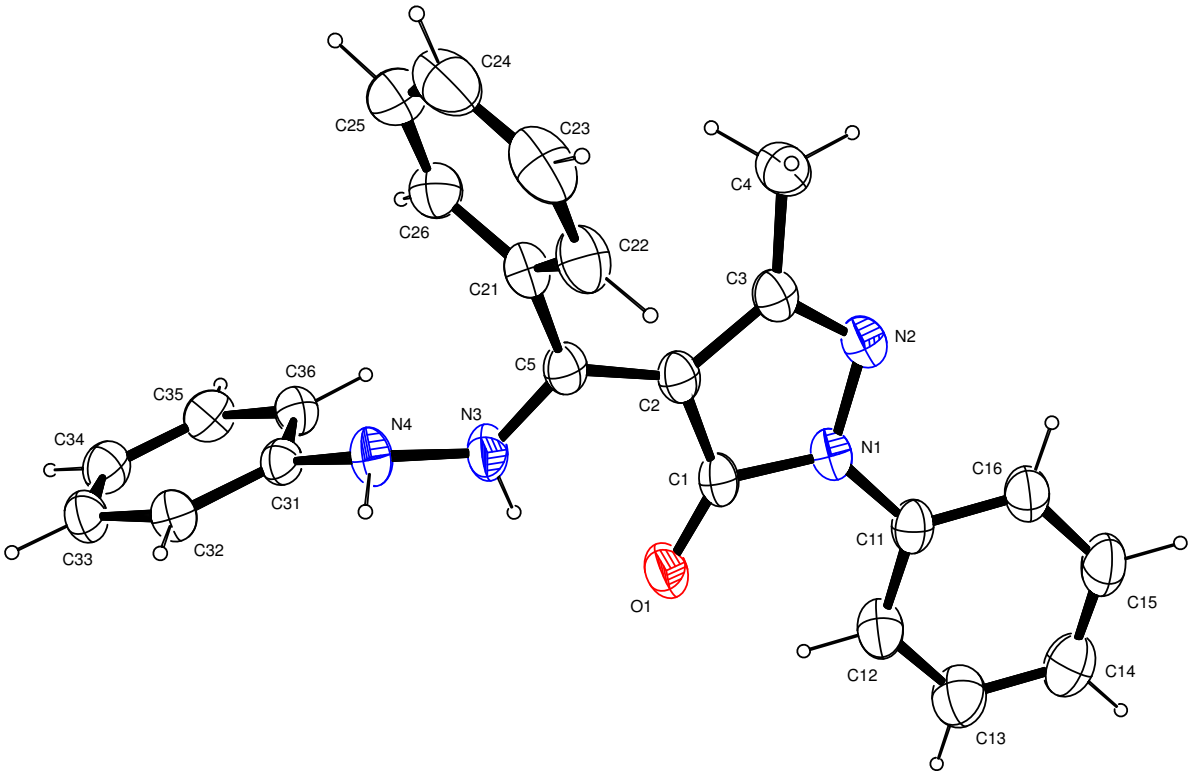

Figure 15. Molecular structure of Bmpp-Ph($C_{23}H_{20}N_4O$)

The dihedral angles formed by the least square planes between the phenyl of the phenylhydrazone group with the pyrazole and the C21-C26 aromatic ring are 85.29(6)° and 77.88(6)°, respectively. The phenyl on the pyrazole group is slight twisted out of the pyrazole plane by 12.84(4)°.Intra molecular C—H····N, C—H····O and N—H····O interactions occur while inter molecular interactions include C—H····O, phenylhydrazone π-stacking and N—H····*π* interactions (Fig.16), for clarity the N—H····π interaction is not shown). The packing diagram of Bmpp-Ph is shown in Fig.17.

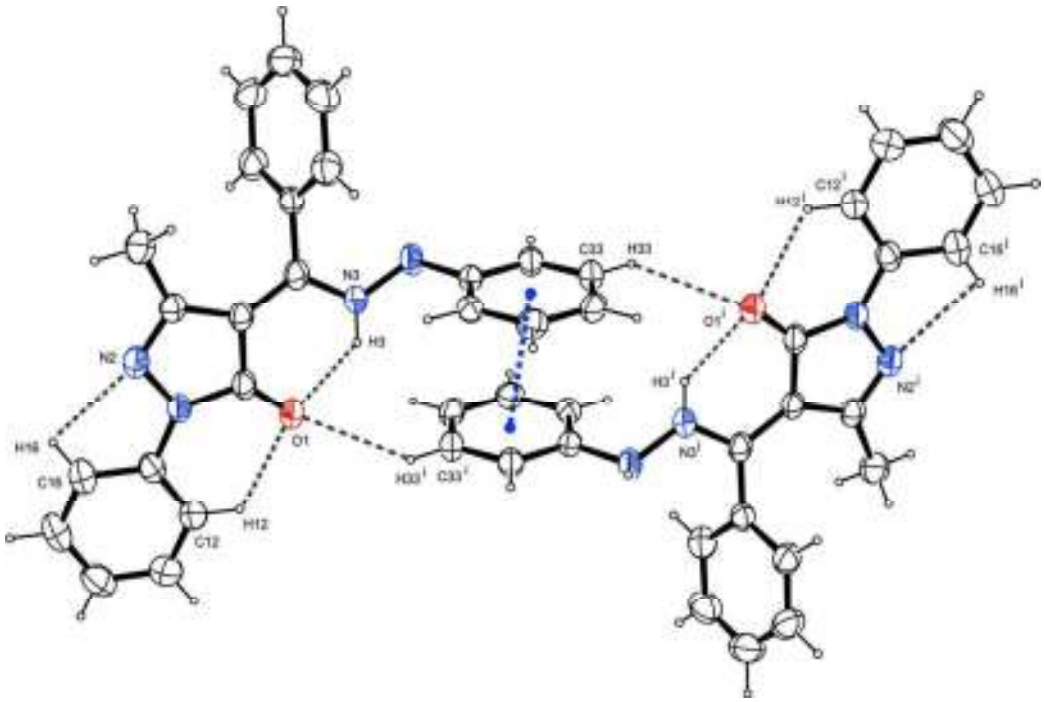

Figure 16. Inter and Intramolecular Hydrogen Bonding in Bmpp-Ph

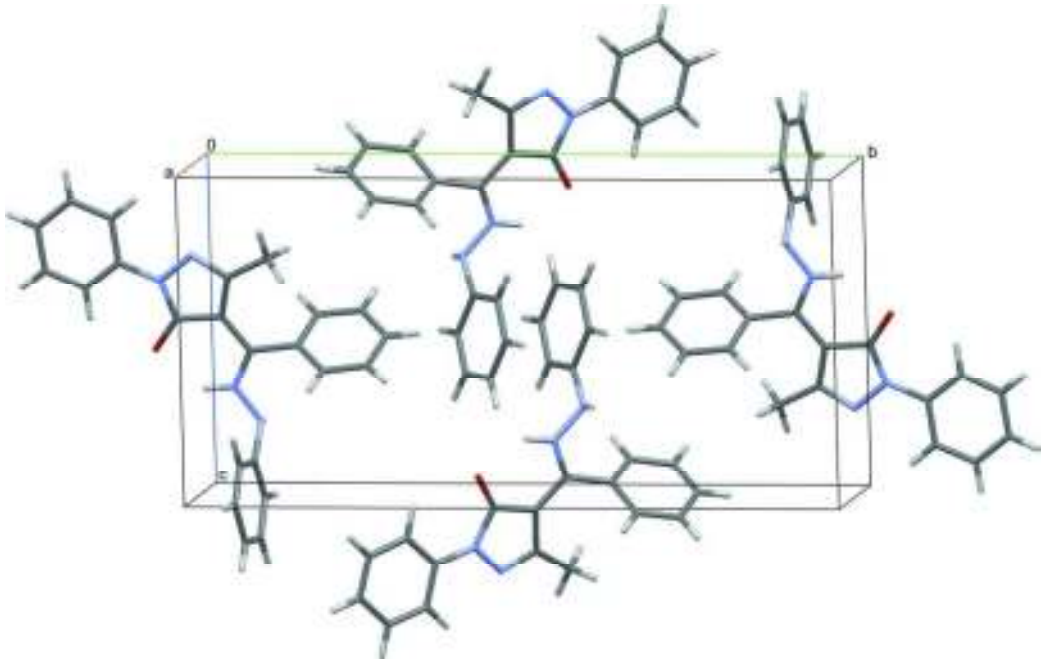

Figure 17. Molecular Packing Diagram of Bmpp-Ph

Despite the good solubility property exhibited by the acetyl derivative of acylpyrazolone phenylhydrazone Ampp-Ph, attempts to grow the crystal structure were not successful. Single crystals of an unprecedented cobalt complex with the 4-benzoyl-3-methyl-1-phenyl-2-pyrazolin-5-one (12AX(E) m1107) were isolated from an ethanolic solution of Bmpp-Ph on slow evaporation at room temperature. This has been attributed to the hydrolysis of the Schiff base ligand before chelation to metal ion occurred, as Schiff bases are known to easily undergo hydrolysis in solution to form its corresponding aldehyde or ketone (59JA475,60JA1773).

Table 5. Crystal and Refinement Data for $C_{38}H_{38}CoN_4O_6$

Compound	Bmpp-Sn
Formula	$[Co(C_{17}H_{13}N_2O_2)_2(C_2H_6O)_2]$
Crystal colour and form	Orange / Block
Formula mass	705.65
Crystal system	Triclinic
Space group	P1
a	11.0484 (3) (Å)
b	11.2282 (3) (Å)
c	14.8425 (4) (Å)
α	89.205 (1)°
β	87.678 (1)°
V	1792.56 (8) ($Å^3$)
Z	2
$D_{(calc)}$	1.307 (Mg cm^{-1})
F(000)	738
θ range	3.8–31.5 (°)
Crystal size	0.49 x 0.36 x 0.12 (mm)
Reflections measured	32307
Independent/observed	8869/7482
Mu(MoKa)	0.71073 (/mm)
Temperature	200 (K)
Parameters	108

The molecular X-ray crystal structure has been reported as bis(4-benzoyl-3-methyl-1-phenyl-1H-pyrazol-5-olato-κ^2O,O′)bis(ethanol-κO)cobalt(II) formulated as $C_{38}H_{38}CoN_4O_6$ (12AX(E) m1107). Crystal data summary is presented in Table 5.

The Co(II) complex crystallizes in a triclinic space group with two 4-benzoyl-3-methyl-1-phenyl-1*H*-pyrazol-5-olate (BMPP) and two ethanol ligands forming an octahedral geometry (Fig. 18). There are two half-molecules of the complex in the asymmetric unit with cobalt ion located at an inversion centre, and for clarity not all atoms label are shown. The ethanol ethyl groups exhibit disorder: in one complex in a ratio of 0.76:0.24 and to a much less extent in the other complex molecule (and hence not modeled). Each BMPP is deprotonated with the negative charge delocalized over O21···C21···C22···C25···O22 and O11···C11···C12···C15···O12. The average Co-O bond length is 2.042 (39) Å and 2.135 (15) Å for the BMPP and ethanol oxygen atoms respectively. The least squares dihedral angles of the BMPP phenyl groups with the pyrazole ring are 16.61(9) and 61.27(9)° for one complex and 24.64(9) and 62.86(10)° for the other. The hydrogen atom of the hydroxyl group of each ethanol is hydrogen bonded to a pyrazole nitrogen in an adjacent BMPP (Fig.19). In this way each complex is hydrogen bonded to four adjacent complex molecules. In addition there are inter and intra molecular contacts and C—H···Cπ-interactions (Fig. 20).

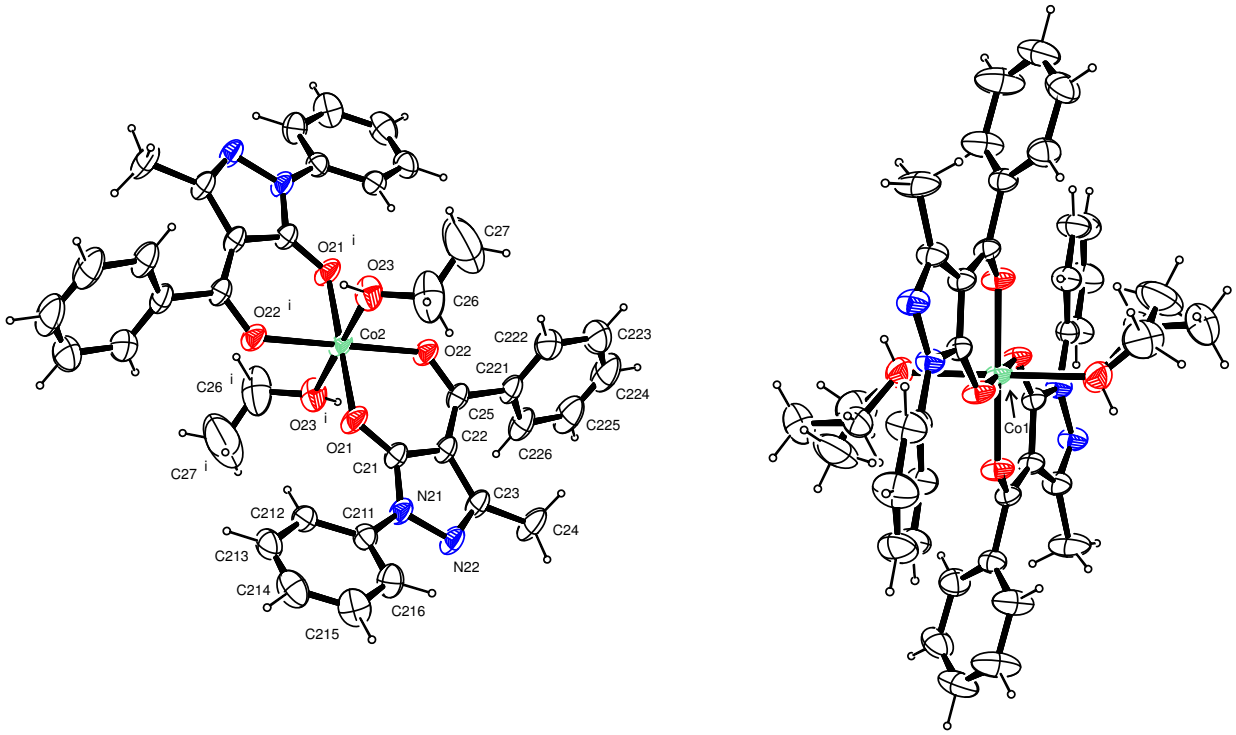

Figure 18.The Molecular Structure of $[Co(C_{17}H_{13}N_2O_2)_2(C_2H_6O)_2]$

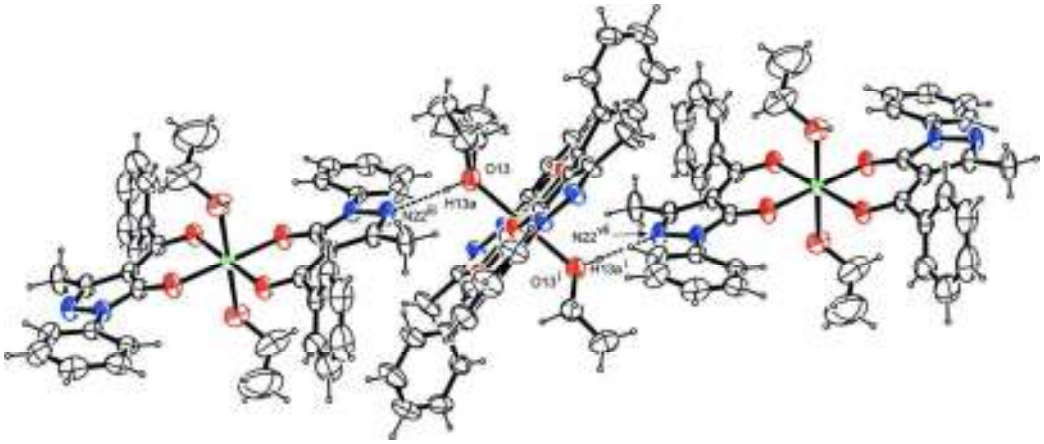

Figure 19. Hydrogen Bonding in $[Co(C_{17}H_{13}N_2O_2)_2(C_2H_6O)_2]$

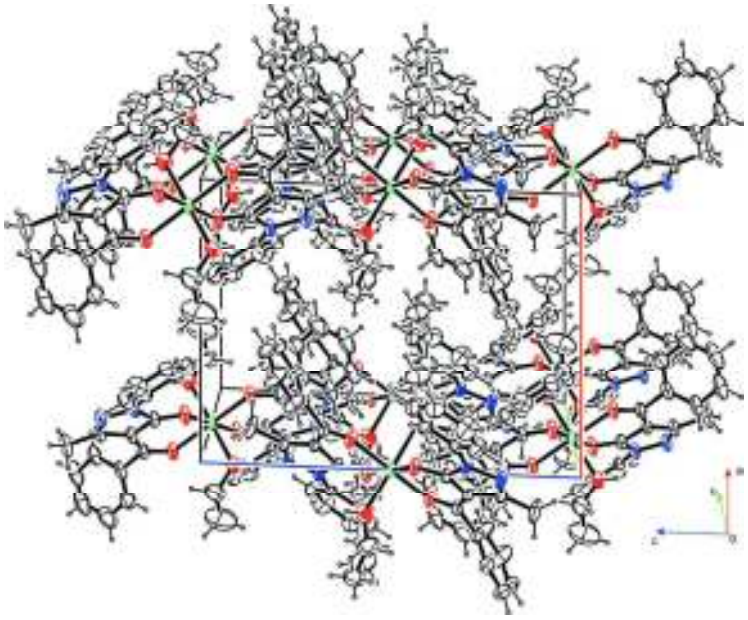

Figure 20. Crystal Packing Diagram of $[Co(C_{17}H_{13}N_2O_2)_2(C_2H_6O)_2]$

4.1.8. Thermogravimetric Studies

To obtain the TGA (thermogravimetric analysis)/DTG (derivative thermomogravimetric) curves of metal complexes, presented in Figs. 21-28, test samples were subjected to thermogravimetric analysis under nitrogen gas at a heating rate of 15 °C min^{-1} from 20 °C to 900 °C. All the metal complexes are generally thermally stable having a steady progressive decomposition with multiple decomposition patterns observed and as a result assigning decomposed components of compounds to the various percentage decompositions in the TG/DTG curve is not favourable. Two coordinated water molecules are common to all metal complexes and are expected to decompose at around 140–300°C (05TMC341), and the uncoordinated water usually decomposes a little earlier. Also, the final mass losses associated with the

thermograms of a good number of the metal complexes corresponding to the percentage mass of the remaining metal oxides.

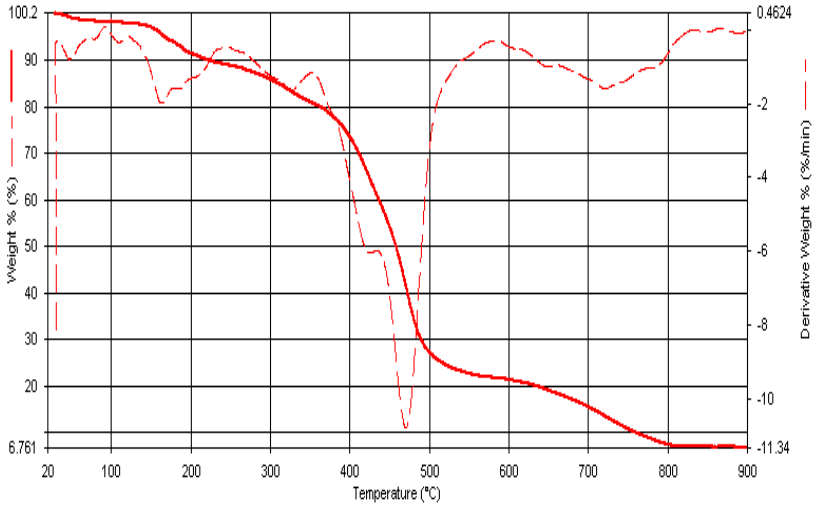

Figure 21. TGA and DTG Curves of $Mn(Bmpp\text{-}Ph)_2(H_2O)_2{\cdot}2H_2O$

In $Mn(Bmpp\text{-}Ph)_2(H_2O)_2{\cdot}2H_2O$, the first few decompositions totaling to about 8.0% at around 200°C may be due to the removal of coordinated and uncoordinated four water molecules calculated as 8.4%. A major decomposition at 475°C with a % weight loss of approximately 48% may be due to the removal of one Schiff base ligand molecule which is theoretically calculated as 43%. A final decomposition at 800°C with a total mass loss of approximately 93% is tentatively due to the removal of the water molecules and decomposition of the Schiff base ligands calculated as approximately 92 %, leaving behind the corresponding manganese oxide with approximately 7% calculated as 8.2%.

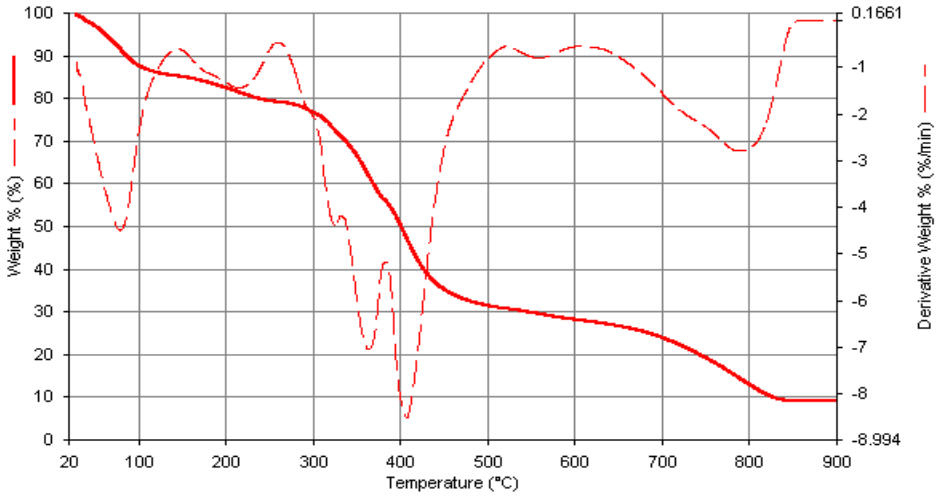

Figure 22. TGA and DTG Curve of $Mn(Ampp\text{-}Ph)_2(H_2O)_2{\cdot}2H_2O$

Thermal analysis for $Mn(Ampp\text{-}Ph)_2(H_2O)_2{\cdot}2H_2O$ shows multiple decompositions obvious from the DTG curve. The first mass losses at around 80°C and at 198°C are due to the removal of the coordinated and lattice water molecules. The final decomposition shows the removal of the two ligand molecules and the water molecules at around 820°C with a total mass loss of approximately 91% calculated as 91%. The leftover manganese oxide is calculated as 9.5 % which observed as 9 % in the TGA curve, Fig.22. The thermal analysis of both cobalt complexes as seen in their thermograms (Figure 23 and 24), exhibited multistep decompositions. However, the decomposition around 170 and 300°C corresponds to the elimination of water molecules. The final mass loss of 92.3% calc as 91.2% at >900°C for $Co(Bmpp\text{-}Ph)_2(H_2O)_2{\cdot}H_2O$ and a final mass loss of 89.9% calc as 90.6% at >900°C for $Co(Ampp\text{-}Ph)_2(H_2O)_2{\cdot}2H_2O$ corresponding to the decomposition of the water molecules and ligands were observed, leaving behind a residue

of cobalt oxide with percentage mass of 10.4% (calc. 9.5%) and 10% (calc. 10.1%), respectively.

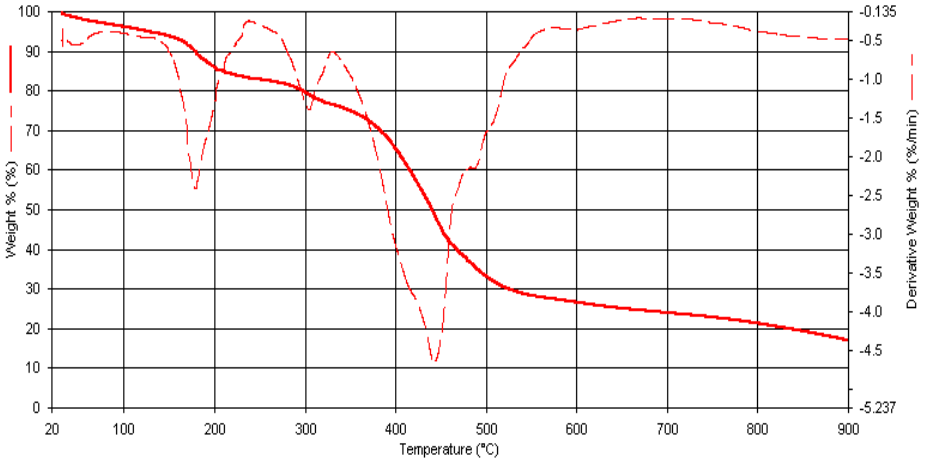

Figure 23. TGA and DTG curve of $Co(Bmpp\text{-}Ph)_2(H_2O)_2{\cdot}H_2O$

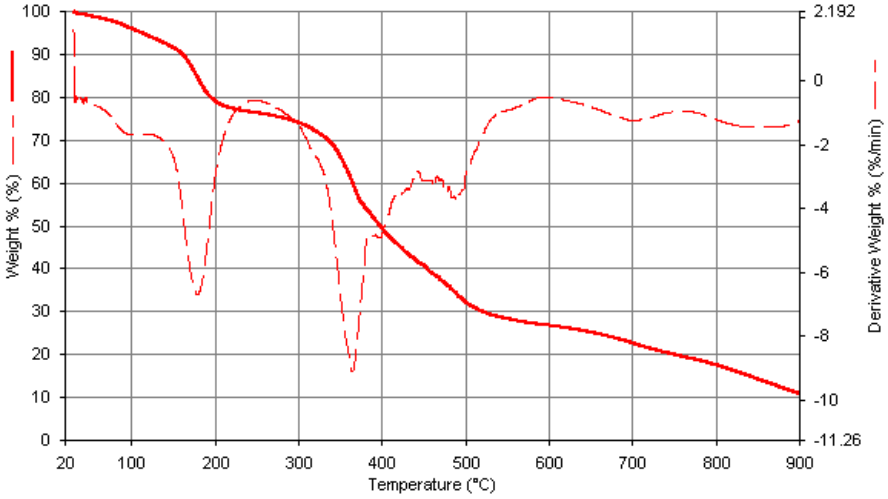

Figure 24.TGA and DTG Curve of $Co(Ampp\text{-}Ph)_2(H_2O)_2{\cdot}2H_2O$

The total mass percent loss of about 12% in two steps observed in $Ni(Bmpp\text{-}Ph)_2(H_2O)_2{\cdot}2H_2O$ thermogram can be attributed to the loss of water molecule (Fig. 25). Also the same trend of decomposition pattern has been observed in $Ni(Ampp\text{-}Dh)_2(H_2O)_2{\cdot}H_2O$ (Fig. 26). A major decomposition is

observed at around 440°C in thermograms for both complexes with a mass percentage loss of 58%, which may be attributed to one molecule of the ligand calculated at approximately 43%. The third decomposition at 760°C in both nickel complexes may be the removal of the second and last ligand molecule, leaving behind a residue of the metal oxide with a mass percentage loss of 8% (calc. as 8.6%) and 10.5% (calc. as 10.3%) for Ni(Bmpp-Ph)$_2$(H$_2$O)$_2$·2H$_2$O and Ni(Ampp-Dh)$_2$(H$_2$O)$_2$·H$_2$O, respectively. This was in agreement with the proposed geometry.

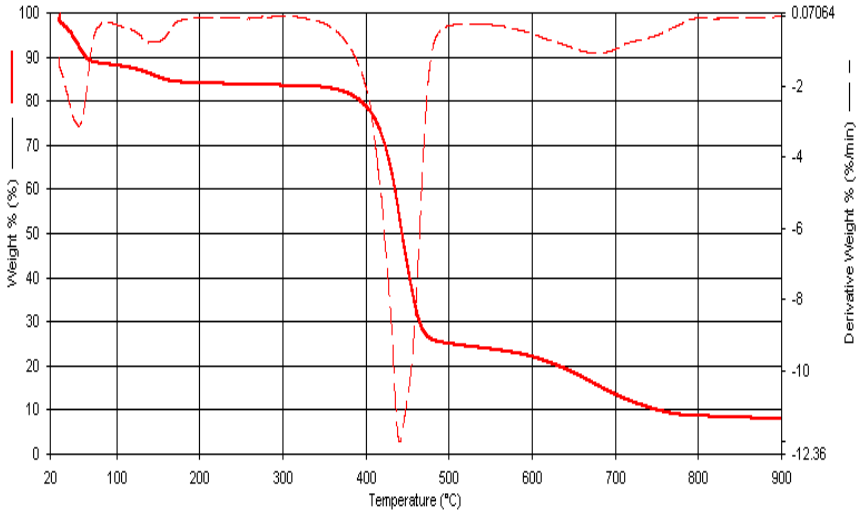

Figure 25.TGA and DTG curve of Ni(Bmpp-Ph)$_2$(H$_2$O)$_2$·2H$_2$O

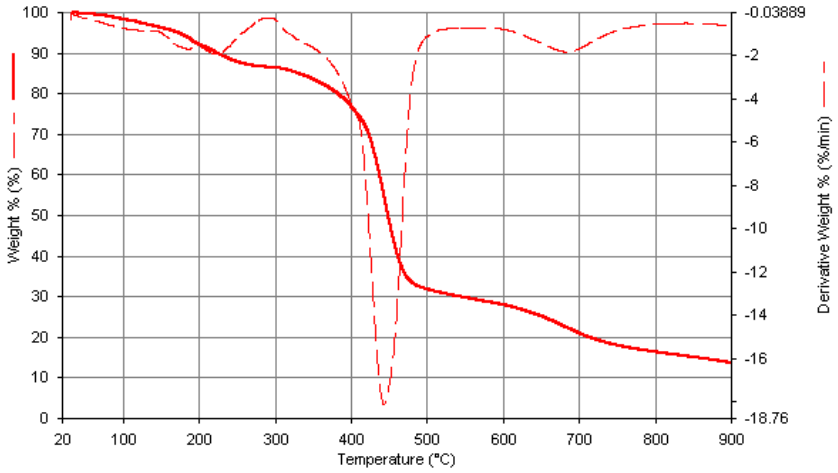

Figure 26.TGA and DTG curve of $Ni(Ampp\text{-}Ph)_2(H_2O)_2{\cdot}H_2O$

Three main decompositions has been observed for $Cu(Bmpp\text{-}Ph)_2(H_2O)_2{\cdot}H_2O$ amongst other decomposition according to DTG curve (Fig. 27) that could not be directly assigned. However, the decomposition at 290°C may be a result of the removal of the two coordinating water molecules, followed by a second major mass percentage loss at 420°C assigned to the removal of a molecule of the Schiff base ligand. The final mass percentage loss at 785°C is equivalent to the removal of the water molecules and the ligands, leaving behind the copper oxide with a remaining mass percentage of approximately 12%, which is calculated as approximately 10%. One major decomposition at 370°C was obtained in the thermogram of $Cu(Ampp\text{-}Dh)_2(H_2O)_2$ (Fig. 28), which may be assigned to the removal of the two coordinating water molecules, although other component of the copper complex cannot be accounted for with the minimal information from its

TG/DTG curves, a final decomposition at >900°C gave a residue of CuO with percentage mass of 11.8% calculated for 11.2%.

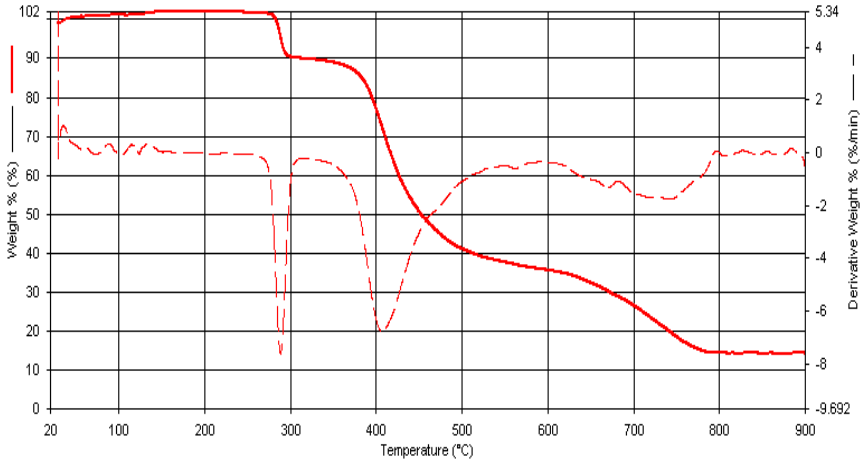

Figure 27. TGA and DTG Curve of $Cu(Bmpp\text{-}Ph)_2(H_2O)_2{\cdot}H_2O$

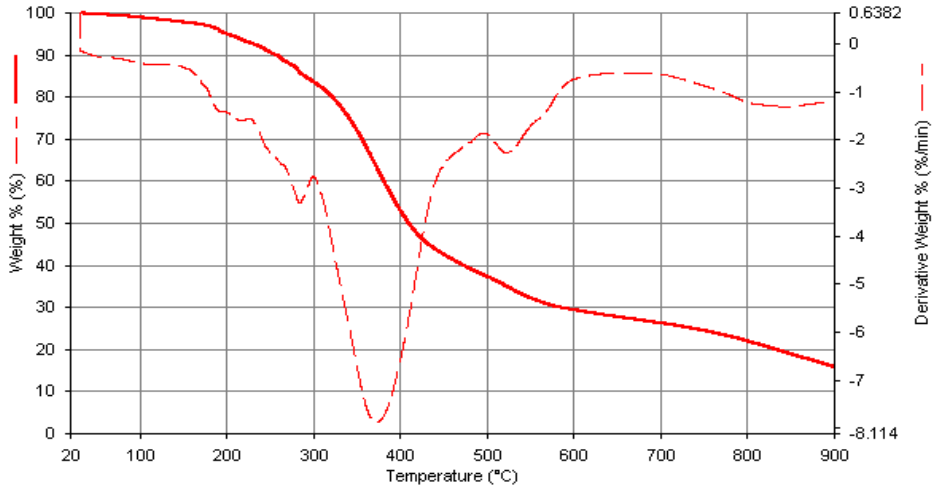

Figure 28. TGA and DTG Curve of $Cu(Ampp\text{-}Ph)_2(H_2O)_2$

On the basis of elemental and characterization techniques presented, the structure of metal complexes can be proposed as follows, **77-86**.

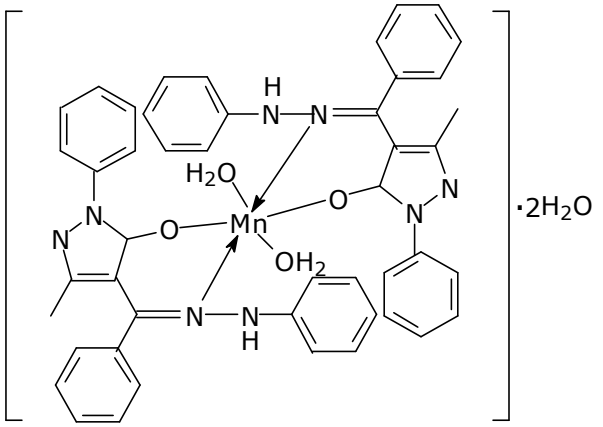

77

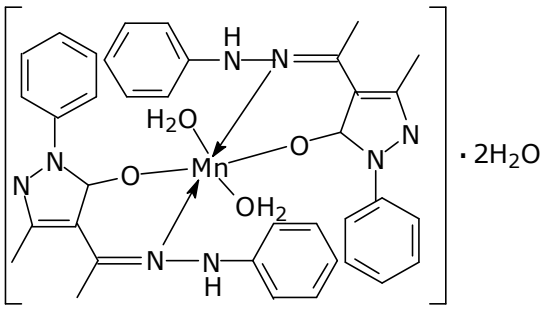

78

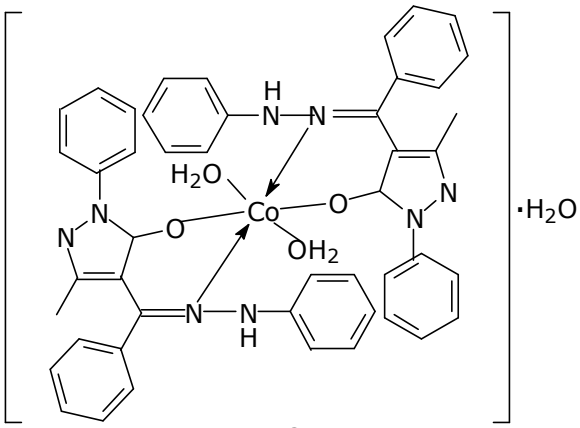

79

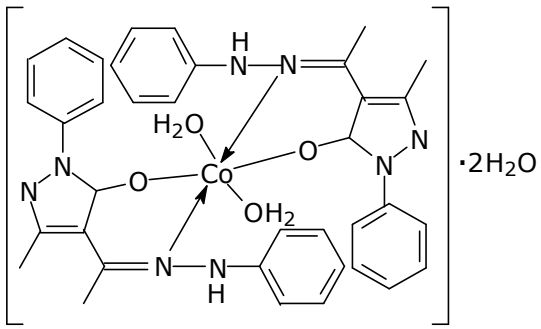

80

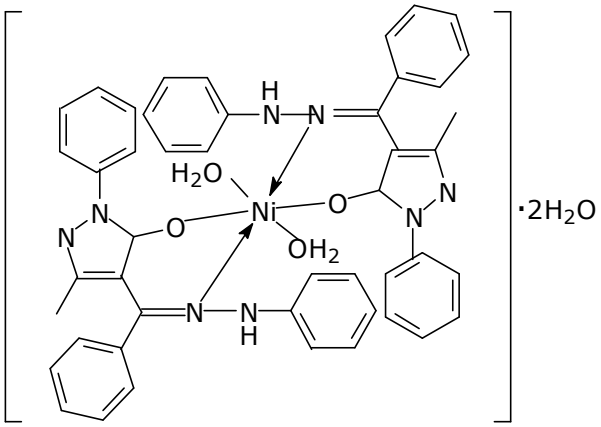

81

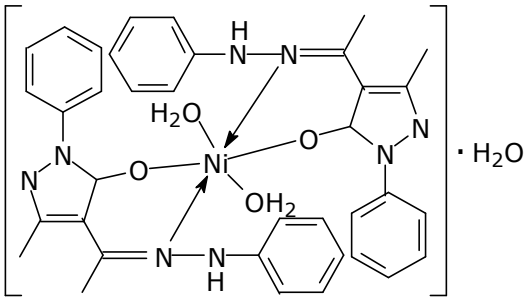

82

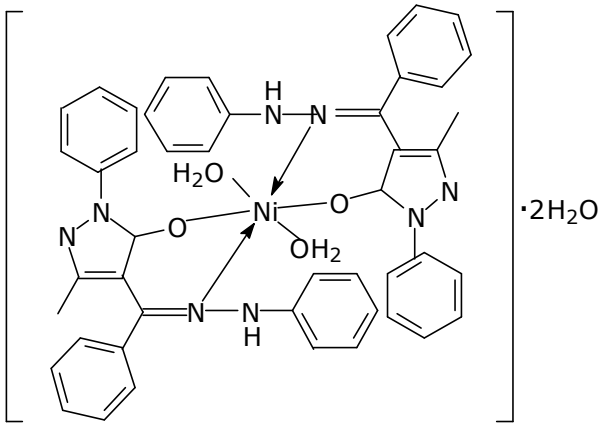

83

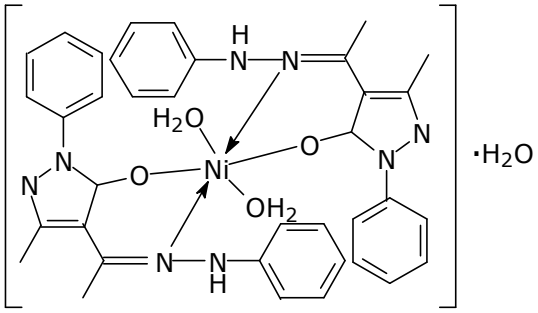

84

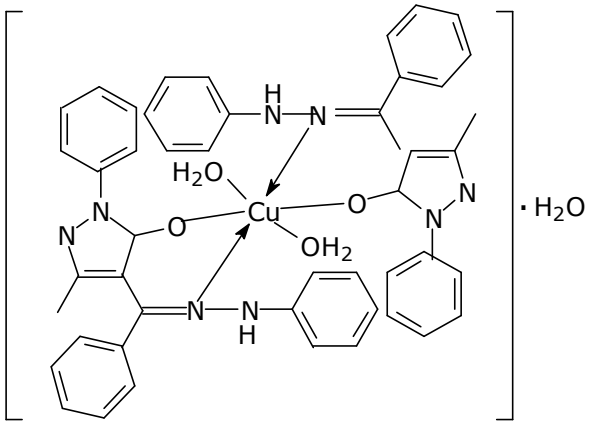

85

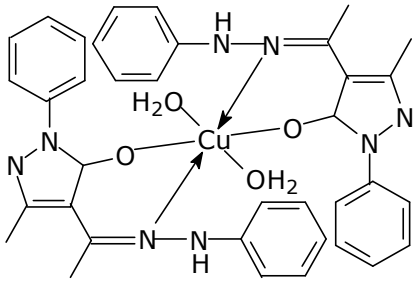

86

4.1.9 Antibacterial Screening

Antibacterial activity of Bmpp.Ph, Ampp-Ph and their metal complexes in DMSO was determined using the disc diffusion method in duplicates. They were screened *in-vitro* against selected Gram positive; *Staphylococus aureus*, *Bacillus pumillus* and Gram negative; *Proteus vulgaris*, *Aeromonas hydrophillia* at 40 mg/ml. Schiff base ligand and their metal complexes have been grouped together and compared with standard drug Chloramphenicol for ease of discussion. A generally low anti bacterial activity has been observed with Bmpp.Ph, Ampp-Ph and metal complexes. Bacterial growth inhi-

bition zones, an indication of antibacterial activity of test samples were recorded in millimeters and presented in Table 6.

Table 6. Zone of Growth Inhibition Exhibited by Ligands and Metal Complexes at 40 mg/mL (mm)

Ligand and complexes	*Staphylococus aureus*	*Bacillus pumillus*	*Proteus vulgaris*	*Aeromonas hydrophillia*
Bmpp-Ph	12.0	10.0	8.0	NI[1]
Ampp-Ph	3.0	NI	4.0	NI
$Mn(Bmpp\text{-}Ph)_2(H_2O)_2{\cdot}2H_2O$	10.0	NI	8.0	NI
$Co(Bmpp\text{-}Ph)_2(H_2O)_2{\cdot}H_2O$	8.0	12.0	NI	NI
$Ni(Bmpp\text{-}Ph)_2(H_2O)_2{\cdot}2H_2O$	NI	8.0	4.0	10.0
$Cu(Bmpp\text{-}Ph)_2(H_2O)_2{\cdot}H_2O$	12.0	6.0	8.0	NI
$Mn(Ampp\text{-}Ph)_2(H_2O)_2{\cdot}2H_2O$	8.0	NI	12.0	NI
$Co(Ampp\text{-}Ph)_2(H_2O)_2{\cdot}2H_2O$	8.0	12.0	NI	6.0
$Ni(Ampp\text{-}Ph)_2(H_2O)_2{\cdot}H_2O$	4.0	4.0	NI	NI
$Cu(Ampp\text{-}Ph)_2(H_2O)_2$	4.0	4.0	NI	NI
Chloramphenicol	30.0	20.0	42.0	40.0
DMSO	NI	NI	NI	NI

[1] NI = no inhibition

The highest zone of inhibition of 12 mm was observed in Bmpp-Ph against *Staphylococus aureus*, in $Co(Bmpp\text{-}Ph)_2(H_2O)_2$ against *Bacillus pumillus*, $Cu(Bmpp\text{-}Ph)_2(H_2O)_2$ against *Staphylococus aureus*, and $Co(Ampp\text{-}Ph)_2(H_2O)_2$ against *Bacillus pumillus*. Benzoyl derivative Bmpp-Ph has a higher activity compared to the acetyl derivative Ampp-Ph as Bmpp-Ph exhibited a generally higher zone of inhibition against more bacterial isolate. Also the metal complexes of Bmpp-Ph seem to be more active as $Ni(Bmpp\text{-}Ph)_2(H_2O)_2$ and $Cu(Bmpp\text{-}Ph)_2(H_2O)_2$ both showed activities against three different bacterial isolates whereas other metal complexes were active against two, even though some of them may have a high zone of inhibition.

In general from Table 6 we can infere that the antibacterial activity of the Schiff base ligand is higher than the metal complexes based on size of zones of inhibition. Although it is on record that chelation of metal ion does increase the possibility of growth inhibition in microbial isolates, but the observed variation may be as a result of impermeability of bacterial isolates cell wall or the nature of their ribosomes (86SRI257).

4.1.10 Antioxidant (Free radical scavenging) activity

Antioxidants can induce reduction capability of DPPH radicals by way of scavenging, which is a measure of the decrease in its absorbance at 517nm (02JAF3444). The Schiff base and metal complexes generally display a moderate to good free radical scavenging activity. At 0.5 mg/mL, a good antioxidant activity compared with ascorbic acid (Table 7) was observed for Bmpp-Ph, $Mn(Bmpp\text{-}Ph)_2(H_2O)_2$, $Mn(Ampp\text{-}Ph)_2(H_2O)_2$, and $Co(Ampp\text{-}Ph)_2(H_2O)_2$, with $Mn(Ampp\text{-}Ph)_2(H_2O)_2$ being the most active, in agreement with reported results on metal chelates of Schiff bases (06JAFC7735, 09SA(A)1901, 12BCA1). $Co(Ampp\text{-}Ph)_2(H_2O)_2$ showed the highest activity amongst the other complexes at 0.25 mg/mL and 0.13 mg/mL. Bmpp-Ph generally displayed a higher activity than Ampp-Ph, but at 0.13 mg/mL the reverse is the case.

Scavenging activity chat of free ligand and their metal complexes (Fig. 29) show that the Schiff base has a higher activity on comparing with stand-

ard drug, ascorbic acid. $Co(Ampp\text{-}Ph)_2(H_2O)_2$ generally has the strongest activity (Fig. 30).

Table 7. Antioxidant Scavenging Activity Data of Phenylhydrazine Schiff Bases and Their Metal Complexes (%)

Ligand and complexes	Percentage antioxidant scavenging activity		
	0.50 mg/ml	0.25 mg/ml	0.13 mg/ml
Bmpp-Ph	62.48	89.11	87.79
Ampp-Ph	31.52	19.15	90.01
$Mn(Bmpp\text{-}Ph)_2(H_2O)_2{\cdot}2H_2O$	52.42	42.76	64.61
$Co(Bmpp\text{-}Ph)_2(H_2O)_2{\cdot}H_2O$	17.22	3.13	32.32
$Ni(Bmpp\text{-}Ph)_2(H_2O)_2{\cdot}2H_2O$	37.33	4.17	40.94
$Cu(Bmpp\text{-}Ph)_2(H_2O)_2{\cdot}H_2O$	–	12.98	1.73
$Mn(Ampp\text{-}Ph)_2(H_2O)_2{\cdot}2H_2O$	70.58	54.00	68.56
$Co(Ampp\text{-}Ph)_2(H_2O)_2{\cdot}2H_2O$	60.07	87.25	80.64
$Ni(Ampp\text{-}Ph)_2(H_2O)_2{\cdot}H_2O$	25.22	81.58	77.07
$Cu(Ampp\text{-}Ph)_2(H_2O)_2$	38.35	57.36	44.76
Ascorbic acid	87.62	93.63	91.99

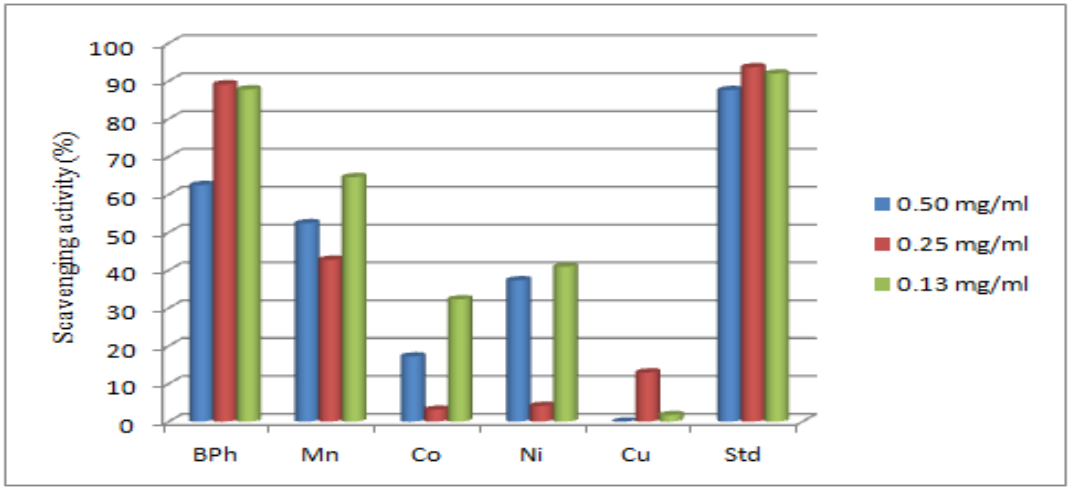

Figure 29. Chart Showing the Scavenging Activity of Bmpp-Ph and its Metal Complexes

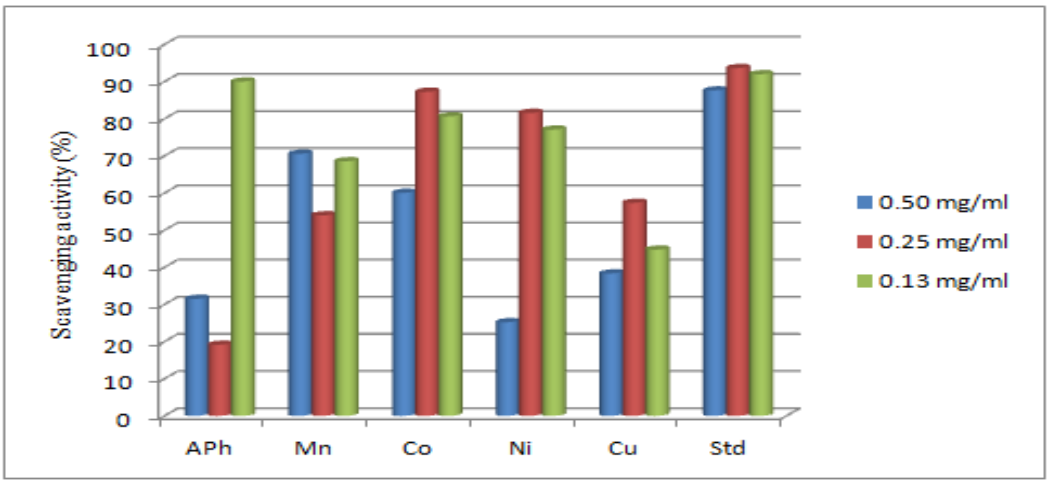

Figure 30. Chart Showing the Scavenging Activity of Ampp-Ph and its Metal Complexes

4.2. Acylpyrazolone Derived Dinitrophenylhydrazine Schiff Bases and Their Metal Complexes

Dinitrophenylhydrazine is a nitro substituted phenylhydrazine at positions 2 and 4 of the phenyl group with the formula $C_6H_6N_4O_4$. The reddish yellow compound **87** was used for a quantitative identification of carbonyl functional groups, developed by Brady and Elsmie (26A77). Presented in this chapter section are the synthesis, characterization, and biological studies of two Schiff base ligands, 4-benzoyl-3-methyl-1-phenyl-2-pyrazolin-5-one dinitrophenylhydrazone Bmpp-Dh and 4-acetyl-3-methyl-1-phenyl-2-pyrazolin-5-one dinitrophenylhydrazone Ampp-Dh with their metal complexes.

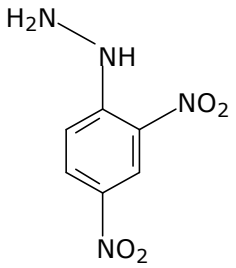

87

4.2.1. Synthesis

Acetyl and benzoyl pyrazolone Schiff base precursors were reacted with dinitrophenylhydrazine in a condensation reaction to afford the Schiff base ligands 4-acetyl-3-methyl-1-phenyl-2-pyrazolin-5-one dinitrophenylhydrazine and 4-benzoyl-3-methyl-1-phenyl-2-pyrazolin-5-one dinitrophenylhydrazine as seen in the synthesis scheme, eq. 5.

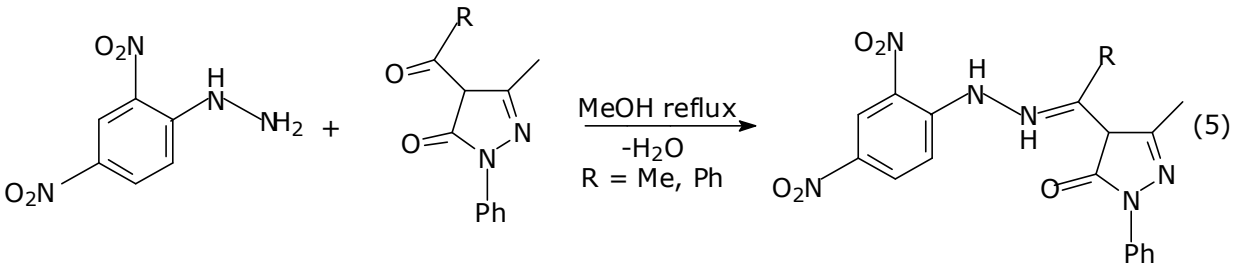

(5)

The synthesized Schiff bases were in solid form and stable at room temperature. They are soluble in methanol, ethanol, and most common organic solvents. Schiff bases were precipitated in a reasonably moderate yield and purity was confirmed by TLC, which was corroborated by a small range melting point. Block-like single crystals of Bmpp-Dh suitable for X-ray crystallography were afforded by a slow evaporation at room temperature from a methanol solution of Bmpp-Dh. They were fully characterized by elemental

analysis, IR-spectroscopy, UV-VIS-spectroscopy, ^{1}H and ^{13}C NMR-spectroscopy, mass-spectroscopy, and X-ray crystallography analysis for Bmpp-Ph.

A total of eight metal complexes were synthesized by the treatment of Bmpp-Dh or Ampp-Dh with the metal salt that corresponds in a synthesis scheme illustrated in eq. 6. They were obtained in an air-stable powder form and in different colors. The complexes are generally insoluble in water, ethanol and in non-coordinating solvents but fairly soluble in methanol and soluble in polar solvents with strong donor strength, like DMF and DMSO. Molar conductance values of metal complexes infer non–electrolytes behaviour in DMF (71CCR81, 75MI1).

$$MX_2 \cdot nH_2O + 2L \xrightarrow[\text{reflux}\quad 4\,h]{AN/H_2O} M(L)_2(H_2O)_2 \cdot nH_2O \quad (6)$$

$M = Mn^{2+}, Co^{2+}, Ni^{2+}$ or Cu^{2+}, $X = Cl^{-}$ or $MeCOO^{-}$
$L = Bmpp-Dh$ or $Ampp-Dh$

4.2.2. Elemental analysis

The percentage composition values of CHN in Bmpp-Dh, Ampp-Dh and metal complexes found were in agreement with calculated values. Octahedral metal complexes with the corresponding Schiff base have been proposed. The complexes have two molecules of the bidentate Schiff base and two water molecules to complete their octahedral geometry. Some of their physical properties, melting point range, elemental composition, conductivity and percentage yield are presented in the experimental chapter.

4.2.3. ^{1}H and ^{13}C NMR Spectroscopy

Structurally Bmpp-Dh and Ampp-Dh is similar to Bmpp-Ph and Ampp-Ph, respectively, discussed above, since dinitrophenylhydrazine is a derivative of phenylhydrazine. Therefore their ^{1}H and ^{13}C NMR spectra looked almost alike in DMSO-d_6 solution, all other conditions remaining constant. In Bmpp-Dh (Fig. 31), the –NH proton and that of the azomethine carbon atom C=NH, respectively, resonated in the downfield region with chemical shift at 11.6 and 8.9 ppm integrating for one proton each. A multiplet due to aromatic hydrogen was observed at 8.5–7.3 ppm, but the integrating protons are not equivalent, which may be due to the overlap of equivalent protons. Finally, the resonance peak due to methyl hydrogen was displayed as a sharp signal upfield of the NMR spectrum at 1.9 ppm integrated for three hydrogen atoms as expected.

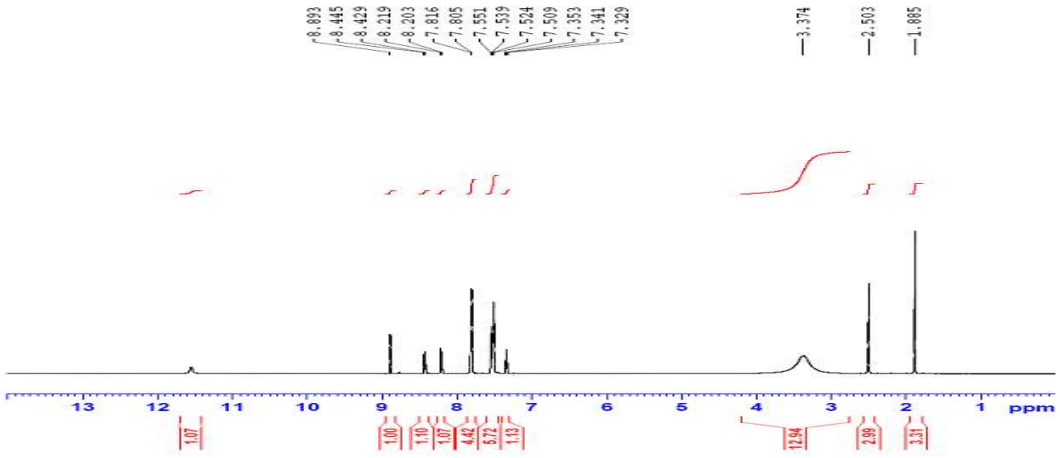

Figure 31. ^{1}H NMR Spectrum of Bmpp-Dh

Ampp-Dh (Fig. 32) showed a singlet with broad base integrating over a wide range for one proton at 10.8 ppm which is assigned to the –NH of the hydrazine. This was followed by another singlet resonating at 8.8 ppm due to hydrogen attached to the azomethine carbon atom C=N. There is a weak signal at 2.4 ppm which may be assigned to the methyl protons but its integration showed otherwise considering that it has been unusually merged with the DMSO peak. However, the mass spectrum molecular peak and fragmentations discussed below, corroborates the proposed composition for Ampp-Dh. Also the aromatic protons H–Ar are observed as a multiplet at 8.4–7.2 ppm.

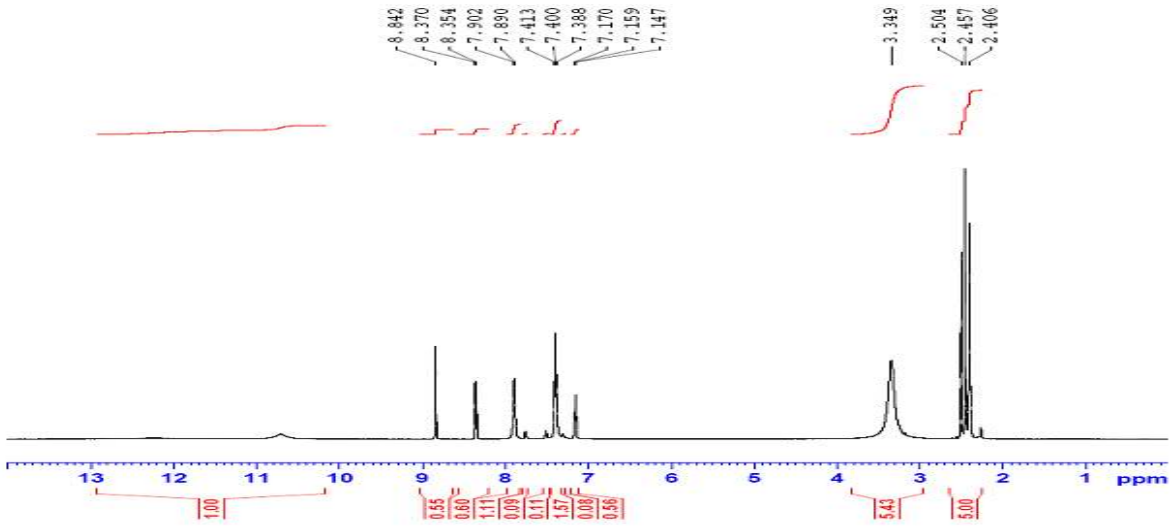

Figure 32. ^{1}H NMR Spectrum of Ampp-Dh

^{13}C NMR spectra of Bmpp-Dh and Ampp-Dh (Fig. 33 and 34) displayed aromatic carbon atoms at a chemical shift of 144.6–117.2 and 137.9–116.02 ppm, respectively. Signals due to azomethine carbon and the pyrazolone

carbonyl C=O is seen at a lower chemical shift value of 147.44 and 148.9 ppm in Bmpp-Dh, which may be a result of dinitrophenylhydrazine steric nature compared to the phenylhydrazine counterpart above. Finally in Bmpp-Dh, the only methyl carbon appears as a single signal in the aliphatic region at 13.6 ppm. In Ampp-Dh, chemical shifts due to C=N and C=O were observed at 137.7 and at 146.2 ppm, respectively. The two methyl groups carbons are observed at 16.2 and 14.9 ppm assigned to the pyrazolone methyl and the acetyl methyl, respectively.

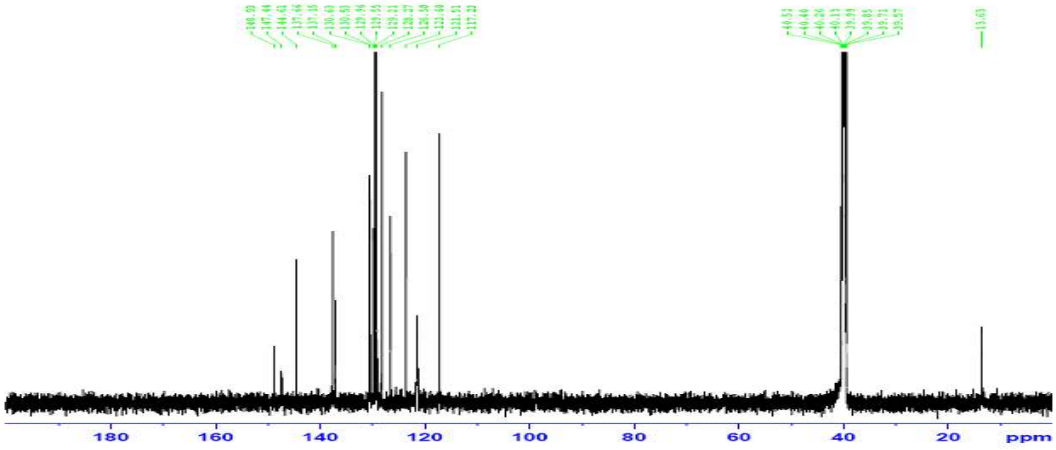

Figure 33. ^{13}C NMR Spectrum of Bmpp-Dh

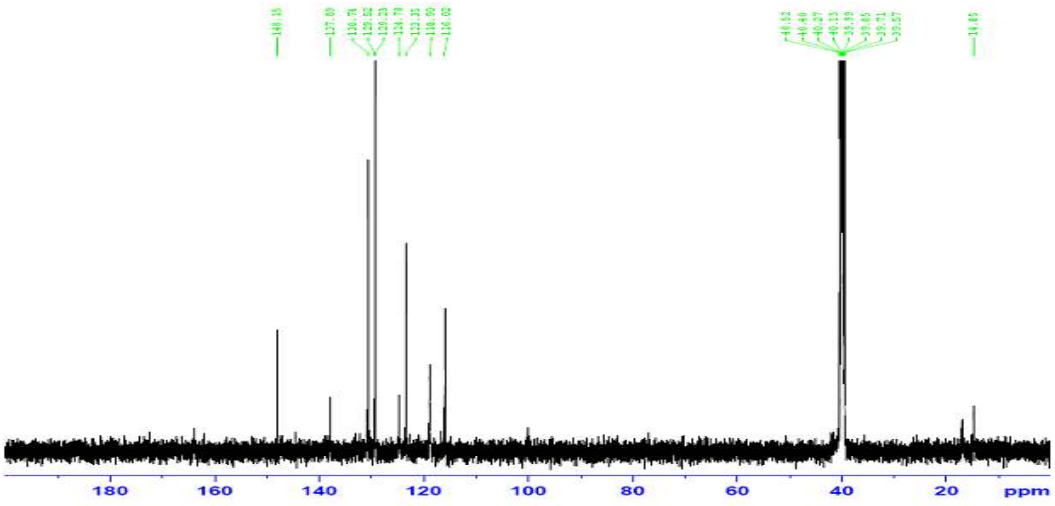

Figure 34. ^{13}C NMR Spectrum of Ampp-Dh

4.2.4. Mass-Spectroscopy

The highest intensity peaks in the mass spectra of Bmpp-Dh and Ampp-Dh corresponds to the molecular ion peak M^+ observed at *m/z* 459 in Bmpp-Dh (Fig.35) and at *m/z* 397 in Ampp-Dh (Figure 36).The fragmentation peak at *m/z* 279 in Bmpp-Dh is due to the protonated benzoyl Schiff base precursor, $C_{17}H_{14}N_2O_2$. The molecular ions observed in both Schiff base ligands confirm the calculated theoretical molar mass plus hydrogen M + H]$^+$.

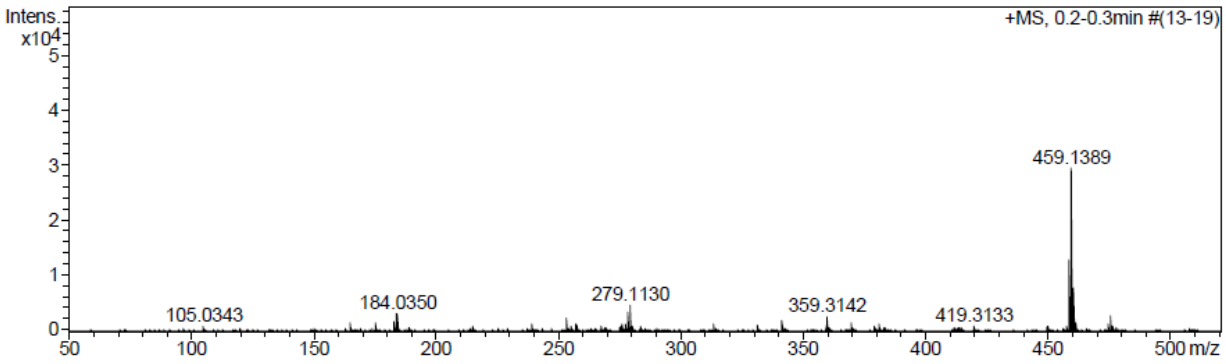

Figure 35. Mass-Spectrum of Bmpp-Dh

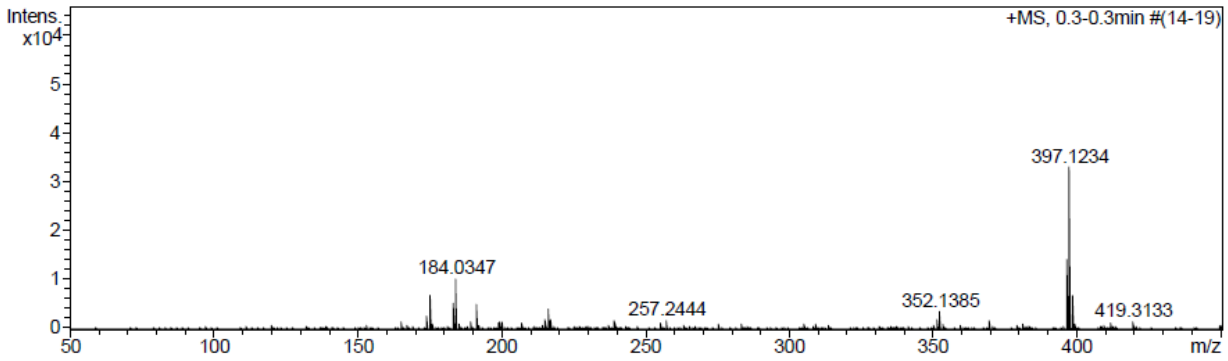

Figure 36. Mass-Spectrum of Ampp-Dh

4.2.5. Infrared Spectroscopy

The IR-spectra of the Schiff base ligands and their metal complexes closely look alike with modifications in the spectra of the metal complexes due to the interaction of the metal ion with the ligands. Octahedral complexes of the synthesized acylpyrazolone ligands have been proposed which were in accordance with previously reported (78JINC793, 81D1241, 94TMC611). Bmpp-Dh and Ampp-Dh existed in keto tautomer form with IR spectra having a strong band vibrating at 1642 and 1627 cm^{-1} corresponding to the azomethine *v*(C=N). The metal ion in the metal complexes coordinates through the donor nitrogen of the azomethine group and based on this the azomethine band in the IR spectra of metals complexes are observed at a significantly lower wavenumber in the range of 1620–1617 cm^{-1}. The broad band at 3489 cm^{-1} in Bmpp-Dh and 3486 cm^{-1} in Ampp-Dh due to inter- and intramolecular hydrogen bonding of the *v*(N–H) stretching band was observed in the range of 3498–3384 cm^{-1} due to *v*(N–H) and *v*(O–H) from the water

molecules. The ketone carbonyl *v*(C=O) group was observed at 1498 and 1501 cm^{-1}, which was absent in the IR-spectra of the metal complexes, an evidence of the coordination of the metal ion through the oxygen of the carbonyl thereby forming –C–O–M bond. The two coordinated water molecules that completed the proposed octahedral geometry of metal complexes can be corroborated with the existence of a new band at around 849–830 cm^{-1}. A new band at around 633–620 cm^{-1} and 492–478 cm^{-1} was assigned to the newly formed *v*(M–N) and *v*(M–O) bonds respectively.

4.2.6. UV-Vis Spectroscopy and Magnetic Moments

The ligands and their complexes showed absorption bands in the UV region due to $\pi \rightarrow \pi^*$ and $n \rightarrow \pi^*$ transitions. The point of absorptions displayed some modifications in the metal complexes as a result of metal ion coordination. In general the electronic spectra of all the metal complexes in this chapter exhibited an unusual display but their magnetic moment values agreed with theoretical predictions in line with reported data. The energy values closeness of different states of transitions may be the reason for the disappearance of some expected bands. Electronic spectra absorption bands and values in nanometers are displayed in the experimental section.

Mn(II) complexes of the dinitrophenylhydrazone with acylpyrazolone show an unusual electronic spectral band in the visible region but close to the UV region (Fig. 37, 38). Two bands were observed at 436 nm and 462 nm in $Mn(Bmpp\text{-}Dh)_2(H_2O)_2$, and a band at 451 nm in Mn(Ampp-

Dh)$_2$(H_2O)$_2$·H_2O. These bands may be attributed to $^6A_{1g} \rightarrow {}^4A_{1g}$ transition a characteristics of an octahedral Mn(II) complex.

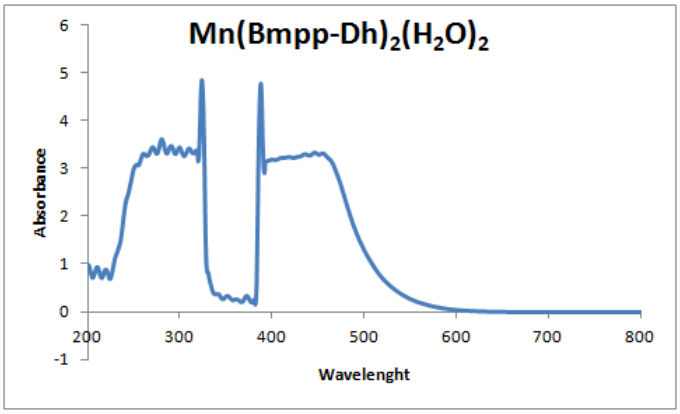

Figure 37. Electronic Spectrum of Mn(Bmpp-Dh)$_2$(H_2O)$_2$

The magnetic moment, of dinitrophenylhydrazone Schiff base complexes with Mn(II), which further confirm their geometry, are 5.65 and 5.67 BM for Mn(Bmpp-Dh)$_2$(H_2O)$_2$ and Mn(Ampp-Dh)$_2$(H_2O)$_2$·H_2O, respectively(07PJP301).

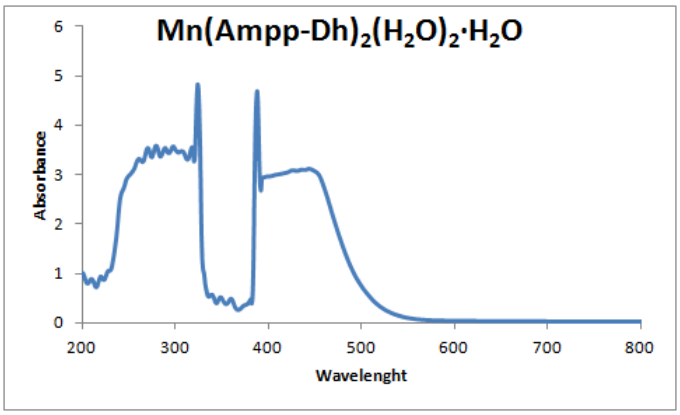

Figure 38. Electronic Spectrum of Mn(Ampp-Dh)$_2$(H_2O)$_2$·H_2O

Electronic spectra of cobalt complexes show similar absorbance in the same region as the manganese complexes. Co(Bmpp-Dh)$_2$(H_2O)$_2$·H_2O dis-

play bands at 425 nm and 460 nm (Fig.39), and $Co(Ampp\text{-}Dh)_2(H_2O)_2$ at 414 nm and 493 nm (Fig. 40) corresponding to ($^4T_{2g} \rightarrow {}^4T_{1g}$) transition of an octahedral Co(II) complex.

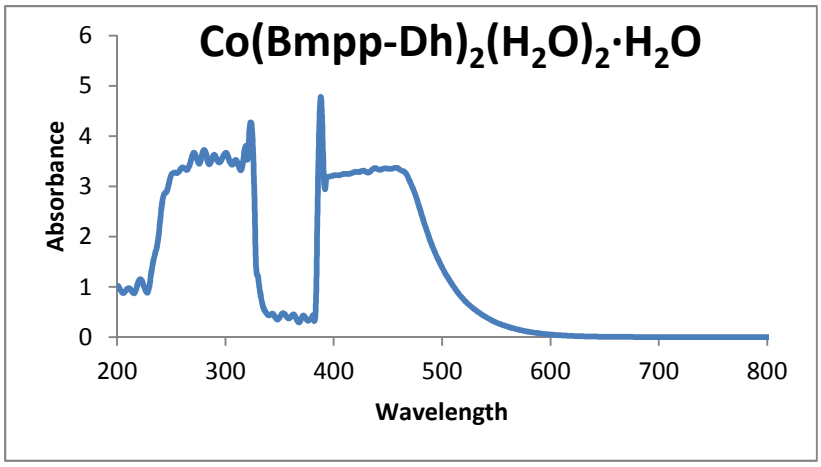

Figure 39. Electronic Spectrum of $Co(Bmpp\text{-}Dh)_2(H_2O)_2 \cdot H_2O$

The measured magnetic moment for $Co(Bmpp\text{-}Dh)_2(H_2O)_2 \cdot H_2O$ was 4.48 BM and 4.47 BM for $Co(Ampp\text{-}Dh)_2(H_2O)_2$ which were in agreement with the expected values for an octahedral Co(II) complex (07EQ7).

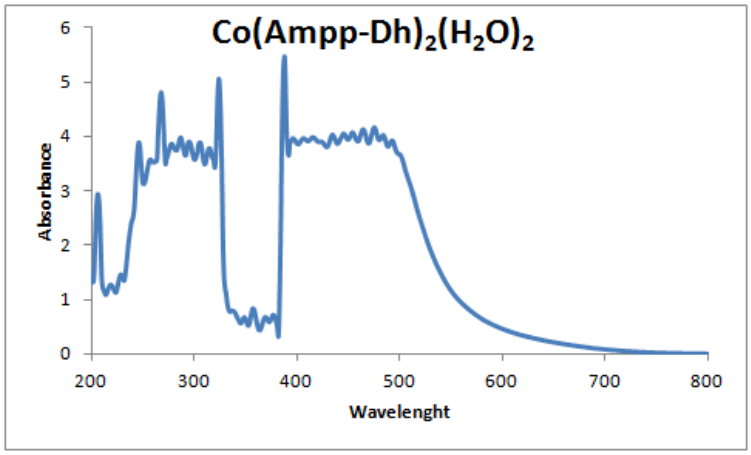

Figure 40. Electronic Spectrum of $Co(Ampp\text{-}Dh)_2(H_2O)_2$

The d-d bands in the visible region were observed in Ni(Bmpp-Dh)$_2$(H$_2$O)$_2$·H$_2$O at 431 nm and 463 nm (Fig. 41). One band was observed for Ni(Ampp-Dh)$_2$(H$_2$O)$_2$ at 436 nm (Fig. 42). However, three different bands are attributed to $^3A_{2g} \rightarrow {}^3T_{1g}(p)$ transition of an octahedral Ni(II).

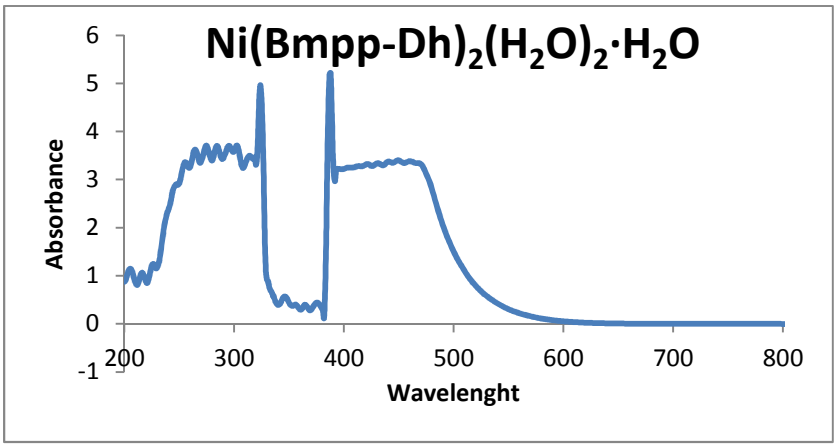

Figure 41. Electronic Spectrum of Ni(Bmpp-Dh)$_2$(H$_2$O)$_2$·H$_2$O

Ni(II) complexes presented herein has a magnetic moment value of 2.90 and 2.92 B.M for Ni(Bmpp-Dh)$_2$(H$_2$O)$_2$·H$_2$O and Ni(Ampp-Dh)$_2$(H$_2$O)$_2$, respectively (02SRI819).

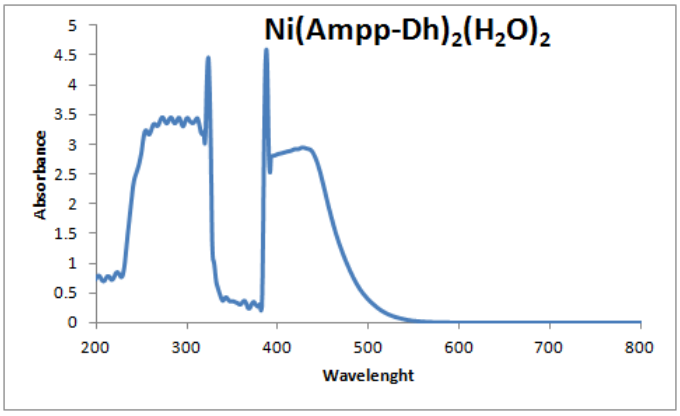

Figure 42. Electronic Spectrum of Ni(Ampp-Dh)$_2$(H$_2$O)$_2$

Like most of the complexes with dinitrophenylhydrazone Schiff base presented here, the copper complexes exhibited d-d transition close to the UV region. $Cu(Bmpp\text{-}Dh)_2(H_2O)_2\cdot 2H_2O$ (Fig. 43) exhibited two bands at 425 nm and 460 nm corresponding to $^2B_{1g}\rightarrow{}^2E_g$ transition associated with a magnetic moment of 1.95 BM. $Cu(Ampp\text{-}Dh)_2(H_2O)_2$(Fig. 44) having a magnetic moment of 1.97 BM, shows a band at 467 nm attributed to $^2B_{1g}\rightarrow{}^2E_g$ transition, and a broad band peculiar to a distorted octahedral Cu(II) at 598 nm corresponding to $^2B_{1g}\rightarrow{}^2B_{2g}$.

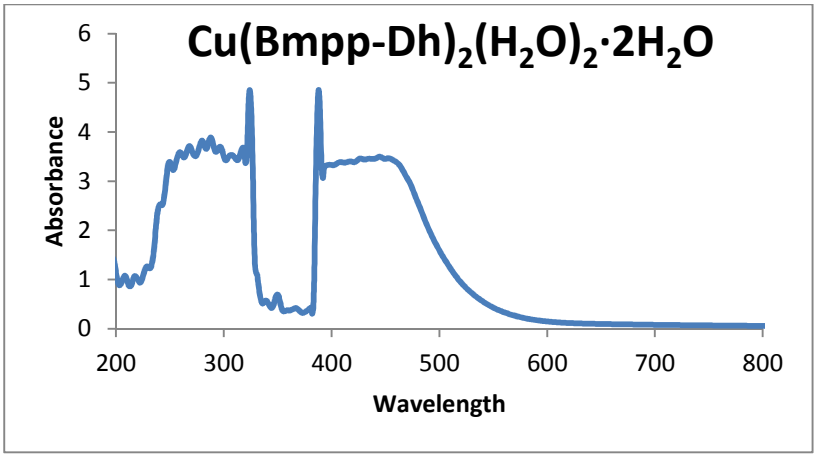

Figure 43. Electronic Spectrum of $Cu(Bmpp\text{-}Dh)_2(H_2O)_2\cdot 2H_2O$

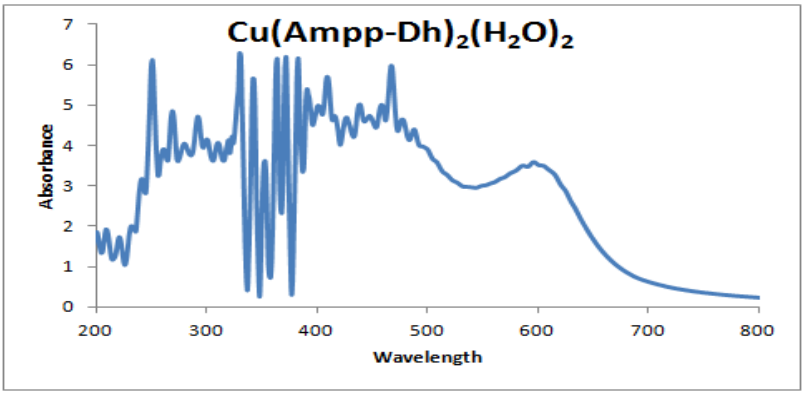

Figure 44. Electronic Spectrum of $Cu(Ampp\text{-}Dh)_2(H_2O)_2$

4.2.7. X-Ray Crystallography

Bmpp-Dh single crystals were obtained from slow evaporation of the methanolic solution at room temperature and subjected to X-ray diffraction. Crystal data summary is presented in Table 8.

Table 8. Crystal and Refinement Data for Bmpp-Dh

Compound	Bmpp-Dh
Formular	$C_{23}H_{18}N_6O_5 \cdot C_2H_6O$
Crystal colour and form	Red / Block
Formula weight	504.50
Crystal system	Monoclinic
Space group	$P2_1/c$
a	12.8289 (4) (Å)
b	14.3247 (4) (Å)
c	14.4213 (4) (Å)
β	111.347 (1)°
V	2468.38 (12) (Å^3)
Z	4
$D_{(calc)}$	1.358 (Mg cm^{-1})
F(000)	1056
θ range	2.9–28.9 (°)
Crystal size	0.16 x 0.43 x 0.39 (mm)
Reflections measured	23873
Independent/observed	6124/5136
Mu(MoKa)	0.71073 (/mm)
Temperature	200 (K)
Parameters	94

In $C_{23}H_{18}N_6O_5 \cdot C_2H_6O$ (Fig. 45), the least square plane of the pyrazolone ring makes a dihedral angle of 53.56(3)° with the least squares plane of all the phenyl rings C_{11}–C_{16}, C_{21}–C_{26}, and C_{31}–C_{36}. The largest deviation distance from the phenyl ring plane is C_{14} at 0.2688(16) Å. The dihedral angles

with the individual least square planes through the phenyl rings with the pyrazolone plane are 45.87(7)°, 58.29(7)° and 55.84(7)°, respectively.

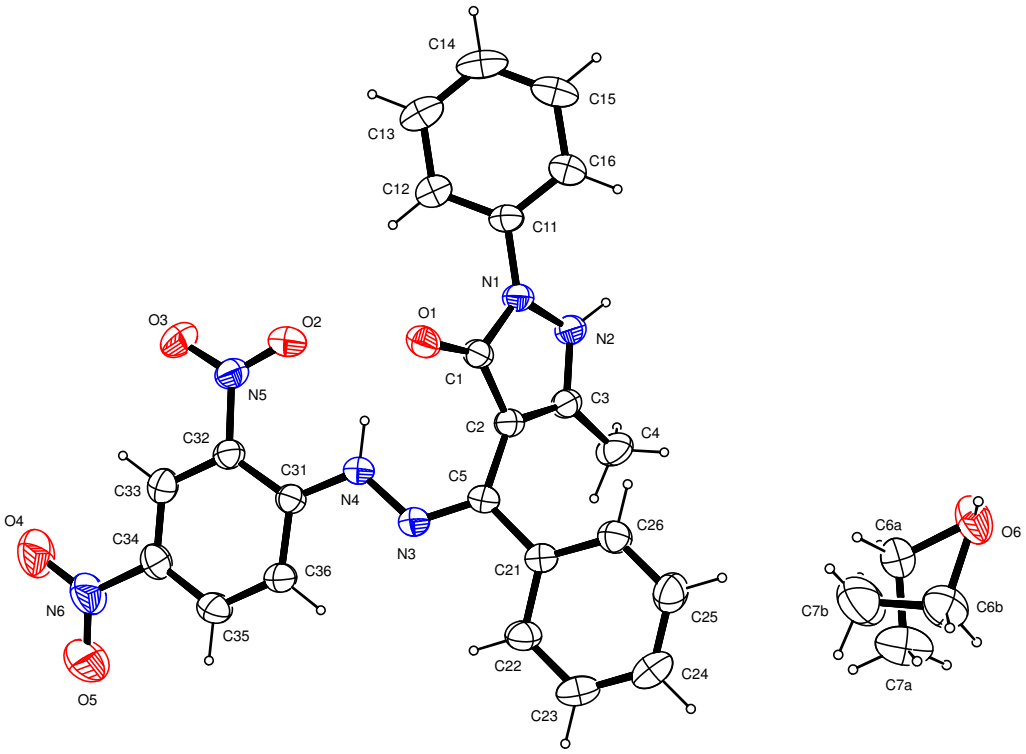

Figure 45. Molecular crystal structure of $C_{23}H_{18}N_6O_5 \cdot C_2H_6O$

The ethyl group of the ethanol solvent molecule is disordered over two set of sites [occupancy ratio 0.762(5):0.238(5)]. H_4N, the hydrogen on N_4, has two intra molecular contacts of 2.023(17) Å and 2.040(17) Å with $O_1$and O_2, respectively. A C_{36}—H_{36}···N_3 intra molecular contact of 2.34 Å also occurs (Fig. 46).

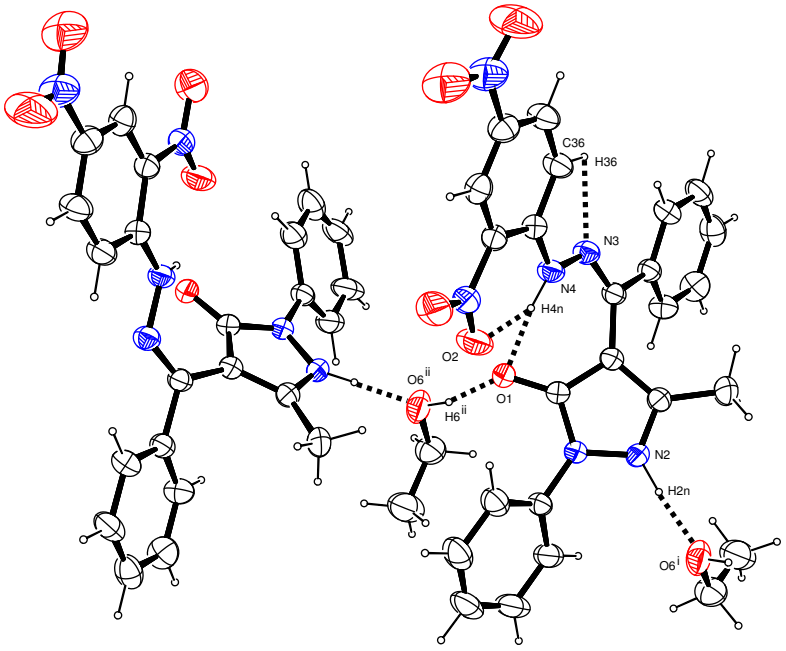

Figure 46. Hydrogen Bonding in $C_{23}H_{18}N_6O_5 \cdot C_2H_6O$

Molecules of the title compound are stacked in the c axis direction and linked via the ethanol solvent molecule with $N_2—H_2N\cdots O_6$ and $O_6—H_6\cdots O_1$ intermolecular contacts of length 1.711(18) Å and 1.72(2) Å, respectively, Fig. 47. Adjacent molecules have a $C_{26}—H_{26}\cdots O_5$ interaction of 2.43 Å.

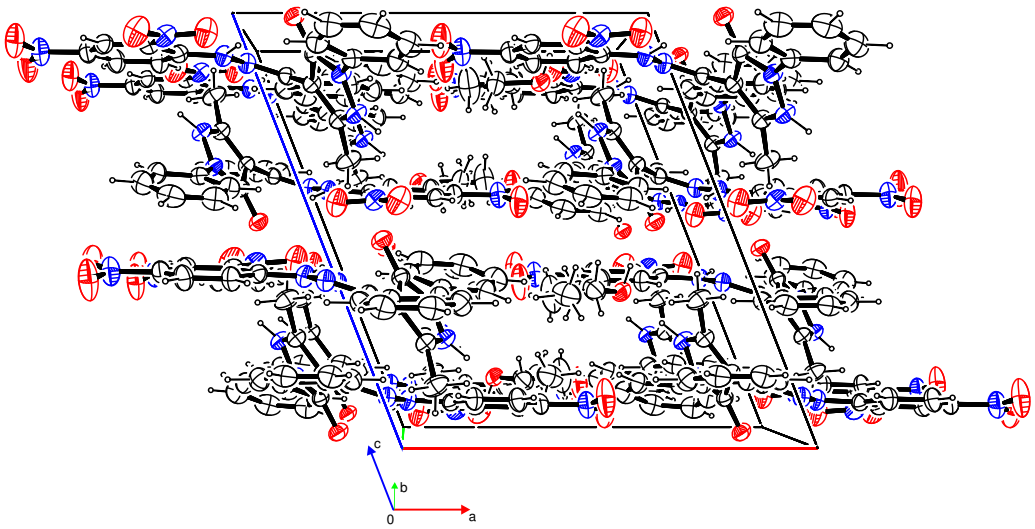

Figure 47. Packing Diagram of $C_{23}H_{18}N_6O_5 \cdot C_2H_6O$

Schiff bases with substituted aryl moieties having more conjugation have been reported to be more easily prepared and stable, hence the reason for the unsuccessful attempts to obtain crystal structure of Ampp-Dh.

4.2.8. Thermogravimetric Studies

Metal complexes of acylpyrazolone dinitrophenylhydrazone Schiff bases are generally thermally stable. In the thermograms presented, a multistep decomposition pattern was observed with the final decomposition occurring beyond 900°C, marking their assignment to be unfavorable. However, it is expected that their final decomposition is equivalent to the mass losses associated with leftover of the corresponding metal oxides. The two coordinated water molecules common to all metal complexes are expected to decompose at around 140–300°C (05TMC341) and the uncoordinated water usually decomposes a little earlier.

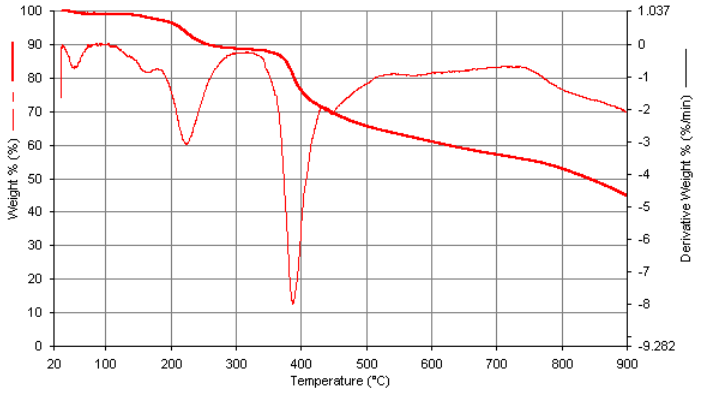

Figure 48. TGA and DTG curves of $Mn(Bmpp\text{-}Dh)_2(H_2O)_2$

Two decompositions of about 11% mass loss was observed in $Mn(Bmpp\text{-}Dh)_2(H_2O)_2$ at 240°C, which may be due to the coordinated water molecules

and others which the complex have absorbed as lattice water (Fig. 48). At around 390°C a major decomposition occurred followed by another one over a wide temperature range extending above 900°C which may be a result of the removal of the Schiff base ligands.

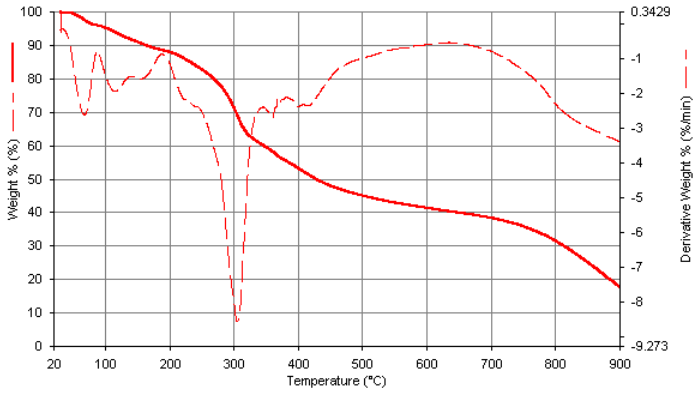

Figure 49. TGA and DTG Curves of $Mn(Ampp\text{-}Dh)_2(H_2O)_2{\cdot}H_2O$

A similar decomposition pattern was observed in $Mn(Ampp\text{-}Dh)_2(H_2O)_2{\cdot}H_2O$ (Fig. 49), having a loss of the coordinated and non coordinated water molecules around 190 °C with a weight percentage loss of 10 %. The major decomposition at around 310 °C may be due to one Schiff base ligand and the wide temperature range decomposition extending beyond 900 °C tentatively due to the second Schiff base ligand molecule leaving behind the metal oxide of manganese.

The removal of the water molecules can be observed in the thermogram of $Co(Bmpp\text{-}Dh)_2(H_2O)_2{\cdot}H_2O$ (Fig. 50), as a multiple decomposition occurring at 240°C with a total mass percentage loss of about 11% which is calculated as 5.3%. The major decomposition at 360°C from DTG curve may be due to

one of the Schiff base ligand but was not clear. Also, the last decomposition observed extend beyond 900°C.

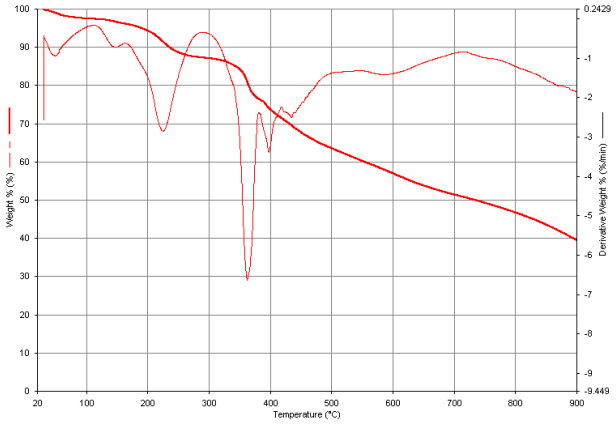

Figure 50. TGA and DTG Curves of $Co(Bmpp\text{-}Dh)_2(H_2O)_2 \cdot H_2O$

The absence of an uncoordinated water molecule can be evident in the thermogram of $Co(Ampp\text{-}Dh)_2(H_2O)_2$, Fig.51. The major decomposition at 370°C may be due to the elimination of two water molecules. The other two decompositions observed from DTG at around 510 and 600°C cannot be assigned. The formation of a gaseous product may be the cause of the unusual thermograms observed.

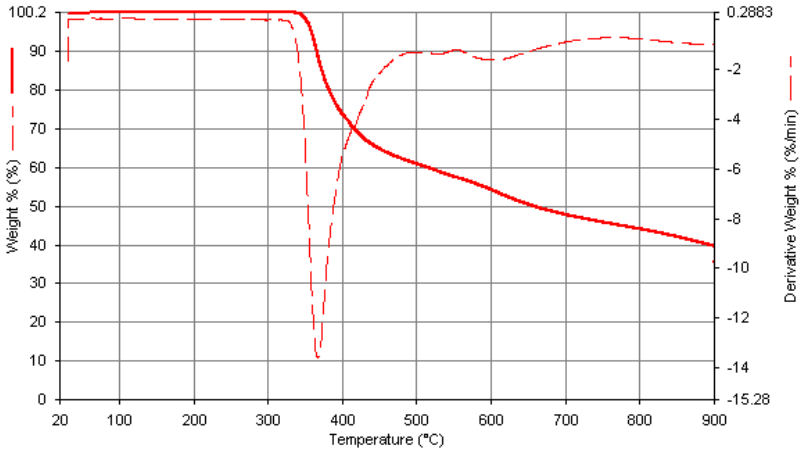

Figure 51.TGA and DTG Curves of $Co(Ampp\text{-}Dh)_2(H_2O)_2$

Removal of the coordinated water molecules in $Ni(Bmpp\text{-}Dh)_2(H_2O)_2 \cdot H_2O$ was evident from the multistep decomposition occurring at around 240°C, Fig. 52, which is followed by a major decomposition at 390°C which may be assigned to the removal of one Schiff base ligand. The last decomposition over a wide range of temperature may be due to the second Schiff base leaving behind the residue of the metal oxide. A similar pattern was observed in $Ni(Ampp\text{-}Dh)_2(H_2O)_2$ (Fig. 53). The water molecule removal was evident from the DTG cure of decomposition at 160°C, the major decomposition at around 298°C may be attributed to the removal of the ligand, although the decomposition temperature is low. Multiple decompositions are observed and complex components assignment was not possible.

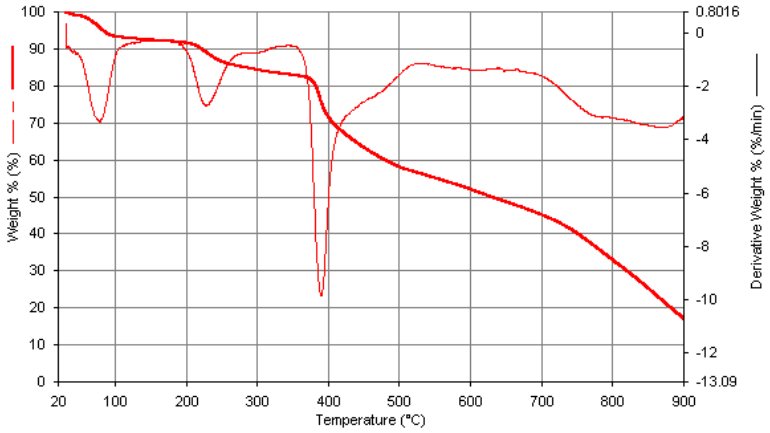

Figure 52. TGA and DTG Curves of $Ni(Bmpp\text{-}Dh)_2(H_2O)_2 \cdot H_2O$

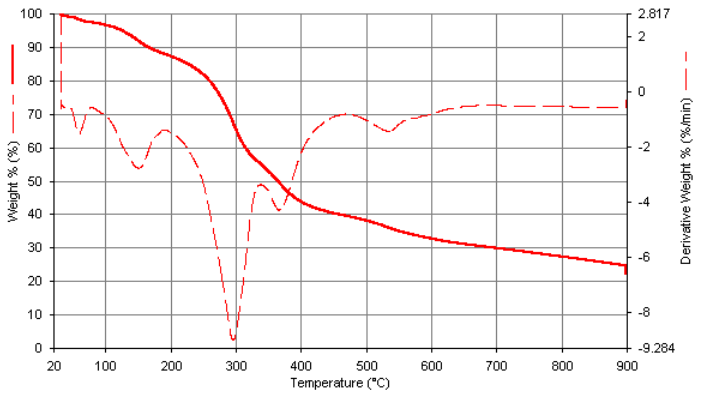

Figure 53. TGA and DTG Curves of $Ni(Ampp\text{-}Dh)_2(H_2O)_2$

Both copper complexes of acylpyrazolone Schiff bases with dinitrophenylhdrazine exhibited a major decomposition at 380°C, this decomposition may be due to the removal of one Schiff base ligand and followed by another decomposition over a wide temperature range which is associated with the removal of the second Schiff base in both cases (Fig. 54 and 55). The presence of the uncoordinated water molecule is obvious in $Cu(Bmpp\text{-}Dh)_2(H_2O)_2{\cdot}2H_2O$ with a decomposition at around 100°C followed by the removal of coordinated water molecule at 200°C. DTG curve reveals some decomposition around 220°C which is due to the coordinated water molecule and absence of any decomposition earlier than this is an evidence of no lattice water molecule.

Based on elemental, spectroscopic and thermal studies the proposed structure for metal complexes is presented in **88**-**95**.

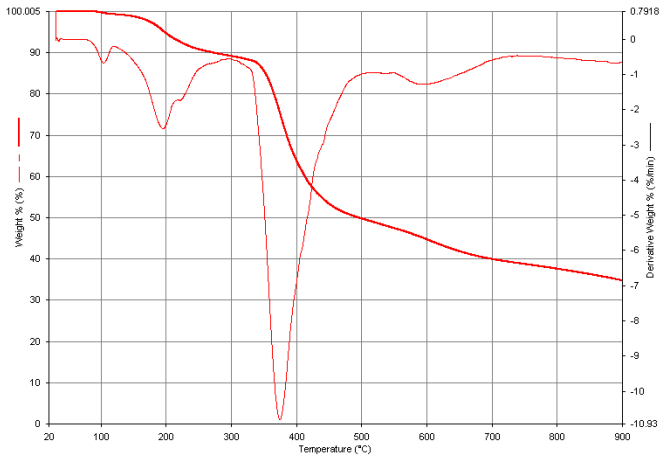

Figure 54. TGA and DTG Curves of $Cu(Bmpp\text{-}Dh)_2(H_2O)_2{\cdot}2H_2O$

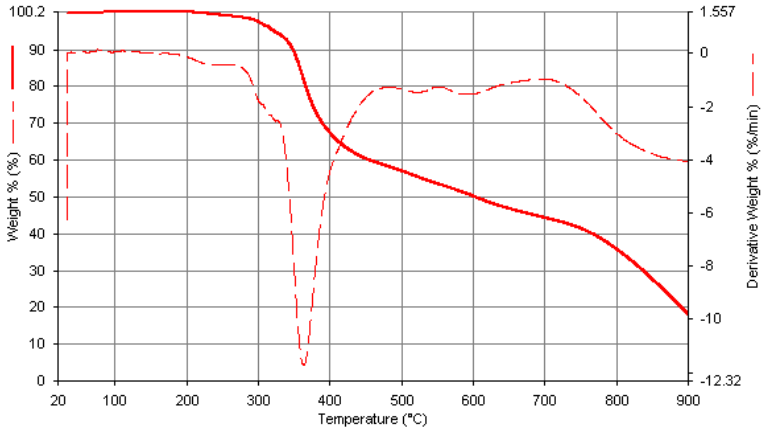

Figure 55. TGA and DTG Curves of $Cu(Ampp\text{-}Dh)_2(H_2O)_2$

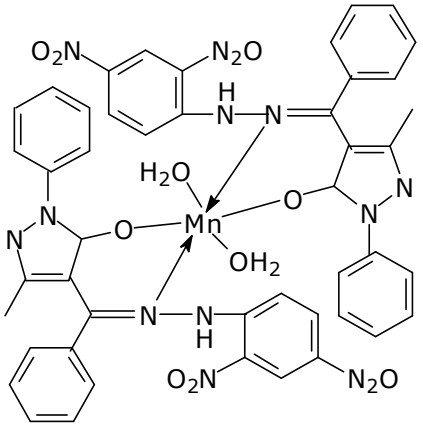

88

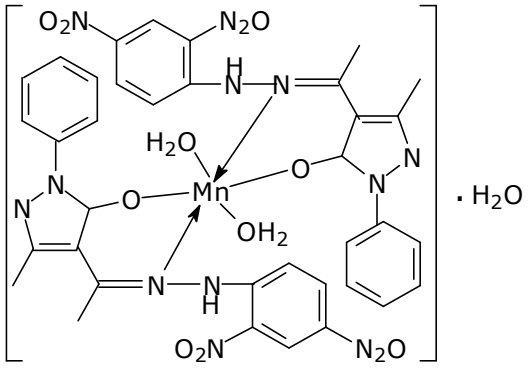

89

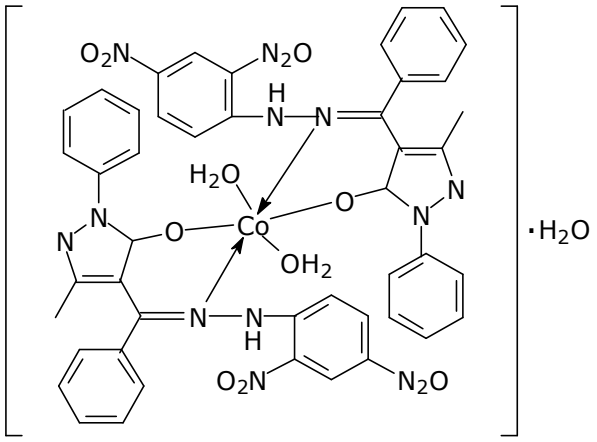

90

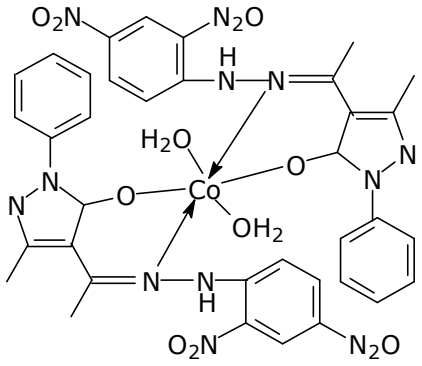

91

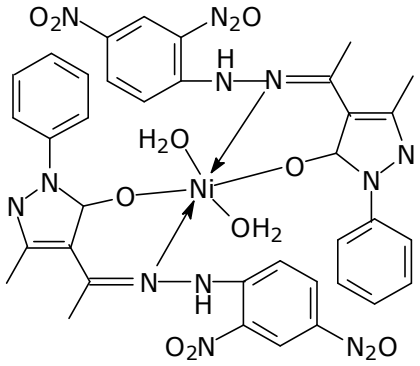

92

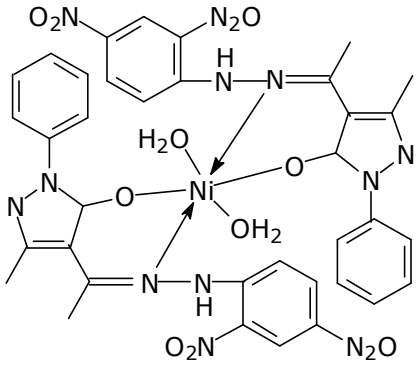

93

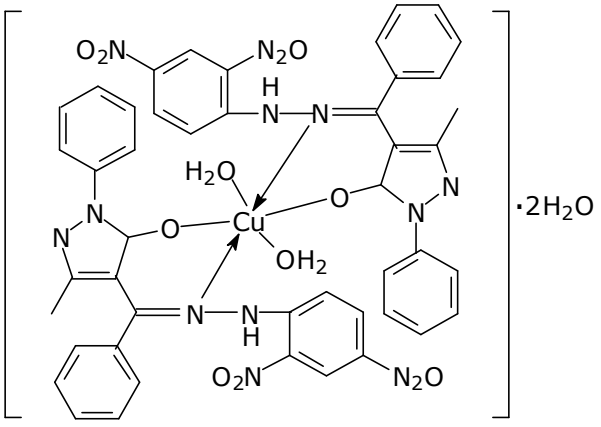

94

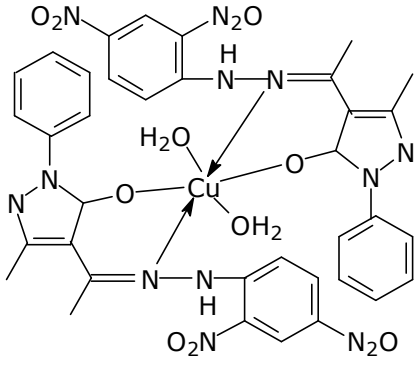

95

4.2.9 Antibacterial Screening

The zones of inhibition from *invitro* antibacterial screening of dinitrophenylhydrazine Schiff base and their metal complexes using the paper disc diffusion method is presented in Table 9. All the reported compounds show a generally low antibacterial activity compared to chloramphenicol. Ampp-Dh showed a highest zone of inhibition at 24 mm against *Staphylococus aureus,* which was followed by $Co(Ampp\text{-}Dh)_2(H_2O)_2$ with 20 mm against Gram negative *Aeromonas hydrophillia.* $Ni(Bmpp\text{-}Dh)_2(H_2O)_2{\cdot}H_2O$ displayed a broad spectrum activity, having a positive activity against all selected bacterial isolates and may be referred to as most active compound on the list (80AAC27).

Table 9. Zone of Growth Inhibition Exhibited by Dinitrophenylhydrazine Schiff Bases and Metal Complexes at 40 mg/mL (mm)

Ligand and complexes	*Staphylococus aureus*	*Bacillus pumillus*	*Proteus vulgaris*	*Aeromonas hydrophillia*
Bmpp-Dh	4.0	8.3	NI	NI
Ampp-Dh	24.0	9.5	NI	4.5
$Mn(Bmpp\text{-}Dh)_2(H_2O)_2$	8.0	7.0	NI	NI
$Co(Bmpp\text{-}Dh)_2(H_2O)_2{\cdot}H_2O$	8.3	7.0	NI	NI
$Ni(Bmpp\text{-}Dh)_2(H_2O)_2{\cdot}H_2O$	10.5	6.0	12.0	12.0
$Cu(Bmpp\text{-}Dh)_2(H_2O)_2{\cdot}2H_2O$	NI	8.5	NI	12.0
$Mn(Ampp\text{-}Dh)_2(H_2O)_2{\cdot}H_2O$	8.0	8.5	9.5	20.0
$Co(Ampp\text{-}Dh)_2(H_2O)_2$	15.5	4.0	NI	5.0
$Ni(Ampp\text{-}Dh)_2(H_2O)_2$	8.0	12.5	NI	8.3
$Cu(Ampp\text{-}Dh)_2(H_2O)_2$	13.0	12.3	NI	20
Chloramphenicol	30.0	20.0	42.0	40.0
DMSO	NI[1]	NI	NI	NI

[1]NI = no inhibition

4.2.10. Antioxidant (Free Radical Scavenging) Activity

Although at 0.50 mg/mL the two Schiff base ligands $Mn(Bmpp\text{-}Dh)_2(H_2O)_2$ and $Co(Ampp\text{-}Dh)_2(H_2O)_2$ did not show any activity, all the compounds under investigation show free-radical scavenging properties with DPPH. $Mn(Ampp\text{-}Dh)_2(H_2O)_2{\cdot}H_2O$ had the strongest antioxidant activity with percentage scavenging activity values close to that of standard drug, ascorbic acid (Table 10). This was in agreement with reported work on synthesized compounds with metal ion coordination (01RJP61).

Table 10. Antioxidant Scavenging Activity Data of Dinitrophenylhydrazine Schiff Bases and Their Metal Complexes (%)

Ligand and complexes	Percentage antioxidant scavenging activity		
	0.50 mg/ml	0.25 mg/ml	0.13 mg/ml
Bmpp-Dh	–	31.05	30.70
Ampp-Dh	–	63.27	76.33
$Mn(Bmpp\text{-}Dh)_2(H_2O)_2$	–	68.83	52.28
$Co(Bmpp\text{-}Dh)_2(H_2O)_2{\cdot}H_2O$	8.58	59.56	47.11
$Ni(Bmpp\text{-}Dh)_2(H_2O)_2{\cdot}H_2O$	87.92	62.80	61.28
$Cu(Bmpp\text{-}Dh)_2(H_2O)_2{\cdot}2H_2O$	2.28	89.90	53.76
$Mn(Ampp\text{-}Dh)_2(H_2O)_2{\cdot}H_2O$	68.48	85.86	87.42
$Co(Ampp\text{-}Dh)_2(H_2O)_2$	–	55.50	55.98
$Ni(Ampp\text{-}Dh)_2(H_2O)_2$	65.32	84.01	84.83
$Cu(Ampp\text{-}Dh)_2(H_2O)_2$	35.73	85.40	82.98
Ascorbic acid	87.62	93.63	91.99

All metal complexes with Bmpp-Dh exhibited a generally increased activity than their ligand, Specifically, $Ni(Bmpp\text{-}Dh)_2(H_2O)_2{\cdot}H_2O$ and $Cu(Bmpp\text{-}Dh)_2(H_2O)_2{\cdot}2H_2O$ showed a significant increase in antioxidant property at 0.5 and 0.25 mg/mL respectively compared to its free Schiff base ligand Bmpp-Dh, Fig.56.

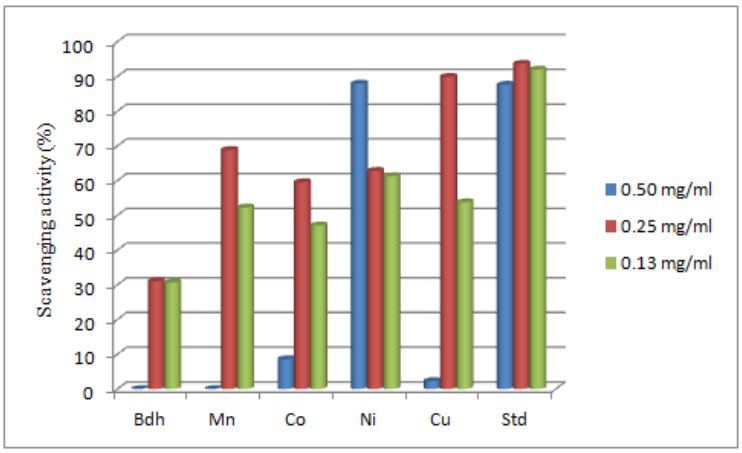

Figure 56. Chart Showing the Scavenging Activity of Bmpp-Dh and its Metal Complexes

A generally higher antioxidant activity for metal complexes have been observed with metal complexes of acetyl pyrazolone Schiff base with dinitrophenylhydrazine as this was peculiar in all different concentrations. $Mn(Ampp\text{-}Dh)_2(H_2O)_2{\cdot}H_2O$ exhibited a strongest activity across all concentration values, Figure 57.

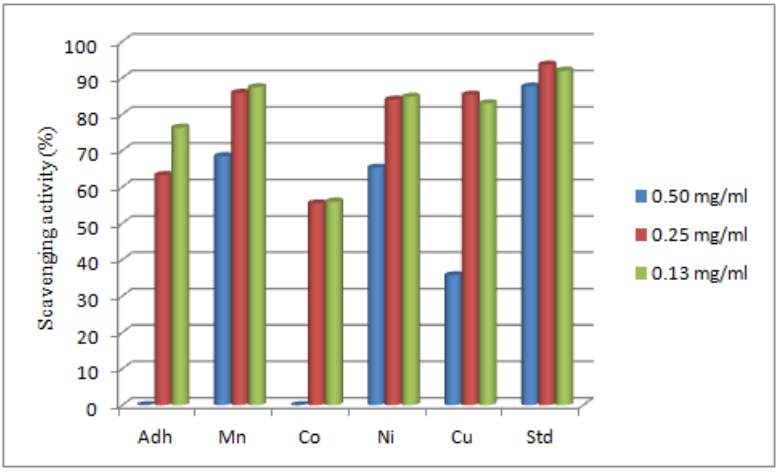

Figure 57. Chart Showing the Scavenging Activity of Ampp-Dh and its Metal Complexes

4.3. Acylpyrazolone Derived Sulfanilamide Schiff Bases and Their Metal Complexes

Sulfanilamide drugs are well-known antimicrobial agents used as therapeutic agents over a century for the prevention and cure of bacterial infections in humans (01D774). Sulfonamides, as they are generally referred were the first set of drugs with a selective action towards various diseases both as a preventive and therapeutic agent (04AOC221, 07SA(A)1271). Structurally, the sulfanilamide group resembles *p*-aminobenzoic acid, a metabolite, which is capable of blocking folic acid synthesis in bacteria, thereby causing cell death; hence the reason for their strong antibacterial activity (05TMC411). Metal complexes of sulfanilamides have also proven to be very significant therapeutic agents and thus have been used as such (92POL1507, 95MBD81, 01D774). Sulfanilamide is the simplest member of the sulfa drugs family having four potential coordinating sites towards metal ions, **96**; the sulfanyl oxygen atoms as well as the amino group nitrogens by deprotonation. The numbers of coordinating chelating sites have been increased by the formation of remarkable Schiff base ligands with even better biological and therapeutic properties (10CJS69). The single crystal structure of sulfanilamide Schiff base with salicylaldehyde was reported in a monoclinic crystal system (10CJSC69). This section discusses the synthesis, characterization, and the biological studies of two Schiff bases ligand of sulfanilamide, 4-benzoyl-3-methyl-1-phenyl-2-pyrazolin-5-one sulfanilamide Bmpp-Sn and 4-

acetyl-3-methyl-1-phenyl-2-pyrazolin-5-one sulfanilamide Ampp-Sn, including their Mn(II), Co(II), Ni(II) and Cu(II) complexes.

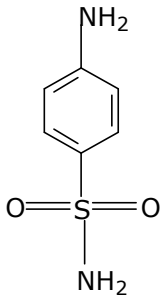

96

4.3.1. Synthesis

Presented in eq. 7 is the synthetic scheme of sulfanilamide Schiff bases obtained from the condensation reaction between the synthesized pyrazolone Schiff base precursors and 4-aminobenzenesulfonamide in a 1:1 molar ratio.

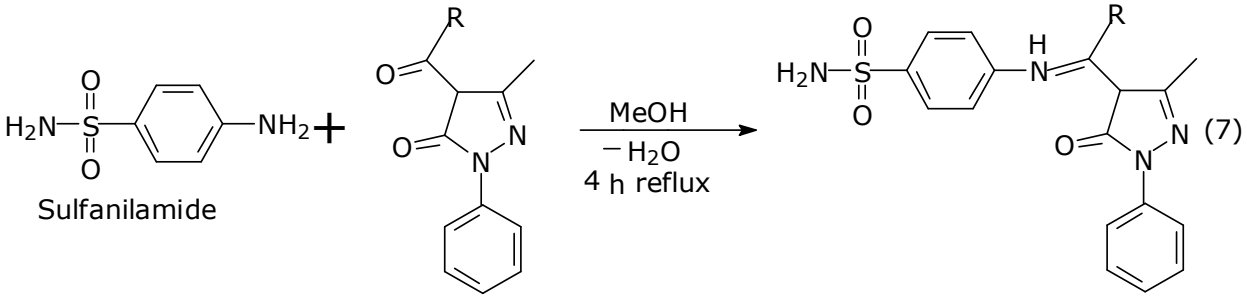

(7)

The Schiff bases were obtained in an air-stable solid form at room temperature and soluble in methanol, ethanol, and most common organic solvents. They were in more than average in yield, and purity was monitored by TLC after continuous washing with methanol. The small melting point

range gave an idea of its purity. Single threadlike crystal structure of Bmpp-Sn distorted with a water molecule was afforded from slow evaporation of a solution of methanol, while that of Ampp-Sn was not successful. The Schiff bases have both been fully characterized by elemental analysis, IR-spectroscopy, UV-VIS-spectroscopy, ^{1}H and ^{13}C NMR spectroscopy, mass spectroscopy and X-ray crystallographic analysis for Bmpp-Sn.

Treatment of Bmpp-Sn or Ampp-Sn with an appropriate metal salt afforded metal complexes as presented in a general synthesis scheme, Eq. 8. They were in a powder form and in different colors. The metal complexes are generally insoluble in water, ethanol, and in most non-coordinating solvents but sparingly soluble in methanol and soluble in DMF and DMSO. Attempts to grow crystal structure for X-ray crystallography were unsuccessful but a single crystal structure of the benzoyl Schiff base precursor with cobalt was obtained instead, from slow evaporation of Bmpp-Sn in DMF. Their molar conductance values infer non–electrolyte behavior in DMF (71CCR81, 75MI1).

$$MX_2 \cdot nH_2O \; + \; 2L \xrightarrow[\text{reflux 4 h}]{EtOH/H_2O} M(L)_2(H_2O)_2 \cdot nH_2O \qquad (8)$$

$M = Mn^{2+}, Co^{2+}, Ni^{2+}$ or Cu^{2+}, $X = Cl^{-}$ or CH_3COO^{-}

L = Bmpp–Sn or Ampp–Sn

4.3.2. Elemental analysis

The CHN elemental analysis result in percentage of Bmpp-Sn, Ampp-Sn, and metal complexes found was in agreement with calculated composition values. Octahedral metal complexes with the corresponding Schiff base are

proposed, having two molecules each of the Schiff base and two molecules of water to complete its octahedral geometry. Some of their physical properties, melting point range, elemental composition and percentage yield are presented in the experimental section.

4.3.3. ^{1}H and ^{13}C NMR Spectroscopy

The ^{1}H NMR spectra of Bmpp-Sn (Fig. 58) showed a multiplet at 7.8–7.1 ppm due to the aromatic protons and a singlet each at 12.8 ppm and at 8.0 ppm assigned, respectively, to the –NH and the azomethine nitrogen H–N=C protons. The resonance peak due to methyl protons is displayed upfield at 2.2 ppm integrating for an unequivalent number of hydrogen atoms.

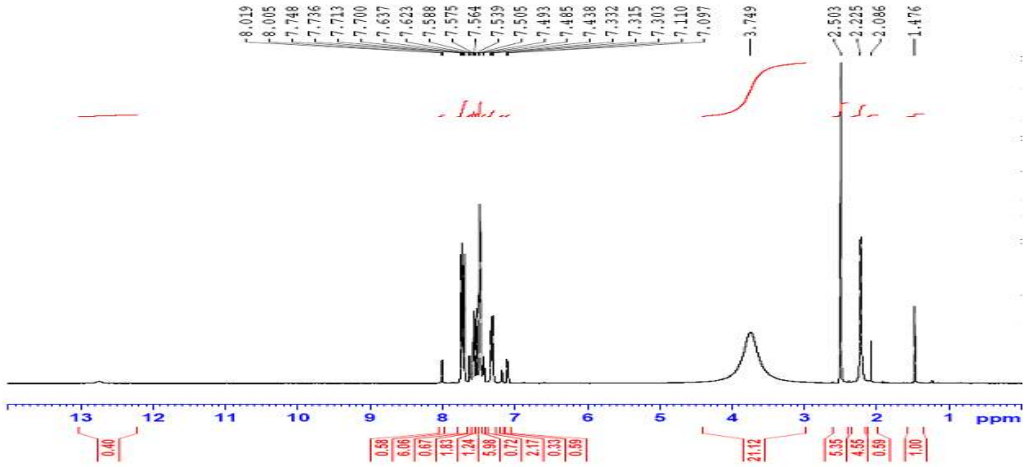

Figure 58.^{1}H NMR Spectrum of Bmpp-Sn

^{1}H NMR spectra of Ampp-Sn (Fig. 59) was inconclusive as resonance peaks were not resolved enough to assign all necessary chemical shifts; however, the peak on the far downfield is due to NH_2 hydrogen –NH at 13.1 ppm integrated for one proton. The two sharp peaks on the far upfield is due

to the methyl proton groups, pyrazolone methyl at 2.5 ppm and the acetyl methyl at 2.4 ppm although integrated for a higher proton value. The signals at 7.9–7.2 ppm are assigned to the aromatic protons while the peak at 8.0 ppm is due to azomethine hydrogen H–N=C.

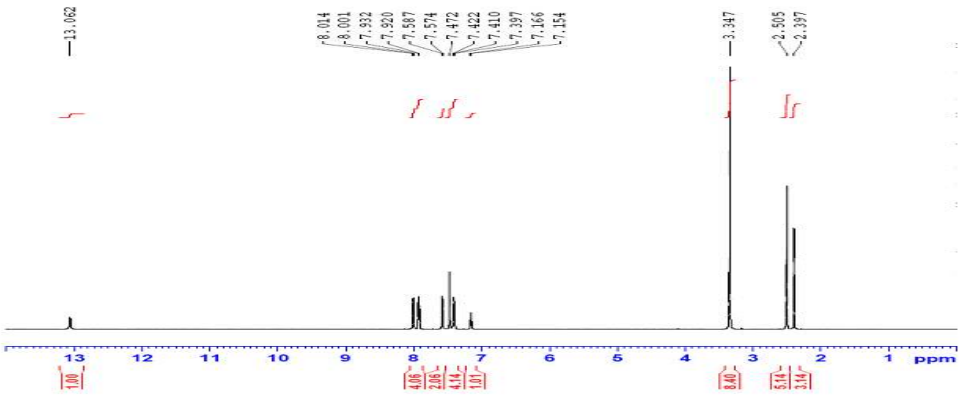

Figure 59. ^{1}H NMR Spectrum of Ampp-Sn

A signal at 190.5 ppm in Bmpp-Sn and that at 165.4 ppm in Ampp-Sn may be assigned to the carbonyl carbon C=O. The azomethine carbon can be observed at 139.3 ppm in Bmpp-Sn (Figure 60), while in Ampp-Sn displayed at 164.5 ppm.

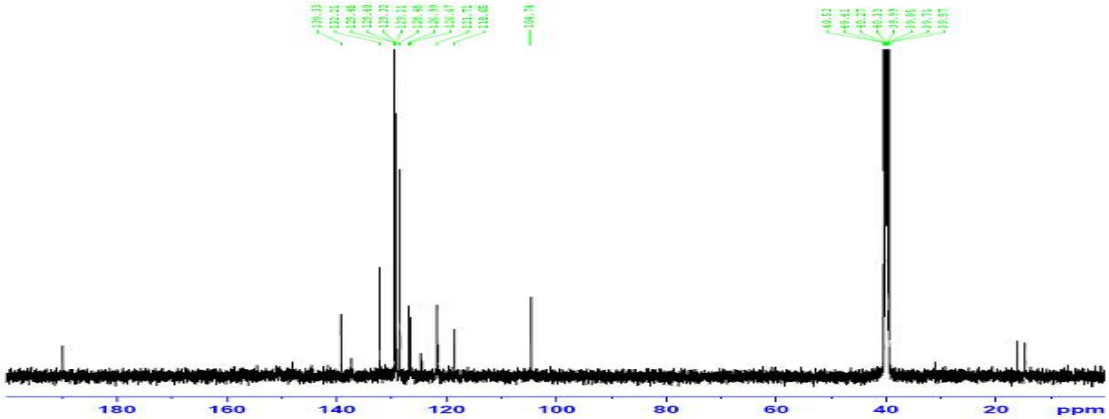

Figure 60. ^{13}C NMR Spectrum of Bmpp-Sn

Signals due to aromatic carbon atoms are resonating at a chemical shift of 132.2–110.7 ppm in Bmpp-Sn and 142.8–116.6 ppm in Ampp-Sn. Aliphatic methyl carbon may be assigned to a signal at around 16.5 ppm in Bmpp-Sn and the two methyl groups in Ampp-Sn is assigned to the signals at 17.6 and 17.5 ppm. The resonance signal due to C–S may be assigned to signal at 148.2 ppm in Ampp-Sn (Fig.61). Unfortunately, this particular signal could not be accounted for in Bmpp-Sn but its mass spectrum and crystal X-ray structure does confirm the proposed molecular structure.

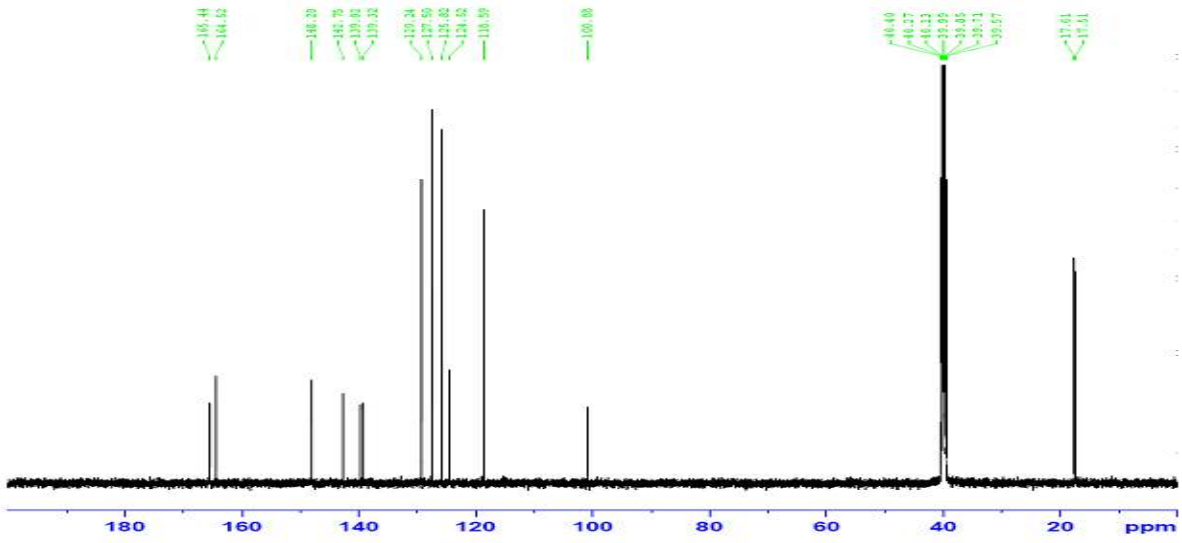

Figure 61. ^{13}C NMR Spectrum of Ampp-Sn

4.3.4. Mass Spectroscopy

The molecular ion peak of the APCI source mass spectrum of Bmpp-Sn and Ampp-Sn was observed at *m/z* 433 and *m/z* 371, respectively, and completely agree with the calculated theoretical molar mass plus one hydro-

gen $[M+H]^+$. Also the protonated benzoyl Schiff base precursor fragmentation peak was observed at *m/z* 279 *i.e.* $C_{17}H_{14}N_2O_2$ in Fig.62, while a fragmentation peak of acetyl Schiff base precursor $C_{12}H_{11}N_2O_2$ was seen at *m/z* 216 in Bmpp-Sn spectrum, Fig.63.

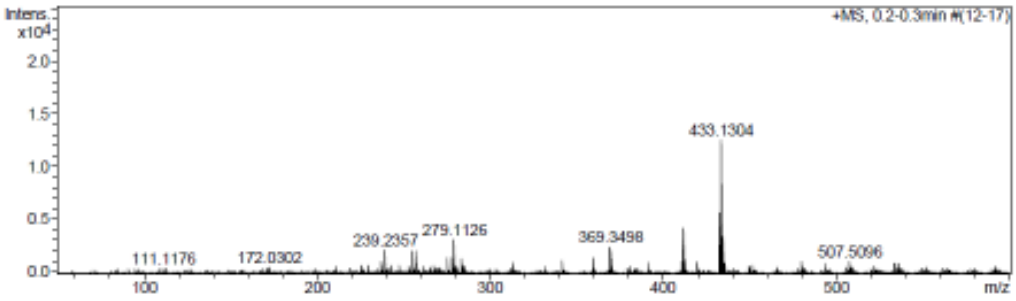

Figure 62. Mass Spectrum of Bmpp-Sn

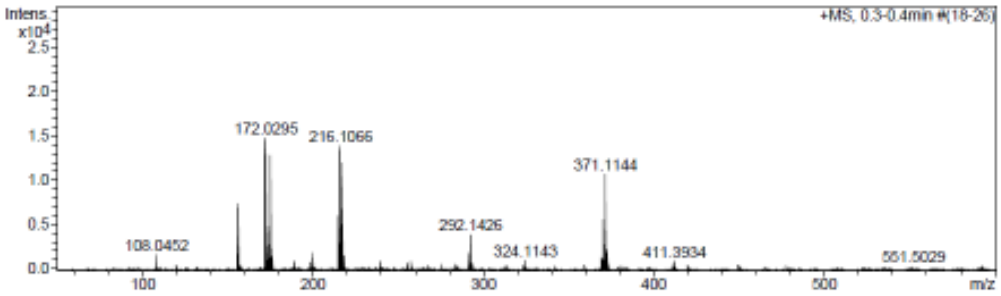

Figure 63. Mass Spectrum of Ampp-Sn

4.3.5. Infrared Spectroscopy

The successful formation of the sulfanilamide Schiff base with acylpyrazolone in a keto tautomer form was evident in the presence of the azomethine (C=N) and ketone carbonyl (C=O) vibrating bands. The (C=N) was observed at 1639 cm^{-1} in Bmpp-Sn and 1633 cm^{-1} in Ampp-Sn which is modified and appeared at a lower wave number region of 1627–1617 cm^{-1} in the IR spectra of metal complexes. Ketone carbonyl group (C=O) was observed at 1504

cm^{-1} in Bmpp-Sn and 1503 cm^{-1} in Ampp-Sn, which was not obvious in the metal complexes spectra showing a transformation of the double bond of carbonyl into a metal oxygen bond –C–O–M. The octahedral Schiff base metal complexes were completed with two water molecules each and this bond can be seen from the formation of a vibrating band at around 850–823 cm^{-1} in addition to the broad band at 3498–3390 cm^{-1} in the metal complexes, which appeared at 3496–3497 cm^{-1} in the Schiff base ligands. The bands that appeared at 634–619 cm^{-1} and 498–470 cm^{-1} are due to metal nitrogen bond M–N and metal oxygen M–O, respectively. The IR spectra of ligands and their respective metal complexes are presented in the Appendix.

4.3.6. UV-Vis Spectroscopy and Magnetic Moment

Bmpp-Sn and Ampp-Sn exhibited the expected bands at the UV region due to $\pi \rightarrow \pi^*$ and $n \rightarrow \pi^*$. Absorption bands and wavelength values carefully assigned are presented in the experimental section. $Mn(Bmpp\text{-}Sn)_2(H_2O)_2$ shows two bands in the visible region at 424 nm and 589 nm assigned to $^6A_{1g} \rightarrow {}^4T_{2g}$ and $^6A_{1g} \rightarrow {}^4T_{1g}$ transitions respectively corresponding to a d^5 octahedral Mn(II) environment (Fig.64). One band at 431 nm is assigned to $^6A_{1g} \rightarrow {}^4T_{2g}$ in $Mn(Ampp\text{-}Sn)_2(H_2O)_2 \cdot H_2O$ (Fig.65). The high spin d^5 octahedral manganese complexes was corroborated with the magnetic moment values of 5.82 and 5.61 BM for $Mn(Bmpp\text{-}Sn)_2(H_2O)_2$ and $Mn(Ampp\text{-}Sn)_2(H_2O)_2 \cdot H_2O$ respectively (07PJP301).

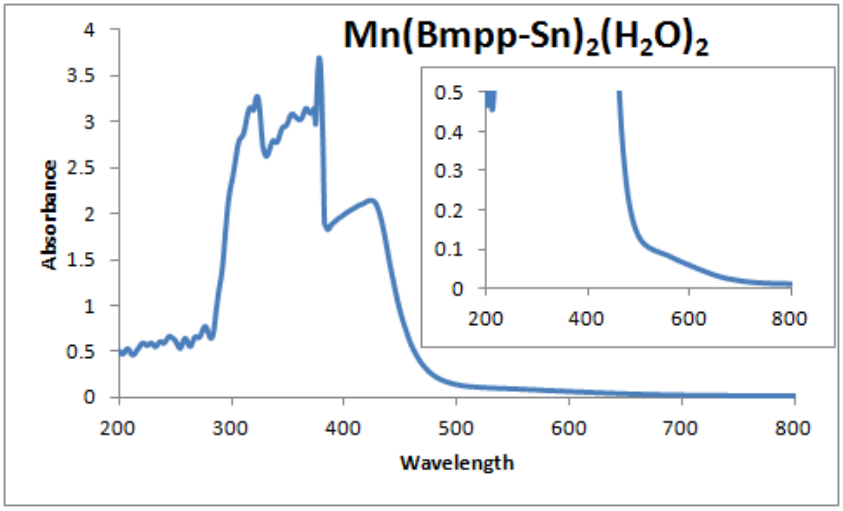

Figure 64. Electronic Spectrum of $Mn(Bmpp\text{-}Sn)_2(H_2O)_2$

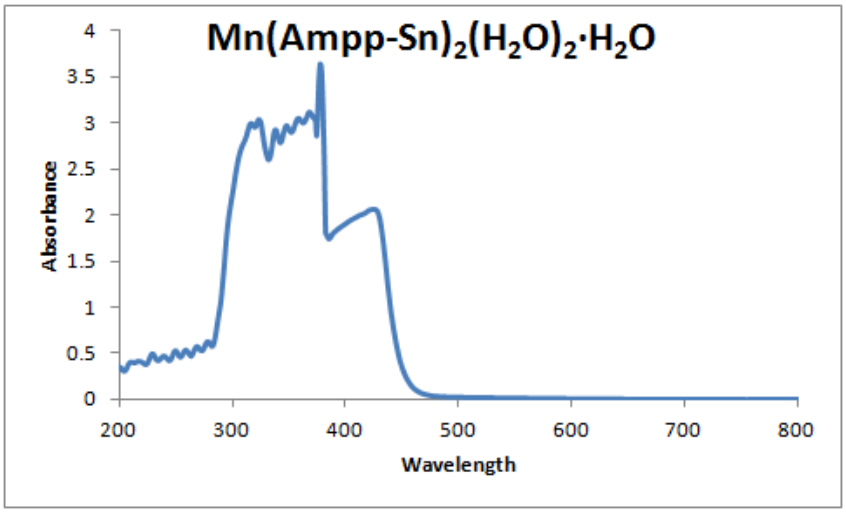

Figure 65. Electronic Spectrum of $Mn(Ampp\text{-}Sn)_2(H_2O)_2{\cdot}H_2O$

$Co(Bmpp\text{-}Sn)_2(H_2O)_2{\cdot}H_2O$ displays two bands in the visible region at 408 nm and 540 nm corresponding to ν_1 ($^4T_{2g}\rightarrow{}^4T_{1g}$), and ($^4A_{2g}\rightarrow{}^4T_{1g}$) transitions respectively, Fig. 66. It also has a magnetic moment value of 4.46 BM expected for an octahedral Co(II). Three bands were observed in the electronic spectra of $Co(Ampp\text{-}Sn)_2(H_2O)_2$ with magnetic moment of 4.43 BM, at 408 nm, 632 nm and 699 nm assigned as ($^4T_{2g}\rightarrow{}^4T_{1g}$), ($^4A_{2g}\rightarrow{}^4T_{1g}$) and

($^4T_{1g}(p) \rightarrow {}^4T_{1g}$) transitions, respectively (Fig. 67), expected of a d^7 octahedral geometry (07EQ7).

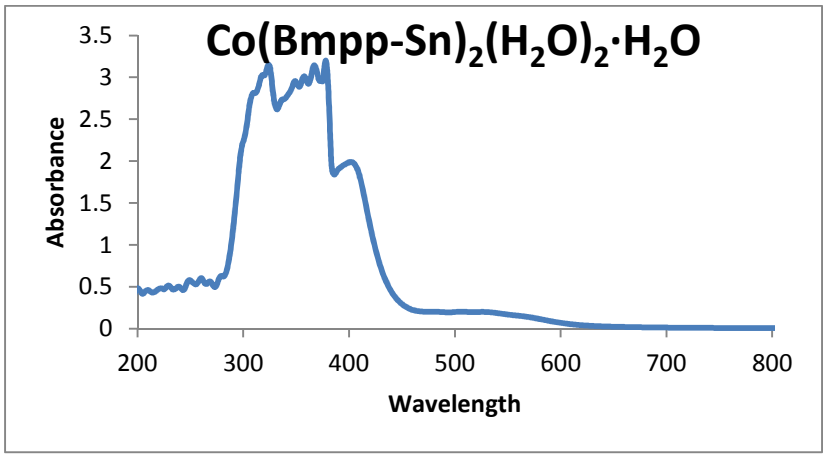

Figure 66. Electronic Spectrum of $Co(Bmpp\text{-}Sn)_2(H_2O)_2 \cdot H_2O$

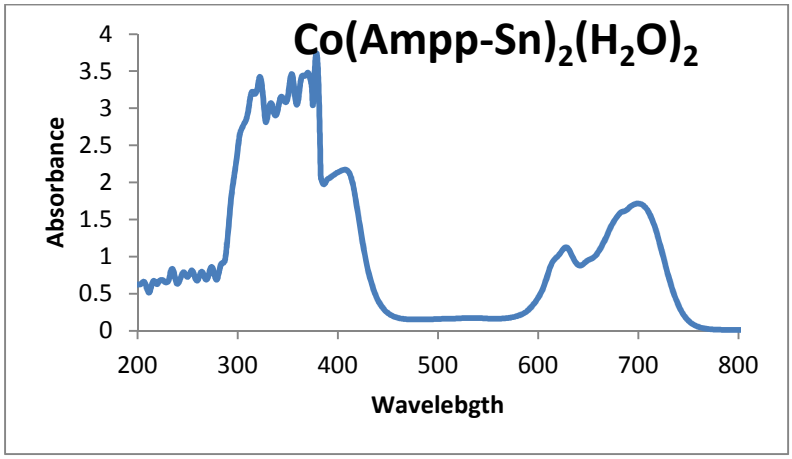

Figure 67. Electronic Spectrum of $Co(Ampp\text{-}Sn)_2(H_2O)_2$

The bands at 410 nm and 683 nm were assigned to $^3A_{2g} \rightarrow {}^3T_{1g}(p)$ and $^3A_{2g} \rightarrow {}^3T_{1g}(F)$, respectively in $Ni(Bmpp\text{-}Sn)_2(H_2O)_2 \cdot H_2O$ (Fig. 68). In $Ni(Ampp\text{-}Sn)_2(H_2O)_2 \cdot H_2O$ the d-d bands at 596 nm and 674 nm is assigned as $^3A_{2g} \rightarrow {}^3T_{1g}(F)$ and $^3A_{2g} \rightarrow {}^3T_{2g}(F)$ respectively, Fig.69. These transitions correspond to a d^8 Ni(II) with octahedral geometry. Their magnetic moment of

2.89 and 2.93 BM for $Ni(Bmpp\text{-}Sn)_2(H_2O)_2\cdot H_2O$ and $Ni(Ampp\text{-}Sn)_2(H_2O)_2\cdot H_2O$, respectively, further justify the predicted geometry (02SRI819).

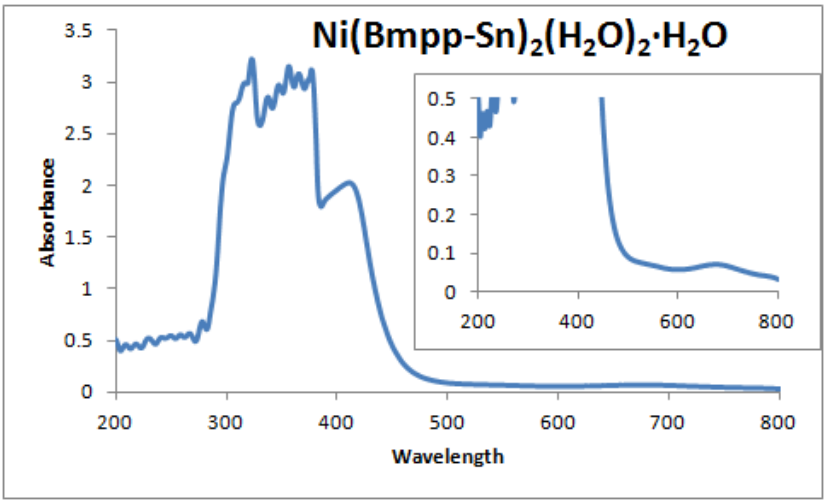

Figure 68. Electronic Spectrum of $Ni(Bmpp\text{-}Sn)_2(H_2O)_2\cdot H_2O$

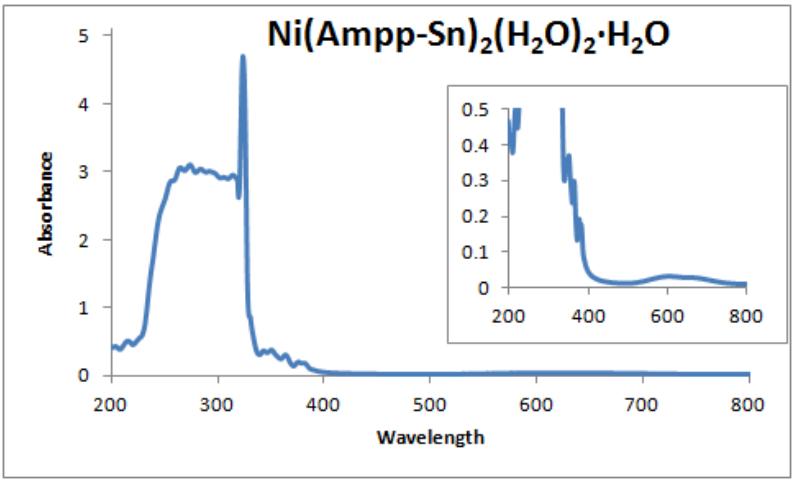

Figure 69. Electronic Spectrum of $Ni(Ampp\text{-}Sn)_2(H_2O)_2\cdot H_2O$

Two bands in the electronic spectra of $Cu(Bmpp\text{-}Sn)_2(H_2O)_2$ observed as a strong band 442 nm and a broad band that peaks at 751 nm were assigned to $^2B_{1g}\rightarrow{}^2E_g$ and $^2B_{1g}\rightarrow{}^2B_{2g}$ transitions, respectively, with a magnetic moment

value of 1.93 BM, Fig.70. $Cu(Ampp\text{-}Sn)_2(H_2O)_2 \cdot H_2O$ exhibited one single broad band characterized by a distorted octahedral Cu(II) at 618 nm which is assigned to $^2B_{1g} \rightarrow {}^2B_{2g}$ transition Fig. 71, with a magnetic moment value of 1.90 BM.

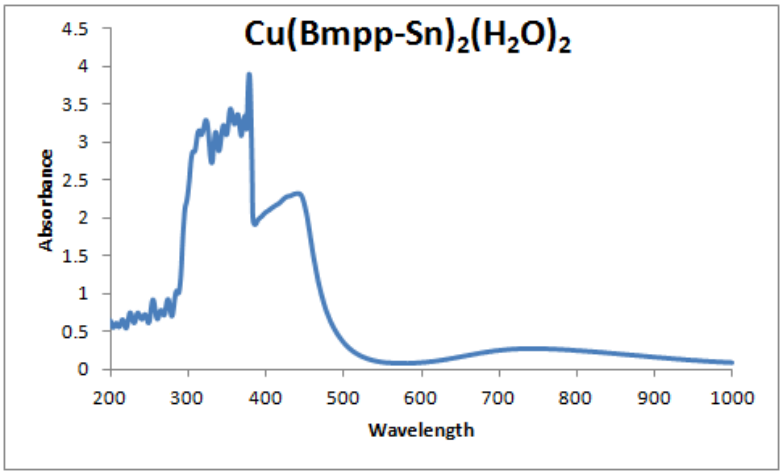

Figure 70. Electronic Spectrum of $Cu(Bmpp\text{-}Sn)_2(H_2O)_2$

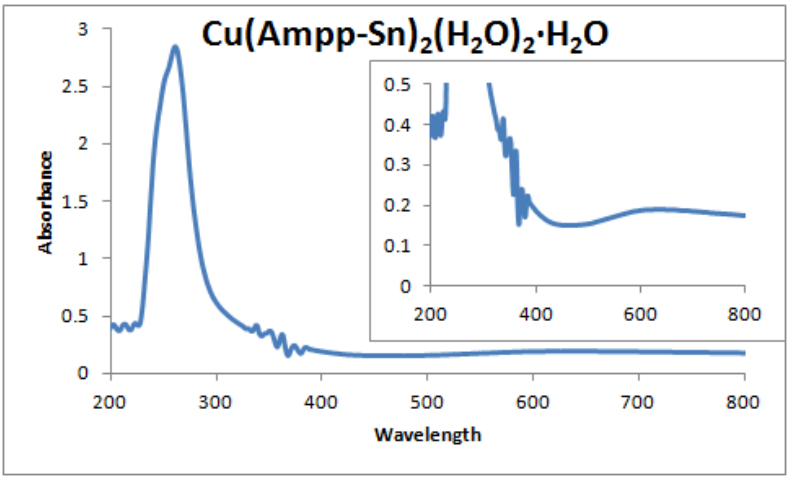

Figure 71. Electronic Spectrum of $Cu(Ampp\text{-}Sn)_2(H_2O)_2 \cdot H_2O$

4.3.7. X-Ray Crystallography

Slow evaporation of Bmpp-Sn solution in methanol afforded needle-like single crystals of Bmpp-Sn with a water molecule distortion formulated as

$C_{23}H_{20}N_4O_3S{\cdot}H_2O$. A summary of crystal data (crystallographic and refinement parameters) is presented in Table 11.

Table 11. Crystal and Refinement Data for Bmpp-Sn

Compound	Bmpp-Sn
Formula	$C_{23}H_{20}N_4O_3S{\cdot}H_2O$
Crystal colour and form	Orange / Block
Formula weight	450.52
Crystal system	Monoclinic
Space group	C2/c
a	23.3366 (4)(Å)
b	14.7706 (3)(Å)
c	12.5787 (2) (Å)
α	90 (1)^o
β	100.727 (1)^o
V	4257.21 (13)(Å^3)
Z	8
$D_{(calc)}$	1.406 (Mg cm^{-1})
F(000)	1888
θ range	2.2–28.3 ($^\circ$)
Crystal size	0.24 x 0.38 x 0.56 (mm)
Reflections measured	19945
Independent/observed	5285/4408
Mu(MoKa)	0.71073 (/mm)
Temperature	296 (K)
Parameters	108

The H atoms on N_1, N_2, and O_4 were located on a difference Fourier map and refined with U(H) set to 1.2U_{eq}(N) and 1.5U_{eq}(O). The SO_2NH_2 group shows rotational disorder, which could not be effectively modeled. The data was corrected for absorption effects using the numerical method implemented in SADABS. Two reflections were omitted from the refinement because they were obscured by the beam-stop. Solid state Bmpp-Sn$\cdot H_2O$ as seen in

Fig. 72, is essentially planar with the plane of the methylpyrazolone group but with the phenyl groups turned out of the plane. The phenyl rings C_{11}–C_{16}, C_{21}–C_{26} and C_{31}–C_{36} make dihedral angles of 39.44(12)°, 66.26(13)° and 34.38(13)°, respectively with the methylpyrazolone group.

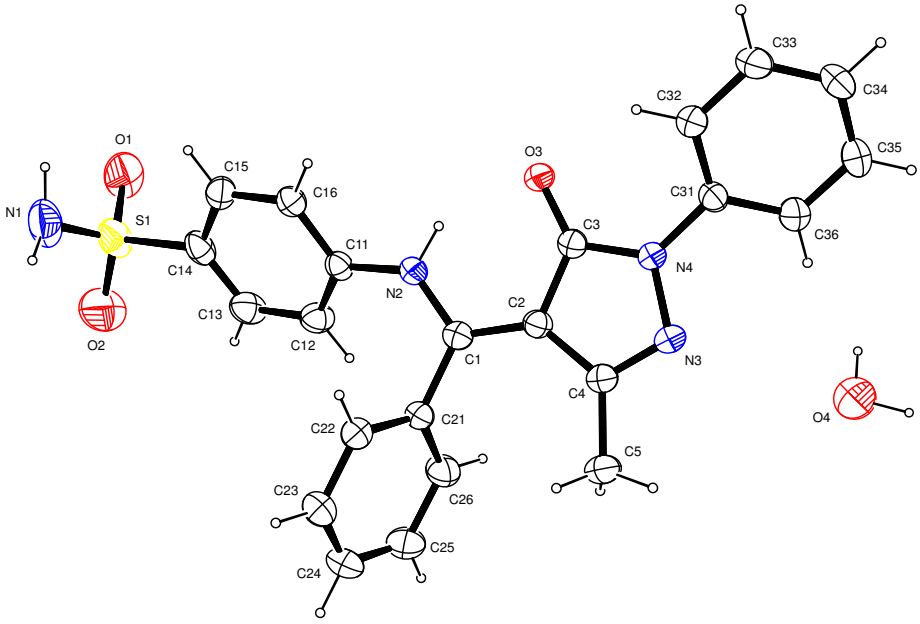

Figure 72. Molecular Crystal Structure of Bmpp-Sn·H_2O

There are three intra-molecular bonds: one short N2···H2···O3 hydrogen bond of 1.90 Å, and two long C13···H13···O2 and C32···H32···O3 hydrogen bonds of 2.48 Å each (Fig. 73). Pairs of Bmpp-Sn·H_2O are alternatively stacked in the c-axis direction and connected with two C22···H22···O3 hydrogen bonds of 2.45 Å, two C16···H16···C (pyrazole ring) π-ring interactions of 2.66 Å, and two N1···H1B···C (C31–C36 phenyl ring) π-ring interaction of 2.70 Å. A water molecule connects adjacent Bmpp-Sn·H_2O in the b-axis di-

rection with two hydrogen bonds N1···H1A···O4···H4B···N4 of length 1.74 and 2.13 Å, respectively.

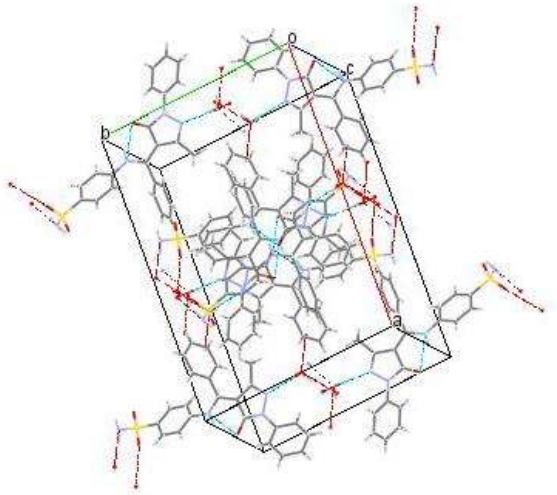

Figure 73. Hydrogen Bonding in Bmpp-Sn·H_2O

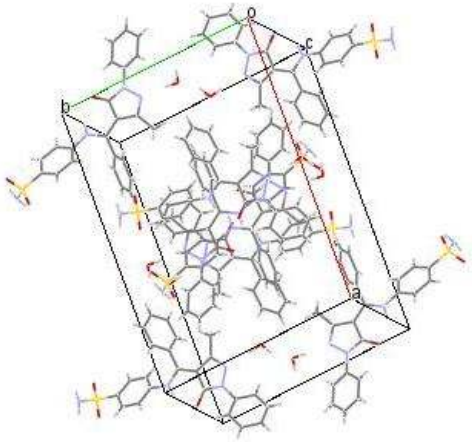

Figure 74. Molecular parking diagram of Bmpp-Sn·H_2O

A Co(II) complex with Bmpp single crystal was obtained from a solution of $Co(Bmpp\text{-}Sn)_2(H_2O)_2\cdot 2H_2O$ in DMF, an unsuccessful attempt to grow the single crystal structure of $Co(Bmpp\text{-}Sn)_2(H_2O)_2\cdot 2H_2O$. The orange block-like crystal has two Bmpp molecules coordinating to the metal ion in a bidentate

form through the ketone oxygen and that of the benzoyl formulated as $C_{40}H_{40}CoN_6O_6$, Fig. 75. Two molecules of DMF complete the octahedral geometry observed (Fig. 76). Summary of crystal data is presented in Table 12.

Table 12. Crystal and Refinement data for $Co(Bmpp)_2(DMF)_2$

Compound	$Co(Bmpp)_2(DMF)_2$
Formular	$C_{40}H_{40}CoN_6O_6$
Crystal colour and form	Orange / Block
Formula weight	759.71
Crystal system	Monoclinic
Space group	P21/c
a	10.1110 (5)(Å)
b	9.3904 (4)(Å)
c	21.3390 (8) (Å)
α	90 (1)°
β	117.241 (2)°
V	1799.43 (14)(Å^3)
Z	2
$D_{(calc)}$	1.402 (Mg cm^{-1})
F(000)	794
θ range	2.1–28.4 (°)
Crystal size	0.22 x 0.44 x 0.56 (mm)
Reflections measured	49492
Independent/observed	4515/4132
Mu(MoKa)	0.534 (/mm)
Temperature	200 (K)

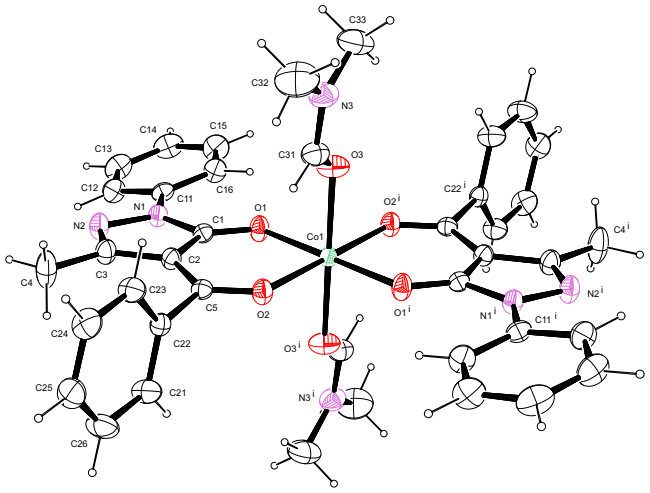

Figure 75. Molecular Crystal Structure of $Co(Bmpp)_2(DMF)_2$

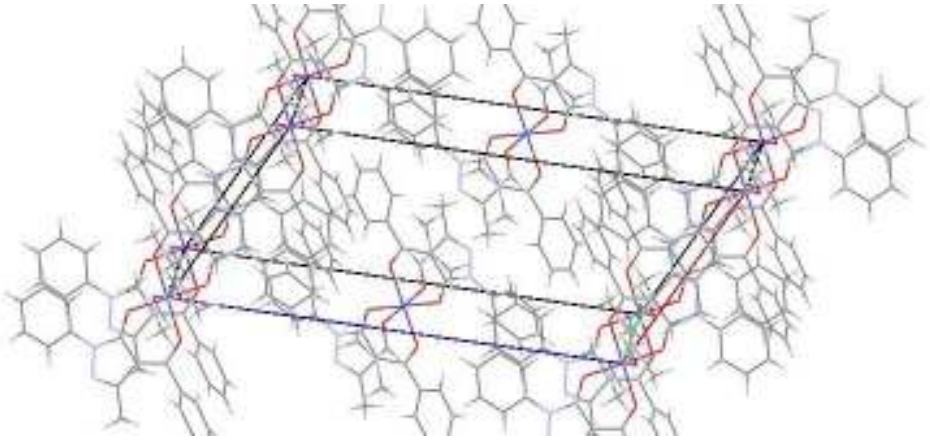

Figure 76. Molecular Packing Diagram of $Co(Bmpp)_2(DMF)_2$

Details of $Co(Bmpp)_2(DMF)_2$ crystal and other single crystals have been submitted to CCDC Cambridge and are presented in the Appendix.

4.3.8. Thermogravimetric Studies

TGA in collaboration with DTG curves shows a similar multistep decomposition pattern in the thermograms of metal complexes of the acylpyrazolone sulfanilamide Schiff base. Generally low thermal decomposition mass losses observed below 300^{o}C are due to the removal of the coordinated and non-

coordinated water molecules, although they have not been observed in some these complexes with coordinated water molecule. Also, most metal complexes exhibited multiple steps, for which assignment was not unequivocal.

In $Mn(Bmpp\text{-}Sn)_2(H_2O)_2{\cdot}H_2O$ (Fig. 77), the removal of the four water molecules have been observed in a decomposition at 220^{o}C. The major decomposition at around 550^{o}C with a mass loss of about 44% may be attributed to the removal of a Schiff base ligand molecule calculated as 45.3%. This decomposition was followed by a second one over a wide temperature range extending beyond 900^{o}C that may be attributed to the second Schiff base ligand leaving a residue of manganese oxide. The $Mn(Ampp\text{-}Sn)_2(H_2O)_2{\cdot}H_2O$ (Fig. 78) exhibited a different trend in decomposition due to the presence of an acetyl derivative Schiff base. Decomposition due to the elimination of the water molecules can be observed at 150 and 290^{o}C. It was followed by a major decomposition at around 450^{o}C attributed to the decomposition of the Schiff base ligand with a mass loss of 40% and calculated as 43.7%. The final decomposition due to the second ligand extends beyond 900^{o}C leaving the metal oxide.

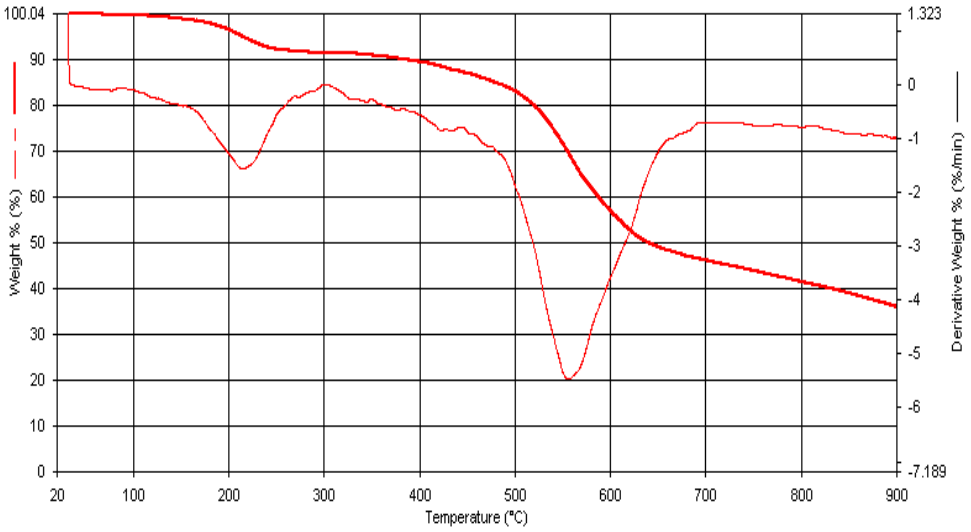

Figure 77. TGA and DTG Curve of $Mn(Bmpp\text{-}Sn)_2(H_2O)_2{\cdot}H_2O$

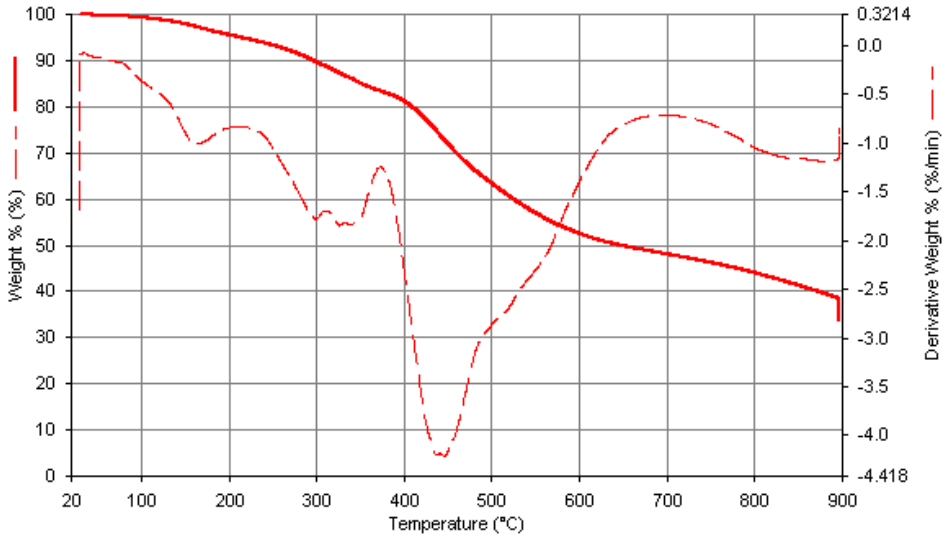

Figure 78. TGA and DTG Curve of $Mn(Ampp\text{-}Sn)_2(H_2O)_2{\cdot}H_2O$

The removal of water molecules from $Co(Bmpp\text{-}Sn)_2(H_2O)_2{\cdot}H_2O$ was observed at around 100°C, Fig.79. The major decomposition at 400°C was attributed to the loss of the Schiff base ligand with a mass percentage of 45% which was calculated as 44.3%. The third decomposition over a wide temperature range was attributed to the second Schiff base ligand leaving a co-

balt oxide residue behind with remaining mass percent of 6.9% and calculated as 7.7%. The thermogram for $Co(Ampp\text{-}Sn)_2(H_2O)_2$ (Fig. 80) exhibited many decompositions bringing about unequivocal assignments. However, the water molecules elimination can be observed in the decomposition at 160°C. The TGA curve extends beyond 900°C.

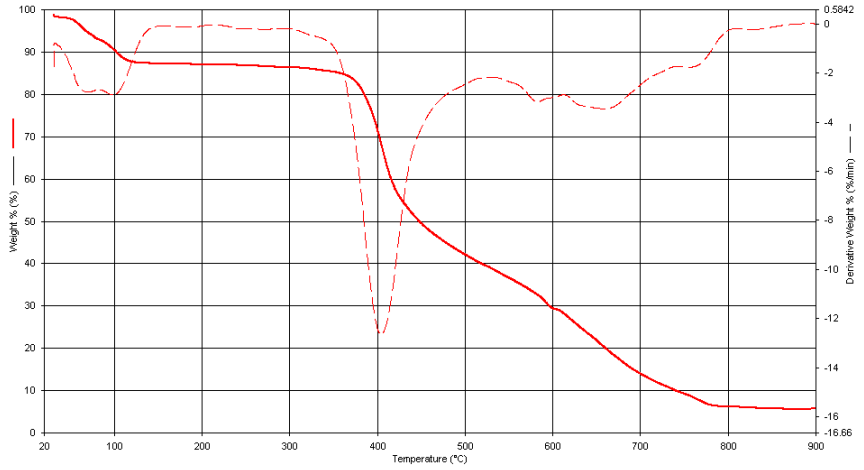

Figure 79. TGA and DTG Curve of $Co(Bmpp\text{-}Sn)_2(H_2O)_2{\cdot}H_2O$

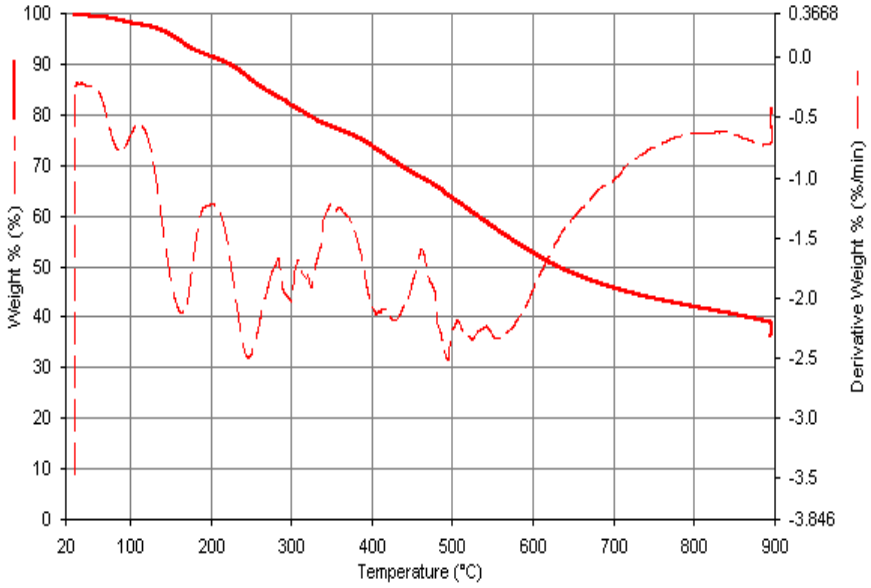

Figure 80. TGA and DTG Curve of $Co(Ampp\text{-}Sn)_2(H_2O)_2$

$Ni(Bmpp\text{-}Sn)_2(H_2O)_2 \cdot H_2O$ exhibited decomposition due to water molecules at around 80 and 140°C (Fig. 81). Its major decomposition occurred at 420°C associated with the removal of a molecule of Schiff base ligand with an equivalent mass loss of 50% and calculated as 50.9%. The final decomposition at around 810°C was attributed to the removal of a total of four molecules of water and two molecules of the Schiff bases ligand leaving behind a nickel oxide residue with mass percent of 9% and calculated as 8.7%. $Ni(Ampp\text{-}Sn)_2(H_2O)_2 \cdot H_2O$ (Fig. 82) exhibited a multistep decomposition. The elimination of the water molecules was evident from the decompositions at 170 and 280°C. A major decomposition due to the removal of one Schiff base molecule was observed at 440°C with a mass loss of 44% which agree with the calculated mass loss of 43.5%. The final decomposition due to the removal of the second Schiff base extends beyond 900°C which was terminated with the left over nickel oxide.

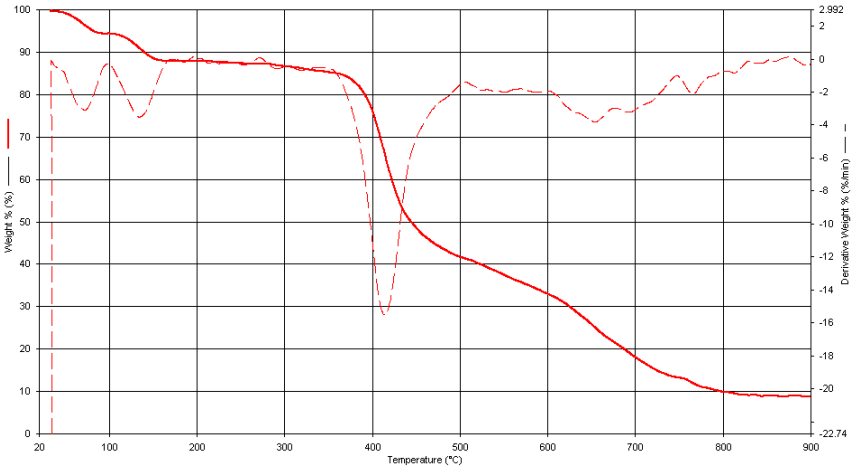

Figure 81. TGA and DTG Curve of $Ni(Bmpp\text{-}Sn)_2(H_2O)_2 \cdot H_2O$

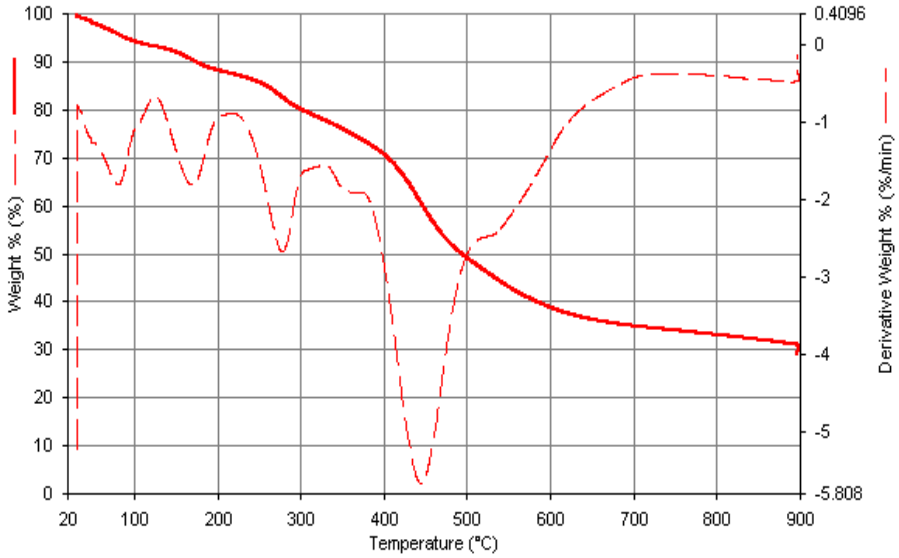

Figure 82. TGA and DTG Curve of Ni(Ampp-Sn)$_2$(H_2O)$_2$·H_2O

The thermal decomposition of Cu(Bmpp-Sn)$_2$(H_2O)$_2$ showed an unexpected one decomposition step at 330^{o}C which cannot be easily assigned, Fig.83. This observation may be due to the formation of gaseous reaction products. Also unexpectedly, the coordinated water molecule in Cu(Ampp-Sn)$_2$(H_2O)$_2$·H_2O (Fig. 84) cannot be accounted for in the TGA curve but a major decomposition at 440^{o}C may be due to the elimination of one Schiff base ligand with a mass loss of 45%, calculated as 43.2%. This was followed by a second and final decomposition attributed to the fragmentation of the last Schiff base liagnd, leaving behind a residue of the metal oxide with a remaining mass of around 11%, calculated as 8.8%.

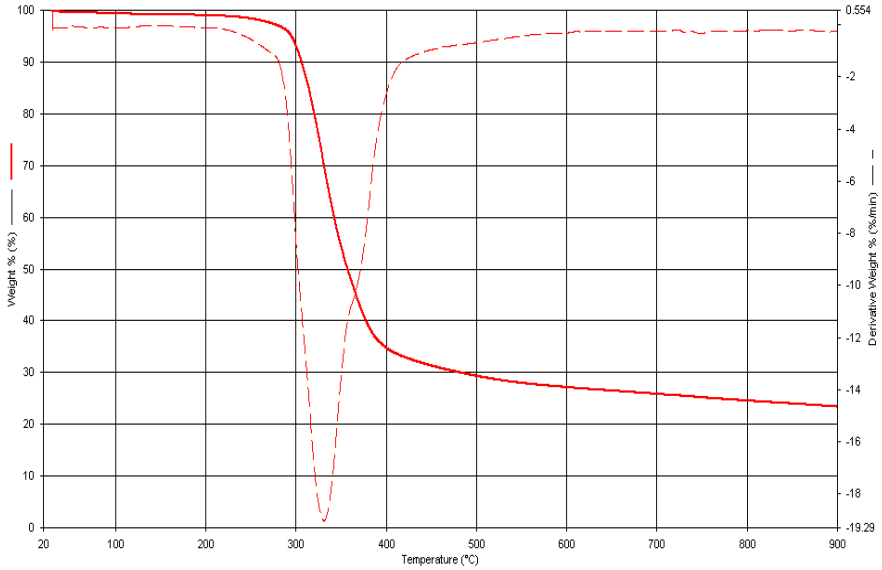

Figure 83. TGA and DTG Curve of $Cu(Bmpp\text{-}Sn)_2(H_2O)_2$

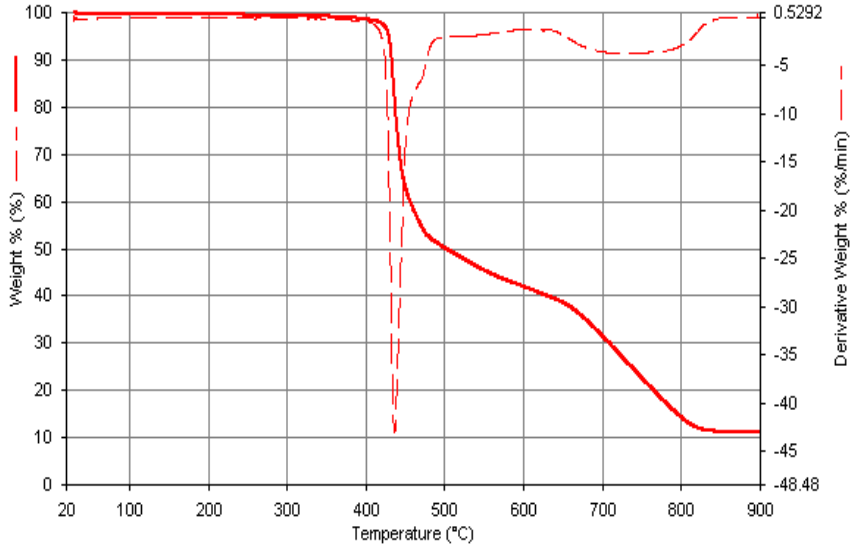

Figure 84. TGA and DTG Curve of $Cu(Ampp\text{-}Sn)_2(H_2O)_2{\cdot}H_2O$

Based on careful analysis of the elemental, analytical, spectroscopic and thermogravimetric studies, the geometry of metal complexes **97**-**104** may be proposed accordingly.

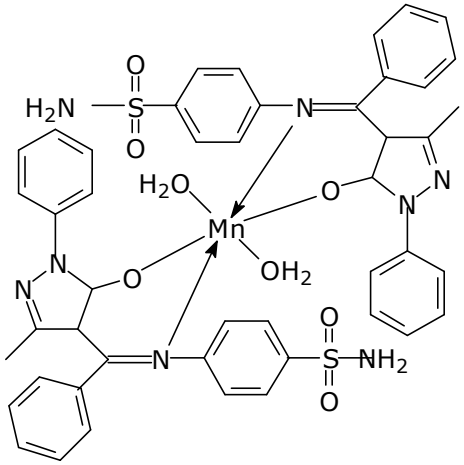

97

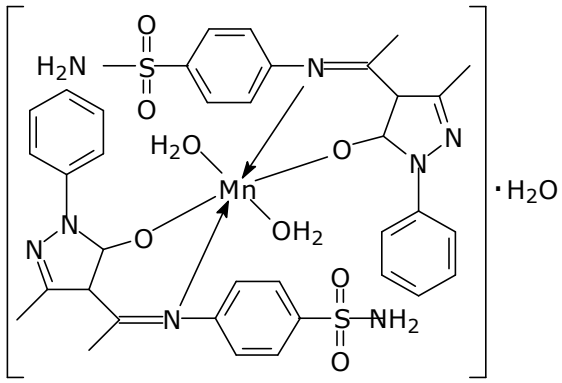

98

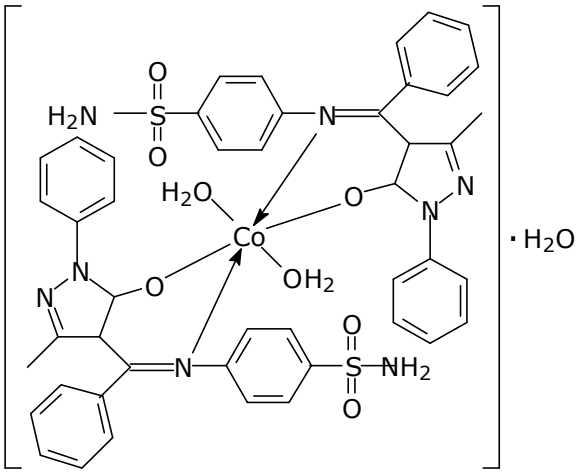

99

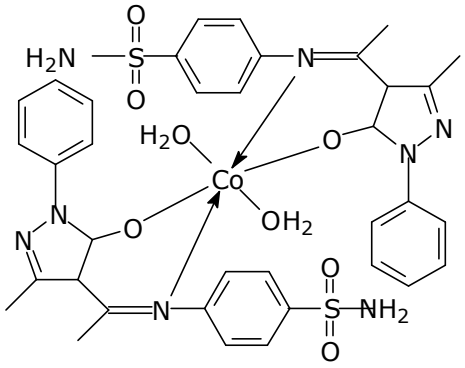

100

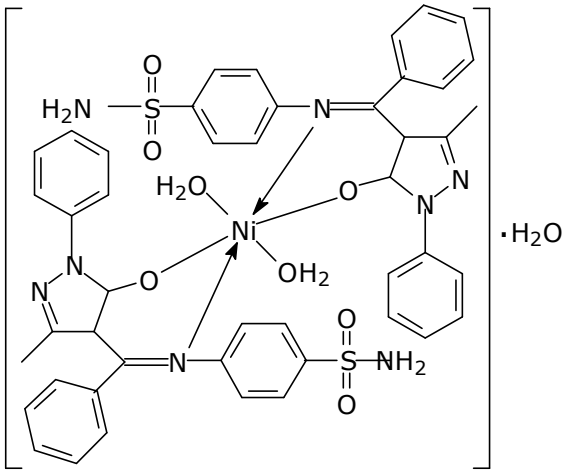

101

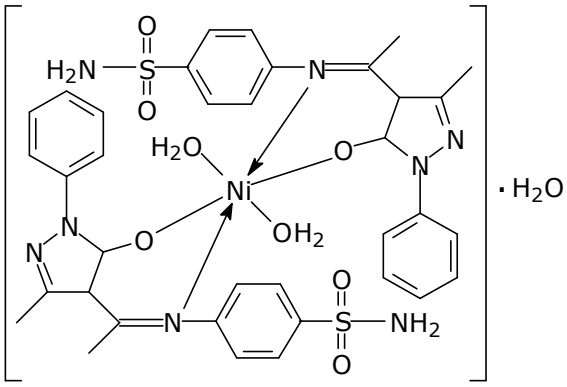

102

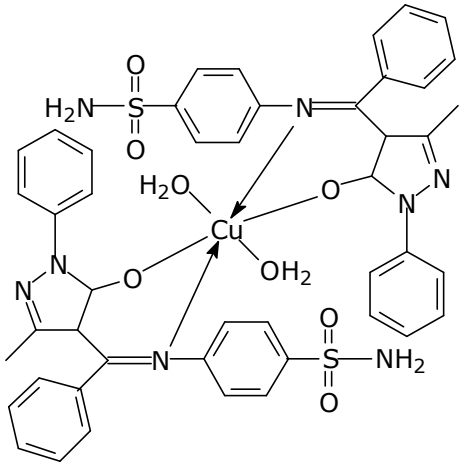

103

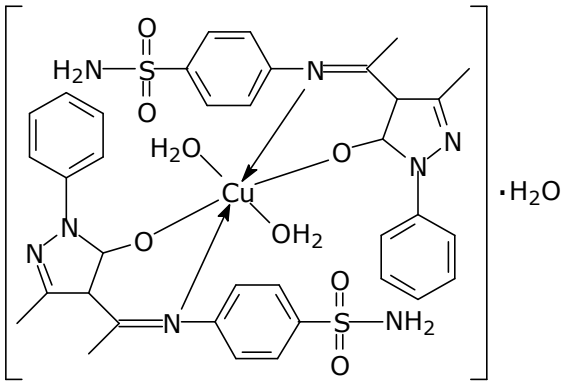

104

4.3.9 Antibacterial Screening

From the zones of inhibition presented in Table 13, the highest zone of inhibition was exhibited by benzoyl derivative Bmpp-Sn against *Aeromonas hydrophillia*. Bmpp-Sn also showed a broad spectrum activity (showing activity against all selected bacterial isolate) an indication of a good bactericidal compared to standard drug. $Co(Bmpp\text{-}Sn)_2(H_2O)_2{\cdot}H_2O$, $Ni(Bmpp\text{-}Sn)_2(H_2O)_2{\cdot}H_2O$, $Ni(Ampp\text{-}Sn)_2(H_2O)_2{\cdot}H_2O$ and Ampp-Sn on the other hand exhibited activity against three selected bacterial isolates. Generally a low to moderate antibacterial activity was observed based on zone of growth inhibition values. Sulfonamide Schiff bases chelated to a metal center have been reported to increase in its biological activity (01JICS474), but in these acylpyrazolone Schiff bases with sulfanilamide presented here in, there have not been any remarkable increased bacterial activities in their metal complexes.

Table 13. Zone of growth inhibition exhibited by sulfanilamide Schiff bases and metal complexes at 40 mg/ml (mm)

Ligand and complexes	*Staphylo-cocus aureus*	*Bacillus pumillus*	*Proteus vulgaris*	*Aeromonas hydrophillia*
Bmpp-Sn	12.5	7.5	10.3	24.0
Ampp-Sn	NI	5.0	8.5	4.0
$Mn(Bmpp\text{-}Sn)_2(H_2O)_2$	8.5	NI	NI	8.0
$Co(Bmpp\text{-}Sn)_2(H_2O)_2{\cdot}H_2O$	13.3	16.0	NI	15.0
$Ni(Bmpp\text{-}Sn)_2(H_2O)_2{\cdot}H_2O$	8.0	NI	11.5	21.0
$Cu(Bmpp\text{-}Sn)_2(H_2O)_2$	NI	10.3	NI	8.0
$Mn(Ampp\text{-}Sn)_2(H_2O)_2{\cdot}H_2O$	NI	NI	NI	8.5
$Co(Ampp\text{-}Sn)_2(H_2O)_2$	NI	9.0	NI	NI
$Ni(Ampp\text{-}Sn)_2(H_2O)_2{\cdot}H_2O$	4.5	6.0	NI	6.0
$Cu(Ampp\text{-}Sn)_2(H_2O)_2{\cdot}H_2O$	NI	NI	8.5	15.0
Chloramphenicol	30.0	20.0	42.0	40.0
DMSO	NI	NI	NI	NI

NI = no inhibition

4.3.10. Antioxidant (Free Radical Scavenging) Activity

There have been reports on the potential antioxidant properties of some naturally occurring ingredients from plants and synthetic analogs having electron-donating groups (08CAM1, 12BCA1, 12TJP285). The inductive effects of the sulfur and nitrogen groups in Bmpp-Sn and Ampp-Sn may push electron density towards the free radicals to produce a relatively stable molecule. The free-radical scavenging properties of most of the metal complexes presented here are low compared to standard drug ascorbic acid (Table 14). However, $Ni(Ampp\text{-}Sn)_2(H_2O)_2{\cdot}H_2O$ showed very strong antioxidant activities having values almost as that of ascorbic acid in all three different concentrations. $Mn(Ampp\text{-}Sn)_2(H_2O)_2{\cdot}H_2O$ as well as $Co(Ampp\text{-}Sn)_2(H_2O)_2$ exhibited strong antioxidant properties higher than their Ampp-Sn Schiff base ligand

which is in agreement with reported compounds coordinated with transition metal ions (01BPH677,04JIB1457, 07MOL1352).

Table 14. Antioxidant Scavenging Activity Data of Sulfanilamide Schiff Bases and Their Metal Complexes (%)

Ligand and complexes	Absorbance at 517 nm wavelength		
	0.50 mg/ml	0.25 mg/ml	0.13 mg/ml
Bmpp-Sn	65.15	46.00	44.88
Ampp-Sn	15.41	44.61	54.10
$Mn(Bmpp\text{-}Sn)_2(H_2O)_2$	–	14.60	–
$Co(Bmpp\text{-}Sn)_2(H_2O)_2{\cdot}H_2O$	–	16.22	30.95
$Ni(Bmpp\text{-}Sn)_2(H_2O)_2{\cdot}H_2O$	–	–	8.50
$Cu(Bmpp\text{-}Sn)_2(H_2O)_2$	–	–	–
$Mn(Ampp\text{-}Sn)_2(H_2O)_2{\cdot}H_2O$	29.42	92.93	90.38
$Co(Ampp\text{-}Sn)_2(H_2O)_2$	24.87	89.69	86.93
$Ni(Ampp\text{-}Sn)_2(H_2O)_2{\cdot}H_2O$	78.98	94.45	85.82
$Cu(Ampp\text{-}Sn)_2(H_2O)_2{\cdot}H_2O$	–	14.60	5.30
Ascorbic acid	87.62	93.63	91.99

On comparing the metal complexes with their corresponding ligands (Fig.85 and 86), the benzoyl pyrazolone derivative Bmpp-Sn showed a stronger free-radical scavenging property at all three different concentrations.

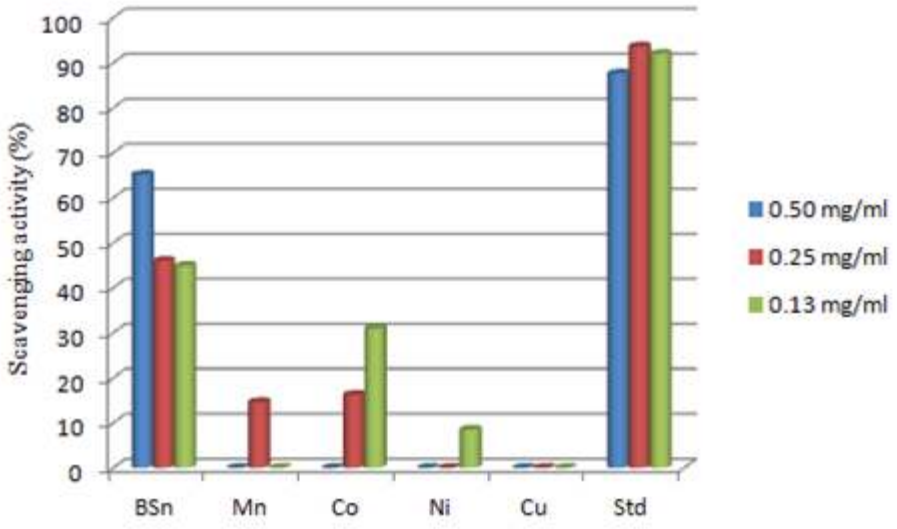

Figure 85. Chart Showing the Scavenging Activity of Bmpp-Sn and its Metal Complexes

However, with Ampp-Sn and its metal complexes, the complexes are stronger antioxidants at concentrations 0.25 and 0.13 mg/mL. Ni(Ampp-Sn)$_2$(H$_2$O)$_2$·H$_2$O exhibited the strongest antioxidant property at 0.25 mg/mL.

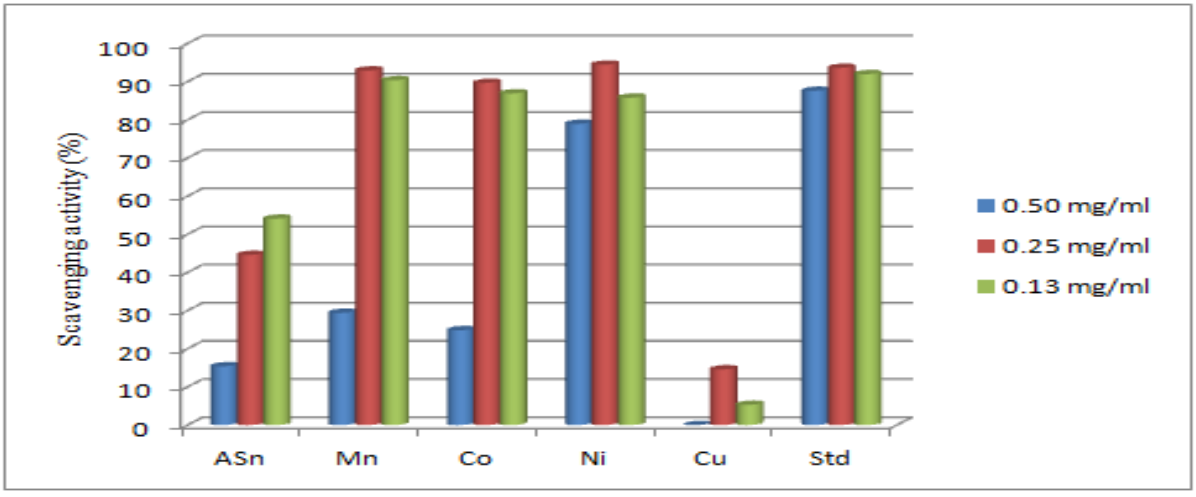

Figure 86. Chart Showing the Scavenging Activity of Ampp-Sn and its Metal Complexes

5. Conclusions

Acetyl and benzoyl derivatives of acylpyrazolone diketones were employed in the synthesis of some new Schiff base ligands with phenylhydrazine, dinitophenylhydrazine, and sulfanilamide, a study that was motivated by interesting biological and chelating properties of acylpyrazolone Schiff bases towards alternative therapeutic agents as a possible replacement for disease-resistant clinically used drugs. These Schiff base ligands have been characterized using a routine set of identification techniques and in some cases X-ray structural analysis.

^{1}H and ^{13}C NMR spectroscopy display resonance of the important newly formed bonds as an evidence of the successful synthesis of the Schiff base, although peaks due to impurities from the dissolving solvent were also observed. Mass spectra for all the Schiff base ligands reveal a molecular ion of $[M + H]^{+}$, which is in close agreement with elemental analysis.

Chelation of Schiff bases to transition metals is known to improve their biological activities. Mn(II), Co(II), Ni(II) and Cu(II) complexes with newly synthesized acylpyrazolones are generally insoluble in polar and non-polar solvents, but soluble in coordinating DMSO and DMF. Non-electrolyte behavior of complexes from conductivity measurement is observed. On comparison of the IR spectra, metal complexes with those for bidentate acypyrazolone Schiff bases, coordination to the transition metal ion through the azomethine nitrogen C=N and ketone oxygen –C-O have been proposed. Octa-

hedral complexes are typically formed with two molecules each of bidentate Schiff base and water.

Electronic spectra of metal complexes along with their magnetic moments from the magnetic susceptibility measurement gave an idea of the preferred coordination of Schiff bases around the metal ions, which is in agreement with proposed structures based on elemental microanalysis and IR spectra.

Thermal (TGA and DTG) studies show generally stable metal complexes. Metal complexes of the benzoyl pyrazolone Schiff base of sulfanilamide (Bmpp-Sn) have a more regular decomposition pattern, which is an indication that they are more thermal stable than their acetyl derivative counterpart.

Invitro antibacterial screening of synthesized compounds using the disc diffusion techniques against selected bacterial isolates show that they are all bactericidal. A few of them have a broad spectrum activity, showing activity against all selected bacterial isolates. The zones of inhibition of bacterial growth alone cannot tell which ligands or metal complexes are more active, hence further studies on the MIC and MBC of the active compounds need to be performed.

Free radical scavenging (antioxidant) capability of the synthesized compounds against DPPH radicals is evident from the values of percentage absorbance obtained. Mn(II), Co(II) and Ni(II) complexes of sulfanilamide Schiff base with the acetylpyrazolone derivative Ampp-Sn, exhibited a very

good radical scavenging property in relation to ascorbic acid, and higher than that of the uncoordinated Schiff base at 0.5, 0.25 and 0.13 g/mL, but not with Cu(II). This group of compounds could be important antitumour candidate, therefore a strong recommendation for their anticancer studies.

New acylpyrazolone Schiff bases obtained from the acetyl and benzoyl derivatives of the pyrazolone ketone along with their transition metal complexes appeared to have interesting therapeutic potential due to their bacterial growth inhibition effect and antioxidant activity. A reasonable number of these metal chelates show a higher biological activity. This study serves as a steering point for subsequent research work towards development of alternative synthetic biological compounds among other applications, and in view of this, the recommendations below will come in handy for possible further work.

Schiff bases and metal complexes reported here are generally insoluble in water. Their poor solubility in water to a great extent limits their biological application, hence possible structural modifications are of importance and strongly recommended in subsequent works. It is evident from crystal structures of the benzoyl acylpyrazolone Schiff base derivative Bmpp, not successful for the acetyl derivative Ampp, that Schiff bases with aromatic groups are more easily synthesized and stable, so the acetyl derivatives could also undergo structural modifications that could introduce more aromatic groups into the system. In addition to the NMR spectra a two dimen-

sional correlation spectra COSY ^{1}H-^{1}H can be recorded. Also heteronuclear single quantum ^{1}H-^{1}H HSQC correlation spectra can be carried out to identify ^{13}C NMR of compounds. And lastly to identify the chemical shifts of carbon not bound to the hydrogen atoms the distantbond ^{1}H-^{13}C HMBC heteronuclear correlation spectra will come in handy. Mixed-ligand metal complexes approach towards structural modifications is also recommended for further studies, to investigate a possible synergic contribution to the efficiency of these metal chelates. A look at the antibacterial activities of the synthesized compounds based on zones of bacterial growth inhibition is not essential to ascertain the actual biological activities, hence the concentration-dependent MIC and MBC determination should be carried out to determine to what extent exactly does this molecule inhibit or kill these bacterial microbes. Because platinum group metals have been significant in cancer chemotherapy, a look at the platinum group metal chelates with these Schiff bases is encouraged, especially with those having high antioxidant properties. It is worth noting that Schiff bases and their metal complexes are very versatile compounds in terms of its reactivity and application of these compounds as catalysts in some important process could become an interesting research focus.

References

83CB546 L. Knorr, *Chem. Ber.*, **17**, 546 (1883).

97JPR145 F. Stoltz, *J. Prakt. Chem.*, **55**, 145 (1897).

26A77 O. L. Brady and G. V. Elsmie, *Analyst*, **51**(599), 77 (1926).

56CRS167 R. W. Brockman, J. R. Thompson, M. J. Bell, and H. E. Skipper, *Cancer Res.*, **16**, 167 (1956).

58NAT1199 M. S. Blois,*Nature*, **26**, 1199 (1958).

59ACS1668 B.S. Jensen, *Acta Chem. Scand.*, **13** 1668 (1959).

59JA475 W. P. Jencks, *J. Am. Chem. Soc.*, **81**, 475 (1959).

60JA1773 B. M. Anderson and W. P. Jencks, *J. Am. Chem. Soc*., **82**, 1773 (1960).

66JIM521 R. Eskenazi, J. Rasavan, and R. Levitus, *J. Inorg. Med. Chem.*, **28**, 521 (1966).

66PIC83 R. H. Holm, G. W. Everett, and A. Chakravorty, *Progr. Inorg. Chem.*, **7**, 83 (1966).

68MI1 A. B. P. Lever, *Inorganic Electronic Spectroscopy*, Elsevier, Amsterdam, 1968, p.376.

68PHE272 A. Saunderson, *Phys. Educ.*, **3**, 272 (1968).

71CCR81 W. J. Geary, *Coord. Chem. Rev.*, **7**, 81 (1971).

75AAC15 D. R. Stalons and C. Thornsberry, *Antimicrob. Agents Chemother.*, **7**, 15 (1975).

75MI1 S. F. A. Kettle, *Coordination Compounds*, Thomas Nelson and Sons, London, 1975,p. 165.

78JINC793 R. J. Hill and C. E. F. Richard, *J. Inorg. Nucl. Chem.*, **40**, 793, (1978).

79JINC1229 M. C. Jain, R. K. Sharma, and P. C. Jain, *J. Inorg. Nucl. Chem.*, **42**, 1229 (1979).

79JME855 D. L. Klayman, J. E. Bartosevich, T. S. Griffin, C. J. Mason, and J. P. Scovil, *J. Med. Chem.*, **22**, 855 (1979).

80AAC27 A. S. Dobek, D. L. Klayman, E. T. Dickson, J. P. Scovill and E. C. Tramont, *Antimicrob. Agents Chemother.*, **18**, 27 (1980).

81BCJ3157 B. G. Ateya, B. E. El-Anadouli, and F. M. A. El-Nizamy, *Bull. Chem. Soc. Jp.*, **54**, 3157 (1981).

81D1241 G. A. Kolawole and K. S. Patel, *J. Chem. Soc., Dalton Trans.*, 1241 (1981).

81NAT270 M. Barber, R. S. Bordoli, R. D. Sedgewick, and A. N. Tyler, *Nature*, **293**, 270 (1981).

82NJM130 B. E Murray, E. R Rensimer, and H. L. DuPont, *N. Engl. J. Med.*, **306**, 130 (1982).

85JID1107 B. E. Murray, T. Alvarado, K. H. Kim, M. Vorachit, P. Jayanetra, M. M. Levine, I. Prenzel, M. Fling, L. Elwell, G.

H. McCracken, G. Madrigal, C. Odio, and L. R. Trabulsi, *J. Infect. Dis.*, **152**, 1107 (1985).

86JA2309 K. Srinivasan, P. Michaud, and J. K. Kochi, *J. Am. Chem. Soc.*, **108**, 2309 (1986).

86SRI257 Y. Anjaneyulu and R. P. Rao, *Synth. React. Inorg. Met. Org. Chem.*, **16**, 257 (1986).

87JIC685 C. G. Saxena and S. V. Srivastava. *J. Ind. Chem. Soc.*, **64**, 685 (1987).

87MI1 A. R. Siedle, in: *Comprehensive Coordination Chemistry I,*G. Wilkinson, R. D. Gillard, and J.A. McCleverty (Eds.), Oxford, Pergamon Press, *Vol. 2*, 1987, p.365.

88AL633 T. Hasan, *Anal. Lett.*, **21**, 633 (1988).

88AL1917 A. Besada, *Anal. Lett.*, **21**, 1917 (1988).

88JEP127 J. L Rios, M. C Recio, and A. Villar, *J. Ethnopharmacol.*, **23**, 127 (1988).

88MI1 H. H. Willard, *Instrumental Methods of Analysis*, Belmont, Wadsworth, 1988, 895 pp.

89AIC197 J. B. Vincent and G. Christou, *Adv. Inorg. Chem.*, **33**, 197 (1989).

89BSF297 A. S. Babaqi, M. S. El-Basiounyi, and R. M. Abdulla, *Bull. Soc. Chim. Fr.*, 297 (1989).

89JAC(23)143 R. Urbina, V. Prado, and E. Canelo. *J. Antimicrob. Chemother.*, **23**, 143 (1989).

89JAC(23)151 A. Lamikanra and R. B. Ndep, *J. Antimicrob. Chemother*., **23**, 151 (1989).

89JAC(24)973 B. A. Wylie and H. J. Koornhof, *J. Antimicrob. Chemother.*, **24**, 973 (1989).

89SCI64 J. B. Fenn, M. Mann, C. K. Meng, S. F. Wong, and C. M. Whitehouse, *Sci*., **246**, 64 (1989).

90AAC515 B. E Murray, J. J. Mathewson, H. L. Dupont, C. D. Ericsson, and R. R. Reves, *Antimicrob. Agents Chemother.*, **34**, 515 (1990).

90BBR686 S. K. Chowdhury, V. Katta, and B. T. Chait, *Biochem. Biophys. Res. Commun.*, **167**, 686 (1990).

90NJM285 S. C. Lester, P. M. Del Pilar, F. Wang, I. P. Schael, H. Jiang, and T. F. O'Brien, *N. Engl. J. Med*., **323**, 285 (1990).

90PHR155 J. M. Ford and W. N. Hait, *Pharmacol. Rev.*, **42**, 155 (1990).

90PIC97 L. Que and A. E. True, *Prog. Inorg. Chem.*, **38**, 97 (1990).

91JA4069 C. Bull, E. C. Neiderhofer, T. Yoshida, and J. A. Fee. *J. Am. Chem. Soc.*, **113**, 4069 (1991).

91TMC276 A. S. Kumbhar, S. B. Padhye, D. X. West, and A. E. Liberta, *Transit. Met. Chem.*, **16**, 276 (1991).

92JME3288 J. Easmon, G. Heinisch, W. Holzer, and B. Rosenwirth,*J. Med. Chem.*, **35**, 3288 (1992).

92POL1507 D. M. L. Goodgame, S. P. W. Hill, and D. J. Williams, *Polyhedron*, **11**, 1507 (1992).

92SCI1055 M. L. Cohen, *Sci*., **257**, 1050 (1992).

92SCI1064 H. C Neu, *Sci*., **257**, 1064 (1992).

93CRS747 M. M. Gottesman, *Cancer Res.*, **53**, 747 (1993).

93IJC(A)446 L. Mishra and V. K. Singh, *Indian J. Chem.*, **A32**, 446 (1993).

93JCT361 R. L. Then, J. Chemother., **5**, 361 (1993).

93TMC221 D. X. West, M. A. Lockwood, A. E. Liberta, X. Chen, and R. D. Willett, *Transit. Met. Chem.*, **18**, 221 (1993).

94IC1875 Y. Inada, K. Sugimoto, K. Ozutsumi, and S. Funahashi, *Inorg. Chem.*, **33**, 1875 (1994).

94IPH87 O. N. Irobi, M. M. Young and W. A. Anderson. *Int. J. Pharmacol.*, **34**, 87 (1994).

94MI1 M. Gerloch and E.C. Constable, *Transition Metal Chemistry*, VCH, Weinheim, 1994, 203 pp.

94TMC611 X. Wang, X. Zhang, L. Hai and X. Min. *Transit. Met. Chem.*, **19**, 611 (1994).

95BCH7773 A. Khindaria, D. P. Barr, and S. D. Aust, *Biochem*., **34**, 7773 (1995).

95JEP109 J. J. M. Meyer and A. J. Afolayan, *J. Ethnopharmacol.*, **47**, 109 (1995).

95MBD81 A. Garcia-Raso, J. J. Fiol, E. Molins, A. M. Calafa, P. A. Marzilli, and L. G. Marzilli, *Met. Based Drugs*, **2**, 81 (1995).

96AJP493 A. W. Bauer, W. M. Kirby, J. C. Sherris, and M. Turck, *Am. J. Clin. Pathol.*, **45**, 493 (1996).

96BCH160 A. K. Whiting, Y. R. Boldt, M. P. Hendrich, L. P. Wackett, and L. Que, *Biochemistry*, **35**, 160 (1996).

96JEP27 F. Salie, P. F. K. Eagles, and H. J. M Lens, *J. Ethnopharmacol.*, **52**, 27 (1996).

96JME3920 K. L. Kees, J. J. Fitzgerald, K. E. Steiner, J. F. Mattes, B. Mihan, T. Tosi, D. Mondoro, and M. L. McCaleb, *J. Med. Chem.*, **39**, 3920 (1996).

96SAB158 F. Dilika, A. J. Afolayan, and J. J. M. Meyer, *S. Afr. J. Bot.*, **63**, 158 (1996).

97EXP291 H. Sies, *Exp. Physiol.*, **82**, 291 (1997).

97JAX565 L. J. Farrugia, *J. Appl. Crystallogr.*, **30**, 565 (1997)

97JEP177 A. J. Afolayan and J. J. M. Meyer, *J. Ethnopharmacol.*, **57**, 177 (1997).

97MI1 K. Nakamato, *Infrared and Raman Spectra of Inorganic and Coordination Compounds*, 5th Ed., Wiley–Interscience, New York, 1997, Part B, p. 1–13.

97POL1171 S. Karabocek and N. Karabocek. *Polyhedron*, **11**, 1771 (1997).

97TMC1 D. X. West, A. K. El-Sawaf, and G. A. Bain, *Transit. Met. Chem.*, **23**, 1 (1997).

98IJC(A)1010 R. Lal De, K. Samanta, C. Samanta, and A. K. Mukherjee, *Ind. J. Chem.*, **A38**,1010 (1998).

98JMI113 M. T. Mendoza, *J. Microbiol. Infect. Dis.*, **27**, 113 (1998).

98MI1 R. J. Fessenden and J. S. Fessenden, *Organic Chemistry*, 6th ed., Brooks/Cole, Pacific Grove, 1998, 1168 pp.

99EJM153 S. G. Kucukguzel, S. Rollas, H. Erdeniz, and M. Kiraz,*Eur. J. Med. Chem.*, **34**, 153 (1999).

99MI1 A. S. Fauci, *Antimicrobial Resistance: The NIH Response to a Growing Problem*, National Institute of Allergy and Infectious Diseases. National Institute of Health, 1999.

00JPP(A)23 X. C. Tanga, D. Z. Jia, K. Liang, X. G. Zhang, X. Xia and Z. Y. Zhou, *J. Photochem. Photobiol.*, **A134**, 23 (2000).

00LAM379 A. Nostro, M. P. Germano, V. D'Angelo, A. Mario, and M. A. Cannatelli, *Lett. Appl. Microbiol.*, **30**, 379 (2000).

00PHC93 A. D. M Mathekga, J. J. M. Meyer, M. M. Horn, and S. E Drewes. *Phytochem*., **53**, 93 (2000).

00POL2599 Z. Y. Yang, R. D. Yang, F. S. Li, and K. B. Yu, *Polyhedron*, **19**, 2599 (2000).

01APR171 H. H. Fahmy and W. EI-Eraky, *Arch. Pharm. Res.*, **24**, 171 (2001).

01BPH677 I. B. Afanasyev, E. A. Ostrakhovitch, E. V. Mikhalchik, G. A. Ibraginova, and L. G. Korkina, *Biochem. Pharmacol.*, **61**, 677 (2001).

01CUS1179 A. K. Tiwari, *Curr Sci (India)*, **81**, 1179 (2001).

01D774 R. X. Yuan, R. G. Xiong, Z. F. Chen, P. Zhang, H. X. Ju, Z. Dai, Z. J. Guo, H. K. Fun, and X. Z. You, *J. Chem. Soc., Dalton Trans.*, 774 (2001).

01JIC474 P. G. More, R. B. Bhalvankar, and S. C. Pattar, *J. Ind. Chem. Soc.*, **78**, 474 (2001).

01JMS15 A. R. Kurbangalieva, A. I. Movchan, O. N. Kataeva, I. A. Litvinov, and G. A. Chmutova, *J. Mol. Struct.*, **595**, 15 (2001).

01PIA257 N. K. Singh, S. B. Singh, A. Srivastava, and S. M. Singh, *Proc. Ind. Acad. Sci., Chem. Sci.*, **113**, 257 (2001).

01RJP61 S. Joshi, V. Pawar, and V. Uma, *Res. J. Pharm., Biol. Chem. Sci.*, **2**, 61 (2001).

01TMC131 N. Raman, A. Kulandaisamy, A. Shunmugasundaram, and K. Jeyasubramanian, *Transit. Met. Chem.*, **26**, 131 (2001).

02BJM97 K. F. Devienne and M. S. G. Raddi, *Braz. J. Microbiol.*, **33**, 97 (2002).

02ECA1365 A. E. Stoyanova and S. D. Peyerimhoff, *Electrochim. Acta*, **47**, 1365 (2002).

02JAF3444 B. Matthaus, *J. Agric. Food Chem.*, **50**, 3444 (2002).

02JCM3574 E. Van Duijkeren, W. J. B. Wannet, D. J. Houwers, and W. Van Pelt, *J. Clin. Microbiol.*, **41**, 3574 (2003).

02JCX255 L. Liu, D. Jia, Y. Qiao, Y. Ji, and K. Yu, *J. Chem. Crystallogr.*, **32**, 255 (2002).

02JCX505 Y. Ji, L. Liu, D. Jia, Y. M. Qiao, and K. Yu, *J. Chem. Crystallogr.*, **32**, 505 (2002).

02SRI819 P. P. Dholakiya and M. N. Patel, *Synth. React. Inorg. Met.-Org, and Nano-Met. Chem.*, **32**, 819 (2002).

02T5357 D. M. Boghaei and S. Mohebi, *Tetrahedron*, **58**, 5357 (2002).

03AX(E)m128 J. L. Wang, F. Ding, and F. M. Miao, *Acta Crystallogr.*, **E59**, m128 (2003).

03CCL263 X. Q. Wei, Z.Y. Lu, P. Zou, and M.G. Xie. *Chin. Chem. Lett.*, **14**, 263 (2003).

03CMI1 EUCAST, *Clin. Microbiol. Infect.*, **9**(8), 1 (2003).

03CRV893 D. A. Horton, G.T. Bourne, and M.L. Smyth, *Chem. Rev.*, **103**, 893 (2003)

03D748 A. R. Cowley, J. R. Dilworth, P. S. Donnelly, and J. W. Shore, *Dalton Trans.*, 748 (2003).

03EJO1209 W. Holzer, K. Hahn, T. Brehmer, R. M. Claramunt, and M. Perez-Torralba, *Eur. J. Org. Chem.*, 1209 (2003).

03JAX7 A. L. Spek, *J. Appl. Crystallogr.*, **36**, 7 (2003).

03JIN61 V. Kumar and R. Dhakarey, *J. Ind. Council Chem.*, **20**, 61 (2003).

03JMS221 L. Liu, D. Z. Jia,, Y. L. Jia, K. B. Yu, *J. Mol. Struct.*, **655**, 221 (2003).

03JPP(A)117 L. Liu, D. Z. Jia, Y. L. Ji, and K. B. Yu, *J. Photochem. Photobiol.*, **A154**, 117 (2003).

03JRN693 G. X. Zheng, Q. F. Wang, and S. G. Luo, *J. Radioanal. Nucl. Chem.*, **258**, 693 (2003).

03MI1 C. Pettinari, F. Marchetti, and A. Drozdov, *Comprehensive Coordination Chemistry II*, J. A. McCleverty and T. J. Meyer (Eds.),Vol. 1, 2003, p. 97.

03MOL439 X. Tai, X. Yin, Q. Chen, and M. Tan. *Molecules*, **8**, 439 (2003).

03MRR697 L. J. Ming, *Med. Res. Rev.*, **6**, 697 (2003).

03TMC229 D. K. Sau, N. Saha, R. J. Butcher, and S. P. Chaudhuri. *Transit. Met. Chem.*, **28**, 229 (2003).

04AOC221 P. Nagpal and R. V. Singh, *Appl. Organomet. Chem.*, **18**, 221 (2004).

04AX(C)o705 J. Belmar, F. R. Perez, Y. Moreno, and R. Baggio, *Acta Crystallogr.*, **C60**, o705 (2004).

04BCA193 N. Katsarosa, M. Katsarosa, S. P. Sovilj, K. Babi-Samardija, and D. M. Mitic. *Bioinorg. Chem. Appl.*, **2**, 193 (2004).

04BKC1121 J. S. Min, K. K. Jung, S. S. Bum, G. S. Bo, N. Zaesung, G. C. Hyae, K. Kwang-Rok, S. S. Young, and R. K. Hyoung, *Bull. Kor. Chem. Soc.*, **25**, 1121 (2004).

04BMB93 E. J. Finehout and K. H. Lee, *Biochem. Mol. Biol. Educ.*, **32**, 93 (2004).

04CSR410 P. G. Cozzi, *Chem. Soc. Rev.*, **33**, 410 (2004).

04D2404 A. R. Cowley, J. R. Dilworth, P. S. Donnelly, A. D. Gee, and J. M. Heslop, *Dalton Trans.*, 2404 (2004).

04ICC1306 L. Zhang, L. Liu, D. Jia, G. Xu, and K. Yu, *Inorg. Chem. Commun.*, **7**, 1306 (2004).

04JEP(94)279 R. D Langfield, F. J. Scarano, M. E. Heitzman, M. Kondo, G. B. Hammond, and C. C. Neto. *J. Ethnopharmacol.*, **94**, 279 (2004).

04JEP(95)253 A. C. U. Lourens, D. Reddy, K. H. C. Baser, A. M. Viljoen, and S. F. Van Vuuren,*J. Ethnopharmacol.*, **95**, 253 (2004).

04JIB1457 M. J. Hynes and M. J. O'Coinceanainn,*J. Inorg. Biochem.*, **98**, 1457 (2004).

04JMS217 B. H. Peng, G. F. Liu, L. Liu, D. Z. Jia, and K. B. Yu, *J. Mol. Struct.*, **692**, 217 (2004).

04JOM2192 C. Y. Wu, L. H. Chen, W. S. Hwang, H. S. Chen, H. Chen, and C. H. Hung. *J. Organomet. Chem.*, **689**, 2192 (2004).

04POL2465 R. N. Jadeja, J. R. Shah, E. Suresh, and P. Paul, *Polyhedron*, **23**, 2465 (2004).

04SRI697 D. S. Raj, N. J. Parmar, and J. R. Shah, *Synth. React. Inorg. Met. Org. Chem.*, **34**, 697 (2004).

05ADD1446 S. B. Levy, *Adv. Drug Del. Rev.*, **57**, 1446 (2005).

05ASx289 Y. Sun, D. Zhang, H. Gao, H. Wang, and R. Tao, *Anal. Sci.*, **22**, x289 (2005).

05JBC179 J. Belmar, F. R. Perez, J. Alderetea, and C. Zuniga, *J. Braz. Chem. Soc.*, **16**, 179 (2005).

05JCX497 G. Liu, L. Liu, D. Jia, and K. Yu, *J. Chem. Crystallogr.*, **35**, 497 (2005).

05JMS(T)61 L. M. R. Valdez, A. M. Villafane, and D. G. Mitnik, *J. Mol. Struct., Theochem,* **716**, 61 (2005).

05JPP(A)243 B. H. Peng, G. F. Liu, L. Liu, D. Z. Jia, and K. B. Yu, *J. Photochem. Photobiol.*, **A171**, 243 (2005).

05MIO779 M. T. G. Silva, S. M. Simas, T. G. F. M. Batsta, P. Cardarelli, and T. C. B. Tomassini. *Mem. Inst. Oswaldo Cruz*, **100**, 779 (2005).

05NJC283 F. R. Perez, J. Belmar, Y. Moreno, R. Baggioc, and O. Pena, *New J. Chem.*, **29**, 283 (2005).

05NRM577 B. Kuster, M. Schirle, P. Mallick, and R. Aebersold, *Nat. Rev. Mol. Cell. Biol.*, **6**, 577 (2005).

05TMC341 S. A. Sallam, *Transit. Met. Chem.*, **30**, 341 (2005).

05TMC411 R. R. Coombs, M. K. Ringer, J. M. Blacquiere, J. C. Smith, J. Scott Neilsen, Y. S. Uh, J. B. Gilbert, L. J. Leger, H. Zhang, A. M. Irving, S. L. Wheaton, C. M. Vogels, and S. A. Westcott, *Transit. Met. Chem.*, **30**, 411 (2005).

06BPH1036 J. Verhoef and A. Fluit, Biochem. Pharmacol., 1036 (2006).

06CAM11 D. K. B. Runyoro, M. I. N. Matee, O. D Ngassapa, C. C. Joseph, and Z. H. Mbwambo, BMC*Complem. Alternat. Med.*, **6**(11), 11 (1996).

06CHJ569 G. F. Liu, L. Liu, D. Z. Jia, and L. Zhang, *Chin. J. Chem.*, **24**, 569 (2006).

06DP71 A. R. Abbasi, Z. Rezvani, and K. Nejati, *Dyes and Pigments*, **70**, 71 (2006).

06JMS24 R. C. Maurya and S. Rajput, *J. Mol. Struct.*, **794**, 24 (2006).

06JAF7735 J. Gabrielska, M. Soczynska-Kordala, J. Hładyszowski, R. Zyłka, J. Miskiewicz, and S. Przestalski, *J. Agric. Food Chem.*, **54**, 7735 (2006).

06JPC(B)8928 B. Gomez, N. V. Likhanova, M. A. D. Aguilar, R. M. Palou, A. Vela, and J. L. Gasquez. *J. Phys. Chem.*, **B110**, 8928 (2006).

06MOL904 T. Rosu, T. Pasculescu, V. Lazar, C. Chifiriuc, and R. Cernat, *Molecules*, **11**, 904 (2006).

06POL1915 Z. Rezvani, B. Divband, A. R. Abbasi, and K. Nejati. *Polyhedron*, **25**, 1915 (2006).

06TJB65 O. Baris, M. Gulluce, F. Sahin, H. Ozer, H. Killic, H. Ozkan, M. Sokmen, and T. Ozbek, *Turk. J. Biol.*, **30**, 65 (2006).

07SC909 Y. Yang, L. Zhang, L. Liu, G. Liu, J. Guo, and D. Jia, *Struct. Chem.*, **18**, 909 (2007).

07CPB1070 A. Iqbal, H. L. Siddiqui, and C. M. Ashraf, *Chem. Pharm. Bull.*, **55**, 1070 (2007).

07DP653 K. Nejati, Z. Rezvani, and B. Massoumi. *Dyes and Pigments*, **75**, 653 (2007).

07EQ7 W. Ferenc, K. Czapla, and J. Sarzy, *Ecl. Quím.*, **32**(3), 7 (2007).

07ICA1599 O. Pouralimardan, A. Chamayou, C. Janiak, and H. Monfared, *Inorg Chim Acta*, **360**, 1599 (2007).

07JIB95 D. Koushik, R. Jagnyeswar, M. Mario, W. Xin-Yi, G. Song, and B. Pradyot, *J. Inorg. Biochem.*, **101**, 95 (2007).

07MI1 Bruker, APEXII, SAINT, SADABS, Bruker AXS Inc., Madison, 2007.

07MOL1352 R. M. S. Pereira, N. E. D. Andrades, N. Paulino, A. C. H. F. Sawaya, M. N. Eberlin, M. C. Marcucci, G. M. Favero, E. M. Novak, and S. P. Bydlowski. *Molecules*, **12**, 1352 (2007).

07MOL1910 S. Rollas andS.G. Kucukguzel, *Molecules*, **12**, 1910 (2007).

07PJP301 A. Bayri and M. Karakaplan, *Pramana – J. Phys*., **69**, 301 (2007).

07POL1677 R. N. Jadeja and J. R. Shah, *Polyhedron*, **26**, 1677 (2007).

07SA(A)1271 C. M. Sharaby. *Spectrochim. Acta*, **A66**, 1271 (2007).

07SRI263 Z. Ling and Z. B. Hua, *Synth. React. Inorg., Metal-Org. Nano-Met. Chem.*, **37**, 263 (2007).

07TJC623 J. Liu, B. Zhang, B. Wu, K. Zhang, and S. Hu, *Turk. J. Chem.*, **31**, 623 (2007).

08ACM60 M. A. Quraishi, R. Sardar, and S. Khan, *Anti Corros. Meth. Mater.*, **35**, 605 (2008).

08AJB1797 N. S. Ncube, A. J. Afolayan, and A. I. Okoh, Afr. J. Biotechnol., **7**, 1797 (2008).

08AX(A)112 G. M. Sheldrick, *Acta Crystallogr.*, **A64**, 112 (2008).

08CAM1 B. Hazra, S. Biswas, and N. Mandal, *BMC Complem. Alternat. Med.*, **8**(63), 1 (2008).

08ECA8287 M. Finsgar, A. Lesar, A. Kokaij, and I. Milosev, *Electrochim. Acta*, **53**, 8287 (2008).

08EJC529 V. Reddy, N. Patil, T. Reddy, and S. D. Angadi. *E-J. Chem.*, **5**, 529 (2008).

08IJC(B)1555 N. Das, A. Verma, P. K. Srivastava, and S. K. Srivastava, *Ind. J. Chem.*, **B47**, 1555 (2008).

08IPS177 K. O. Ogunniran, K. O. James, O. O. Ajani, C. O. Nwinyi, and M. A. Allensela, *Int. J. Phys. Sci.*, **3**(8), 177 (2008).

08JAX466 C. F. Macrae, I. J. Bruno, J. A. Chisholm, P. R. Edgington, P. McCabe, E. Pidcock, L. Rodriguez-Monge, R. Taylor, J. van de Streek, and P. A. Wood, *J. Appl. Crystallogr.*, **41**, 466 (2008).

08JCH1689 Y. Moreno, J. Belmar, F. Brovelli, A. Buljan, O. Pena, and L. Moreno, J. Chil. Chem. Soc., **53**, 1689 (2008).

08JCX837 L. Zhang, L. Liu, G. C. Xu, and D. Z. Jia, *J. Chem. Crystallogr.*, **38**, 837 (2008).

08TMC1013 P. Hou, Z.L. You, L. Zhang, X.L. Ma, and L.L. Ni, *Transit. Met. Chem.*, **33**, 1013 (2008).

09APP169 S. U. Khan, P. Mullick, S. Pandit, and D. Kaushik, *Acta Pol. Pharm. Drug Res.*, **66**, 169 (2009).

09EJM3480 M. Abdel–Aziz, G. E. A. Abuo-Rahma, and A. A. Hasan, *Eur. J. Med. Chem.*, **44**. 3480 (2009).

09IPH220 O. A. Georgewill, U. O. Georgewill, and R. N. P. Nwankwoala, *Int. J. Pharmacol.*, **7**, 220 (2009).

09JCC156 H. Naeimi and M. Moradian, *J. Coord. Chem.*, **62**, 156 (2009).

09JCC2388 N. J. Parmar and S. B. Teraiya, *J. Coord. Chem.*, **62**, 2388 (2009).

09JIR738 N. Ramana, L. Mitub, A. Sakthivela, and M. S. S. Pandi, *J. Iran. Chem. Soc.*, **6**, 738 (2009).

09JSC1159 A. S. Amarasekara, O. S. Owereh, K. A. Lyssenko, and T. V. Timofeeva, *J. Struct. Chem.*, **50**, 1159 (2009).

09JSI181 S. Kumar, D. N. Dhar, and P. N. Saxena, *J. Sci. Ind. Res*., **68**, 181 (2009).

09JIR345 R. A. Khalil, A. H. Jalil, and A. Y. Abd-Alrazzak, *J. Iran. Chem. Soc.*, **6**, 345 (2009).

09SA(A)901 S. B. Bukhari, S. Memon, M. Mahroof-Tahir, and M. I. Bhanger, *Spectrochim. Acta*, **A71** 1901 (2009).

10CJS69 Y. Z. Tang, H. R. Wen, J. Zhang and Y. H. Tan. *Chin. J. Struct. Chem.*, **29**, 69 (2010).

10COC281 M. Dolaz, V. McKee, A. Gölcü, and M. Tümer, *Curr. Org. Chem.*, **14**, 281 (2010).

10EJM3196 Z. L. You, L. L. Ni, D. H. Shi, and S. Bai, *Eur. J. Med. Chem.*, **45**, 3196 (2010).

10ICC996 Z. L. You, L. Zhang, D. H. Shi, X. L. Wang, X. F. Li, and Y. P. Ma, *Inorg. Chem. Commun.*, **13**, 996 (2010).

10IJM2473 E. E. Ebenso, D. A. Isabirye, and N. O. Eddy, *Int. J. Mol. Sci.*, **11**, 2473 (2010).

10JCPR558 J. Yadav, S. N. Pandeya, G. Nath, and S. P. Singh, *J. Chem. Pharm. Res.*, **2**, 558 (2010).

10JEI599 Z. H. Chohan and S. H. Sumrra. *J. Enzyme Inhib. Med. Chem.*, **25**, 599 (2010).

10JIB851 M. J. Xie, X. D. Yang, W. P. Liu, S. P. Yan, and Z. H. Meng, *J. Inorg. Biochem.*, **104**, 851 (2010).

10JPA68 N. P. Moorjani, K. M. Vyas, and R. N. Jadeja, *J. Pure Appl. Sci.*, **18**, 68 (2010).

10JPH2856 G. Mariappan, B. P. Saha, L. Sutharson, G. Ankits, L. Pandey, and D. Kumar, *J. Pharm. Res.*, **3**, 2856 (2010).

10MI1 P. W. Atkins, T. L. Overton, J. P. Rourke, M. T. Weller and F. A. Armstrong, Shriver and Atkins' Inorganic Chemistry, 5th Edn., Oxford University Press, 2010, p. 473.

10NBT695 P. Mallick and B. Kuster, *Nat Biotechnol.*, **28**, 695 (2010).

10OC14 S. Bouzroura, Y.Bentarzi, R. Kaoua, B. Nedjar-Kolli, S. Poulain-Martini, and E. Dunach, *Org. Commun.*, **3**, 8 (2010).

11ICC636 Z. L. You, Y. M. Cui, Y. P. Ma, C. Wang, X. S. Zhou, and K. Li, *Inorg. Chem. Commun.*, **14**, 636 (2011).

11ICC1636 N. Zhang, C. Y. Huang, D. H. Shi, and Z. L. You, *Inorg. Chem. Commun.*, **14**, 1636 (2011).

11IJP26 M. Singh and N. Raghav, *Int. J. Pharm. Pharm Sci.*, **3**(4), 26 (2011).

11JAX1281 C. B.Hubschle, G. M. Sheldrick, and B. Dittrich, *J. Appl. Crystallogr.*, **44**, 1281 (2011).

12AX(E)o1280 O. G. Idemudia, A. P. Sadimenko, A. J. Afolayan and E. C. Hosten. Acta Crystallogr., **E68**, o1280 (2012).

12AJ52 N. D. Ekekwe, A. J. Arinze, L. A. Nnanna, C. F. Ukpabi, A. Agwu , and M. O. C. Ogwuegbu. *Am. J. Chem.*, **2**, 52 (2012).

12AX(E)m1107 O. G.Idemudia and E. C. Hosten, *Acta Crystallogr*., **E68**, m1107 (2012).

12BCA1 A. A. Al-Amiery, A. H. Kadhum, and A. Mohamad, *Bio-inorg. Chem. Appl.*, Article ID 795812, 1–6 (2012).

12BCE95 A. A. Abeer, A. S. Shayma, A. Y. Wagee, M. A. Hapipah, and A. A. Mahmood, *Bull. Chem. Soc. Ethiop.*, **26**, 95 (2012).

12IC1152 S. Parihar, S. Pathan, R. N. Jadeja, A. Patel, and V. K. Gupta, *Inorg. Chem.*, **51**, 1152 (2012).

12IJE3222 A. K. Singh and M. A. Quraishi, *Int. J. Electrochem. Sci.*, **7**, 3222 (2012).

12MI1 K. Todar, *Bacterial Resistance to Antibiotics*, The Microbial World, Lectures in Microbiology, Online Textbook, Department of Bacteriology, University of Wisconsin-Madison, Retrieved January 6, 2012.

12TJP285 M. N. Alam, T. B. Wahed, F. Sultana, J. Ahmed, and M. Hasan, *Turk. J. Pharm. Sci.*, **9**, 285 (2012).

13JCHE1 S. Goel, S. Chandra and S. D, Dwivedi, *J. Chem., Article* ID 742915(2013).

Appendix

A1. IR Spectra of Metal Complexes

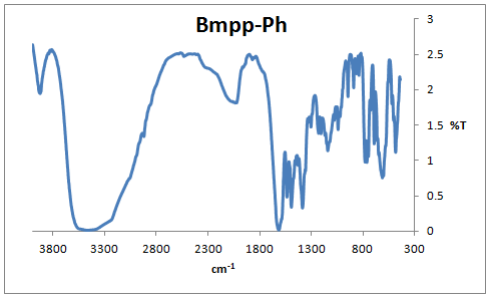

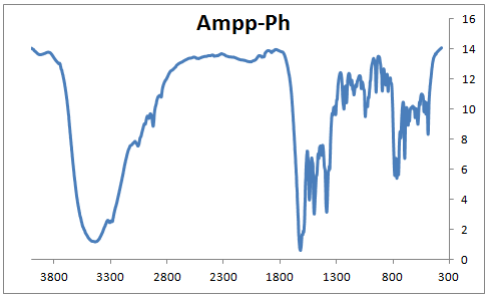

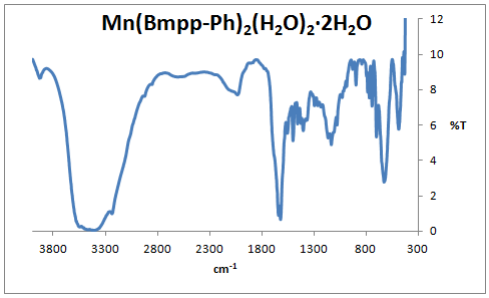

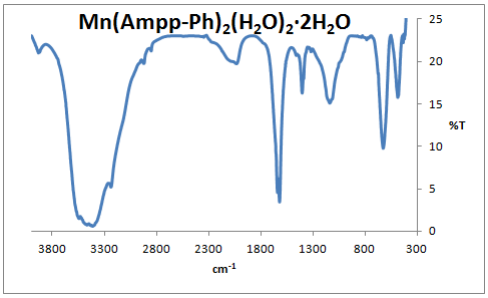

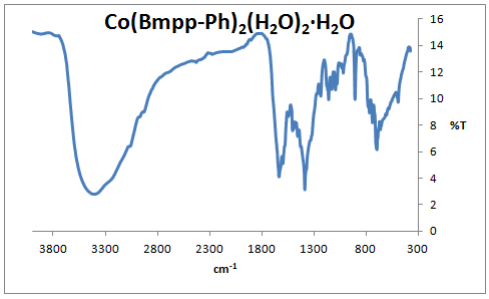

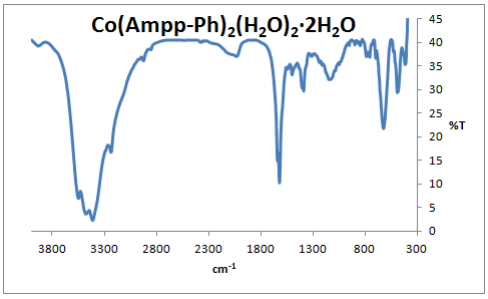

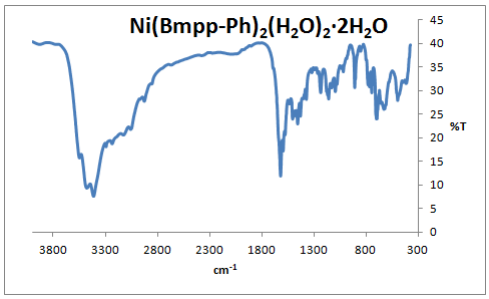

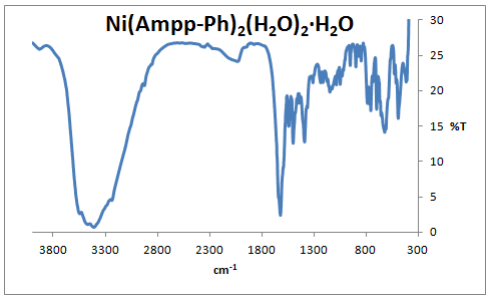

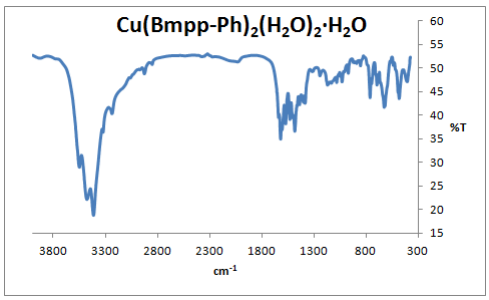
Cu(Bmpp-Ph)2(H2O)2·H2O
%T
cm-1

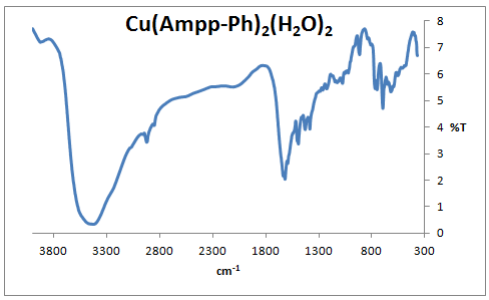
Cu(Ampp-Ph)2(H2O)2
%T
cm-1

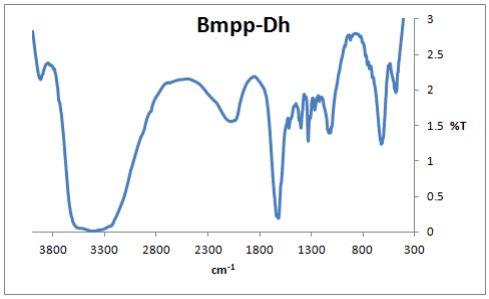
Bmpp-Dh
%T
cm-1

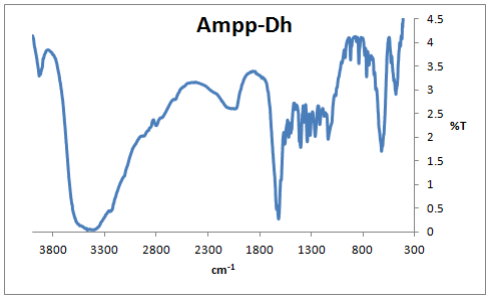
Ampp-Dh
%T
cm-1

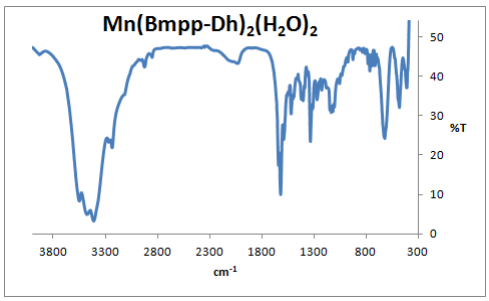
Mn(Bmpp-Dh)2(H2O)2
%T
cm-1

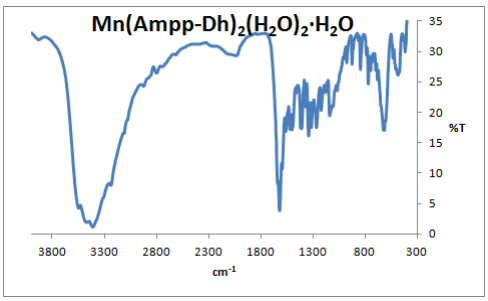
Mn(Ampp-Dh)2(H2O)2·H2O
%T
cm-1

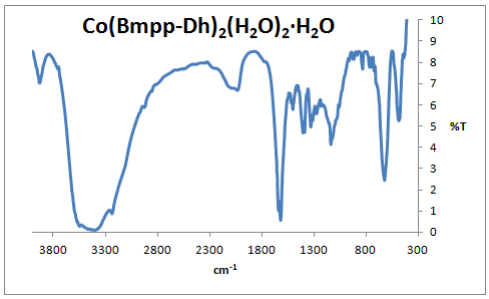
Co(Bmpp-Dh)2(H2O)2·H2O
%T
cm-1

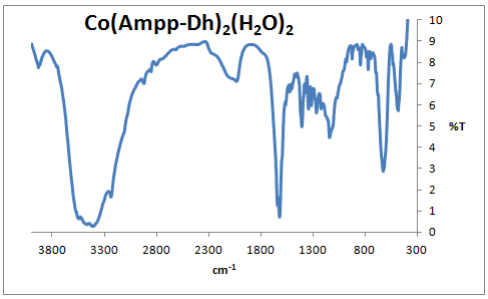
Co(Ampp-Dh)2(H2O)2
%T
cm-1

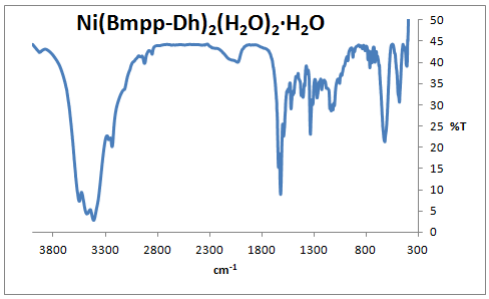
Ni(Bmpp-Dh)2(H2O)2·H2O
%T
cm-1

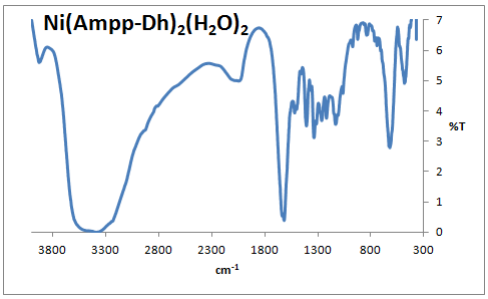
Ni(Ampp-Dh)2(H2O)2
%T
cm-1

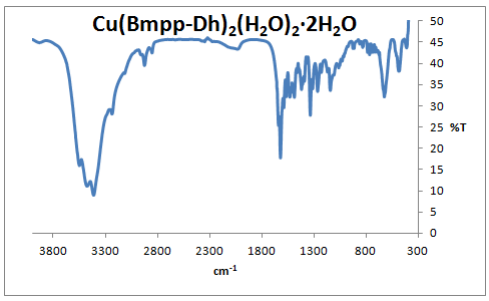
Cu(Bmpp-Dh)2(H2O)2·2H2O
%T
cm-1

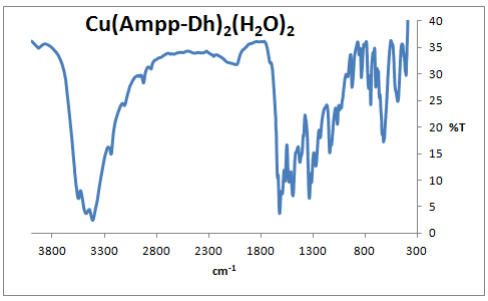
Cu(Ampp-Dh)2(H2O)2
%T
cm-1

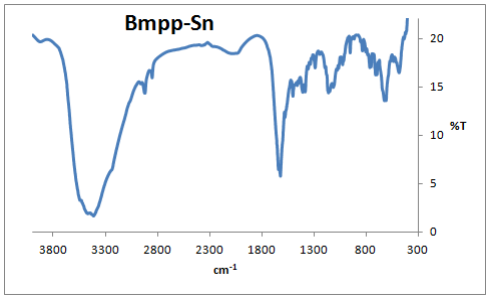
Bmpp-Sn
%T
cm-1

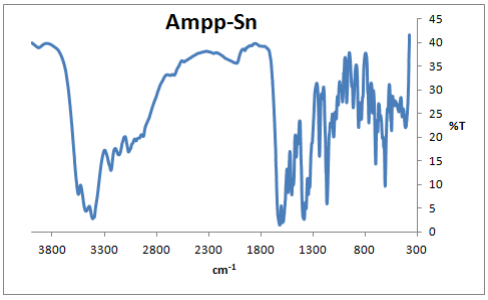
Ampp-Sn
%T
cm-1

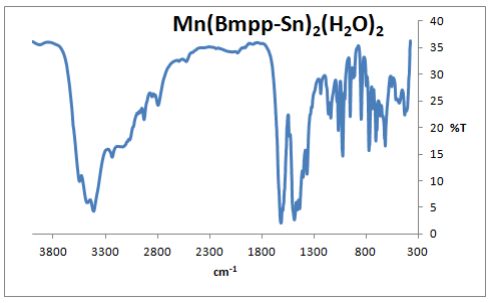
Mn(Bmpp-Sn)2(H2O)2
%T
cm-1

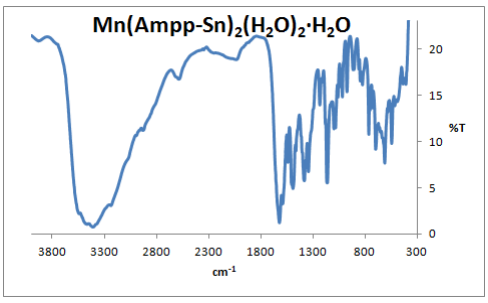
Mn(Ampp-Sn)2(H2O)2·H2O
%T
cm-1

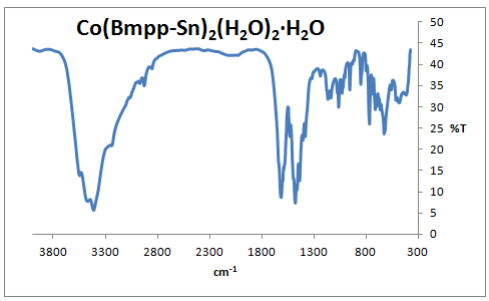
Co(Bmpp-Sn)2(H2O)2·H2O
%T
cm-1

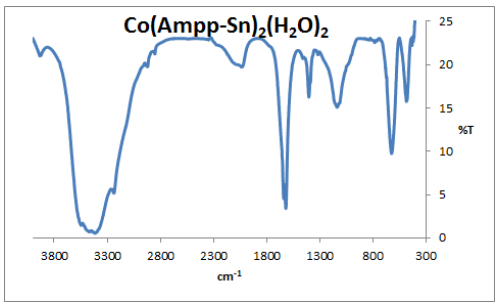
Co(Ampp-Sn)2(H2O)2
%T
cm-1

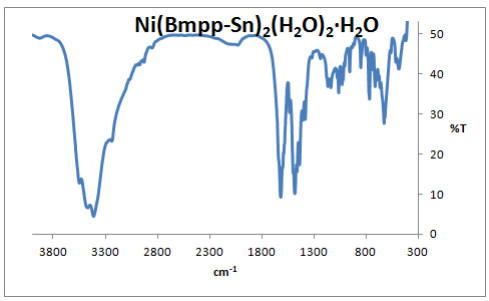
Ni(Bmpp-Sn)2(H2O)2·H2O
%T
cm-1

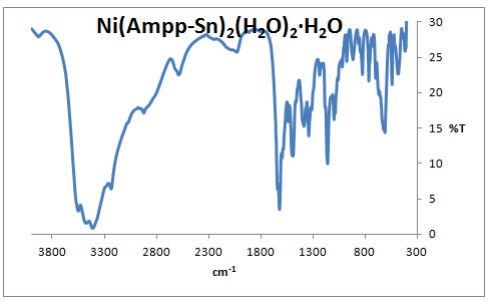
Ni(Ampp-Sn)2(H2O)2·H2O
%T
cm-1

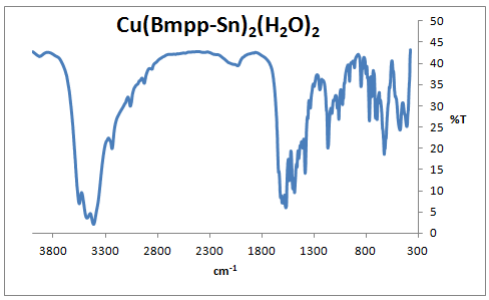
Cu(Bmpp-Sn)2(H2O)2
50
45
40
35
30
25
20
15
10
5
0
%T
3800
3300
2800
2300
1800
1300
800
300
cm-1

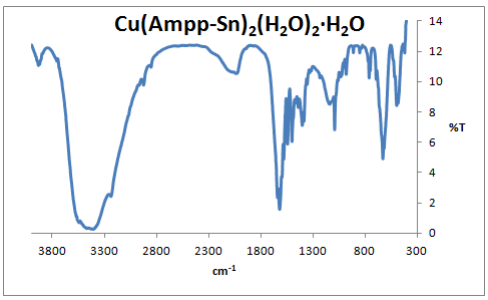
Cu(Ampp-Sn)2(H2O)2·H2O
14
12
10
8
6
4
2
0
%T
3800
3300
2800
2300
1800
1300
800
300
cm-1

A2. Crystal Structures Data

Bmpp-Ph R = 0.04 : Jan 25 13:55:49 2012

Contents

Table S1 - Crystal Data and Details of the Structure Determination
for: ca013 R = 0.04

Table S2 - Final Coordinates and Equivalent Isotropic Displacement Parameters of the non-Hydrogen atoms
for: ca013 R = 0.04

Table S3 - Hydrogen Atom Positions and Isotropic Displacement Parameters
for: ca013 R = 0.04

Table S4 - (An)isotropic Displacement Parameters
for: ca013 R = 0.04

Table S5 - Bond Distances (Angstrom)
for: ca013 R = 0.04

Table S6 - Bond Angles (Degrees)
for: ca013 R = 0.04

Table S7 - Torsion Angles (Degrees)
for: ca013 R = 0.04

Table S8 - Contact Distances(Angstrom)
for: ca013 R = 0.04

Table S9 - Hydrogen Bonds (Angstrom, Deg)
for: ca013 R = 0.04

Table S1 - Crystal Data and Details of the Structure Determination
for: ca013 R = 0.04

	Crystal Data
Formula	C23 H20 N4 O
Formula Weight	368.43
Crystal System	Monoclinic
Space group	P21/c (No. 14)
a, b, c [Angstrom]	8.6806(2) 20.4319(4) 10.6100(2)
alpha, beta, gamma [deg]	90 99.713(1) 90
V [Ang**3]	1854.83(7)
Z	4
D(calc) [g/cm**3]	1.319
Mu(MoKa) [/mm]	0.084
F(000)	776
Crystal Size [mm]	0.22 x 0.40 x 0.59

Data Collection

Temperature (K)	200
Radiation [Angstrom]	MoKa 0.71073
Theta Min-Max [Deg]	2.4, 28.3
Dataset	-11: 11 ; -27: 26 ; -14: 14
Tot., Uniq. Data, R(int)	17965, 4607, 0.014
Observed data [I > 2.0 sigma(I)]	3891

Refinement

Nref, Npar	4607, 262
R, wR2, S	0.0391, 0.1079, 1.04

w=1/[\s^2^(Fo^2^)+(0.0506P)^2^+0.4920P]
where P=(Fo^2^+2Fc^2^)/3 Max. and Av. Shift/Error 0.00, 0.00
Min. and Max. Resd. Dens. [e/Ang^3] -0.17, 0.27

Table S2 - Final Coordinates and Equivalent Isotropic Displacement Parameters of the non-Hydrogen atoms
for: ca013 R = 0.04

Atom	x	y	z	U(eq) [Ang^2]
O1	0.37112(10)	-0.06816(4)	0.56481(8)	0.0414(3)
N1	0.19594(11)	-0.06784(5)	0.37026(8)	0.0317(3)
N2	0.08885(10)	-0.02411(5)	0.30147(9)	0.0326(3)
N3	0.35993(12)	0.04986(5)	0.68161(8)	0.0351(3)
N4	0.42974(12)	0.09280(5)	0.77706(8)	0.0333(3)
C1	0.27317(13)	-0.04046(6)	0.48275(9)	0.0314(3)
C2	0.21562(12)	0.02578(5)	0.48023(9)	0.0301(3)
C3	0.10127(12)	0.03072(5)	0.36586(10)	0.0308(3)
C4	0.00114(14)	0.08688(6)	0.31689(12)	0.0410(3)
C5	0.27016(12)	0.07110(5)	0.57521(9)	0.0295(3)
C11	0.22094(13)	-0.12928(5)	0.31617(10)	0.0317(3)
C12	0.31193(16)	-0.17665(6)	0.38711(12)	0.0423(4)
C13	0.33855(19)	-0.23605(7)	0.33154(14)	0.0521(4)
C14	0.27385(18)	-0.24925(7)	0.20636(14)	0.0516(4)
C15	0.18389(16)	-0.20201(7)	0.13574(12)	0.0477(4)
C16	0.15679(14)	-0.14194(6)	0.18873(11)	0.0390(3)
C21	0.23894(12)	0.14208(5)	0.56126(10)	0.0316(3)
C22	0.29871(15)	0.17609(6)	0.46630(11)	0.0410(4)
C23	0.27886(18)	0.24303(7)	0.45546(14)	0.0526(4)
C24	0.19696(19)	0.27574(7)	0.53651(15)	0.0575(5)
C25	0.13434(18)	0.24193(7)	0.62892(15)	0.0534(4)
C26	0.15687(14)	0.17513(6)	0.64279(12)	0.0401(4)
C31	0.40268(12)	0.07932(5)	0.90166(9)	0.0275(3)
C32	0.51420(13)	0.09944(5)	1.00413(10)	0.0314(3)
C33	0.48897(14)	0.08995(6)	1.12813(10)	0.0348(3)
C34	0.35439(14)	0.05974(6)	1.15146(10)	0.0364(3)
C35	0.24276(13)	0.04011(6)	1.04931(11)	0.0359(3)
C36	0.26506(13)	0.05003(5)	0.92422(10)	0.0315(3)

U(eq) = 1/3 of the trace of the orthogonalized U Tensor

Table S3 - Hydrogen Atom Positions and Isotropic Displacement Parameters
for: ca013 R = 0.04

Atom	x	y	z	U(iso) [Ang^2]
H3	0.3866(18)	0.0073(8)	0.6855(14)	0.049(4)
H4	0.529(2)	0.0996(8)	0.7705(16)	0.055(4)
H4A	0.06120	0.12050	0.28290	0.0620
H4B	0.04800	0.10540	0.38680	0.0620
H4C	-0.08400	0.07170	0.24880	0.0620
H12	0.35600	-0.16830	0.47380	0.0510
H13	0.40210	-0.26800	0.38020	0.0630
H14	0.29100	-0.29030	0.16920	0.0620
H15	0.13970	-0.21080	0.04930	0.0570
H16	0.09530	-0.10970	0.13890	0.0470
H22	0.35290	0.15330	0.40920	0.0490
H23	0.32160	0.26650	0.39220	0.0630
H24	0.18340	0.32180	0.52890	0.0690
H25	0.07570	0.26470	0.68300	0.0640
H26	0.11640	0.15210	0.70780	0.0480
H32	0.60780	0.11970	0.98900	0.0380
H33	0.56490	0.10430	1.19780	0.0420
H34	0.33840	0.05250	1.23680	0.0440
H35	0.14970	0.01960	1.06510	0.0430
H36	0.18730	0.03700	0.85470	0.0380

The Temperature Factor has the Form of Exp(-T) where
T = 8*(Pi**2)*U*(Sin(Theta)/Lambda)**2 for Isotropic Atoms

Table S4 - (An)isotropic Displacement Parameters
for: ca013 R = 0.04

Atom	U(1,1)	U(2,2)	U(3,3)	U(2,3)	U(1,3)	U(1,2)
O1	0.0531(5)	0.0408(5)	0.0266(4)	-0.0013(3)	-0.0043(3)	0.0052(4)
N1	0.0352(5)	0.0358(5)	0.0233(4)	-0.0006(3)	0.0026(3)	-0.0036(4)
N2	0.0315(4)	0.0386(5)	0.0269(4)	0.0017(4)	0.0028(3)	-0.0043(4)
N3	0.0482(6)	0.0343(5)	0.0215(4)	-0.0021(4)	0.0023(4)	-0.0007(4)
N4	0.0386(5)	0.0394(5)	0.0217(4)	-0.0014(4)	0.0048(4)	-0.0079(4)
C1	0.0365(5)	0.0374(6)	0.0207(4)	-0.0008(4)	0.0056(4)	-0.0040(4)
C2	0.0332(5)	0.0359(5)	0.0218(5)	0.0012(4)	0.0068(4)	-0.0031(4)
C3	0.0295(5)	0.0375(6)	0.0261(5)	0.0019(4)	0.0069(4)	-0.0053(4)
C4	0.0387(6)	0.0424(6)	0.0394(6)	0.0016(5)	-0.0008(5)	0.0009(5)
C5	0.0316(5)	0.0359(5)	0.0224(4)	0.0011(4)	0.0089(4)	-0.0033(4)
C11	0.0338(5)	0.0360(5)	0.0268(5)	-0.0031(4)	0.0091(4)	-0.0089(4)
C12	0.0570(7)	0.0376(6)	0.0313(6)	-0.0010(5)	0.0048(5)	-0.0038(5)
C13	0.0703(9)	0.0385(7)	0.0465(7)	-0.0017(6)	0.0069(7)	0.0016(6)
C14	0.0616(8)	0.0440(7)	0.0502(8)	-0.0145(6)	0.0126(6)	-0.0049(6)
C15	0.0476(7)	0.0586(8)	0.0366(6)	-0.0175(6)	0.0065(5)	-0.0082(6)
C16	0.0371(6)	0.0493(7)	0.0304(5)	-0.0060(5)	0.0051(4)	-0.0048(5)
C21	0.0338(5)	0.0342(5)	0.0258(5)	-0.0003(4)	0.0022(4)	-0.0055(4)
C22	0.0480(7)	0.0428(7)	0.0318(6)	0.0034(5)	0.0057(5)	-0.0101(5)
C23	0.0622(9)	0.0438(7)	0.0465(7)	0.0118(6)	-0.0060(6)	-0.0173(6)
C24	0.0667(9)	0.0340(6)	0.0615(9)	0.0021(6)	-0.0189(7)	-0.0028(6)
C25	0.0573(8)	0.0465(7)	0.0519(8)	-0.0093(6)	-0.0036(6)	0.0131(6)
C26	0.0403(6)	0.0444(7)	0.0355(6)	-0.0009(5)	0.0060(5)	0.0027(5)
C31	0.0333(5)	0.0267(5)	0.0226(4)	0.0004(4)	0.0050(4)	0.0014(4)
C32	0.0326(5)	0.0336(5)	0.0276(5)	-0.0001(4)	0.0040(4)	-0.0032(4)
C33	0.0404(6)	0.0378(6)	0.0246(5)	-0.0015(4)	0.0006(4)	0.0008(4)
C34	0.0463(6)	0.0387(6)	0.0258(5)	0.0029(4)	0.0110(4)	0.0029(5)
C35	0.0374(6)	0.0359(6)	0.0367(6)	0.0021(4)	0.0132(4)	-0.0030(4)
C36	0.0334(5)	0.0309(5)	0.0293(5)	-0.0019(4)	0.0030(4)	-0.0029(4)

The Temperature Factor has the Form of Exp(-T) where T = 8*(Pi**2)*U*(Sin(Theta)/Lambda)**2 for isotropic atoms T = 2*(Pi**2)*Sumij(h(i)*h(j)*U(i,j)*Astar(i)*Astar(j)), foranisotropic atoms. Astar(i) are reciprocal axial lengths andh(i) are the reflection indices.

Table S5 - Bond Distances (Angstrom)
for: ca013 R = 0.04

O1-C1	1.2456(14)	C25-C26	1.3831(19)
N1-N2	1.4022(14)	C31-C36	1.3925(15)
N1-C1	1.3845(13)	C31-C32	1.3903(15)
N1-C11	1.4122(14)	C32-C33	1.3834(15)
N2-C3	1.3071(14)	C33-C34	1.3801(17)
N3-N4	1.3984(13)	C34-C35	1.3857(16)
N3-C5	1.3316(13)	C35-C36	1.3881(16)
N4-C31	1.4084(13)	C4-H4A	0.9800
N3-H3	0.899(16)	C4-H4B	0.9800
N4-H4	0.887(18)	C4-H4C	0.9800
C1-C2	1.4414(16)	C12-H12	0.9500
C2-C5	1.3915(14)	C13-H13	0.9500
C2-C3	1.4358(14)	C14-H14	0.9500
C3-C4	1.4903(16)	C15-H15	0.9500
C5-C21	1.4782(14)	C16-H16	0.9500
C11-C12	1.3880(17)	C22-H22	0.9500
C11-C16	1.3969(16)	C23-H23	0.9500
C12-C13	1.3856(19)	C24-H24	0.9500
C13-C14	1.379(2)	C25-H25	0.9500
C14-C15	1.380(2)	C26-H26	0.9500
C15-C16	1.3865(19)	C32-H32	0.9500
C21-C26	1.3856(16)	C33-H33	0.9500
C21-C22	1.3941(16)	C34-H34	0.9500
C22-C23	1.3809(19)	C35-H35	0.9500
C23-C24	1.378(2)	C36-H36	0.9500
C24-C25	1.383(2)		

Table S6 Bond Angles (Degrees) for: ca013 R = 0.04

N2-N1-C1	111.92(9)	C14-C15-C16	121.20(12)
N2-N1-C11	119.26(8)	C11-C16-C15	119.29(11)
C1-N1-C11	128.63(10)	C5-C21-C22	118.50(10)
N1-N2-C3	106.56(9)	C5-C21-C26	121.37(10)
N4-N3-C5	121.98(10)	C22-C21-C26	120.10(10)
N3-N4-C31	115.89(9)	C21-C22-C23	119.83(12)
C5-N3-H3	117.6(9)	C22-C23-C24	119.92(13)
N4-N3-H3	119.8(10)	C23-C24-C25	120.40(13)
C31-N4-H4	115.0(11)	C24-C25-C26	120.18(14)
N3-N4-H4	110.5(11)	C21-C26-C25	119.53(12)
O1-C1-N1	126.38(11)	N4-C31-C32	118.15(10)
N1-C1-C2	104.33(9)	N4-C31-C36	121.95(9)
O1-C1-C2	129.29(10)	C32-C31-C36	119.80(9)
C1-C2-C3	105.65(8)	C31-C32-C33	120.08(10)
C1-C2-C5	122.47(9)	C32-C33-C34	120.52(10)
C3-C2-C5	131.88(10)	C33-C34-C35	119.38(10)
C2-C3-C4	129.45(10)	C34-C35-C36	120.91(11)
N2-C3-C4	119.07(10)	C31-C36-C35	119.29(10)
N2-C3-C2	111.46(9)	C3-C4-H4A	110.00
N3-C5-C21	118.41(9)	C3-C4-H4B	109.00
C2-C5-C21	123.10(9)	C3-C4-H4C	110.00
N3-C5-C2	118.43(9)	H4A-C4-H4B	109.00
N1-C11-C12	120.79(10)	H4A-C4-H4C	109.00
N1-C11-C16	119.64(10)	H4B-C4-H4C	109.00
C12-C11-C16	119.55(10)	C11-C12-H12	120.00
C11-C12-C13	120.03(12)	C13-C12-H12	120.00
C12-C13-C14	120.75(13)	C12-C13-H13	120.00
C13-C14-C15	119.17(13)	C14-C13-H13	120.00
C13-C14-H14	120.00	C26-C25-H25	120.00
C15-C14-H14	120.00	C21-C26-H26	120.00
C14-C15-H15	119.00	C25-C26-H26	120.00
C16-C15-H15	119.00	C31-C32-H32	120.00
C11-C16-H16	120.00	C33-C32-H32	120.00
C15-C16-H16	120.00	C32-C33-H33	120.00
C21-C22-H22	120.00	C34-C33-H33	120.00
C23-C22-H22	120.00	C33-C34-H34	120.00
C22-C23-H23	120.00	C35-C34-H34	120.00
C24-C23-H23	120.00	C34-C35-H35	120.00
C23-C24-H24	120.00	C36-C35-H35	120.00
C25-C24-H24	120.00	C31-C36-H36	120.00
C24-C25-H25	120.00	C35-C36-H36	120.00

Table S7 - Torsion Angles (Degrees) for: ca013R = 0.04

C1-N1-N2-C3	2.24(12)	C11-N1-N2-C3	-173.09(9)
N2-N1-C1-O1	177.77(11)	N2-N1-C1-C2	-2.98(12)
C11-N1-C1-O1	-7.46(19)	C11-N1-C1-C2	171.79(10)
N2-N1-C11-C12	-172.48(11)	N2-N1-C11-C16	9.22(15)
C1-N1-C11-C12	13.08(18)	C1-N1-C11-C16	-165.22(11)
N1-N2-C3-C2	-0.46(12)	N1-N2-C3-C4	-179.01(9)
C5-N3-N4-C31	127.25(11)	N4-N3-C5-C2	174.74(10)
N4-N3-C5-C21	-2.61(15)	N3-N4-C31-C32	152.77(10)
N3-N4-C31-C36	-30.80(15)	O1-C1-C2-C3	-178.24(11)
O1-C1-C2-C5	2.00(18)	N1-C1-C2-C3	2.53(11)
N1-C1-C2-C5	-177.23(10)	C1-C2-C3-N2	-1.33(12)
C1-C2-C3-C4	177.03(11)	C5-C2-C3-N2	178.39(11)
C5-C2-C3-C4	-3.3(2)	C1-C2-C5-N3	-10.79(16)
C1-C2-C5-C21	166.43(10)	C3-C2-C5-N3	169.52(11)
C3-C2-C5-C21	-13.26(18)	N3-C5-C21-C22	113.82(12)
N3-C5-C21-C26	-64.01(15)	C2-C5-C21-C22	-63.40(15)
C2-C5-C21-C26	118.77(12)	N1-C11-C12-C13	-178.35(12)
C16-C11-C12-C13	-0.1(2)	N1-C11-C16-C15	179.00(11)
C12-C11-C16-C15	0.69(18)	C11-C12-C13-C14	-0.9(2)
C12-C13-C14-C15	1.1(2)	C13-C14-C15-C16	-0.5(2)
C14-C15-C16-C11	-0.4(2)	C5-C21-C22-C23	-176.45(11)
C26-C21-C22-C23	1.41(18)	C5-C21-C26-C25	178.02(12)
C22-C21-C26-C25	0.22(18)	C21-C22-C23-C24	-1.5(2)
C22-C23-C24-C25	0.0(2)	C23-C24-C25-C26	1.6(2)
C24-C25-C26-C21	-1.7(2)	N4-C31-C32-C33	176.97(10)
C36-C31-C32-C33	0.47(16)	N4-C31-C36-C35	-177.71(10)
C32-C31-C36-C35	-1.34(16)	C31-C32-C33-C34	0.88(17)
C32-C33-C34-C35	-1.33(18)	C33-C34-C35-C36	0.44(18)
C34-C35-C36-C31	0.89(17)		

Table S8 - Contact Distances (Angstrom) for: ca013 R = 0.04

O1.N3	2.7204(13)	C22.C12	3.4740(19)	O1.C12	2.8992(15)
C22.C3	3.5041(16)	O1.C33	3.3094(14)	C22.C4	3.3493(18)
O1.H3	1.994(16)	C23.C25	3.494(2)	O1.H12	2.2600
C24.C15	3.527(2)	O1.H33	2.5900	C25.C23	3.494(2)
N2.C35	3.4454(15)	C26.C16	3.5653(17)	N3.O1	2.7204(13)
C26.C11	3.5078(17)	N4.C11	3.4265(15)	C26.N4	3.0547(16)
N4.C26	3.0547(16)	C33.O1	3.3094(14)	N2.H35	2.8000
C34.C3	3.4700(16)	N2.H34	2.8500	C35.N2	3.4454(15)
N2.H36	2.6900	C1.H4B	2.9000	N2.H16	2.4600
C1.H12	2.7200	N3.H36	2.5700	C1.H3	2.416(15)
C1.C4	3.5621(16)	C2.H34	3.0100	C3.C34	3.4700(16)
C2.H22	3.0100	C3.C22	3.5041(16)	C3.H34	2.6900
C4C1	3.5621(16)	C11.H26	2.9300	C4.C22	3.3493(18)
C11.H4	2.569(17)	C4.C21	3.2426(16)	C12.H4	2.821(17)
C11.C26	3.5078(17)	C15.H32	2.9400	C11.N4	3.4265(15)
C16.H26	2.7800	C12.O1	2.8992(15)	C16.H32	3.0400
C12.C22	3.4740(19)	C16.H4	2.824(18)	C15.C24	3.527(2)
C2.H4B	2.9400	C16.C26	3.5653(17)	C22.H4A	2.8200
C21.C4	3.2426(16)	C22.H12	2.9600	C23.H13	3.0600
H12.O1	2.2600	C24.H15	2.9200	H12.C1	2.7200
C25.H23	2.9900	H12.C22	2.9600	C25.H15	2.9400
H12.H14	2.3900	C26.H23	3.0300	H13.C32	3.0100
C32.H13	3.0100	H13.C33	3.0600	C33.H3	2.882(16)
H13.C23	3.0600	C33.H13	3.0600	H14.H12	2.3900
C34.H3	2.935(16)	H15.C24	2.9200	C34.H24	3.0200
H15.C25	2.9400	C35.H24	2.8700	H16.N2	2.4600
C36.H3	3.032(15)	H22.C2	3.0100	C36.H24	2.9800
H23.C25	2.9900	H3.O1	1.994(16)	H23.C26	3.0300
H3.C1	2.416(15)	H24.C34	3.0200	H3.C36	3.032(15)
H24.C35	2.8700	H3.C33	2.882(16)	H24.C36	2.9800
H3.C34	2.935(16)	H25.H4A	2.5900	H3.H33	2.5900
H26.C11	2.9300	H4.H32	2.3400	H26.C16	2.7800
H4.C11	2.569(17)	H32.H4	2.3400	H4.C12	2.821(17)
H32.C15	2.9400	H4.C16	2.824(17)	H32.C16	3.0400
H4A.C22	2.8200	H33.O1	2.5900	H4A.H25	2.5900
H33.H3	2.5900	H4B.C21	2.9400	H34.N2	2.8500
H4B.C1	2.9000	H34.C2	3.0100	H4C.H36	2.5700
H34.C3	2.6900	H35.N2	2.8000	H36.N2	2.6900
H36.N3	2.5700	H36.H4C	2.5700		

Table S9 - Hydrogen Bonds (Angstrom, Deg)
for: ca013 R = 0.04

N3--H3..O1	0.899(16)	1.994(16)	2.7204(13)	136.8(13)
C12--H12..O1	0.9500	2.2600	2.8992(15)	124.00
C16--H16..N2	0.9500	2.4600	2.7951(16)	100.00
C33--H33..O1	0.9500	2.5900	3.3094(14)	132.00

Translation of Symmetry Code to Equiv.Pos

a = [3657.00] = [3_657] =1-x,-y,2-z
b = [1554.00] = [1_554] =x,y,-1+z
c = [3556.00] = [3_556] =-x,-y,1-z
d = [3656.00] = [3_656] =1-x,-y,1-z
e = [2545.00] = [2_545] =-x,-1/2+y,1/2-z
f = [4554.00] = [4_565] =x,1/2-y,-1/2+z
g = [2555.00] = [2_555] =-x,1/2+y,1/2-z
h = [4555.00] = [4_566] =x,1/2-y,1/2+z
i = [2656.00] = [2_656] =1-x,1/2+y,3/2-z
j = [1556.00] = [1_556] =x,y,1+z
k = [4545.00] = [4_556] =x,-1/2-y,1/2+z
l = [2646.00] = [2_646] =1-x,-1/2+y,3/2-z
m= [4544.00] = [4_555] =x,-1/2-y,-1/2+z

$Co(Bmpp)_2(EtoH)_2$ R = 0.03 : May 14 13:17:39 2012

Contents

Table S1 - Crystal Data and Details of the Structure Determination
for: ca104 R = 0.03

Table S2 - Final Coordinates and Equivalent Isotropic Displacement Parameters of the non-Hydrogen atoms
for: ca104 R = 0.03

Table S3 - Hydrogen Atom Positions and Isotropic Displacement Parameters
for: ca104 R = 0.03

Table S4 - (An)isotropic Displacement Parameters
for: ca104 R = 0.03

Table S5 - Bond Distances (Angstrom)
for: ca104 R = 0.03

Table S6 - Bond Angles (Degrees)
for: ca104 R = 0.03

Table S7 - Torsion Angles (Degrees)
for: ca104 R = 0.03

Table S8 - Contact Distances(Angstrom)
for: ca104 R = 0.03

Table S9 - Hydrogen Bonds (Angstrom, Deg)
for: ca104 R = 0.03

Table S1 - Crystal Data and Details of the Structure Determination
for: ca104 R = 0.03

Crystal Data

Formula	C38 H38 Co N4 O6
Formula Weight	705.65
Crystal System	Triclinic
Space group	P-1 (No 2)
a, b, c [Angstrom]	11.0484(3) 11.2282(3) 14.8425(4)
alpha, beta, gamma [deg]	89.205(1) 87.678(1) 76.997(1)
V [Ang**3]	1792.56(8)
Z	2
D(calc) [g/cm**3]	1.307
Mu(MoKa) [/mm]	0.529
F(000)	738
Crystal Size [mm]	0.12 x 0.36 x 0.49

Data Collection

Temperature (K)	200
Radiation [Angstrom]	MoKa 0.71073
Theta Min-Max [Deg]	2.3, 28.3
Dataset	-14: 14; -14: 14; -19: 19
Tot., Uniq. Data, R(int)	32307, 8869, 0.015
Observed data [I > 2.0 sigma(I)]	7482

Refinement

Nref, Npar	8869, 471
R, wR2, S	0.0344, 0.0950, 1.02
w = 1/[\s^2^(Fo^2^)+(0.0422P)^2^+0.9543P]	
where P=(Fo^2^+2Fc^2^)/3	
Max. and Av. Shift/Error	0.00, 0.00
Min. and Max. Resd. Dens. [e/Ang^3]	-0.47, 0.51

Table S2 Final Coordinates and Equivalent Isotropic Displacement Parameters of the non-Hydrogen Atoms for: ca104 R = 0.03

Atom	x	y	z	U(eq) [Ang^2]
Co1	0	0	½	0.0264(1)
O11	-0.06104(10)	0.16165(9)	0.56233(6)	0.0315(3)
O12	0.11939(10)	-0.05987(10)	0.60361(7)	0.0336(3)
O13	0.14538(12)	0.06673(12)	0.43001(9)	0.0466(4)
N11	-0.10305(11)	0.27443(11)	0.69400(8)	0.0280(3)
N12	-0.05984(13)	0.26925(12)	0.78148(8)	0.0341(4)
C11	-0.03970(13)	0.17640(12)	0.64384(9)	0.0252(4)
C12	0.04931(14)	0.10603(13)	0.70179(9)	0.0279(4)
C13	0.02963(15)	0.17038(14)	0.78577(9)	0.0335(4)
C14	0.0899(2)	0.1371(2)	0.87390(11)	0.0562(6)
C15	0.13206(13)	-0.00484(13)	0.67443(9)	0.0275(4)
*C16A	0.2742(3)	-0.0041(4)	0.4279(2)	0.0534(10)
*C17A	0.3656(3)	0.0719(3)	0.4045(2)	0.0641(11)
C111	-0.19608(13)	0.37569(13)	0.66632(10)	0.0286(4)
C112	-0.25930(15)	0.37105(15)	0.58784(11)	0.0371(4)
C113	-0.34801(17)	0.47218(18)	0.56156(13)	0.0481(6)
C114	-0.37636(19)	0.57684(18)	0.61289(15)	0.0535(6)
C115	-0.3129(2)	0.58125(18)	0.68994(16)	0.0578(7)
C116	-0.22273(18)	0.48182(16)	0.71716(13)	0.0463(6)
C121	0.24248(14)	-0.06123(14)	0.72766(9)	0.0310(4)
C122	0.2658(2)	-0.18464(17)	0.74798(15)	0.0533(6)
C123	0.3715(2)	-0.2392(2)	0.79362(18)	0.0699(8)
C124	0.45441(19)	-0.1725(2)	0.81670(14)	0.0581(7)
C125	0.43434(17)	-0.0511(2)	0.79472(13)	0.0521(6)
C126	0.32726(17)	0.00593(17)	0.75092(12)	0.0428(5)
*C16B	0.2583(12)	0.0716(13)	0.4401(8)	0.070(4)
*C17B	0.3450(12)	-0.0480(17)	0.4284(10)	0.106(6)
Co2	1	½	0	0.0303(1)
O21	1.07029(12)	0.34177(11)	0.06276(7)	0.0395(3)
O22	0.87771(11)	0.54948(10)	0.11026(7)	0.0359(3)
O23	0.87494(12)	0.41461(12)	-0.06579(8)	0.0462(4)
N21	1.11456(13)	0.22367(12)	0.19080(8)	0.0336(4)
N22	1.07617(14)	0.22544(13)	0.28176(8)	0.0375(4)
C21	1.05355(15)	0.32601(14)	0.14632(9)	0.0316(4)
C22	0.97286(15)	0.39911(14)	0.21254(9)	0.0321(4)
C23	0.99378(16)	0.32862(15)	0.29435(10)	0.0362(5)
C24	0.9383(2)	0.35577(17)	0.38780(11)	0.0532(6)
C25	0.88599(15)	0.50747(14)	0.18943(9)	0.0318(4)
C26	0.7822(3)	0.3650(3)	-0.01816(18)	0.0823(10)
C27	0.6610(3)	0.4357(5)	-0.0300(4)	0.155(3)
C211	1.19389(14)	0.11779(14)	0.15297(10)	0.0318(4)
C212	1.26245(15)	0.12585(17)	0.07298(10)	0.0382(5)
C213	1.33730(16)	0.02042(19)	0.03630(12)	0.0463(5)
C214	1.34711(18)	-0.09108(19)	0.07852(14)	0.0516(6)
C215	1.28032(19)	-0.09846(17)	0.15823(15)	0.0514(6)
C216	1.20287(17)	0.00521(16)	0.19519(12)	0.0418(5)
C221	0.79264(16)	0.57662(15)	0.25689(10)	0.0375(5)
C222	0.66813(19)	0.5958(2)	0.23946(14)	0.0560(7)
C223	0.5791(2)	0.6608(3)	0.30081(18)	0.0756(9)
C224	0.6170(3)	0.7090(2)	0.37703(16)	0.0758(9)
C225	0.7401(3)	0.69350(19)	0.39334(14)	0.0635(8)
C226	0.8290(2)	0.62677(16)	0.33398(11)	0.0459(6)

U(eq) = 1/3 of the trace of the orthogonalized U Tensor Starred Atom sites have a S.O.F less than 1.0

Table S3 - Hydrogen Atom Positions and Isotropic Displacement Parameters for: ca104 R = 0.03

Atom	x	y	z	U(iso) [Ang^2]
H12A	0.31250	0.09070	0.73700	0.0510
H14B	0.04020	0.18630	0.92210	0.0840
H13A	0.12590	0.10750	0.38640	0.060(7)
H14A	0.09530	0.05020	0.88660	0.0840
*H16B	0.29270	-0.04240	0.48780	0.0640
*H17A	0.45000	0.02060	0.40480	0.0960
*H17B	0.35730	0.13740	0.44880	0.0960
*H17C	0.34960	0.10780	0.34430	0.0960
H112	-0.24180	0.29890	0.55240	0.0450
H113	-0.39000	0.46930	0.50730	0.0580
H114	-0.43890	0.64490	0.59520	0.0640
H115	-0.33110	0.65350	0.72520	0.0690
H116	-0.17930	0.48630	0.77050	0.0560
H122	0.20960	-0.23210	0.73070	0.0640
H123	0.38620	-0.32350	0.80890	0.0840
H124	0.52630	-0.21040	0.84810	0.0700
H125	0.49360	-0.00550	0.80940	0.0630
H14C	0.17360	0.15310	0.87080	0.0840
*H16A	0.28360	-0.07050	0.38320	0.0640
*H16A	0.26630	0.10270	0.50120	0.0840
*H16B	0.28140	0.13020	0.39580	0.0840
*H17A	0.36690	-0.06200	0.36420	0.1590
*H17B	0.30530	-0.11250	0.45190	0.1590
*H17C	0.42040	-0.04930	0.46140	0.1590
H23A	0.89850	0.36900	-0.11430	0.062(7)
H24A	0.84790	0.38440	0.38500	0.0800
H24B	0.97320	0.41920	0.41470	0.0800
H24C	0.95750	0.28140	0.42470	0.0800
H26A	0.78710	0.28090	-0.03950	0.0990
H26B	0.79930	0.36040	0.04690	0.0990
H27A	0.65980	0.52220	-0.02090	0.2320
H27B	0.60320	0.40990	0.01390	0.2320
H27C	0.63570	0.42400	-0.09120	0.2320
H212	1.25790	0.20260	0.04400	0.0460
H213	1.38260	0.02520	-0.01890	0.0560
H214	1.39950	-0.16240	0.05300	0.0620
H215	1.28750	-0.17510	0.18790	0.0620
H216	1.15590	-0.00080	0.24940	0.0500
H222	0.64290	0.56480	0.18580	0.0670
H223	0.49310	0.67190	0.29010	0.0910
H224	0.55650	0.75350	0.41870	0.0910
H225	0.76500	0.72850	0.44550	0.0760
H226	0.91470	0.61510	0.34580	0.0550

The Temperature Factor has the Form of Exp(-T) Where T = 8*(Pi**2)*U*(Sin(Theta)/Lambda)**2 for Isotropic Atoms

Table S4 (An)isotropic Displacement Parameters for: ca104 R = 0.03

Atom	U(1,1) or U	U(2,2)	U(3,3)	U(2,3)	U(1,3)	U(1,2)
Co1	0.0358(2)	0.0252(1)	0.0152(1)	-0.0041(1)	-0.0046(1)	0.0007(1)
O11	0.0441(6)	0.0282(5)	0.0180(4)	-0.0049(4)	-0.0068(4)	0.0022(4)
O12	0.0445(6)	0.0306(5)	0.0216(5)	-0.0060(4)	-0.0091(4)	0.0021(4)
O13	0.0443(7)	0.0425(7)	0.0467(7)	0.0110(6)	0.0090(5)	0.0012(5)
N11	0.0322(6)	0.0298(6)	0.0199(5)	-0.0068(4)	-0.0034(4)	-0.0019(5)
N12	0.0400(7)	0.0393(7)	0.0200(5)	-0.0098(5)	-0.0062(5)	-0.0013(6)
C11	0.0298(7)	0.0255(6)	0.0196(6)	-0.0041(5)	-0.0013(5)	-0.0045(5)
C12	0.0329(7)	0.0309(7)	0.0186(6)	-0.0045(5)	-0.0047(5)	-0.0038(6)
C13	0.0380(8)	0.0381(8)	0.0218(6)	-0.0079(6)	-0.0063(6)	-0.0018(6)
C14	0.0680(13)	0.0625(12)	0.0253(8)	-0.0149(8)	-0.0182(8)	0.0159(10)
C15	0.0324(7)	0.0293(7)	0.0199(6)	-0.0005(5)	-0.0042(5)	-0.0046(5)
C16A	0.0383(16)	0.055(2)	0.0609(17)	0.0128(14)	0.0033(12)	0.0003(14)
C17A	0.0478(17)	0.072(2)	0.073(2)	-0.0167(16)	0.0098(14)	-0.0154(14)
C111	0.0271(7)	0.0295(7)	0.0274(7)	-0.0030(5)	0.0015(5)	-0.0031(5)
C112	0.0369(8)	0.0387(8)	0.0316(7)	-0.0059(6)	-0.0040(6)	0.0007(7)
C113	0.0428(10)	0.0523(11)	0.0417(9)	-0.0007(8)	-0.0103(7)	0.0066(8)
C114	0.0479(11)	0.0429(10)	0.0596(12)	0.0010(8)	-0.0060(9)	0.0119(8)
C115	0.0609(13)	0.0366(9)	0.0669(13)	-0.0157(9)	-0.0095(10)	0.0100(9)
C116	0.0484(10)	0.0384(9)	0.0476(10)	-0.0150(7)	-0.0113(8)	0.0022(7)
C121	0.0332(7)	0.0337(7)	0.0232(6)	-0.0050(5)	-0.0048(5)	-0.0008(6)
C122	0.0572(12)	0.0383(9)	0.0645(12)	0.0048(8)	-0.0304(10)	-0.0062(8)
C123	0.0739(15)	0.0438(11)	0.0865(17)	0.0066(11)	0.0421(13)	0.0045(10)
C124	0.0432(10)	0.0688(14)	0.0531(11)	-0.0118(10)	-0.0203(9)	0.0107(9)
C125	0.0369(9)	0.0748(14)	0.0462(10)	-0.0100(9)	-0.0103(8)	-0.0138(9)
C126	0.0444(9)	0.0461(10)	0.0392(9)	-0.0016(7)	-0.0092(7)	-0.0117(8)
C16B	0.083(8)	0.059(7)	0.083(7)	0.007(6)	-0.025(6)	-0.043(6)
C17B	0.047(7)	0.152(15)	0.098(10)	0.011(9)	-0.013(6)	0.022(8)
Co2	0.0410(2)	0.0330(2)	0.0148(1)	-0.0039(1)	0.0024(1)	-0.0045(1)
O21	0.0552(7)	0.0384(6)	0.0188(5)	-0.0016(4)	0.0073(4)	0.0007(5)
O22	0.0456(6)	0.0379(6)	0.0209(5)	-0.0029(4)	0.0045(4)	-0.0031(5)
O23	0.0487(7)	0.0593(8)	0.0324(6)	-0.0235(5)	0.0078(5)	-0.0162(6)
N21	0.0415(7)	0.0373(7)	0.0195(5)	-0.0018(5)	0.0052(5)	-0.0049(6)
N22	0.0508(8)	0.0387(7)	0.0205(6)	-0.0001(5)	0.0079(5)	-0.0065(6)
C21	0.0389(8)	0.0337(7)	0.0217(6)	-0.0028(5)	0.0035(5)	-0.0081(6)
C22	0.0426(8)	0.0335(7)	0.0200(6)	-0.0035(5)	0.0062(6)	-0.0094(6)
C23	0.0493(9)	0.0364(8)	0.0220(7)	-0.0013(6)	0.0072(6)	-0.0093(7)
C24	0.0847(15)	0.0415(9)	0.0252(8)	0.0016(7)	0.0183(8)	-0.0007(9)
C25	0.0412(8)	0.0339(7)	0.0211(6)	-0.0051(5)	0.0052(6)	0.0108(6)
C26	0.0781(17)	0.118(2)	0.0662(15)	-0.0505(15)	0.0244(13)	-0.0562(17)
C27	0.066(2)	0.212(6)	0.173(5)	-0.017(4)	0.028(3)	-0.009(3)
C211	0.0302(7)	0.0381(8)	0.0268(7)	-0.0065(6)	0.0002(5)	-0.0072(6)
C212	0.0333(8)	0.0508(10)	0.0278(7)	-0.0014(6)	-0.0001(6)	-0.0039(7)
C213	0.0337(8)	0.0670(12)	0.0339(8)	-0.0119(8)	0.0031(6)	-0.0023(8)
C214	0.0435(10)	0.0516(11)	0.0573(11)	-0.0246(9)	0.0050(8)	-0.0056(8)
C215	0.0536(11)	0.0357(9)	0.0656(12)	-0.0110(8)	0.0071(9)	-0.0125(8)
C216	0.0468(10)	0.0374(9)	0.0424(9)	-0.0062(7)	0.0093(7)	-0.0138(7)
C221	0.0493(9)	0.0329(8)	0.0263(7)	0.0001(6)	0.0128(6)	-0.0035(7)
C222	0.0509(11)	0.0668(13)	0.0429(10)	0.0024(9)	0.0082(8)	0.0005(10)
C223	0.0549(13)	0.0874(18)	0.0668(15)	0.0144(13)	0.0210(11)	0.0166(12)
C224	0.095(2)	0.0621(14)	0.0505(13)	0.0018(10)	0.0379(13)	0.0167(13)
C225	0.0972(18)	0.0469(11)	0.0376(10)	-0.0102(8)	0.0259(11)	0.0019(11)
C226	0.0682(12)	0.0375(9)	0.0301(8)	-0.0065(6)	0.0154(8)	-0.0107(8)

The Temperature Factor has the Form of Exp(-T)
WhereT = 8*(Pi**2)*U*(Sin(Theta)/Lambda)**2 for Isotropic Atoms T = 2*(Pi**2)*Sumij(h(i)*h(j)*U(i,j)*Astar(i)*Astar(j)), for Anisotropic Atoms. Astar(i) are Reciprocal Axial Lengths and h(i) are the Reflection Indices.

Table S5 - Bond Distances (Angstrom) for: ca104 R = 0.03

Co1-O11	2.0125(10)	N22-C23	1.313(2)
Co1-O12	2.0721(11)	C11-C12	1.425(2)
Co1-O13	2.1460(14)	C12-C15	1.422(2)
Co1-O11a	2.0125(10)	C12-C13	1.4337(19)
Co1-O12a	2.0721(11)	C13-C14	1.496(2)
Co1-O13a	2.1460(14)	C15-C121	1.493(2)
Co2-O23	2.1245(13)	C16A-C17A	1.490(5)
Co2-O21b	2.0048(12)	C16B-C17B	1.47(2)
Co2-O22b	2.0786(11)	C111-C112	1.390(2)
Co2-O23b	2.1245(13)	C111-C116	1.388(2)
Co2-O21	2.0048(12)	C112-C113	1.386(3)
Co2-O22	2.0786(11)	C113-C114	1.378(3)
O11-C11	1.2621(16)	C114-C115	1.373(3)
O12-C15	1.2551(17)	C14-H14C	0.9800
O13-C16B	1.276(14)	C14-H14A	0.9800
O13-C16A	1.465(4)	C14-H14B	0.9800
O13-H13A	0.8000	C115-C116	1.386(3)
O21-C21	1.2624(17)	C16A-H16B	0.9900
O22-C25	1.2592(17)	C16A-H16A	0.9900
O23-C26	1.431(3)	C16B-H16A	0.9900
O23-H23A	0.8900	C16B-H16B	0.9900
N11-C111	1.4189(19)	C17A-H17C	0.9800
N11-N12	1.3974(17)	C17A-H17B	0.9800
N11-C11	1.3746(18)	C17A-H17A	0.9800
N12-C13	1.313(2)	C17B-H17B	0.9800
N21-C211	1.417(2)	C17B-H17C	0.9800
N21-C21	1.370(2)	C17B-H17A	0.9800
N21-N22	1.3977(17)	C121-C122	1.383(2)
C121-C126	1.384(2)	C27-H27B	0.9800
C122-C123	1.389(3)	C27-H27C	0.9800
C123-C124	1.363(3)	C27-H27A	0.9800
C124-C125	1.368(3)	C211-C216	1.388(2)
C125-C126	1.394(3)	C211-C212	1.395(2)
C112-H112	0.9500	C212-C213	1.387(3)
C113-H113	0.9500	C213-C214	1.376(3)
C114-H114	0.9500	C214-C215	1.380(3)
C115-H115	0.9500	C215-C216	1.386(3)
C116-H116	0.9500	C221-C226	1.395(2)
C21-C22	1.434(2)	C221-C222	1.378(3)
C22-C23	1.438(2)	C222-C223	1.397(3)
C22-C25	1.417(2)	C223-C224	1.380(4)
C122-H122	0.9500	C224-C225	1.363(5)
C123-H123	0.9500	C225-C226	1.385(3)
C23-C24	1.500(2)	C212-H212	0.9500
C124-H124	0.9500	C213-H213	0.9500
C125-H125	0.9500	C214-H214	0.9500
C25-C221	1.499(2)	C215-H215	0.9500
C26-C27	1.411(5)	C216-H216	0.9500
C126-H12A	0.9500	C222-H222	0.9500
C24-H24B	0.9800	C223-H223	0.9500
C24-H24C	0.9800	C224-H224	0.9500
C24-H24A	0.9800	C225-H225	0.9500
C26-H26A	0.9900	C226-H226	0.9500
C26-H26B	0.9900		

Table S6 Bond Angles (Degrees) for: ca104 R = 0.03

O11-Co1-O12	90.12(4)	O21-Co2-O22b	91.27(4)
O11-Co1-O13	90.93(5)	O21-Co2-O23b	90.46(5)
O11-Co1-O11a	180.00	Co1-O11-C11	121.85(9)
O11-Co1-O12a	89.88(4)	Co1-O12-C15	128.43(10)
O11-Co1-O13a	89.07(5)	Co1-O13-C16A	121.11(17)
O12-Co1-O13	89.14(5)	Co1-O13-C16B	139.4(6)
O11a-Co1-O12	89.88(4)	C16B-O13-H13A	104.00
O12-Co1-O12a	180.00	Co1-O13 -H13A	116.00
O12-Co1-O13a	90.87(5)	C16A-O13-H13A	115.00
O11a-Co1-O13	89.07(5)	Co2-O21-C21	122.73(11)
O12a-Co1-O13	90.87(5)	Co2-O22-C25	128.58(11)
O13-Co1-O13a	180.00	Co2-O23-C26	122.94(13)
O11a-Co1-O12a	90.12(4)	C26-O23-H23A	107.00
O11a-Co1-O13a	90.93(5)	Co2-O23-H23A	122.00
O12a-Co1-O13a	89.14(5)	C11-N11-C111	128.63(12)
O22-Co2-O23	92.76(5)	N12-N11-C111	120.15(12)
O21b-Co2-O22	91.27(4)	N12-N11-C11	111.14(11)
O22-Co2-O22b	180.00	N11-N12-C13	106.47(11)
O22-Co2-O23b	87.24(5)	C21-N21-C211	127.65(12)
O21b-Co2-O23	90.46(5)	N22-N21-C211	120.37(12)
O22b-Co2-O23	87.24(5)	N22-N21-C21	111.42(12)
O23-Co2-O23b	180.00	N21-N22-C23	106.32(12)
O21b-Co2-O22b	88.73(4)	O11-C11-N11	122.94(13)
O21b-Co2-O23b	89.54(5)	N11-C11-C12	105.98(12)
O22b-Co2-O23b	92.76(5)	O11-C11-C12	131.06(13)
O21-Co2-O21b	180.00	C13-C12-C15	132.25(13)
O21-Co2-O22	88.73(4)	C11-C12-C15	122.89(12)
O21-Co2-O23	89.54(5)	C11-C12-C13	104.83(12)
N12-C13-C14	118.61(14)	O13-C16B-H16A	109.00
C12-C13-C14	129.72(15)	C17B-C16B-H16A	109.00
N12-C13-C12	111.57(13)	C17B-C16B-H16B	109.00
C12-C15-C121	121.51(12)	O13-C16B-H16B	109.00
O12-C15-C121	115.73(13)	C16A-C17A-H17C	109.00
O12-C15-C12	122.74(13)	H17A-C17A-H17B	109.00
O13-C16A-C17A	112.8(3)	H17A-C17A-H17C	109.00
O13-C16B-C17B	112.7(11)	H17B-C17A-H17C	109.00
N11-C111-C116	119.69(14)	C16A-C17A-H17B	110.00
C112-C111-C116	119.40(15)	C16A-C17A-H17A	109.00
N11-C111-C112	120.90(13)	C16B-C17B-H17C	110.00
C111-C112-C113	119.63(15)	C16B-C17B-H17B	109.00
C112-C113-C114	121.06(18)	C16B-C17B-H17A	109.00

C113-C114-C115	119.03(19)	H17B-C17B-H17C	109.00
C13-C14-H14B	109.00	H17A-C17B-H17B	109.00
C13-C14-H14C	109.00	H17A-C17B-H17C	110.00
H14A-C14-H14C	110.00	C15-C121-C122	119.55(15)
H14A-C14-H14B	109.00	C15-C121-C126	120.97(14)
H14B-C14-H14C	109.00	C122-C121-C126	119.28(16)
C13-C14-H14A	109.00	C121-C122-C123	120.01(19)
C114-C115-C116	121.02(19)	C122-C123-C124	120.4(2)
C111-C116-C115	119.84(18)	C123-C124-C125	120.2(2)
H16A-C16A-H16B	108.00	C124-C125-C126	120.20(19)
C17A-C16A-H16B	109.00	C121-C126-C125	119.86(17)
C17A-C16A-H16A	109.00	C113-C112-H112	120.00
O13-C16A-H16A	109.00	C111-C112-H112	120.00
O13-C16A-H16B	109.00	C112-C113-H113	119.00
H16A-C16B-H16B	108.00	C114-C113-H113	119.00
C113-C114-H114	120.00	O23-C26-C27	112.4(3)
C115-C114-H114	120.00	H24A-C24-H24C	109.00
C116-C115-H115	119.00	C23-C24-H24A	109.00
C114-C115-H115	120.00	C23-C24-H24B	109.00
C115-C116-H116	120.00	C23-C24-H24C	109.00
C111-C116-H116	120.00	H24A-C24-H24B	109.00
N21-C21-C22	106.12(12)	H24B-C24-H24C	109.00
O21-C21-N21	122.37(14)	O23-C26-H26B	109.00
O21-C21-C22	131.50(14)	O23-C26-H26A	109.00
C123-C122-H122	120.00	H26A-C26-H26B	108.00
C21-C22-C23	104.25(13)	C27-C26-H26A	109.00
C23-C22-C25	133.13(14)	C27-C26-H26B	109.00
C121-C122-H122	120.00	C26-C27-H27C	109.00
C21-C22-C25	122.19(12)	C26-C27-H27A	110.00
N22-C23-C24	117.69(14)	C26-C27-H27B	109.00
C22-C23-C24	130.42(15)	H27A-C27-H27B	109.00
C122-C123-H123	120.00	H27A-C27-H27C	110.00
N22-C23-C22	111.88(13)	H27B-C27-H27C	109.00
C124-C123-H123	120.00	C212-C211-C216	119.73(15)
C125-C124-H124	120.00	N21-C211-C212	120.32(14)
C123-C124-H124	120.00	N21-C211-C216	119.95(14)
C22-C25-C221	122.13(12)	C211-C212-C213	119.18(16)
C126-C125-H125	120.00	C212-C213-C214	121.12(17)
O22-C25-C22	122.65(14)	C213-C214-C215	119.52(18)
O22-C25-C221	115.15(14)	C214-C215-C216	120.40(18)
C124-C125-H125	120.00	C211-C216-C215	120.02(17)
C121-C126-H12A	120.00	C25-C221-C222	118.69(15)
C125-C126-H12A	120.00	C25-C221-C226	121.65(16)

C222-C221-C226	119.58(17)	C216-C215-H215	120.00
C221-C222-C223	119.93(19)	C211-C216-H216	120.00
C222-C223-C224	119.5(2)	C215-C216-H216	120.00
C223-C224-C225	120.8(2)	C221-C222-H222	120.00
C224-C225-C226	120.1(2)	C223-C222-H222	120.00
C221-C226-C225	120.0(2)	C222-C223-H223	120.00
C211-C212-H212	120.00	C224-C223-H223	120.00
C213-C212-H212	120.00	C223-C224-H224	120.00
C212-C213-H213	119.00	C225-C224-H224	120.00
C214-C213-H213	119.00	C224-C225-H225	120.00
C213-C214-H214	120.00	C226-C225-H225	120.00
C215-C214-H214	120.00	C221-C226-H226	120.00
C214-C215-H215	120.00	C225-C226-H226	120.00

Table S7 - Torsion Angles (Degrees) for: ca104 R = 0.03

O12-Co1-O11-C11	-14.75(11)	O13-Co1-O11-C11	-103.89(12)
O12a-Co1-O11-C11	165.25(11)	O13a-Co1-O11-C11	76.11(12)
O11-Co1-O12-C15	2.28(13)	O13-Co1-O12-C15	93.21(13)
O11a-Co1-O12-C15	-177.72(13)	O13a-Co1-O12-C15	-86.79(13)
O11-Co1-O13-C16A	131.19(18)	O12-Co1-O13-C16A	41.08(18)
O11a-Co1-O13-C16A -	48.81(18)	O12a-Co1-O13-C16A	-138.92(18)
O21-Co2-O22-C25	19.90(14)	O23-Co2-O22-C25	109.38(14)
O21b-Co2-O22-C25	-160.10(14)	O22-Co2-O21-C21	-17.42(14)
O23-Co2-O21-C21	-110.20(14)	O22b-Co2-O21-C21	162.58(14)
O23b-Co2-O21-C21	69.81(14)	O22b-Co2-O23-C26	153.81(18)
O21-Co2-O23-C26	62.51(18)	O22-Co2-O23-C26	-26.19(18)
O23b-Co2-O22-C25	-70.62(14)	O21b-Co2-O23-C26	-117.49(18)
Co1-O11-C11-C12	17.8(2)	Co1-O11-C11-N11	-164.27(10)
Co1-O12-C15-C12	9.8(2)	Co1-O12-C15-C121	-168.50(9)
Co1-O13-C16A-C17A	-160.59(17)	Co2-O21-C21-N21	-171.43(12)
Co2-O21-C21-C22	10.5(3)	Co2-O22-C25-C22	-12.6(2)
Co2-O22-C25-C221	170.58(11)	Co2-O23-C26-C27	108.5(3)
C111-N11-N12-C13	-176.35(13)	N12-N11-C11-O11	-179.12(13)
C111-N11-C11-O11	-2.6(2)	C111-N11-C11-C12	175.81(14)
N12-N11-C11-C12	-0.73(16)	C11-N11-N12-C13	0.53(17)
C11-N11-C111-C112	17.8(2)	C11-N11-C111-C116	-160.85(16)
N12-N11-C111-C112 -	165.91(14)	N12-N11-C111-C116	15.4(2)
N11-N12-C13-C12	-0.09(18)	N11-N12-C13-C14	-176.89(15)
C211-N21-C21-O21	-6.1(3)	C21-N21-N22-C23	-1.07(19)
C211-N21-N22-C23	-173.12(15)	N22-N21-C21-O21	-177.42(15)
N22-N21-C21-C22	1.09(18)	N22-N21-C211-C216	20.3(2)
C211-N21-C21-C22	172.42(15)	N22-N21-C211-C212	-160.23(15)
C21-N21-C211-C212	29.1(2)	C21-N21-C211-C216	-150.36(17)
N21-N22-C23-C24	-178.80(15)	N21-N22-C23-C22	0.60(19)
O11-C11-C12-C13	178.84(15)	N11-C11-C12-C13	0.64(16)
N11-C11-C12-C15	178.95(14)	O11-C11-C12-C15	-2.9(3)
C15-C12-C13-N12	-178.43(16)	C15-C12-C13-C14	-2.1(3)
C11-C12-C13-N12	-0.34(18)	C11-C12-C13-C14	176.00(17)
C11-C12-C15-C121	165.68(14)	C13-C12-C15-O12	165.28(16)
C11-C12-C15-O12	-12.5(2)	C13-C12-C15-C121	-16.5(3)
O12-C15-C121-C122	-49.3(2)	C12-C15-C121-C122	132.42(17)
O12-C15-C121-C126	125.62(16)	C12-C15-C121-C126	-52.7(2)
C112-C111-C116-C115	0.8(3)	N11-C111-C112-C113	-178.76(15)
N11-C111-C116-C115	179.51(17)	C116-C111-C112-C113	-0.1(3)
C111-C112-C113-C114	-1.2(3)	C112-C113-C114-C115	1.7(3)
C113-C114-C115-C116	-1.0(3)	C114-C115-C116-C111	-0.3(3)
C15-C121-C122-C123	176.86(18)	C126-C121-C122-C123	1.9(3)
C122-C121-C126-C125	-0.3(3)	C15-C121-C126-C125	-175.20(15)
C121-C122-C123-C124	-1.6(3)	C122-C123-C124-C125	-0.3(4)
C123-C124-C125-C126	1.9(3)	C124-C125-C126-C121	-1.6(3)
O21-C21-C22-C23	177.64(18)	O21-C21-C22-C25	4.3(3)
N21-C21-C22-C23	-0.67(18)	N21-C21-C22-C25	-173.99(15)
C21-C22-C23-N22	0.04(19)	C21-C22-C23-C24	179.34(18)
C25-C22-C23-N22	172.28(18)	C25-C22-C23-C24	-8.4(3)
C21-C22-C25-O22	-3.2(3)	C21-C22-C25-C221	173.43(15)
C23-C22-C25-O22	-174.33(17)	C23-C22-C25-C221	2.3(3)
O22-C25-C221-C226	-122.06(17)	O22-C25-C221-C222	54.7(2)
C22-C25-C221-C222	-122.19(19)	C22-C25-C221-C226	61.1(2)
N21-C211-C212-C213	-178.58(15)	C216-C211-C212-C213	0.9(2)
N21-C211-C216-C215	179.93(17)	C212-C211-C216-C215	0.4(3)
C211-C212-C213-C214	-1.5(3)	C212-C213-C214-C215	0.7(3)
C213-C214-C215-C216	0.7(3)	C214-C215-C216-C211	-1.2(3)
C25-C221-C222-C223	-179.5(2)	C226-C221-C222-C223	-2.7(3)
C25-C221-C226-C225	177.90(16)	C222-C221-C226-C225	1.2(3)
C221-C222-C223-C224	2.3(4)	C222-C223-C224-C225	-0.3(4)
C223-C224-C225-C226	-1.2(4)	C224-C225-C226-C221	0.8(3)

Table S8 Contact Distances (Angstrom) for: ca104 R = 0.03

Co1.H24Cc	3.2800	O21.C212	2.847(2)	Co1.H17B	3.3800
O21.O23	2.9092(18)	Co1.H24Cd	3.2800	O21.C25	3.0372(19)
Co1.H17Ba	3.3800	O21.C26	3.401(4)	O11.O12	2.8916(15)
O22.C26	3.208(3)	O11.O13	2.9657(17)	O22.O23b	2.8998(18)
O11.C15	3.0366(17)	O22.O23	3.0429(16)	O11.C24c	3.361(2)
O22.C21	2.8653(19)	O11.C112	2.848(2)	O22.O21	2.8556(17)
O11.O13a	2.9181(17)	O22.O21b	2.9198(15)	O11.C16Aa	3.246(4)
O23.O22	3.0429(16)	O11.O12a	2.8855(14)	O23.O21b	2.9328(18)
O12.O13	2.9605(17)	O23.O21	2.9092(18)	O12.C11	2.8887(17)
O23.C21b	3.376(2)	O12.C16B	3.323(13)	O23.O22b	2.8998(18)
O12.O11	2.8916(15)	O23.N12m	2.7862(17)	O12.O13a	3.0055(18)
O11.H17Ba	2.8900	O12.C16A	3.193(3)	O11.H24Cc	2.4600
O12.O11a	2.8855(14)	O11.H112	2.2400	O13.O11a	2.9181(17)
O12.H24Cd	2.8500	O13.O12	2.9605(17)	O12.H16B	2.5600
O13.N22c	2.8313(19)	O12.H122	2.7300	O13.O11	2.9657(17)
O12.H13Aa	2.8800	O13.C11a	3.4115(19)	O13.H216c	2.7900
O13.O12a	3.0055(18)	O13.H24Cc	2.8100	O21.O23b	2.9328(18)
O21.H212	2.3100	O21.O2b	2.9198(15)	O21.H14Bm	2.8200
O21.O22	2.8556(17)	O22.H26B	2.6600	O22.H23Ab	2.8300
C22.C116o	3.526(3)	O22.H222	2.7500	C23.C226	3.478(2)
O23.H14Bm	2.8000	C24.C226	3.117(3)	O23.H116m	2.6000
C24.O11n	3.361(2)	N12.C226e	3.426(2)	C24.C112n	3.596(2)
N12.C26f	3.445(3)	C24.C221	3.292(2)	N12.O23f	2.7862(17)
C26.N12m	3.445(3)	N22.O13n	2.8313(19)	C11.H112	2.7400
N22.C16Bn	3.356(13)	C11.H216d	2.9900	N11.H226e	2.6900
C11.H226e	2.9800	N12.H116	2.5000	C12.H12A	2.9400
N12.H23Af	1.9000	C112.O11	2.848(2)	N12.H226e	2.9100
C12.H216d	2.8500	N22.H13An	2.0400	C112.C24c	3.596(2)
N22.H216	2.5400	C13.H23Af	2.7800	N22.H16Bn	2.8800
C14.H12A	3.0800	C11.C226e	3.579(3)	C14.H23Af	2.9600
C12.C226e	3.578(2)	C116.C22e	3.526(3)	C12.C216d	3.582(2)
C16A.H216c	3.0000	C13.C216d	3.574(2)	C16B.H225e	2.7900
C13.C226e	3.471(2)	C17B.H224l	2.8400	C13.C126	3.413(3)
C21.H212	2.7700	C14.C212f	3.566(2)	C21.H116o	3.0700
C14.C126	3.214(3)	C121.C14	3.265(2)	C14.C121	3.265(2)
C22.H226	3.0900	C16A.C216c	3.569(3)	C22.H116o	2.8800
C16B.N22c	3.356(13)	C23.H122g	2.7500	C17A.C125g	3.597(4)
C23.H13An	2.9300	C24.H122g	3.0000	C213.H213r	3.0200
C24.H226	2.9300	C213.H125q	2.9900	C24.H13An	3.0800
C214.H125q	2.8600	C25.H26B	3.0200	C214.H26As	2.9300
C125.C17Ag	3.597(4)	C215.H125q	3.0400	C126.C14	3.214(3)

C215.H26As	2.9600	C126.C13	3.413(3)	C216.H13An	3.0900
C27.H27Bp	3.0400	C216.H16An	3.0200	C212.O21	2.847(2)
C221.H24A	2.8300	C212.C14m	3.566(2)	C224.H12Ao	3.0200
C113.H113h	3.0400	C225.H16Ao	2.7800	C216.C16An	3.569(3)
C225.H12Ao	3.0500	C216.C12g	3.582(2)	C225.H17Bo	3.0400
C116.H23Af	3.0100	C226.H24B	2.7900	C216.C13g	3.574(2)
C226.H24A	2.7800	C221.C24	3.292(2)	H16A.C216c	3.0200
C121.H14A	2.9400	H16A.H216c	2.5000	C124.H115i	3.0000
H16A.H225e	2.0200	C125.H213f	2.9000	H16A.C225e	2.7800
C125.H17Cg	3.0500	H16B.O12	2.5600	C226.N12o	3.426(2)
H16B.N22c	2.8800	C126.H14C	2.7100	H17B.C225e	3.0400
C226.C13o	3.471(2)	H17B.H225e	2.3500	C226.C12o	3.578(2)
H17B.Co1	3.3800	C226.C11o	3.579(3)	H17B.O11a	2.8900
C226.C23	3.478(2)	H17B.H112a	2.3500	C226.C24	3.117(3)
H17C.H224l	2.4600	C212.H124q	3.0000	H17C.C125g	3.0500
H17C.H17Cg	2.5900	H24B.C226	2.7900	H17C.H13A	2.5300
H24B.H226	2.3800	H12A.C12	2.9400	H24C.O11n	2.4600
H12A.H14C	2.4700	H24C.O13n	2.8100	H12A.C225e	3.0500
H24C.Co1n	3.2800	H12A.C224e	3.0200	H24C.H13An	2.4300
H12A.C14	3.0800	H24C.Co1g	3.2800	H13A.C24c	3.0800
H24C.O12g	2.8500	H13A.C216c	3.0900	H26A.C215s	2.9600
H13A.H216c	2.3600	H26A.C214s	2.9300	H13A.H24Cc	2.4300
H26B.O22	2.6600	H13A.N22c	2.0400	H26B.C25	3.0200
H13A.H17C	2.5300	H27B.C27p	3.0400	H13A.C23c	2.9300
H112.H17Ba	2.3500	H14A.C121	2.9400	H112.C11	2.7400
H14B.O23f	2.8000	H112.O11	2.2400	H14B.H23Af	2.3500
H113.C113h	3.0400	H14B.O21f	2.8200	H113.H113h	2.3900
H14C .H12A	2.4700	H115.C124j	3.0000	H14C.C126	2.7100
H116.O23f	2.6000	H23A.H116m	2.2200	H116.N12	2.5000
H23A.H14Bm	2.3500	H116.H23Af	2.2200	H23A.N12m	1.9000
H116.C21e	3.0700	H23A.C13m	2.7800	H116.C22e	2.8800
H23A.C14m	2.9600	H122.O12	2.7300	H23A.C116m	3.0100
H122.C23d	2.7500	H24A.C221	2.8300	H122.C24d	3.0000
H24A.C226	2.7800	H124.C212k	3.0000	H125.C213k	2.9900
H216.C12g	2.8500	H125.C214k	2.8600	H222.O22	2.7500
H125.C215k	3.0400	H224.C17Bt	2.8400	H212.O21	2.3100
H224.H17Ct	2.4600	H212.C21	2.7700	H225.H17Bo	2.3500
H213.C125m	2.9000	H225.C16Bo	2.7900	H213.C213r	3.0200
H225.H16Ao	2.0200	H216.O13n	2.7900	H226.C22	3.0900
H216.N22	2.5400	H226.C24	2.9300	H216.C16An	3.0000
H22.H24B	2.3800	H216.H13An	2.3600	H226.N11o	2.6900
H216.H16An	2.5000	H226.N12o	2.9100	H216.C11g	2.9900
H226.C11o	2.9800				

Table S9 Hydrogen Bonds (Angstrom, Deg) for: ca104 R = 0.03

O13--H13A..N22	0.8000	2.0400	2.8313(19)	175.00	1_455
O23--H23A..N12	0.8900	1.9000	2.7862(17)	177.00	1_654
C16A--H16B..O12	0.9900	2.5600	3.193(3)	122.00	
C24-- H24C..O11	0.9800	2.4600	3.361(2)	153.00	1_655
C112--H112..O11	0.9500	2.2400	2.848(2)	121.00	
C116-- H116..O23	0.9500	2.6000	3.458(2)	151.00	1_456
C116--H116..N12	0.9500	2.5000	2.827(2)	100.00	
C212--H212..O21	0.9500	2.3100	2.847(2)	115.00	

Translation of Symmetry Code to Equiv.Pos

a =[2556.00] = [2_556] =-x,-y,1-z
b =[2765.00] = [2_765] =2-x,1-y,-z
c =[1455.00] = [1_455] =-1+x,y,z
d =[2656.00] = [2_656] =1-x,-y,1-z
e =[2666.00] = [2_666] =1-x,1-y,1-z
f =[1456.00] = [1_456] =-1+x,y,1+z
g =[2656.00] = [2_656] =1-x,-y,1-z
h =[2466.00] = [2_466] =-1-x,1-y,1-z
i =[1645.00] = [1_645] =1+x,-1+y,z
j =[1465.00] = [1_465] =-1+x,1+y,z
k =[2756.00] = [2_756] =2-x,-y,1-z
l =[1545.00] = [1_545] =x,-1+y,z
m =[1654.00] = [1_654] =1+x,y,-1+z
n =[1655.00] = [1_655] =1+x,y,z
o =[2666.00] = [2_666] =1-x,1-y,1-z
p =[2665.00] = [2_665] =1-x,1-y,-z
q =[2756.00] = [2_756] =2-x,-y,1-z
r =[2855.00] = [2_855] =3-x,-y,-z
s =[2755.00] = [2_755] =2-x,-y,-z
t =[1565.00] = [1_565] =x,1+y,z

Bmpp-Dh R = 0.04 : Jun 26 10:57:16 2012

Contents

Table S1 - Crystal Data and Details of the Structure Determination
for: ca092 R = 0.04

Table S2 - Final Coordinates and Equivalent Isotropic Displacement Parameters of the non-Hydrogen atoms
for: ca092 R = 0.04

Table S3 - Hydrogen Atom Positions and Isotropic Displacement Parameters
for: ca092 R = 0.04

Table S4 - (An)isotropic Displacement Parameters
for: ca092 R = 0.04

Table S5 - Bond Distances (Angstrom)
for: ca092 R = 0.04

Table S6 - Bond Angles (Degrees)
for: ca092 R = 0.04

Table S7 - Torsion Angles (Degrees)
for: ca092 R = 0.04

Table S8 - Contact Distances(Angstrom)
for: ca092 R = 0.04

Table S9 - Hydrogen Bonds (Angstrom, Deg)
for: ca092 R = 0.04

Table S1 - Crystal Data and Details of the Structure Determination
for: ca092 R = 0.04

Crystal Data

Formula	C23 H18 N6 O5, C2 H6 O
Formula Weight	504.50
Crystal System	Monoclinic
Space group	P21/c (No. 14)
a, b, c [Angstrom]	12.8289(4) 14.3247(4) 14.4213(4)
alpha, beta, gamma [deg]	90 111.347(1) 90
V [Ang**3]	2468.38(13)
Z	4
D(calc) [g/cm**3]	1.358
Mu(MoKa) [/mm]	0.100
F(000)	1056
Crystal Size [mm]	0.39 x 0.43 x 0.61

Data Collection

Temperature (K)	200
Radiation [Angstrom]	MoKa 0.71073
Theta Min-Max [Deg]	2.2, 28.3
Dataset	-16: 17 ; -13: 19 ; -19: 19
Tot., Uniq. Data, R(int)	23873, 6124, 0.014
Observed data [I > 2.0 sigma(I)]	5136

Refinement

Nref, Npar	6124, 368
R, wR2, S	0.0417, 0.1161, 1.04
Max.andAv. Shift/Error	0.00, 0.00
Min. and Max. Resd. Dens. [e/Ang^3]	-0.22, 0.28

W=1/[\s^2^(Fo^2^)+(0.0507P)^2^+0.8242P]
where P=(Fo^2^+2Fc^2^)/3

Table S2 Final Coordinates and Equivalent Isotropic Displacement Parameters of the non-Hydrogen atoms for: ca092 R = 0.04

Atom	x	y	z	U(eq) [Ang^2]
O1	0.14776(8)	0.69594(6)	0.47229(6)	0.0383(3)
O2	-0.07049(9)	0.77842(7)	0.42852(9)	0.0544(4)
O3	-0.22537(11)	0.83873(7)	0.42516(10)	0.0588(4)
O4	-0.53149(10)	0.65498(10)	0.42226(12)	0.0730(5)
O5	-0.53782(10)	0.50904(11)	0.38432(14)	0.0876(6)
N1	0.20431(9)	0.73686(7)	0.34187(7)	0.0317(3)
N2	0.20240(9)	0.69518(7)	0.25557(8)	0.0340(3)
N3	-0.01147(8)	0.51321(7)	0.38324(8)	0.0326(3)
N4	-0.05711(9)	0.59824(7)	0.39281(8)	0.0328(3)
N5	-0.16820(10)	0.77102(7)	0.42199(8)	0.0399(3)
N6	-0.48924(10)	0.58418(10)	0.40330(11)	0.0553(5)
C1	0.15772(9)	0.67707(8)	0.39078(8)	0.0299(3)
C2	0.12604(9)	0.59567(8)	0.33014(8)	0.0294(3)
C3	0.15677(10)	0.61039(8)	0.24838(9)	0.0321(3)
C4	0.14119(14)	0.55220(10)	0.15841(10)	0.0466(4)
C5	0.07256(9)	0.51282(8)	0.35381(8)	0.0292(3)
C11	0.24261(10)	0.82994(8)	0.36714(9)	0.0322(3)
C12	0.17815(12)	0.89102(9)	0.39821(11)	0.0425(4)
C13	0.21730(15)	0.98106(10)	0.42595(12)	0.0514(5)
C14	0.31808(15)	1.00912(10)	0.42101(12)	0.0531(5)
C15	0.38033(14)	0.94861(11)	0.38782(12)	0.0520(5)
C16	0.34373(11)	0.85755(9)	0.36157(10)	0.0410(4)
C21	0.11659(10)	0.41870(8)	0.34431(8)	0.0304(3)
C22	0.05139(11)	0.33871(9)	0.33661(10)	0.0376(3)
C23	0.09362(13)	0.25170(9)	0.32782(11)	0.0453(4)
C24	0.20034(13)	0.24258(10)	0.32641(10)	0.0461(4)
C25	0.26619(12)	0.32073(10)	0.33591(11)	0.0455(4)
C26	0.22459(11)	0.40835(9)	0.34526(10)	0.0379(4)
C31	-0.16063(10)	0.59744(8)	0.39772(8)	0.0302(3)
C32	-0.21772(10)	0.67863(8)	0.41052(9)	0.0322(3)
C33	-0.32476(11)	0.67409(9)	0.41267(9)	0.0364(3)
C34	-0.37698(10)	0.58920(10)	0.40188(10)	0.0393(4)
C35	-0.32465(11)	0.50752(10)	0.38895(11)	0.0422(4)
C36	-0.21948(11)	0.51165(9)	0.38672(10)	0.0378(4)
O6	0.69603(9)	0.26440(9)	0.35941(8)	0.0517(4)
*C6A	0.58374(18)	0.25573(15)	0.35662(17)	0.0497(7)
*C7A	0.5500(3)	0.1568(2)	0.35424(19)	0.0669(10)
*C7B	0.5168(8)	0.2239(8)	0.3541(10)	0.091(4)
*C6B	0.6238(6)	0.1806(5)	0.3640(5)	0.054(3)

U(eq) = 1/3 of the trace of the orthogonalized U Tensor. Starred Atom sites have a S.O.F less than 1.0

Table S3 - Hydrogen Atom Positions and Isotropic Displacement Parameters
for: ca092 R = 0.04

Atom	x	y	z	U(iso) [Ang^2]
H2N	0.2371(14)	0.7212(12)	0.2146(13)	0.054(5)
H4A	0.11620	0.59190	0.09900	0.0700
H4B	0.08480	0.50400	0.15220	0.0700
H4C	0.21230	0.52250	0.16490	0.0700
H4N	-0.0119(14)	0.6495(12)	0.4120(12)	0.050(4)
H12	0.10830	0.87160	0.40050	0.0510
H13	0.17460	1.02340	0.44840	0.0620
H14	0.34470	1.07060	0.44060	0.0640
H15	0.44850	0.96910	0.38280	0.0620
H16	0.38730	0.81510	0.34020	0.0490
H22	-0.02210	0.34420	0.33740	0.0450
H23	0.04890	0.19770	0.32270	0.0540
H24	0.22820	0.18270	0.31890	0.0550
H25	0.34000	0.31470	0.33610	0.0550
H26	0.27060	0.46180	0.35240	0.0450
H33	-0.36140	0.72910	0.42150	0.0440
H35	-0.36220	0.44930	0.38170	0.0510
H36	-0.18460	0.45570	0.37760	0.0450
*H6AB	0.57780	0.28640	0.41600	0.0600
*H7AA	0.47080	0.15330	0.34610	0.1000
*H7AC	0.56110	0.12510	0.29830	0.1000
H6	0.7439(18)	0.2723(14)	0.4213(17)	0.072(6)
*H7AB	0.59560	0.12630	0.41670	0.1000
*H6AA	0.53220	0.28810	0.29690	0.0600
*H6BA	0.61480	0.13640	0.30870	0.0640
*H6BB	0.65670	0.14710	0.42810	0.0640
*H7BA	0.48950	0.26110	0.29290	0.1360
*H7BB	0.52730	0.26440	0.41150	0.1360
*H7BC	0.46210	0.17520	0.35120	0.1360

The Temperature Factor has the Form of Exp(-T)
Where T = 8*(Pi**2)*U*(Sin(Theta)/Lambda)**2 for Isotropic Atoms

Table S4 - (An)isotropic Displacement Parameters for: ca092 R = 0.04

Atom	U(1,1) or U	U(2,2)	U(3,3)	U(2,3)	U(1,3)	U(1,2)
O1	0.0441(5)	0.0430(5)	0.0328(4)	-0.0091(4)	0.0200(4)	-0.0148(4)
O2	0.0559(6)	0.0345(5)	0.0824(8)	-0.0076(5)	0.0368(6)	-0.0116(4)
O3	0.0760(8)	0.0300(5)	0.0843(8)	-0.0046(5)	0.0457(7)	0.0055(5)
O4	0.0488(6)	0.0734(8)	0.1089(11)	0.0078(8)	0.0432(7)	0.0175(6)
O5	0.0437(7)	0.0796(10)	0.1479(15)	-0.0171(9)	0.0448(8)	-0.0183(6)
N1	0.0401(5)	0.0269(5)	0.0327(5)	-0.0038(4)	0.0186(4)	-0.0068(4)
N2	0.0466(6)	0.0290(5)	0.0335(5)	-0.0024(4)	0.0229(4)	-0.0046(4)
N3	0.0329(5)	0.0267(5)	0.0399(5)	-0.0001(4)	0.0154(4)	-0.0011(4)
N4	0.0347(5)	0.0252(5)	0.0423(5)	-0.0012(4)	0.0185(4)	-0.0032(4)
N5	0.0526(7)	0.0289(5)	0.0443(6)	-0.0027(4)	0.0249(5)	-0.0025(5)
N6	0.0333(6)	0.0630(9)	0.0725(9)	0.0030(7)	0.0227(6)	0.0017(6)
C1	0.0308(5)	0.0297(5)	0.0305(5)	-0.0017(4)	0.0129(4)	-0.0050(4)
C2	0.0323(5)	0.0259(5)	0.0314(5)	-0.0012(4)	0.0134(4)	-0.0024(4)
C3	0.0383(6)	0.0267(5)	0.0338(6)	-0.0015(4)	0.0162(5)	-0.0006(4)
C4	0.0689(9)	0.0375(7)	0.0414(7)	-0.0093(5)	0.0297(7)	-0.0057(6)
C5	0.0296(5)	0.0269(5)	0.0302(5)	-0.0006(4)	0.0098(4)	-0.0041(4)
C11	0.0394(6)	0.0254(5)	0.0311(5)	-0.0003(4)	0.0119(5)	-0.0054(4)
C12	0.0466(7)	0.0338(6)	0.0478(7)	-0.0054(5)	0.0182(6)	-0.0022(5)
C13	0.0679(10)	0.0303(7)	0.0527(8)	-0.0058(6)	0.0181(7)	0.0016(6)
C14	0.0717(10)	0.0267(6)	0.0499(8)	0.0011(6)	0.0089(7)	-0.0124(6)
C15	0.0540(8)	0.0406(8)	0.0571(9)	0.0049(6)	0.0151(7)	-0.0187(7)
C16	0.0425(7)	0.0354(6)	0.0466(7)	0.0018(5)	0.0181(6)	-0.0072(5)
C21	0.0328(6)	0.0273(5)	0.0298(5)	-0.0001(4)	0.0098(4)	-0.0020(4)
C22	0.0366(6)	0.0318(6)	0.0414(6)	-0.0041(5)	0.0108(5)	-0.0067(5)
C23	0.0542(8)	0.0294(6)	0.0461(7)	-0.0064(5)	0.0110(6)	-0.0078(6)
C24	0.0596(9)	0.0319(6)	0.0423(7)	-0.0015(5)	0.0132(6)	0.0098(6)
C25	0.0431(7)	0.0435(7)	0.0509(8)	0.0043(6)	0.0184(6)	0.0108(6)
C26	0.0348(6)	0.0330(6)	0.0465(7)	0.0034(5)	0.0155(5)	-0.0002(5)
C31	0.0317(5)	0.0293(5)	0.0306(5)	-0.0004(4)	0.0124(4)	-0.0022(4)
C32	0.0384(6)	0.0280(6)	0.0317(5)	-0.0002(4)	0.0145(5)	-0.0011(5)
C33	0.0375(6)	0.0374(6)	0.0354(6)	0.0016(5)	0.0147(5)	0.0061(5)
C34	0.0284(6)	0.0458(7)	0.0442(7)	0.0007(5)	0.0137(5)	0.0004(5)
C35	0.0341(6)	0.0367(7)	0.0555(8)	-0.0049(6)	0.0159(6)	-0.0072(5)
C36	0.0342(6)	0.0295(6)	0.0511(7)	-0.0050(5)	0.0172(5)	-0.0033(5)
O6	0.0405(5)	0.0805(8)	0.0385(5)	-0.0182(5)	0.0197(4)	-0.0101(5)
C6A	0.0436(12)	0.0495(12)	0.0643(13)	-0.0051(9)	0.0296(9)	-0.0020(9)
C7A	0.072(2)	0.0563(16)	0.0620(14)	0.0037(11)	0.0121(12)	-0.0192(13)
C7B	0.052(5)	0.074(7)	0.150(10)	0.025(6)	0.041(6)	0.005(4)
C6B	0.044(4)	0.060(5)	0.049(4)	0.001(3)	0.008(3)	-0.006(3)

The Temperature Factor has the Form of Exp(-T)
Where T = 8*(Pi**2)*U*(Sin(Theta)/Lambda)**2 for Isotropic Atoms

T = 2*(Pi**2)*Sumij(h(i)*h(j)*U(i,j)*Astar(i)*Astar(j)), for Anisotropic Atoms. Astar(i) are Reciprocal Axial Lengths and h(i) are the Reflection Indices.

Table S5 - Bond Distances (Angstrom) for: ca092 R = 0.04

O1-C1	1.2572(14)	C14-C15	1.377(2)	O2-N5	1.2270(18)
C15-C16	1.391(2)	O3-N5	1.2269(17)	C21-C22	1.3990(18)
O4-N6	1.227(2)	C21-C26	1.389(2)	O5-N6	1.224(2)
C22-C23	1.3831(19)	O6-C6A	1.432(3)	C23-C24	1.383(2)
O6-C6B	1.533(8)	C24-C25	1.379(2)	O6-H6	0.89(2)
C25-C26	1.390(2)	N1-N2	1.3725(15)	C31-C36	1.4206(18)
N1-C11	1.4219(15)	C31-C32	1.4218(17)	N1-C1	1.3767(16)
C32-C33	1.386(2)	N2-C3	1.3358(16)	C33-C34	1.3696(19)
N3-C5	1.2944(16)	C34-C35	1.395(2)	N3-N4	1.3800(15)
C35-C36	1.363(2)	N4-C31	1.3555(18)	C4-H4A	0.9800
N5-C32	1.4512(16)	C4-H4C	0.9800	N6-C34	1.450(2)
C4-H4B	0.9800	N2-H2N	0.937(18)	C12-H12	0.9500
N4-H4N	0.914(18)	C13-H13	0.9500	C1-C2	1.4251(16)
C14-H14	0.9500	C2-C3	1.3887(17)	C15-H15	0.9500
C2-C5	1.4718(17)	C16-H16	0.9500	C3-C4	1.4931(18)
C22-H22	0.9500	C5-C21	1.4873(17)	C23-H23	0.9500
C11-C16	1.386(2)	C24-H24	0.9500	C11-C12	1.386(2)
C25-H25	0.9500	C12-C13	1.389(2)	C26-H26	0.9500
C13-C14	1.380(3)	C33-H33	0.9500	C35-H35	0.9500
C6B-H6BB	0.9900	C36-H36	0.9500	C7A-H7AC	0.9800
C6A-C7A	1.479(4)	C7A-H7AA	0.9800	C6B-C7B	1.465(14)
C7A-H7AB	0.9800	C6A-H6AA	0.9900	C7B-H7BA	0.9800
C6A-H6AB	0.9900	C7B-H7BB	0.9800	C6B-H6BA	0.9900
C7B-H7BC	0.9800				

Table S6 - Bond Angles (Degrees) for: ca092 R = 0.04

C6B-O6-H6	105.3(14)	N3-C5-C2	125.93(11)
C6A-O6-H6	111.1(16)	N3-C5-C21	115.07(11)
N2-N1-C11	122.06(10)	C12-C11-C16	121.32(12)
N2-N1-C1	109.04(9)	N1-C11-C16	119.74(11)
C1-N1-C11	128.76(10)	N1-C11-C12	118.93(12)
N1-N2-C3	109.18(10)	C11-C12-C13	118.93(15)
N4-N3-C5	118.10(10)	C12-C13-C14	120.19(16)
N3-N4-C31	117.21(10)	C13-C14-C15	120.48(14)
O2-N5-C32	118.70(11)	C14-C15-C16	120.25(16)
O3-N5-C32	118.84(13)	C11-C16-C15	118.81(14)
O2-N5-O3	122.46(12)	C22-C21-C26	118.62(12)
O5-N6-C34	117.92(14)	C5-C21-C22	120.91(12)
O4-N6-O5	123.13(15)	C5-C21-C26	120.46(11)
O4-N6-C34	118.95(14)	C21-C22-C23	120.17(14)
N1-N2-H2N	122.9(11)	C22-C23-C24	120.63(14)
C3-N2-H2N	127.5(11)	C23-C24-C25	119.73(14)
N3-N4-H4N	119.6(12)	C24-C25-C26	120.00(15)
C31-N4-H4N	121.1(12)	C21-C26-C25	120.84(13)
N1-C1-C2	105.94(10)	C32-C31-C36	116.37(12)
O1-C1-C2	130.27(11)	N4-C31-C36	119.50(11)
O1-C1-N1	123.79(10)	N4-C31-C32	124.10(11)
C3-C2-C5	128.30(10)	N5-C32-C31	122.41(12)
C1-C2-C3	106.92(10)	C31-C32-C33	121.72(11)
C1-C2-C5	124.77(10)	N5-C32-C33	115.87(11)
N2-C3-C2	108.90(11)	C32-C33-C34	119.12(12)
N2-C3-C4	119.43(12)	C33-C34-C35	121.38(13)
C2-C3-C4	131.56(12)	N6-C34-C33	119.33(13)
C2-C5-C21	119.01(11)	N6-C34-C35	119.29(13)
C34-C35-C36	119.71(13)	C32-C33-H33	120.00
C31-C36-C35	121.70(13)	C34-C33-H33	120.00
C3-C4-H4C	110.00	C36-C35-H35	120.00
C3-C4-H4A	109.00	C34-C35-H35	120.00
C3-C4-H4B	109.00	C31-C36 -H36	119.00
H4B-C4-H4C	109.00	C35-C36-H36	119.00
H4A-C4-H4C	109.00	O6-C6A-C7A	111.5(2)
H4A-C4-H4B	109.00	O6-C6B-C7B	102.9(6)
C13-C12-H12	121.00	O6-C6A-H6AA	109.00
C11-C12-H12	121.00	O6-C6A-H6AB	109.00
C12-C13-H13	120.00	C7A-C6A-H6AA	109.00
C14-C13-H13	120.00	C7A-C6A-H6AB	109.00
C15-C14-H14	120.00	H6AA-C6A-H6AB	108.00
C13-C14-H14	120.00	O6-C6B-H6BB	111.00
C16-C15-H15	120.00	C7B-C6B-H6BA	111.00
C14-C15-H15	120.00	C7B-C6B-H6BB	111.00
C15-C16-H16	121.00	H6BA-C6B-H6BB	109.00
C11-C16-H16	121.00	O6-C6B-H6BA	111.00
C21-C22-H22	120.00	H7AA-C7A-H7AC	109.00
C23-C22-H22	120.00	H7AB-C7A-H7AC	109.00
C22-C23-H23	120.00	C6A-C7A-H7AA	109.00
C24-C23-H23	120.00	C6A-C7A-H7AB	110.00
C23-C24-H24	120.00	C6A-C7A-H7AC	110.00
C25-C24-H24	120.00	H7AA-C7A-H7AB	109.00
C26-C25-H25	120.00	C6B-C7B-H7BA	109.00
C24-C25-H25	120.00	C6B-C7B-H7BB	109.00
C21-C26-H26	120.00	C6B-C7B-H7BC	110.00
C25-C26-H26	120.00	H7BA-C7B-H7BB	109.00
H7BA-C7B-H7BC	109.00	H7BB-C7B-H7BC	110.00

Table S7 - Torsion Angles (Degrees) for: ca092 R = 0.04

C1-N1-N2-C3	-0.45(14)	C11-N-N2-C3	-176.44(12)
N2-N1-C1-O1	-179.98(11)	N2-N1-C1-C2	-0.23(13)
C11-N1-C1-O1	-4.3(2)	C11-N1-C1-C2	175.41(12)
N2-N1-C11-C12	131.90(13)	N2-N1-C11-C16	-48.92(17)
C1-N1-C11-C12	-43.23(19)	C1-N1-C11-C16	135.95(14)
N1-N2-C3-C2	0.97(15)	N1-N2-C3-C4	177.64(12)
C5-N3-N4-C31	163.07(11)	N4-N3-C5-C2	0.72(17)
N4-N3-C5-C21	-179.44(10)	N3-N4-C31-C32	178.08(11)
N3-N4-C31-C36	-3.89(16)	O2-N5-C32-C31	-5.72(18)
O2-N5-C32-C33	174.35(12)	O3-N5-C32-C31	174.54(12)
O3-N5-C32-C33	-5.39(17)	O4-N6-C34-C33	-5.9(2)
O4-N6-C34-C35	174.49(15)	O5-N6-C34-C33	173.35(15)
O5-N6-C34-C35	-6.3(2)	O1-C1-C2-C3	-179.48(13)
O1-C1-C2-C5	-0.3(2)	N1-C1-C2-C3	0.80(13)
N1-C1-C2-C5	179.97(11)	C1-C2-C3-N2	-1.10(14)
C1-C2-C3-C4	-177.22(14)	C5-C2-C3-N2	179.77(12)
C5-C2-C3-C4	3.7(2)	C1-C2-C5-N3	46.97(18)
C1-C2-C5-C21	-132.86(12)	C3-C2-C5-N3	-134.05(14)
C3-C2-C5-C21	46.12(17)	N3-C5-C21-C22	19.35(16)
N3-C5-C21-C26	-159.14(11)	C2-C5-C21-C22	-160.80(11)
C2-C5-C21-C26	20.71(16)	N1-C11-C12-C13	177.95(12)
C16-C11-C12-C13	-1.2(2)	N1-C11-C16-C15	-179.21(12)
C12-C11-C16-C15	-0.1(2)	C11-C12-C13-C14	1.0(2)
C12-C13-C14-C15	0.6(2)	C13-C14-C15-C16	-1.8(2)
C14-C15-C16-C11	1.6(2)	C5-C21-C22-C23	180.00(12)
C26-C21-C22-C23	-1.49(19)	C5-C21-C26-C25	-179.67(12)
C22-C21-C26-C25	1.82(19)	C21-C22-C23-C24	-0.1(2)
C22-C23-C24-C25	1.3(2)	C23-C24-C25-C26	-1.0(2)
C24-C25-C26-C21	-0.6(2)	N4-C31-C32-N5	-1.49(18)
N4-C31-C32-C33	178.43(11)	C36-C31-C32-N5	-179.59(11)
C36-C31-C32-C33	0.34(17)	N4-C31-C36-C35	-178.57(12)
C32-C31-C36-C35	-0.39(18)	N5-C32-C33-C34	179.73(11)
C31-C32-C33-C34	-0.20(18)	C32-C33-C34-N6	-179.52(12)
C32-C33-C34-C35	0.1(2)	N6-C34-C35-C36	179.48(13)
C33-C34-C35-C36	-0.1(2)	C34-C35-C36-C31	0.3(2)

Table S8 - Contact Distances(Angstrom) for: ca092 R = 0.04

O1.O2	2.8892(16)	O6.H16p	2.7800	O1.N4	2.8261(15)
O6.H2Np	1.710(18)	O1.C12	3.0669(16)	N2.C6Bf	3.284(8)
O1.O6a	2.5862(14)	N2.O6f	2.6464(17)	O2.O1	2.8892(16)
N3.N3g	3.2939(15)	O2.N4	2.6497(14)	N4.O2	2.6497(14)
O3.C13b	3.3352(19)	N4.N5	2.9615(15)	O4.C16c	3.276(2)
N4.C1	2.9884(17)	O5.N6e	3.242(2)	N4.O1	2.8261(15)
O5.C26c	3.231(2)	N5.N4	2.9615(15)	O5.O5e	3.128(3)
N5.C23g	3.3950(18)	O6.N2p	2.6464(17)	N6.O5e	3.242(2)
O6.C16p	3.3186(17)	N2.H6BAf	2.9400	O6.O1q	2.5862(14)
N2.H16	2.8200	O1.H12	2.7000	N3.H36	2.3400
O1.H4N	2.024(18)	N3.H22	2.5000	O1.H6a	1.72(2)
N5.H4N	2.699(18)	O2.H4N	2.040(18)	N6.H7Ach	2.7700
O2.H12	2.8100	C1.N4	2.9884(17)	O3.H13b	2.6000
C3.C26	3.1938(17)	O3.H33	2.3300	C4.C26	3.2485(19)
O4.H7BBd	2.6400	C4.C21	3.4000(19)	O4.H16c	2.6200
C5.C36g	3.5415(17)	O4.H33	2.4300	C6B.C12q	3.595(7)
O4.H6ABd	2.7400	C6B.N2p	3.284(8)	O5.H35	2.4200
C7B.C25	3.423(12)	O5.H26c	2.4300	C12.O1	3.0669(16)
O6.H35k	2.8000	C12.C6Ba	3.595(7)	C13.O3b	3.3352(19)
C3.H26	2.7100	C16.O6f	3.3186(17)	C3.H23i	2.7600
C16.O4k	3.276(2)	C4.H26	2.9800	C21.C31g	3.5613(15)
C5.H4B	2.9700C21	C4	3.4000(19)	C6A.H2Np	2.881(19)
C21.C32g	3.5761(16)	C6A.H35k	2.8500	C22.C32g	3.4998(18)
C6B.H2Np	2.51(2)	C23.N5g	3.3950(18)	C7A.H15n	3.0800
C25.C33g	3.4254(19)	C7B.H25	2.5400	C25.C7B	3.423(12)
C11.H6BBa	2.7800	C26.C4	3.2485(19)	C12.H6BBa	2.6800
C26.C33g	3.4593(18)	C13.H7	3.0500	C26.C3	3.1938(17)
C13.H6	2.8200	C26.O5	3.231(2)	C14.H24	2.9100
C26.C34	3.4541(19)	C14.H6	3.0600	C31.C21	3.5613(15)
C14.H7	2.9300	C32.C22	3.4998(18)	C15.H7	2.9300
C32.C21	3.5761(16)	C16.H2	2.840(17)	C33.C25	3.4254(19)
C16.H6	3.0400	C33.C26	3.4593(18)	C16.H7	3.0100
C34.C26	3.4541(19)	C21.H4B	2.9200	C36.C5	3.5416(17)
C26.H4	3.0300	C1.H4	2.339(19)	C26.H4	3.0300
C1.H12	2.8700	C34.H7	3.0400	C1.H6	2.64(2)
H6.H16	2.5700	C2.H23	2.9000	H6.O4	2.7400
C2.H26	2.6100	H6.H35	2.5600	C2.H4	2.577(18)
H2N.C16	2.840(17)	H2N.H4	2.5900	H6.C11	2.7800
H2N.H16	2.5000	H6.C12	2.6800	H2N.H6	2.19(3)
H6.C13	2.8200	H2N.C6	2.51(2)	H6.C16	3.0400
H2N.O6	1.710(18)	H6.C14	3.0600	H2N.C6	2.881(19)
H7.H25	2.3500	H2N.H6	2.3800	H7.O4	2.6400
H7.C15	2.9300	H7.H25	2.3600	H7AB.C13	3.0500
H7BC.H25	2.5000	H7AB.C16	3.0100	H12.C1	2.8700
H7AB.C14	2.9300	H12.O1	2.7000	H4A.H2N	2.5900
H12.O2	2.8100	H4B.C26	3.0300	H13.O3b	2.6000
H4B.C21	2.9200	H14.H24	2.4500	H4B.C5	2.9700
H15.C7	3.0800	H4C.C26	3.0300	H16.H2N	2.5000
H4N.N5	2.699(18)	H16.N2	2.8200	H4N.O2	2.040(18)
H16.O4	2.6200	H4N.O1	2.024(18)	H16.O6f	2.7800
H4N.C1	2.339(19)	H16.H6AAf	2.5700	H4N.C2	2.577(18)
H22.N3	2.5000	H7AC.N6m	2.7700	H23.C2m	2.9000
H7AC.C34	3.0400	H23.C3	2.7600	H6.O1	1.72(2)
H24.H14	2.4500	H6.C1	2.64(2)	H24.C14	2.9100
H6.H2N	2.19(3)	H25.H7BA	2.3500	H6BA.N2	2.9400
H25.H7BB	2.3600	H6BA.H2N	2.3800	H25.C7B	2.5400
H25.H7BC	2.5000	H33.O4	2.4300	H26.C3	2.7100
H35.O5	2.4200	H26.C4	2.9800	H35.H6ABo	2.5600
H26.O5k	2.4300	H35.O6o	2.8000	H26.C2	2.6100
H35.C6Ao	2.8500	H33.O3	2.3300	H36.N3	2.3400

Table S9 - Hydrogen Bonds (Angstrom, Deg) for: ca092 R = 0.04

N2--H2N..O6	0.937(18)	1.710(18)	2.6464(17)	177.5(16)	2_655
N4--H4N..O1	0.914(18)	2.024(18)	2.8261(15)	145.6(15)	
N4--H4N..O2	0.914(18)	2.040(18)	2.6497(14)	122.9(15)	
O6--H6..O1	0.89(2)	1.72(2)	2.5862(14)	67(2)	3_666
C26--H26..O5	0.9500	2.4300	3.231(2)	142.00	1_655
C36--H36..N3	0.9500	2.3400	2.6873(19)	101.00	

Translation of Symmetry Code to Equiv.Pos

a = [3666.00] = [3_666] =1-x,1-y,1-z
b = [3576.00] = [3_576] =-x,2-y,1-z
c = [1455.00] = [1_455] =-1+x,y,z
d = [3566.00] = [3_566] =-x,1-y,1-z
e = [3466.00] = [3_466] =-1-x,1-y,1-z
f = [2655.00] = [2_655] =1-x,1/2+y,1/2-z
g = [3566.00] = [3_566] =-x,1-y,1-z
h = [2555.00] = [2_555] =-x,1/2+y,1/2-z
i = [2555.00] = [2_555] =-x,1/2+y,1/2-z
j = [1565.00] = [1_565] =x,1+y,z
k = [1655.00] = [1_655] =1+x,y,z
l = [1565.00] = [1_565] =x,1+y,z
m = [2545.00] = [2_545] =-x,-1/2+y,1/2-z
n = [1545.00] = [1_545] =x,-1+y,z
o = [1455.00] = [1_455] =-1+x,y,z
p = [2645.00] = [2_645] =1-x,-1/2+y,1/2-z
q = [3666.00] = [3_666] =1-x,1-y,1-z

Bmpp-Sn R = 0.07 : May 31 13:38:01 2012

Contents

Table S1 - Crystal Data and Details of the Structure Determination
for: ca113 R = 0.07

Table S2 - Final Coordinates and Equivalent Isotropic Displacement Parameters of the non-Hydrogen atoms
for: ca113 R = 0.07

Table S3 - Hydrogen Atom Positions and Isotropic Displacement Parameters
for: ca113 R = 0.07

Table S4 - (An)isotropic Displacement Parameters
for: ca113 R = 0.07

Table S5 - Bond Distances (Angstrom)
for: ca113 R = 0.07

Table S6 - Bond Angles (Degrees)
for: ca113 R = 0.07

Table S7 - Torsion Angles (Degrees)
for: ca113 R = 0.07

Table S8 - Contact Distances(Angstrom)
for: ca113 R = 0.07

Table S9 - Hydrogen Bonds (Angstrom, Deg)
for: ca113 R = 0.07

Table S1 - Crystal Data and Details of the Structure Determination
for: ca113 R = 0.07

Crystal Data

Formula	C23 H20 N4 O3 S, H2 O
Formula Weight	450.52
Crystal System	Monoclinic
Space group	C2/c (No. 15)
a, b, c [Angstrom]	23.3366(4) 14.7706(3) 12.5787(2)
alpha, beta, gamma [deg]	90 100.927(1) 90
V [Ang**3]	4257.21(13)
Z	8
D(calc) [g/cm**3]	1.406
Mu(MoKa) [/mm]	0.191
F(000)	1888
Crystal Size [mm]	0.24 x 0.38 x 0.56

Data Collection

Temperature (K)	296
Radiation [Angstrom]	MoKa 0.71073
Theta Min-Max [Deg]	2.2, 28.3
Dataset	-31: 31 ; -19: 17 ; -16: 16
Tot., Uniq. Data, R(int)	19945, 5285, 0.014
Observed data [I > 2.0 sigma(I)]	4408

Refinement

Nref, Npar	5285, 295
R, wR2, S	0.0651, 0.1806, 1.05

w = 1/[\s^2^(Fo^2^)+(0.0787P)^2^+11.9450P]
where P=(Fo^2^+2Fc^2^)/

Max. and Av. Shift/Error	0.51, 0.00
Min. and Max. Resd. Dens. [e/Ang^3]	-1.28, 1.83

Table S2 - Final Coordinates and Equivalent Isotropic Displacement Parameters of the non-Hydrogen atoms for: ca113 R = 0.07

Atom	x	y	z	U(eq) [Ang^2]
S1	0.12191(3)	-0.36730(5)	0.78538(6)	0.0456(2)
O1	0.08003(12)	-0.40409(16)	0.7001(2)	0.0615(8)
O2	0.18096(12)	-0.35637(18)	0.7677(3)	0.0725(10)
O3	-0.06168(7)	0.08927(11)	0.84448(13)	0.0264(4)
N1	0.12469(14)	-0.42757(19)	0.8891(3)	0.0603(10)
N2	0.03935(8)	-0.00073(13)	0.87790(15)	0.0250(5)
N3	0.00391(8)	0.30070(14)	0.90748(17)	0.0306(6)
N4	-0.04430(8)	0.24360(13)	0.87464(16)	0.0265(5)
C1	0.06811(9)	0.07755(15)	0.90030(17)	0.0241(6)
C2	0.03535(9)	0.15636(15)	0.89605(18)	0.0247(6)
C3	-0.02805(9)	0.15514(15)	0.86799(17)	0.0242(6)
C4	0.05035(10)	0.24937(16)	0.92100(19)	0.0280(6)
C5	0.10857(11)	0.29281(19)	0.9599(3)	0.0394(8)
C11	0.06118(9)	-0.08680(15)	0.85686(17)	0.0247(6)
C12	0.10950(11)	-0.09765(18)	0.8079(2)	0.0335(7)
C13	0.12767(11)	-0.18375(19)	0.7868(2)	0.0380(8)
C14	0.09767(11)	-0.25835(18)	0.8140(2)	0.0343(7)
C15	0.04800(11)	-0.24799(16)	0.85929(19)	0.0308(7)
C16	0.02984(10)	-0.16200(16)	0.87996(17)	0.0262(6)
C21	0.13256(9)	0.07562(15)	0.93661(19)	0.0261(6)
C22	0.15517(11)	0.03029(17)	1.0325(2)	0.0322(7)
C23	0.21501(12)	0.0275(2)	1.0689(3)	0.0449(8)
C24	0.25204(12)	0.0691(2)	1.0102(3)	0.0512(9)
C25	0.22970(12)	0.1135(2)	0.9151(3)	0.0469(9)
C26	0.16983(11)	0.11732(19)	0.8779(2)	0.0357(7)
C31	-0.10148(9)	0.27998(15)	0.86559(19)	0.0271(6)
C32	-0.14525(10)	0.22863(16)	0.8967(2)	0.0305(7)
C33	-0.20042(11)	0.26617(19)	0.8897(2)	0.0385(8)
C34	-0.21129(12)	0.3546(2)	0.8555(3)	0.0463(9)
C35	-0.16744(13)	0.4048(2)	0.8251(3)	0.0488(9)
C36	-0.11254(11)	0.36773(18)	0.8283(2)	0.0393(8)
O4	0.01818(16)	0.5070(2)	0.4000(5)	0.143(2)

U(eq) = 1/3 of the trace of the orthogonalized U Tensor

Table S3 - Hydrogen Atom Positions and Isotropic Displacement Parameters
for: ca113 R = 0.07

Atom	x	y	z	U(iso) [Ang^2]
H1A	0.14900	-0.41100	0.95260	0.112(19)
H1B	0.08400	-0.44910	0.89380	0.054(10)
H2	0.00140	0.00560	0.86500	0.040(8)
H5A	0.10300	0.35310	0.98450	0.0590
H5B	0.12980	0.29520	0.90170	0.0590
H5C	0.13020	0.25800	1.01850	0.0590
H12	0.12940	-0.04720	0.78950	0.0400
H13	0.16000	-0.19150	0.75440	0.0460
H15	0.02740	-0.29840	0.87540	0.0370
H16	-0.00350	-0.15430	0.90950	0.0320
H22	0.13030	0.00210	1.07180	0.0390
H23	0.23030	-0.00240	1.13310	0.0540
H24	0.29220	0.06710	1.03510	0.0610
H25	0.25480	0.14090	0.87560	0.0560
H26	0.15480	0.14770	0.81400	0.0430
H32	-0.13780	0.16980	0.92190	0.0370
H33	-0.23030	0.23150	0.90820	0.0460
H34	-0.24800	0.37990	0.85300	0.0550
H35	-0.17470	0.46430	0.80220	0.0590
H36	-0.08340	0.40150	0.80570	0.0470
H4A	-0.01550	0.48530	0.34760	1.2(5)
H4B	0.01030	0.57480	0.40290	2.0(13)

The Temperature Factor has the Form of Exp(-T)
WhereT = 8*(Pi**2)*U*(Sin(Theta)/Lambda)**2 for Isotropic Atoms

Table S4 - (An)isotropic Displacement Parameters for: ca113 R = 0.07

Atom	U(1,1) or U	U(2,2)	U(3,3)	U(2,3)	U(1,3)	U(1,2)
S1	0.0448(4)	0.0353(4)	0.0523(4)	0.0170(3)	0.0020(3)	0.0117(3)
O1	0.0756(17)	0.0411(12)	0.0590(14)	-0.0209(11)	-0.0094(12)	0.0037(11)
O2	0.0528(14)	0.0576(15)	0.110(2)	0.0284(15)	0.0232(14)	0.0109(12)
O3	0.0237(7)	0.0236(8)	0.0319(8)	-0.0024(6)	0.0051(6)	-0.0022(6)
N1	0.0677(19)	0.0397(14)	0.0651(18)	-0.0031(13)	-0.0089(15)	0.0151(13)
N2	0.0209(8)	0.0243(9)	0.0298(9)	-0.0005(7)	0.0050(7)	0.0014(7)
N3	0.0258(9)	0.0238(9)	0.0412(11)	-0.0006(8)	0.0038(8)	-0.0047(7)
N4	0.0222(9)	0.0213(9)	0.0353(10)	-0.0003(7)	0.0034(7)	-0.0012(7)
C1	0.0233(10)	0.0281(11)	0.0212(9)	0.0011(8)	0.0053(7)	-0.0007(8)
C2	0.0222(10)	0.0260(10)	0.0260(10)	-0.0004(8)	0.0045(8)	-0.0003(8)
C3	0.0244(10)	0.0252(10)	0.0230(9)	0.0002(8)	0.0042(8)	0.0000(8)
C4	0.0247(10)	0.0270(11)	0.0324(11)	-0.0008(9)	0.0054(8)	-0.0025(8)
C5	0.0275(12)	0.0326(13)	0.0568(16)	-0.0076(12)	0.0047(11)	-0.0063(10)
C11	0.0239(10)	0.0258(10)	0.0232(10)	-0.0019(8)	0.0012(8)	0.0026(8)
C12	0.0286(11)	0.0350(13)	0.0382(13)	-0.0060(10)	0.0098(10)	-0.0013(9)
C13	0.0294(12)	0.0407(14)	0.0446(14)	-0.0138(11)	0.0090(10)	0.0025(10)
C14	0.0317(12)	0.0330(12)	0.0343(12)	-0.0101(10)	-0.0034(9)	0.0094(10)
C15	0.0360(12)	0.0263(11)	0.0274(11)	-0.0013(9)	-0.0009(9)	-0.0001(9)
C16	0.0263(10)	0.0288(11)	0.0229(10)	-0.0009(8)	0.0028(8)	0.0015(8)
C21	0.0221(10)	0.0254(10)	0.0303(11)	-0.0011(8)	0.0038(8)	0.0004(8)
C22	0.0306(11)	0.0285(11)	0.0354(12)	0.0025(9)	0.0013(9)	-0.0018(9)
C23	0.0358(13)	0.0393(14)	0.0524(16)	0.0072(12)	-0.0101(12)	0.0012(11)
C24	0.0228(11)	0.0455(16)	0.080(2)	0.0023(15)	-0.0037(12)	0.0000(11)
C25	0.0267(12)	0.0463(16)	0.070(2)	0.0042(14)	0.0150(12)	-0.0043(11)
C26	0.0281(11)	0.0396(14)	0.0408(13)	0.0060(11)	0.0101(10)	0.0001(10)
C31	0.0236(10)	0.0259(11)	0.0301(11)	-0.0014(8)	0.0009(8)	0.0023(8)
C32	0.0272(11)	0.0261(11)	0.0377(12)	-0.0017(9)	0.0053(9)	0.0000(9)
C33	0.0253(11)	0.0382(14)	0.0524(16)	-0.0045(12)	0.0082(10)	-0.0015(10)
C34	0.0246(12)	0.0410(15)	0.070(2)	-0.0016(14)	0.0005(12)	0.0073(10)
C35	0.0357(14)	0.0321(14)	0.074(2)	0.0126(14)	-0.0009(13)	0.0087(11)
C36	0.0303(12)	0.0306(13)	0.0553(16)	0.0100(11)	0.0039(11)	0.0015(10)
O4	0.070(2)	0.061(2)	0.273(6)	-0.045(3)	-0.028(3)	0.0034(17)

The Temperature Factor has the Form of Exp(-T)
Where T = 8*(Pi**2)*U*(Sin(Theta)/Lambda)**2 for Isotropic Atoms
T = 2*(Pi**2)*Sumij(h(i)*h(j)*U(i,j)*Astar(i)*Astar(j)), for Anisotropic Atoms. Astar(i) are Reciprocal Axial Lengths and h(i) are the Reflection Indices.

Table S5 - Bond Distances (Angstrom) for: ca113 R = 0.07

S1-O1	1.416(3)	C21-C26	1.387(3)	S1-O2	1.446(3)
C22-C23	1.385(4)	S1-N1	1.571(4)	C23-C24	1.383(4)
S1-C14	1.765(3)	C24-C25	1.377(5)	O3-C3	1.250(3)
C25-C26	1.388(4)	O4-H4A	0.9800	C31-C36	1.386(3)
O4-H4B	1.0200	C31-C32	1.387(3)	N2-C1	1.340(3)
C32-C33	1.389(4)	N2-C11	1.413(3)	C33-C34	1.384(4)
N3-N4	1.404(3)	C34-C35	1.375(4)	N3-C4	1.307(3)
C35-C36	1.387(4)	N4-C3	1.368(3)	C5-H5B	0.9600
N4-C31	1.423(3)	C5-H5A	0.9600	N1-H1A	0.9200
C5-H5C	0.9600	N1-H1B	1.0100	C12-H12	0.9300
N2-H2	0.8700	C13-H13	0.9300	C1-C2	1.388(3)
C15-H15	0.9300	C1-C21	1.487(3)	C16-H16	0.9300
C2-C4	1.438(3)	C22-H22	0.9300	C2-C3	1.455(3)
C23-H23	0.9300	C4-C5	1.498(4)	C24-H24	0.9300
C11-C16	1.391(3)	C25-H25	0.9300	C11-C12	1.393(3)
C26-H26	0.9300	C12-C13	1.382(4)	C32-H32	0.9300
C13-C14	1.383(4)	C33-H33	0.9300	C14-C15	1.394(4)
C34-H34	0.9300	C15-C16	1.379(3)	C35-H35	0.9300
C21-C22	1.393(3)	C36-H36	0.9300		

Table S6 - Bond Angles (Degrees) for: ca113 R = 0.07

O1-S1-O2	117.88(19)	N3-C4-C5	118.2(2)	O1-S1-N1	109.01(16)
C12-C11-C16	120.2(2)	O1-S1-C14	107.61(14)	N2-C11-C16	117.19(19)
O2-S1-N1	107.49(19)	N2-C11-C12	122.5(2)	O2-S1-C14	106.33(14)
C11-C12-C13	119.6(2)	N1-S1-C14	108.16(15)	C12-C13-C14	119.8(2)
H4A-O4-H4B	103.00	S1-C14-C15	120.5(2)	C1-N2-C11	129.18(19)
S1-C14-C13	118.6(2)	N4-N3-C4	106.75(19)	C13-C14-C15	120.9(2)
N3-N4-C3	112.08(18)	C14-C15-C16	119.2(2)	N3-N4-C31	118.92(18)
C11-C16-C15	120.2(2)	C3-N4-C31	128.51(19)	C1-C21-C	22118.1(2)
S1-N1-H1B	110.00	C22-C21-C26	120.1(2)	H1A-N1-H1B	118.00
C1-C21-C26	121.9(2)	S1-N1-H1A	119.00	C21-C22-C23	119.6(2)
C1-N2-H2	113.00	C22-C23-C24	120.2(3)	C11-N2-H2	117.00
C23-C24-C25	120.2(3)	N2-C1-C21	119.03(19)	C24-C25-C26	120.2(3)
C2-C1-C21	123.1(2)	C21-C26-C25	119.7(2)	N2-C1-C2	117.7(2)
N4-C31-C32	120.0(2)	C1-C2-C3	121.8(2)	C32-C31-C36	120.5(2)
C3-C2-C4	105.02(19)	N4-C31-C36	119.5(2)	C1-C2-C4	133.1(2)
C31-C32-C33	119.2(2)	O3-C3-N4	126.1(2)	C32-C33-C34	120.6(2)
O3-C3-C2	129.1(2)	C33-C34-C35	119.6(3)	N4-C3-C2	104.74(18)
C34-C35-C36	120.7(3)	C2-C4-C5	130.4(2)	C31-C36-C35	119.4(2)
N3-C4-C2	111.4(2)	C4-C5-H5B	110.00	C4-C5-H5C	109.00
C23-C24-H24	120.00	C4-C5-H5A	109.00	C25-C24-H24	120.00
H5A-C5-H5C	109.00	C26-C25-H25	120.00	H5B-C5-H5C	109.00
C24-C25-H25	120.00	H5A-C5-H5B	109.00	C21-C26-H26	120.00
C13-C12-H12	120.00	C25-C26-H26	120.00	C11-C12-H12	120.00
C33-C32-H32	120.00	C12-C13-H13	120.00	C31-C32-H32	120.00
C14-C13-H13	120.00	C32-C33-H33	120.00	C14-C15-H15	120.00
C34-C33-H33	120.00	C16-C15-H15	120.00	C35-C34-H34	120.00
C15-C16-H16	120.00	C33-C34-H34	120.00	C11-C16-H16	120.00
C34-C35-H35	120.00	C21-C22-H22	120.00	C36-C35-H35	120.00
C23-C22-H22	120.00	C31-C36-H36	120.00	C24-C23-H23	120.00
C35-C36-H36	120.00	C22-C23-H23	120.00		

Table S7 - Torsion Angles (Degrees) for: ca113 R = 0.07

O1-S1-C14-C13	109.8(2)	O1-S1-C14-C15	67.9(2)
O2-S1-C14-C13	17.4(3)	O2-S1-C14-C15	-165.0(2)
N1-S1-C14-C13	132.6(2)	N1-S1-C14-C15	-49.8(3)
C11-N2-C1-C2	167.1(2)	C11-N2-C1-C21	-17.7(3)
C1-N2-C11-C12	-30.7(3)	C1-N2-C11-C16	153.9(2)
C4-N3-N4-C3	0.4(3)	C4-N3-N4-C31	173.0(2)
N4-N3-C4-C2	1.0(3)	N4-N3-C4-C5	-178.1(2)
N3-N4-C3-O3	177.4(2)	N3-N4-C3-C2	-1.5(2)
C31-N4-C3-O3	5.6(4)	C31-N4-C3-C2	-173.3(2)
N3-N4-C31-C32	-141.8(2)	N3-N4-C31-C36	36.5(3)
C3-N4-C31-C32	29.5(4)	C3-N4-C31-C36	-152.2(2)
N2-C1-C2-C3	-0.2(3)	N2-C1-C2-C4	175.5(2)
C21-C1-C2-C3	-175.3(2)	C21-C1-C2-C4	0.4(4)
N2-C1-C21-C22	-61.5(3)	N2-C1-C21-C26	118.5(3)
C2-C1-C21-C22	113.5(3)	C2-C1-C21-C26	-66.5(3)
C1-C2-C3-O3	-0.2(4)	C1-C2-C3-N4	178.7(2)
C4-C2-C3-O3	-176.9(2)	C4-C2-C3-N4	2.0(2)
C1-C2-C4-N3	-178.1(2)	C1-C2-C4-C5	0.8(5)
C3-C2-C4-N3	-1.9(3)	C3-C2-C4-C5	177.0(3)
N2-C11-C12-C13	-178.2(2)	C16-C11-C12-C13	-2.9(3)
N2-C11-C16-C15	178.7(2)	C12-C11-C16-C15	3.1(3)
C11-C12-C13-C14	0.3(4)	C12-C13-C14-S1	179.8(2)
C12-C13-C14-C15	2.2(4)	S1-C14-C15-C16	-179.49(18)
C13-C14-C15-C16	-2.0(4)	C14-C15-C16-C11	-0.7(3)
C1-C21-C22-C23	-179.7(2)	C26-C21-C22-C23	0.3(4)
C1-C21-C26-C25	-179.9(2)	C22-C21-C26-C25	0.1(4)
C21-C22-C23-C24	-0.3(4)	C22-C23-C24-C25	-0.1(5)
C23-C24-C25-C26	0.4(5)	C24-C25-C26-C21	-0.5(4)
N4-C31-C32-C33	178.5(2)	C36-C31-C32-C33	0.2(4)
N4-C31-C36-C35	-176.5(3)	C32-C31-C36-C35	1.8(4)
C31-C32-C33-C34	-2.1(4)	C32-C33-C34-C35	2.0(5)
C33-C34-C35-C36	0.0(5)	C34-C35-C36-C31	-1.9(5)

Table S8 - Contact Distances(Angstrom) for: ca113 R = 0.07

S1.H35	3.0700	O4.H5A	2.9200	O1.O4	2.838(5)
N1.O4	2.775(5)	O2.C25	3.413(5)	N2.O3	2.670(3)
O2.C33	3.418(4)	N2.O3	3.227(2)	O3.C32	2.993(3)
N3.O4	2.864(4)	O3.C22	3.399(3)	N4.C15	3.365(3)
O3.N2	2.670(3)	N4.C16	3.271(3)	O3.N2	3.227(2)
N1.H15	2.9500	O3.C2	3.349(3)	N1.H24	2.8700
O3.C1	3.059(3)	N2.H22	2.9100	O3.C26	3.419(3)
N3.H36	2.6500	O4.N3	2.864(4)	N3.H4B	1.8500
O4.O4	2.811(8)	C1.O3	3.059(3)	O4.O1	2.838(5)
C1.C3	3.519(3)	O4.N1	2.775(5)	C2.C3	3.293(3)
O1.H4A	1.9300	C2.O3	3.349(3)	O1.H36	2.8700
C2.C16	3.447(3)	O2.H13	2.4800	C3.C3	3.464(3)
O2.H33	2.7800	C3.C16	3.180(3)	O2.H35	2.7900
C3.C2	3.293(3)	O2.H25	2.5500	C3.C1	3.519(3)
O3.H12	2.9000	C4.C26	3.528(4)	O3.H22	2.4800
C5.C26	3.223(4)	O3.H26	2.7900	C5.C21	3.279(4)
O3.H2	1.9000	C11.C11	3.531(3)	O3.H32	2.4800
C11.C22	3.293(3)	O4.H36	2.7900	C11.C16	3.496(3)
O4.H1B	1.7700	C12.C21	3.022(3)	C12.C22	3.398(4)
C2.H16	2.6900	C12.C26	3.517(4)	C3.H2	2.3200
C15.C31	3.481(3)	C3.H32	2.7800	C15.C15	3.201(3)
C3.H16	2.7600	C15.N4	3.365(3)	C4.H16	2.9300
C15.C16	3.449(3)	C4.H4B	2.7500	C15.C32	3.466(3)
C5.H24	3.1000	C16.N4	3.271(3)	C5.H4B	3.0000
C16.C15	3.449(3)	C13.H34	3.0100	C16.C2	3.447(3)
C15.H1B	3.1000	C16.C3	3.180(3)	C21.H12	2.5800
C16.C11	3.496(3)	C21.H5C	2.8900	C16.C16	3.302(3)
C22.H32	3.0500	C21.C12	3.022(3)	C26.H5C	2.9900
C21.C5	3.279(4)	C26.H5B	2.8200	C22.C11	3.293(3)
C26.H12	2.7600	C22.C12	3.398(4)	C31.H26	3.0700
C22.O3	3.399(3)	C32.H26	2.8800	C25.O2	3.413(5)
C33.H1A	3.0100	C26.C4	3.528(4)	C34.H1A	2.7000
C26.C12	3.517(4)	C35.H1A	2.7500	C26.O3	3.419(3)
C36.H5B	3.0400	C26.C5	3.223(4)	C36.H4B	2.9700
C31.C15	3.481(3)	H1A.C33	3.010	C32.O3	2.993(3)
H1A.C34	2.7000	C32.C15	3.466(3)	H1A.C35	2.7500
C33.O2	3.418(4)	H1B.C15	3.1000	C1.H12	2.8500
H1B.H15	2.5800	H1B.O4	1.7700	H13.H34	2.5000
H1B.H4A	2.3500	H15.H1B	2.5800	H1B.H4B	2.5500
H15.N1	2.9500	H2.H16	2.4300	H16.H2	2.4300
H2.O3	1.9000	H16.C2	2.6900	H2.C3	2.3200
H16.C4	2.9300	H4A.O1	1.9300	H16.C3	2.7600
H4A.H1B	2.3500	H22.N2	2.9100	H4A.H36	2.3000
H22.H32	2.5500	H4B.C4	2.7500	H22.O3	2.4800
H4B.H1B	2.5500	H24.N1	2.8700	H4B.C5	3.0000
H24.C5	3.1000	H4B.C36	2.9700	H25.O2	2.5500
H4B.N3	1.8500	H26.H5B	2.5600	H4B.H36	2.3200
H26.O3	2.7900	H4B.H5A	2.4500	H26.C32	2.8800
H5A.H4B	2.4500	H26.C31	3.0700	H5A.O4	2.9200
H32.C22	3.0500	H5B.C36	3.0400	H32.H22	2.5500
H5B.C26	2.8200	H32.C3	2.7800	H5B.H26	2.5600
H32.O3	2.4800	H5C.C26	2.9900	H33.O2	2.7800
H5C.C21	2.8900	H34.H13	2.5000	H12.C21	2.5800
H34.C13	3.0100	H12.C1	2.8500	H35.O2	2.7900
H12.C26	2.7600	H35.S1	3.0700	H12.O3	2.9000
H36.O1	2.8700	H13.O2	2.4800	H36.N3	2.6500
H36.H4B	2.3200	H36.H4A	2.3000	H36.O4	2.7900

Table S9 - Hydrogen Bonds (Angstrom, Deg) for: ca113 R = 0.07

N1--H1B..O4	1.0100	1.7700	2.775(5)	169.00	4_555
N2--H2..O3	0.8700	1.9000	2.670(3)	146.00	
O4-- H4A..O1	0.9800	1.9300	2.838(5)	153.00	3_556
O4--H4B..N3	1.0200	1.8500	2.864(4)	174.00	4_564
C13--H13..O2	0.9300	2.4800	2.867(4)	105.00	
C22--H22..O3	0.9300	2.4800	3.399(3)	172.00	3_557
C25--H25..O2	20.9300	2.5500	3.413(5)	154.00	6_556
C32--H32..O3	0.9300	2.4800	2.993(3)	115.00	

Translation of Symmetry Code to Equiv.Pos

a = [2546.00] = [2_546] =-x,-1+y,3/2-z
b = [3556.00] = [5_556] =-x,-y,1-z
c = [5545.00] = [3_545] =1/2+x,-1/2+y,z
d = [6546.00] = [4_546] =1/2-x,-1/2+y,3/2-z
e = [2556.00] = [2_556] =-x,y,3/2-z
f = [3557.00] = [5_557] =-x,-y,2-z
g = [4555.00] = [6_556] =x,-y,1/2+z
h = [7547.00] = [7_547] =1/2-x,-1/2-y,2-z
i = [4565.00] = [6_566] =x,1-y,1/2+z
j = [7557.00] = [7_557] =1/2-x,1/2-y,2-z
k = [6556.00] = [4_556] =1/2-x,1/2+y,3/2-z
l = [5455.00] = [3_455] =-1/2+x,1/2+y,z
m = [2566.00] = [2_566] =-x,1+y,3/2-z
n = [3556.00] = [5_556] =-x,-y,1-z
o = [3566.00] = [5_566] =-x,1-y,1-z
p = [4554.00] = [6_555] =x,-y,-1/2+z
q = [4564.00] = [6_565] =x,1-y,-1/2+z

$Co(Bmpp)_2(DMF)_2$ P 21/c R = 0.03 : Jul 15 10:48:38 2013

Contents

Table S1 - Crystal Data and Details of the Structure Determination
for: da158 P 21/c R = 0.03

Table S2 - Final Coordinates and Equivalent Isotropic Displacement Parameters of the non-Hydrogen atoms
for: da158 P 21/c R = 0.03

Table S3 - Hydrogen Atom Positions and Isotropic Displacement Parameters
for: da158 P 21/c R = 0.03

Table S4 - (An)isotropic Displacement Parameters
for: da158 P 21/c R = 0.03

Table S5 - Bond Distances (Angstrom)
for: da158 P 21/c R = 0.03

Table S6 - Bond Angles (Degrees)
for: da158 P 21/c R = 0.03

Table S7 - Torsion Angles (Degrees)
for: da158 P 21/c R = 0.03

Table S8 - Contact Distances(Angstrom)
for: da158 P 21/c R = 0.03

Table S9 - Hydrogen Bonds (Angstrom, Deg)
for: da158 P 21/c R = 0.03

Table S1 - Crystal Data and Details of the Structure Determination
for: da158 P 21/c R = 0.03

Crystal Data

Formula	C40 H40 Co N6 O6
Formula Weight	759.71
Crystal System	monoclinic
Space group	P21/c (No. 14)
a, b, c [Angstrom]	10.1110(5) 9.3804(4) 21.3390(8)
alpha, beta, gamma [deg]	90 117.241(2) 90
V [Ang**3]	1799.43(14)
Z	2
D(calc) [g/cm**3]	1.402
Mu(MoKa) [/mm]	0.534
F(000)	794
Crystal Size [mm]	0.22 x 0.44 x 0.56

Data Collection

Temperature (K)	200
Radiation [Angstrom]	MoKa 0.71073
Theta Min-Max [Deg]	2.1, 28.4
Dataset	-13: 13 ; -12: 12 ; -28: 28
Tot., Uniq. Data, R(int)	49492, 4515, 0.020
Observed data [I > 2.0 sigma(I)]	4132

Refinement

Nref, Npar	4515, 244
R, wR2, S	0.0270, 0.0743, 1.06
w = ^2^(FO^2^)+(0.0361P)^2^+0.6867P]	
WHERE P=(FO^2^+2FC^2^)/3'	
Max. and Av. Shift/Error	0.00, 0.00
Min. and Max. Resd. Dens. [e/Ang^3]	-0.34, 0.34

Table S2 Final Coordinates and Equivalent Isotropic Displacement Parameters of the non-Hydrogen atoms for da158 P 21/c R = 0.03

Atom	x	y	z	U(eq) [Ang^2]
Co1	0	0	0	0.0185(1)
O1	0.07304(8)	0.09842(9)	-0.06357(4)	0.0255(2)
O2	0.20998(9)	0.02131(9)	0.08676(4)	0.0244(2)
O3	0.05540(11)	-0.20357(10)	-0.02413(5)	0.0337(3)
N1	0.25950(10)	0.20444(10)	-0.08279(5)	0.0216(3)
N2	0.41066(10)	0.23714(12)	-0.04498(5)	0.0268(3)
N3	0.18512(13)	-0.40936(11)	0.00477(6)	0.0328(3)
C1	0.20635(11)	0.13720(11)	-0.04155(5)	0.0193(3)
C2	0.33134(11)	0.12829(12)	0.02701(5)	0.0202(3)
C3	0.45214(12)	0.19208(13)	0.01946(6)	0.0253(3)
C4	0.61111(14)	0.21211(19)	0.07231(7)	0.0412(4)
C5	0.32388(11)	0.07645(11)	0.08752(5)	0.0189(3)
C11	0.18336(12)	0.24706(12)	-0.15444(5)	0.0217(3)
C12	0.25288(14)	0.34117(13)	-0.18050(6)	0.0284(3)
C13	0.18246(16)	0.37857(15)	-0.25133(7)	0.0348(4)
C14	0.04367(16)	0.32533(15)	-0.29608(7)	0.0361(4)
C15	-0.02525(15)	0.23409(16)	-0.26932(6)	0.0350(3)
C16	0.04308(13)	0.19418(14)	-0.19878(6)	0.0282(3)
C21	0.47455(14)	0.20892(14)	0.19972(6)	0.0303(3)
C22	0.45882(11)	0.09085(11)	0.15778(5)	0.0197(3)
C23	0.57010(13)	-0.01118(12)	0.18009(6)	0.0276(3)
C24	0.69800(14)	0.00591(14)	0.24367(7)	0.0332(4)
C25	0.71488(14)	0.12532(16)	0.28419(6)	0.0346(4)
C26	0.60366(15)	0.22675(16)	0.26267(7)	0.0371(4)
C31	0.15923(14)	-0.27687(13)	0.01748(6)	0.0294(3)
C32	0.3144(2)	-0.48764(18)	0.05506(11)	0.0566(6)
C33	0.0904(2)	-0.47853(16)	-0.06152(9)	0.0478(5)

U(eq) = 1/3 of the trace of the orthogonalized U Tensor

Table S3 - Hydrogen Atom Positions and Isotropic Displacement Parameters for: da158 P 21/c R = 0.03

Atom	x	y	z	U(iso) [Ang^2]
H4A	0.66380	0.26300	0.05040	0.0620
H4B	0.65760	0.11880	0.08900	0.0620
H4C	0.61620	0.26760	0.11230	0.0620
H12	0.34780	0.37950	-0.15000	0.0340
H13	0.23050	0.44170	-0.26920	0.0420
H14	-0.00370	0.35100	-0.34450	0.0430
H15	-0.12130	0.19790	-0.29980	0.0420
H16	-0.00570	0.13140	-0.18110	0.0340
H21	0.39710	0.27760	0.18540	0.0360
H23	0.55900	-0.09300	0.15190	0.0330
H24	0.77370	-0.06470	0.25910	0.0400
H25	0.80330	0.13800	0.32710	0.0410
H26	0.61540	0.30870	0.29090	0.0440
H31	0.22510	-0.23580	0.06150	0.0350
H32A	0.38060	-0.50810	0.03410	0.0850
H32B	0.28200	-0.57740	0.06720	0.0850
H32C	0.36750	-0.43020	0.09770	0.0850
H33A	0.14380	-0.48710	-0.08980	0.0720
H33B	0.00010	-0.42160	-0.08730	0.0720
H33C	0.06310	-0.57370	-0.05230	0.0720

The Temperature Factor has the Form of Exp(-T)
Where T = 8*(Pi**2)*U*(Sin(Theta)/Lambda)**2 for Isotropic Atoms

Table S4 - Anisotropic Displacement Parameters for: da158 P 21/c R = 0.03

Atom	U(1,1) or U	U(2,2)	U(3,3)	U(2,3)	U(1,3)	U(1,2)
Co1	0.0168(1)	0.0220(1)	0.0169(1)	0.0002(1)	0.0078(1)	-0.0010(1)
O1	0.0191(4)	0.0364(4)	0.0192(4)	0.0031(3)	0.0073(3)	-0.0044(3)
O2	0.0201(4)	0.0323(4)	0.0197(4)	0.0016(3)	0.0083(3)	-0.0038(3)
O3	0.0425(5)	0.0293(4)	0.0276(4)	-0.0014(3)	0.0145(4)	0.0087(4)
N1	0.0186(4)	0.0280(5)	0.0175(4)	0.0022(3)	0.0077(3)	-0.0012(3)
N2	0.0194(4)	0.0380(5)	0.0218(4)	0.0026(4)	0.0085(4)	-0.0047(4)
N3	0.0411(6)	0.0248(5)	0.0381(6)	0.0019(4)	0.0231(5)	0.0050(4)
C1	0.0203(5)	0.0204(5)	0.0179(5)	0.0003(4)	0.0094(4)	0.0009(4)
C2	0.0174(4)	0.0243(5)	0.0178(5)	0.0006(4)	0.0071(4)	-0.0003(4)
C3	0.0209(5)	0.0336(6)	0.0206(5)	0.0016(4)	0.0089(4)	-0.0028(4)
C4	0.0217(6)	0.0717(10)	0.0259(6)	0.0086(6)	0.0071(5)	-0.0125(6)
C5	0.0190(4)	0.0182(5)	0.0186(5)	0.0001(4)	0.0078(4)	0.0023(4)
C11	0.0243(5)	0.0239(5)	0.0179(5)	0.0026(4)	0.0106(4)	0.0052(4)
C12	0.0299(6)	0.0299(6)	0.0270(6)	0.0048(5)	0.0144(5)	0.0013(5)
C13	0.0441(7)	0.0353(7)	0.0312(6)	0.0127(5)	0.0225(6)	0.0081(5)
C14	0.0435(7)	0.0413(7)	0.0218(5)	0.0103(5)	0.0135(5)	0.0142(6)
C15	0.0300(6)	0.0459(7)	0.0214(5)	0.0040(5)	0.0052(5)	0.0054(5)
C16	0.0257(5)	0.0351(6)	0.0218(5)	0.0032(4)	0.0091(4)	0.0013(5)
C21	0.0296(6)	0.0313(6)	0.0246(5)	-0.0027(5)	0.0077(5)	0.0074(5)
C22	0.0188(5)	0.0233(5)	0.0171(4)	0.0024(4)	0.0084(4)	-0.0001(4)
C23	0.0251(5)	0.0273(6)	0.0263(6)	-0.0008(4)	0.0083(5)	0.0047(4)
C24	0.0236(6)	0.0408(7)	0.0288(6)	0.0050(5)	0.0066(5)	0.0102(5)
C25	0.0245(5)	0.0511(8)	0.0207(5)	-0.0012(5)	0.0040(4)	-0.0005(5)
C26	0.0371(7)	0.0407(7)	0.0254(6)	-0.0109(5)	0.0074(5)	0.0005(6)
C31	0.0373(6)	0.0263(6)	0.0281(6)	0.0001(5)	0.0180(5)	0.0018(5)
C32	0.0626(11)	0.0410(9)	0.0607(11)	0.0091(7)	0.0235(9)	0.0237(8)
C33	0.0637(10)	0.0322(7)	0.0495(9)	-0.0113(6)	0.0276(8)	-0.0006(7)

The Temperature Factor has the Form of Exp(-T)
Where T = 8*(Pi**2)*U*(Sin(Theta)/Lambda)**2 for Isotropic Atoms
T = 2*(Pi**2)*Sumij(h(i)*h(j)*U(i,j)*Astar(i)*Astar(j)), for Anisotropic Atoms. Astar(i) are Reciprocal Axial Lengths and h(i) are the Reflection Indices.

Table S5 - Bond Distances (Angstrom) for da158 P 21/c R = 0.03

Co1-O1	2.0384(8)	C21-C22	1.3866(16)	Co1-O2	2.0921(9)
C21-C26	1.3897(19)	Co1-O3	2.1188(10)	C22-C23	1.3850(17)
Co1-O1	2.0384(8)	C23-C24	1.3902(18)	Co1-O2	2.0921(9)
C24-C25	1.3771(19)	Co1-O3	2.1188(10)	C25-C26	1.381(2)
O1-C1	1.2610(15)	C4-H4A	0.9800	O2-C5	1.2558(15)
C4-H4B	0.9800	O3-C31	1.2288(16)	C4-H4C	0.9800
N1-N2	1.3972(15)	C12-H12	0.9500	N1-C1	1.3762(15)
C13-H13	0.9500	N1-C11	1.4187(14)	C14-H14	0.9500
N2-C3	1.3105(15)	C15-H15	0.9500	N3-C31	1.3235(16)
C16-H16	0.9500	N3-C32	1.454(2)	C21-H21	0.9500
N3-C33	1.449(2)	C23-H23	0.9500	C1-C2	1.4324(14)
C24-H24	0.9500	C2-C3	1.4339(18)	C25-H25	0.9500
C2-C5	1.4137(15)	C26-H26	0.9500	C3-C4	1.4937(19)
C31-H31	0.9500	C5-C22	1.5017(14)	C32-H32A	0.9800
C11-C12	1.3930(18)	C32-H32B	0.9800	C11-C16	1.3873(18)
C32-H32C	0.9800	C12-C13	1.3890(18)	C33-H33A	0.9800
C13-C14	1.380(2)	C33-H33B	0.9800	C14-C15	1.382(2)
C33-H33C	0.9800	C15-C16	1.3897(16)		

Table S6 - Bond Angles (Degrees) for: da158 P 21/c R = 0.03

O1-Co1-O2	90.89(3)	C1-C2-C3	105.04(9)
O1-Co1-O3	91.71(4)	C1-C2-C5	124.19(11)
O1-Co1-O1	180.00	C3-C2-C5	130.58(10)
O1-Co1-O2	89.11(3)	N2-C3-C2	111.87(11)
O1-Co1-O3	88.29(4)	N2-C3-C4	117.94(12)
O2-Co1-O3	91.55(4)	C2-C3-C4	130.18(11)
O1-Co1-O2	89.11(3)	O2-C5-C2	124.19(10)
O2-Co1-O2	180.00	O2-C5-C22	117.30(9)
O2-Co1-O3	88.45(4)	C2-C5-C22	118.49(10)
O1-Co1-O3	88.29(4)	N1-C11-C12	119.00(11)
O2Co1-O3	88.45(4)	N1-C11-C16	121.02(11)
O3-Co1-O3	180.00	C12-C11-C16	119.97(10)
O1-Co1-O2	90.89(3)	C11-C12-C13	119.57(12)
O1-Co1-O3	91.71(4)	C12-C13-C14	120.94(14)
O2-Co1-O3	91.55(4)	C13-C14-C1	118.94(12)
Co1-O1-C1	122.26(7)	C14-C15-C16	121.32(13)
Co1-O2-C5	127.16(7)	C11-C16-C15	119.25(12)
Co1-O3-C3	1124.21(8)	C22-C21-C2	119.97(13)
N2-N1-C1	112.05(9)	C5-C22-C21	119.98(10)
N2-N1-C11	118.10(10)	C5-C22-C23	120.33(9)
C1-N1-C11	129.81(11)	C21-C22-C23	119.67(10)
N1-N2-C3	105.98(10)	C22-C23-C24	120.15(11)
C31-N3-C32	121.21(12)	C23-C24-C25	119.94(13)
C31-N3-C33	121.08(12)	C24-C25-C26	120.23(12)
C32-N3-C33	117.61(12)	C21-C26-C25	120.00(13)
O1-C1-N1	123.89(9)	O3-C31-N3	124.13(12)
O1-C1-C2	131.04(10)	C3-C4-H4A	109.00
N1-C1-C2	105.05(10)	C3-C4-H4B	109.00
C3-C4-H4C	109.00	C25-C24-H24	120.00
H4A-C4-H4B	109.00	C24-C25-H25	120.00
H4A-C4-H4C	109.00	C26-C25-H25	120.00
H4B-C4-H4C	109.00	C21-C26-H26	120.00
C11-C12-H12	120.00	C25-C26-H26	120.00
C13-C12-H12	120.00	O3-C31-H31	118.00
C12-C13-H13	120.00	N3-C31-H31	118.00
C14-C13-H13	120.00	N3-C32-H32A	109.00
C13-C14-H14	121.00	N3-C32-H32B	109.00
C15-C14-H14	121.00	N3-C32-H32C	109.00
C14 -C15-H15	119.00	H32A-C32-H32B	109.00
C16-C15-H15	119.00	H32A-C32-H32C	109.00
C11-C16-H16	120.00	H32B-C32-H32C	110.00
C15-C16-H16	120.00	N3-C33-H33A	109.00
C22-C21-H21	120.00	N3-C33-H33B	109.00
C26-C21-H21	120.00	N3-C33-H33C	109.00
C22-C23-H23	120.00	H33A-C33-H33B	109.00
C24-C23-H23	120.00	H33A-C33-H33C	110.00
C23-C24-H24	120.00	H33B-C33-H33C	109.00

Table S7 - Torsion Angles (Degrees) for: da158 P 21/c R = 0.03

O2-Co1-O1-C1	3.06(9)	O3-Co1-O1-C1	-88.52(9)
O2-Co1-O1-C1	-176.94(9)	O3-Co1-O1-C1	91.48(9)
O1-Co1-O2-C5	-0.65(9)	O3-Co1-O2-C5	91.09(10)
O1-Co1-O2-C5	179.35(9)	O3-Co1-O2-C5	-88.91(10)
O1-Co1-O3-C31	108.89(12)	O2-Co1-O3-C31	17.95(12)
O1-Co1-O3-C31	-71.11(12)	O2-Co1-O3-C31	-162.05(12)
Co1-O1-C1-N1	-179.69(8)	Co1-O1-C1-C2	-1.60(17)
Co1-O2-C5-C2	-3.59(16)	Co1-O2-C5-C22	174.84(7)
Co1-O3-C31-N3	173.20(11)	C1-N1-N2-C3	-0.47(13)
C11-N1-N2-C3	177.51(10)	N2-N1-C1-O1	179.26(10)
N2-N1-C1-C2	0.75(12)	C11-N1-C1-O1	1.59(18)
C11-N1-C1-C2	-176.92(11)	N2-N1-C11-C12	-11.73(16)
N2-N1-C11-C16	166.90(11)	C1-N1-C11-C12	165.82(12)
C1-N1-C11-C16	-15.55(19)	N1-N2-C3-C2	-0.03(15)
N1-N2-C3-C4	179.54(11)	C32-N3-C31-O3	176.97(16)
C33-N3-C31-O3	0.6(2)	O1-C1-C-C3	-179.07(12)
O1-C1-C2-C5	-3.58(19)	N1-C1-C2-C3	-0.71(12)
N1-C1-C2-C5	174.77(10)	C1-C2-C3-N2	0.48(14)
C1-C2-C3-C4	-179.02(13)	C5-C2-C3-N2	-174.61(12)
C5-C2-C3-C4	5.9(2)	C1-C2-C5-O2	6.34(18)
C1-C2-C5-C22	-172.08(10)	C3-C2-C5-O2	-179.40(12)
C3-C2-C5-C22	2.18(18)	O2-C5-C22-C21	-85.66(14)
O2-C5-C22-C23	96.30(14)	C2-C5-C22-C21	92.87(14)
C2-C5-C22-C23	-85.18(14)	N1-C11-C12-C13	177.02(12)
C16-C11-C12-C13	-1.6(2)	N1-C11-C16-C15	-177.41(12)
C12-C11-C16-C15	1.21(19)	C11-C12-C13-C14	0.9(2)
C12-C13-C14-C15	0.3(2)	C13-C14-C15-C16	-0.7(2)
C14-C15-C16-C11	0.0(2)	C26-C21-C22-C5	-175.93(12)
C26-C21-C22-C23	2.1(2)	C22-C21-C26-C25	-1.4(2)
C5-C22-C23-C24	177.00(12)	C21-C22-C23-C24	-1.06(19
C22-C23-C24-C25	-0.7(2)	C23-C24-C25-C26	1.5(2)
C24-C25-C26-C21	-0.4(2)		

Table S8 - Contact Distances(Angstrom) for: da158 P 21/c R = 0.03

Co1.C2	3.3521(12)	N2.C2	2.2745(15)	Co1.C2	3.3521(12)
N1.H16	2.6300	Co1.H31	3.0100	N1.H12	2.5900
Co1.H31	3.0100	N2.H4A	2.4500	O1.O2	2.9436(11)
N2.H12	2.4300	O1.O3	2.9837(13)	N2.H23	2.7900
O1.C11	2.9880(14)	N3.H4A	2.6900	O1.C16	2.9023(14)
C1.O2	2.9305(13)	O1.O3	2.8960(14)	C1.C3	2.2747(17)
O1.O2	2.8981(13)	C1.C16	3.0327(15)	O2.O1	2.9436(11)
C2.N2	2.2745(15)	O2.C23	3.2678(17)	C2.C21	3.3713(15)
O2.O3	2.9370(14)	C2.Co1	3.3521(12)	O2.O3	3.0177(13)
C2.C23	3.3152(15)	O2.C21	3.1875(16)	C3.C1	2.2747(17)
O2.O1	2.8981(13)	C3.C11	3.4914(15)	O3.O1_a	2.8960(14)
C3.C32	3.537(2)	O3.O1	2.9837(13)	C3.C22	3.0718(16)
O3.C33	2.7700(18)	C4.C22	3.0923(19)	O3.O2	2.9370(14)
C4.C21	3.569(2)	O3.O2	3.0177(13)	C4.C5	3.320(2)
O1.H16	2.2800	C4.C23	3.274(2)	O1.H14	2.9100
C5.C4	3.320(2)	O2.H31	2.4900	C5.O1	3.0633(13)
O3.H14	2.6600	C11.C24	3.5758(18)	O3.H33B	2.3700
C11.C3	3.4914(15)	N1.C2	2.2293(14)	C11.C23	3.5579(18)
N2.C12	2.7635(15)	C11.C14	2.7859(17)	C11.O1	2.9880(14)
C23.C26	3.548(2)	C12.N2	2.7635(15)	C23.C4	3.274(2)
C12.C23	3.5737(18)	C24.C11	3.5758(18)	C12.C15	2.762(2)
C24.C21	2.770(2)	C13.C16	3.588(2)	C25.C22	2.7732(16)
C13.C16	2.772(2)	C25.C16	3.593(2)	C14.C11	2.7859(17)
C25.C15	3.563(2)	C14.C16	3.559(2)	C26.C23	2.7666(19)
C15.C25	3.563(2)	C26.C23	3.548(2)	C15.C12	2.762(2)
C31.O1	3.3763(17)	C16.C1	3.0327(15)	C31.O2	3.0948(15)
C16.C13	2.772(2)	C32.C3	3.537(2)	C16.C13	3.588(2)
C33.O3	2.7700(18)	C16.C14	3.559(2)	C1.H33C	3.0300
C16.O1	2.9023(14)	C1.H16	2.7600	C16.C25	3.593(2)
C2.H4B	2.9400	C21.C24	2.770(2)	C2.H4C	2.9200
C21.C2	3.3713(15)	C2.H32B	3.0000	C21.O2	3.1875(16)
C3.H32A	2.9600	C21.C4	3.569(2)	C4.H15	2.9500
C22.C4	3.0923(19)	C5.H23	2.6600	C22.C3	3.0718(16)
C5.H21	2.6600	C22.C25	2.7732(16)	C5.H31	3.0600
C23.C11	3.5579(18)	C11.H23	2.9600	C23.O2	3.2678(17)
C11.H33A	2.9600	C23.C26	2.7666(19)	C11.H24	3.0000
C23.C2	3.3152(15)	C12.H33A	3.0800	C23.C12	3.5737(18)
C12.H24	3.0300	C12.H23	2.8900	H4A.N2	2.4500
C13.H24	2.9900	H4A.N3	2.6900	C13.H16	2.9200
H4A.C31	2.7700	C14.H16	2.9100	H4B.C2	2.9400
C14.H24	2.9500	H4B.C22	2.9900	C15.H24	2.9200

H4B.C23	2.7600	C16.H24	2.9600	H4C.C2	2.9200
C21.H4C	2.8800	H4C.C21	2.8800	C22.H4B	2.9900
H4C.C22	2.7600	C22.H26	3.0900	H4C.H15	2.4700
C22.H4C	2.7600	H12.N1	2.5900	C23.H26	2.8000
H12.N2	2.4300	C23.H4B	2.7600	H12.H13	2.3400
C24.H21	3.0200	H13.H12	2.3400	C25.H32C	3.0400
H13.H14	2.3300	C31.H32A	3.0200	H14.H13	2.3300
C31.H32B	3.0700	H14.H15	2.3300	C31.H33C	3.1000
H14.O1	2.9100	C31.H33A	2.9700	H14.O3	2.6600
C31.H33B	2.4800	H15.H14	2.3300	C31.H33C	3.0200
H15.H16	2.3400	C31.H32C	2.4800	H15.C4	2.9500
C31.H4A	2.7700	H15.H4C	2.4700	C32.H33A	2.7700
H16.O1	2.2800	C32.H33C	2.6500	H16.N1	2.6300
C32.H31	2.5600	H16.C12	7600	C33.H32A	2.7100
H16.H15	2.3400	C33.H32B	2.7000	H16.C13	2.9200
H16.C14	2.9100	H31.C5	3.0600	H21.C5	2.6600
H31.C32	2.5600	H21.H26	2.3400	H31.H32C	2.2300
H21.C24	3.0200	H32A.C3	2.9600	H23.C5	2.6600
H32A.C31	3.0200	H23.H24	2.3400	H32A.C33	2.7100
H23.N2	2.7900	H32B.C2	3.0000	H23.C11	2.9600
H32B.C31	3.0700	H23.C12	2.8900	H32B.C33	2.7000
H24.H23	2.3400	H32B.H33C	2.5000	H24.H25	2.3300
H32C.C31	2.4800	H24.C11	3.0000	H32C.H31	2.2300
H24.C12	3.0300	H32C.C25	3.0400	H24.C13	2.9900
H33A.C11	2.9600	H24.C14	2.9500	H33A.C12	3.0800
H24.C15	2.9200	H33A.C31	2.9700	H24.C16	2.9600
H33A.C32	2.7700	H25.H24	2.3300	H33B.O3	2.3700
H25.H26	2.3300	H33B.C31	2.4800	H26.H21	2.3400
H33C.C1	3.0300	H26.H25	2.3300	H33C.C31	3.1000
H26.C22	3.0900	H33C.C32	2.6500	H26.C23	2.8000
H33C.H32B	2.5000	H31.Co1	3.0100	H33C.C31	3.0200
H31.O2	2.4900				

Table S9 - Hydrogen Bonds (Angstrom, Deg) for: da158 P 21/c R = 0.03

C12--H12..N2	0.9500	2.4300	2.7635(15)	100.00
C16--H16..O1	0.9500	2.2800	2.9023(14)	123.00
C31--H31..O2	0.9500	2.4900	3.0948(15)	121.00
C33--H33B..O3	0.9800	2.3700	2.7700(18)	104.00

Translation of Symmetry Code to Equiv.Pos

a = [3555.00] = [3_555] =-x,-y,-z
b = [2544.00] = [2_544] =-x,-1/2+y,-1/2-z
c = [3655.00] = [3_655] =1-x,-y,-z
d = [1565.00] = [1_565] =x,1+y,z
e = [4655.00] = [4_666] =1+x,1/2-y,1/2+z
f = [2554.00] = [2_554] =-x,1/2+y,-1/2-z
g = [4454.00] = [4_465] =-1+x,1/2-y,-1/2+z
h = [2645.00] = [2_645] =1-x,-1/2+y,1/2-z
i = [2655.00] = [2_655] =1-x,1/2+y,1/2-z
j = [3545.00] = [3_545] =-x,-1-y,-z
k = [1545.00] = [1_545] =x,-1+y,z